Nanoparticles and microfluidics for future tuberculosis vaccines

Neustrup, M.A.

NANOPARTICLES AND MICROFLUIDICS FOR FUTURE TUBERCULOSIS VACCINES

Malene Aaby Neustrup

NANOPARTICLES AND MICROFLUIDICS FOR FUTURE TUBERCULOSIS VACCINES

Proefschrift

ter verkrijging van
de graad van doctor aan de Universiteit Leiden,
op gezag van rector magnificus prof.dr.ir. H. Bijl,
volgens besluit van het college voor promoties
te verdedigen op dinsdag 23 september 2025
klokke 13:00 uur

door

Malene Aaby Neustrup

The research described in this dissertation was conducted at the Division of BioTherapeutics, Leiden Academic Centre for Drug Research (LACDR), Leiden University, and at the Department of Infectious Diseases, Leiden University Medical Center (LUMC), both located in Leiden, The Netherlands. This work was made possible through the grant 'TTW 15240' provided by the Dutch Research Council (NWO) domain Applied and Engineering Sciences (TTW).

Layout and cover design by Malene Aaby Neustrup. The cover design was created using the fluid simulator 'Haxiomic' by George Corney.

ISBN: 978-94-6496-418-9
Printed by Gildeprint — www.gildeprint.nl

Promotores: Prof.dr. J.A. Bouwstra
Prof.dr. T.H.M. Ottenhoff

Co-promotor: Dr. K. van der Maaden

Promotiecommissie: Prof.dr. H. Irth
Prof.dr. E.C.M. de Lange
Prof.dr. F.A. Ossendorp
Prof.dr. Y. Perrie — University of Strathclyde
Prof.dr. G.F.A. Kersten
Prof.dr. R. Rissmann

TABLE OF CONTENTS

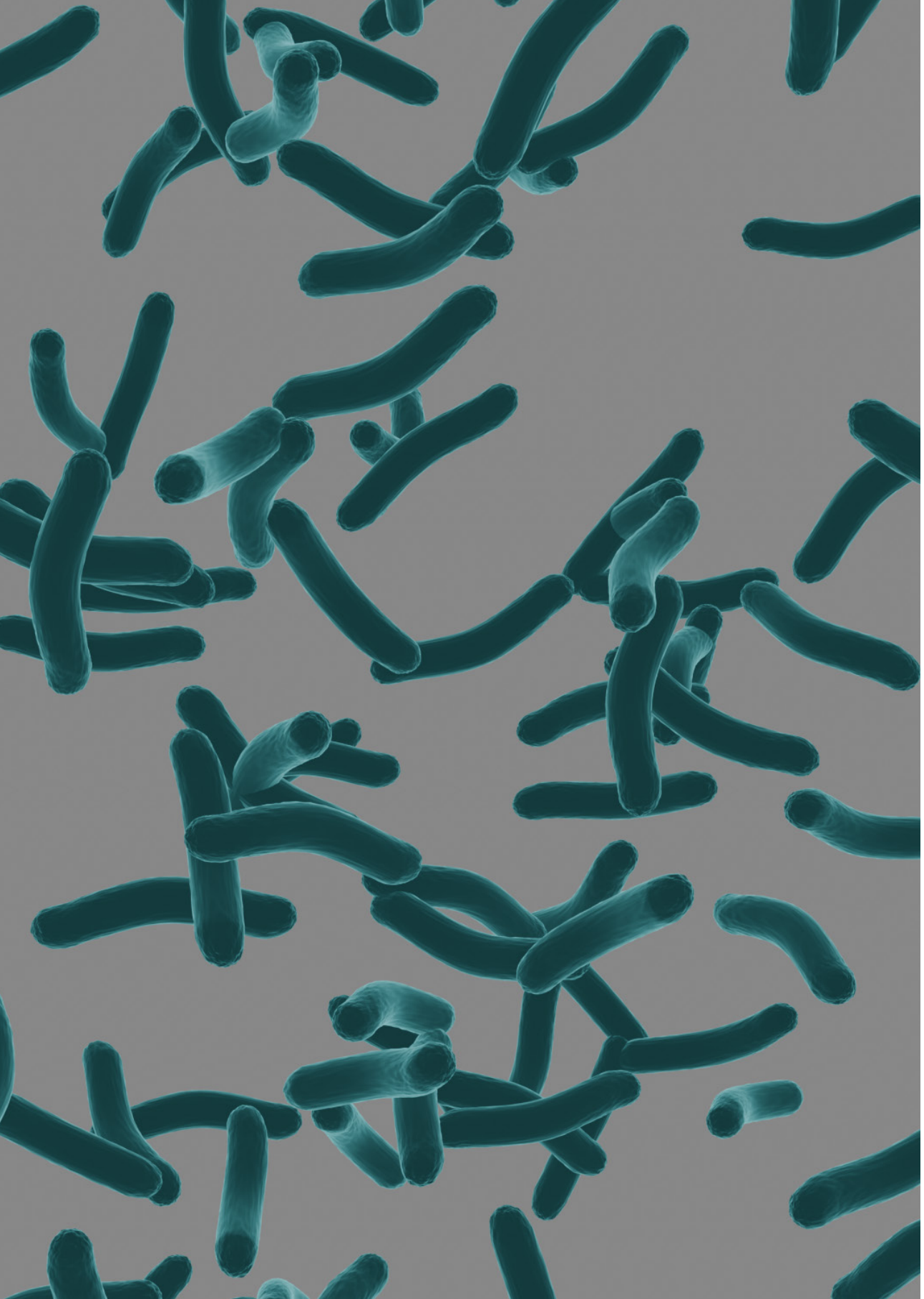

CHAPTER 1

GENERAL INTRODUCTION
DISSERTATION AIM AND OUTLINE

GENERAL INTRODUCTION

"One can think of the middle of the twentieth century as the end of one of the most important social revolutions in history, the virtual elimination of infectious diseases as a significant factor in social life [1]." Wrote Sir Frank MacFarlane Burnet, the 1960 co-winner of the Nobel Prize in Medicine, in 1962.

This optimistic statement was presumably based on the improved living conditions in the Western World caused by better nutrition, sanitation, housing, and the development of vaccines and antibiotics that had decreased the mortality and morbidity of infectious diseases [2]. However, the statement was shortly after disproven, as a series of outbreaks and epidemics of new, re-emerging, and drug-resistant pathogens, e.g., the AIDS outbreak (1981: first official reporting [3]) and Ebola (1976: first recognition of the disease [4]) refuted the notion that infectious diseases were no longer a threat to human health [2]. We have still not "virtually eliminated" infectious diseases. One of humans' oldest enemies, tuberculosis (TB), which has been with us for at least 10,500 years [5], is still going strong. TB is the deadliest infectious disease in recent times, only recently surpassed (on a death/year basis) by COVID-19 [6, 7].

Tuberculosis

TB is caused by the *Mycobacterium tuberculosis* complex, a group of closely related mycobacteria, including the *Mycobacterium tuberculosis* (Mtb), which is the main cause of TB in humans [8, 9]. Mtb is transmitted through airborne droplets, called liquid aerosols, which expire when individuals with pulmonary TB cough, sneeze, talk, and even breathe [10]. TB mainly affects the lungs, causing symptoms such as fever, chest pain, and cough with sputum and sometimes blood [11]. When Mtb is transmitted to a new host, it can either be eradicated by the immune system [12], lead to the symptomatic (active) disease, or be (mainly) contained in granulomas by the body as an asymptomatic infection that possibly can lead to the active disease later in life [13–15]. If active TB is left untreated, it may cause death by septic shock, respiratory failure, or suffocation [16].

It is estimated that one-quarter of the world's population is infected (mostly latently) with TB and that it killed around 1.3 million people in 2022 [7]. This is despite TB being manageable/curable with a strict regimen of antibiotics [7]. According to the World Health Organization (WHO), TB is especially a problem in the regions of Southeast Asia (46%), Africa (23%), and the Western Pacific (18%), regions which mainly consist of low-income countries [7]. TB is a severe health problem in these countries due to, among others, low TB case detection [17] and low adherence to and availability of medication [18–20].

Vaccination can potentially reduce the TB burden, as it has lowered the incidence rates of other diseases, e.g. measles and polio, and even eradicated smallpox [21]. However, the only vaccine registered against TB, the live-attenuated vaccine *Mycobacterium bovis* Bacille Calmette-Guérin (BCG) (already administered since 1921 [22]), is inadequate, as it has a high variable efficiency (the protection varies between 0 and 80%), fails to prevent active pulmonary TB in adults, and can cause severe side effects in immunocompromised individuals [23, 24]. The variable efficacy of the BCG vaccine against TB has several controversial and diverse reasons. Such as, but not limited to, i) TB not only being caused by one, but several mycobacteria in the Mtb complex, ii) previous exposure to mycobacteria may interfere with the BCG response, iii) lack of essential antigens in the vaccine, and iv) vaccine manufacturing differences [25]. In the past century, these differences in manufacturing have been caused by the usage of different strains of the BCG vaccine, e.g., BCG Russia, Copenhagen, and Japan, and batch-to-batch variations [25, 26]. Therefore, a new, more effective vaccine and/or vaccination strategy is needed to increase the effectiveness and protection rate of TB vaccines. The studies described in this dissertation will explore different vaccine formulations, administration routes, and methodologies, as a first step toward a new vaccine against TB.

A promising antigen for a new TB vaccine is Ag85B-ESAT6-Rv2034 (AER), which we have focussed on in this dissertation. AER is a fusion protein consisting of Antigen 85B (Ag85B), one of the proteins that is most abundant in Mtb and BCG culture supernatants [27, 28], the 6 kDa early secretory antigenic target (ESAT-6); a protein secreted by Mtb and other mycobacteria, but not BCG [29–31], and Rv2034; a protein that is expressed during inflammatory pulmonary infections in mice [32] and strongly recognised by human T cells [33]. By choosing a protein, the possibility of strain differences is complety avoided. In a preclinical study, AER adjuvanted (from Latin: adjuvare; to help) with CAF01 exhibited promising results in HLA-DR3 mice, which are transgenic mice that have the human leucocyte antigen variant DR3 (a major allele present in 20% of the human population) instead of murine major histocompatibility complex (MHC) class II [33]. It reduced the colony-forming units of Mtb in lungs and spleens in guinea pigs to the same level as BCG 30 days post-infection, which is better than described in other studies performed with Ag85B-ESAT6 [33]. However, the protective efficacy is still only at the same level as BCG, the suboptimal vaccine. Therefore, the vaccine could be further optimised.

Mounting of an immune response against TB

To formulate a vaccine against TB, it is important to know how Mtb infects the body and which response is necessary to eradicate the bacteria. Mtb is (usually) transmitted after inhalation of Mtb-containing aerosols into the respiratory tract, which comprises the upper respiratory tract (the oral and nasal cavity down to the larynx above the vocal cords [34]) and the lower respiratory tract (the larynx below the vocal cords down to the alveoli [35, 36]). The respiratory tract is mostly lined with a mucous membrane, the first line of defence against Mtb [35]. The mucous membrane consists of the lamina propria (a connective tissue layer) and tightly bound epithelial cells covered in mucus [37].

Little is known about the early Mtb infection [38]. However, it is believed that if the mucosal barrier functions do not clear the Mtb bacteria, they can travel to the mucosa-free alveolar sacs and infect alveolar macrophages, which are both the primary immune cell type in the alveoli and the cell type that Mtb mainly infects [38, 39]. Alveolar macrophages recognise pathogen-associated molecular patterns located (PAMPs) on Mtb with their pattern-recognition receptors (PRRs) that, among others, initiate phagocytosis [40]. Phagocytosis is a process by which the pathogen is taken up through an extension of the cell membrane, which fuses and creates a vesicle inside the macrophage called the phagosome. The phagosome fuses with other vesicles inside the macrophage called lysosomes, which contain enzymes and other substances, which the macrophage uses to kill the pathogen [41]. However, Mtb avoids destruction in various ways, e.g., by preventing phagosome-lysosome fusion [41]. Therefore, Mtb is able to reproduce slowly (an approximate generation time of 20 h [38]) inside the phagosomal compartments [41].

Mtb-infected alveolar macrophages can traverse the airway epithelium and gain access to the lung interstitium [39]. Mtb replicates for approximately one week inside the macrophages, whereafter the bacteria escape and are phagocytosed by other cells, e.g., neutrophils, migratory inflammatory monocytes, and the professional antigen-presenting cell dendritic cells (DCs) [42]. The inflammatory monocytes and the DCs transport Mtb to the draining lymph node in the lung and transfer the antigen to uninfected lymphoid-tissue resident immature DCs [42]. The immature DCs differentiate into mature DCs when their PRRs interact with PAMPs on the Mtb [43, 44].

Antigens that the DCs have sampled are presented on their MHC molecules, which can interact with T cells through their α:β T cell receptor (TCR) [45]. Classical MHC molecules are polymorphic and can be divided into MHC class I molecules and MHC class II molecules [46]. For antigen presentation to the cluster of differentiation (CD)4$^+$ T cell, the antigen has to be presented on a MHC class II molecule, and the T cell's co-receptor CD4 has to interact with the MHC molecule [45]. For the T cell type CD8$^+$ T cell, the antigen has to be presented on a MHC class I molecule, with the co-receptor CD8 interacting with the MHC molecule [45]. Additional costimulatory signals are transmitted by the interaction of surface molecules and the secretion of cytokines, see Fig. 1. The best characterised costimulatory signals for the CD4$^+$ T cells are provided by CD80 and CD86 molecules, which are present in high levels on activated antigen-presenting cells (APCs) [47]. These molecules bind to the CD28 molecule on the CD4$^+$ T cell, and additional costimulatory signals in the form of cytokines, produced by the DC or other cells, bind to the CD4$^+$ T cell's cytokine receptors and direct the differentiation into various subsets of effector CD4$^+$ T cells [47].

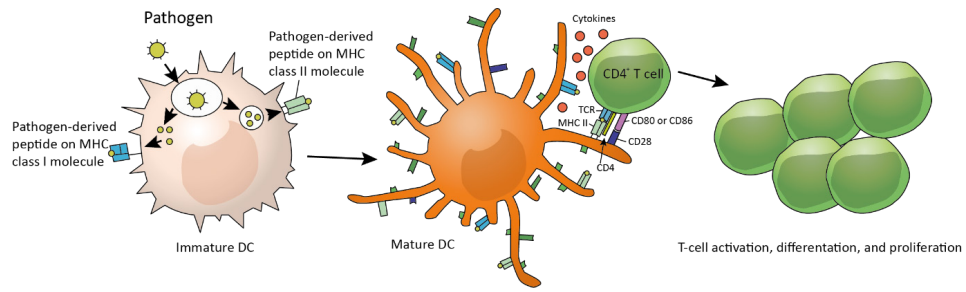

Figure 1. Simplified illustration of (pathogen-derived) antigen presentation on an MHC class I molecule and an MHC class II molecule on a DC. The DC is activated via PRRs from the pathogen and can hereafter activate T cells by presenting the antigen on MHC molecules to the TCR while supplying costimulatory signals (here shown for CD4$^+$ T cells), which leads to activation, differentiation, and proliferation of the T cell. CD: cluster of differentiation, DC: dendritic cell, MHC: major histocompatibility complex.

Based on the costimulatory signals given during the activation of CD4$^+$ T cells, they develop into different effector cells. The major subsets are T helper (Th)1, Th2, Th17, regulatory T (T_{reg}) cells, and T follicular helper (T_{FH}) cells. The subsets are characterised by their cytokine profiles associated with their effector functions [47]. Th1 cells help macrophages clear intravesical infections; Th2 cells help to control infections by extracellular organisms, e.g., parasites [47, 48]; Th17 cells help to protect against extracellular organisms and have been associated with autoimmunity and stimulation of neutrophils [49, 50]; T_{FH} cells provide help to the B cells [51], and; T_{reg} cells have a role in dampening immune responses and maintaining immunological self-tolerance by inhibiting conventional T-cell responses [52]. The activated CD8$^+$ T cell differentiates into the effector cell, the cytotoxic T cell [53]. Once pathogens have entered host cells, they are inaccessible to antibodies and phagocytic cells. By recognising pathogen-derived antigens on MHC class I molecules of the infected cell, the cytotoxic T cell reorganises its cytoskeleton and exocytose granules, which fuse with the cell membrane and release its content in the synapse between the cytotoxic T cell and the infected cell [54]. The content in the granules consists of preformed effector molecules such as granzymes and perforins, which penetrate the cell membrane and induce the apoptosis, programmed cell death, of the host cell [54].

The inflammatory milieu of the Mtb infection promotes Mtb-specific T_{reg} cells that restrict priming and proliferation of effector T cells, therefore delaying their arrival in the lung (T-cell responses against Mtb are on average detected 45 days after Mtb exposure, whereas T-cell response typically peak at 7-14 days for most infections), and when these effector T cells finally reach the site of infection, there is a sizeable bacterial burden, regulatory cell types and immunosuppressive factors [42]. Therefore, Mtb gets encapsulated in large granulomas consisting of various cell types, where it can be contained for decades [55]. Sometimes, the structural organisation in the granuloma is altered, which can lead to necrosis of the granuloma and, thereby, the release of bacteria [55]. As the normal immune response against TB often is insufficient, it is important to identify the essential factors in containing/

eradicating the TB infection. However, which kind of immune responses correlate with protection against TB is not entirely determined.

It has been shown that B cell-deficient mice (B cells can develop into plasma cells that produce antibodies) demonstrate increased susceptibility to TB and more severe lesion formation [56]. However, other groups have shown little to no role of B cells [56]. Therefore, the role of B cells and antibodies in protection against TB is yet to be determined. $CD4^+$ T cells are, on the other hand, crucial as HIV-infected individuals depleted of $CD4^+$ T cells are restricted in their ability to contain TB [42]. Mice with a deletion of the interferon (IFN)-γ gene have shown extreme susceptibility to TB; however, IFN-γ-deficient BCG-vaccinated mice have also shown to exhibit significant protection against Mtb, which indicates that an IFN-γ independent mechanism to limit Mtb does exist and that IFN-γ might not be a reliable correlate of protection against TB [57].

As the immunological response to BCG seems to depend on the animal model, dose, BCG strain, and administration route, among others, it is hard to determine what makes BCG inadequate to protect against TB [57]. BCG induces both humoral and cellular responses, but it might be that the response is not adequate in regards to the central-memory T-cell response, Th17 response, and/or $CD8^+$ T-cell response [57]; however, it is not determined. Therefore, it is hard to conclude exactly which kind of response a vaccine should elicit to confer protection. However, it is believed that an effective vaccine against TB should comprise both a $CD4^+$ and a $CD8^+$ T-cell response [24].

Different vaccine types and adjuvants

Early vaccines were based on live-attenuated or inactivated-whole pathogens. Live-attenuated (weakened) vaccines are based on living viruses or bacteria that have been modified, usually by repeated culturing [58]. They cause a mild infection and induce an immune response similar to that of the wild-type strain infections; however, they can cause disease in immunosuppressed people, as seen with disseminated BCGosis in HIV-infected infants [26], and have the potential for reversion to the virulent form, as it has been documented with the oral polio vaccine [59]. Vaccines based on inactivated whole pathogens, produced by inactivating/killing the pathogens with heat, chemicals, or radiation [60], are safer than live-attenuated vaccines as they cannot revert to the virulent form while still containing pathogen components, which act as intrinsic adjuvants [61]. However, inactivated-whole pathogen vaccines are unsuitable when the natural infection does not convey long-standing immunity [61] and can sometimes not be produced in large quantities, as seen with hepatitis B [62].

Since the early days of vaccine production, other types of vaccines have emerged, such as subunit vaccines [63]. Subunit vaccines are based on purified antigens, usually proteins [62], and often have fewer adverse effects than whole inactivated pathogens, e.g., as seen for the pertussis vaccine [63]. Subunit vaccines often lack adjuvant effects and are, therefore, usually poorly immunogenic [61]. It is thus necessary to add adjuvants to these vaccines, as adjuvants can help improve the potency and redirect the immune system toward an effective response [61]. Adjuvants can be divided into two groups: particulate and molecular [64, 65]. In 1926, the immune-enhancing effects of the particulate adjuvant type aluminium salts, also called alum, were reported [62]. This led to the first licensed adjuvanted vaccine, which remained the only licensed adjuvant for more than half a century [61]. Aluminium adjuvants are associated with enhanced antibody responses and are skewed towards a Th2 response [62, 66]. Since then, other classes of adjuvants have entered the market. For example, emulsions, e.g., the oil-in-water emulsion adjuvant MF59® based on squalene first licensed in 1997 [67, 68], as well as liposomes, e.g., AS01, which also contains monophosphoryl lipid A and Quillaja Saponaria-21, used against shingles [62]. This dissertation will focus mainly on the three particulate adjuvant types: liposomes, poly(lactic-*co*-glycolic acid) (PLGA) particles, and lipid-PLGA hybrids.

Adjuvants: liposomes, PLGA (nano)particles, and lipid-PLGA hybrids

Particulate adjuvants consist of small particles. Different types of particulate adjuvants exist, but some common denominators have been identified. Particulate adjuvants can act as carrier systems for the antigens and molecular adjuvants, thereby ensuring co-delivery, which has been shown to enhance the immune response [69]. Factors such as size, charge, and rigidity are important determinants for generating a particular immune response [70].

There are discrepancies among experimental results regarding nanoparticle size in different studies, probably due to differences in the experimental setup [71]. However, when it comes to uptake in immune cells such as macrophages and Langerhans cells, phagocytosis is most efficient for particles with a size of around 3 μm, and clathrin-mediated endocytosis is optimal for particles of about 100 nm [71]. Nanoparticles also seem to be better at cross-presenting their antigenic cargo in DCs and hereby being better at activating $CD8^+$ T cells, as particles around 800 nm were processed by the proteasome in DCs, indicating that they escaped from the lumen of the endosome into the cytosol, whereas 3 μm sized particles were processed by endolysosomal proteases [72]. Furthermore, nanoparticles (around 50 nm and also 300-600 nm) are more likely to induce Th1 responses than micrometre-sized particles (2-8 μm) that are more prone to trigger Th2 responses [71, 73]. Therefore, nanoparticles seem to be preferred for a vaccine that should induce Th1 and $CD8^+$ T-cell responses.

Particles can be neutral, positively or negatively charged. Positively charged particles typically form a depot at the injection site and are efficiently taken up by APCs [70]. It has been shown that positively charged particles are taken up more efficiently than neutral and negatively charged particles and induce higher $CD4^+$ and $CD8^+$ T-cell responses [74]. Regarding rigidity, studies have shown that rigid particles are more readily taken up by macrophages, endothelial cells, and DCs than less rigid particles [70, 75]. Only a few studies have been published on the relationship between rigidity and immunogenicity;

however, more rigid particles tend to induce Th1 responses [70, 71]. The particulate adjuvant types this dissertation will focus on (cationic liposomes, PLGA particles, and lipid-PLGA hybrids) have different physicochemical properties and have been shown to affect the immune system in various ways.

Cationic liposomes can induce maturation of DCs that subsequently can trigger $CD4^+$ (skewed towards a Th1-response) and $CD8^+$ T-cell responses [74, 76, 77]. A subgroup of cationic liposomes is the pH-sensitive cationic liposomes. They are stable at physiological pH; however, when they are internalised by APCs and exposed to the decreasing pH in the endosomes, where the liposomal bilayer becomes unstable, fuses with the endosomal membrane and the content leaks into the cytosol [78, 79]. This can promote $CD8^+$ T-cell responses [80].

PLGA nanoparticles have an excellent safety profile, being both biodegradable and biocompatible [81], and their properties (hydrophilicity/hydrophobicity, drug loading, drug release rate, etc.) are tuneable, which allows for the customisation of their properties to fit specific applications [82]. PLGA nanoparticles, without any added molecular adjuvants, do not elicit much of an immune response [76]. The small response can be slightly Th2-biased [73]. However, with a molecular adjuvant included, PLGA nanoparticles can induce Th1-response in mice [76].

Lipid-PLGA hybrids combine liposomes and PLGA nanoparticles by being nanoparticles with a PLGA core covered by lipids [73]. Lipid-PLGA hybrids have successfully been used in drug and vaccine delivery preclinical research, where they induced equal $IFN\gamma^+CD4^+CD44^{high}$ (Th1)-cell responses to liposomes with the same lipid composition in vivo [73].

Microfluidics and PLGA particle production

Currently, PLGA particles are mainly produced by two methods: emulsion-based methods, where a water-immiscible or partly water-immiscible organic solvent containing dissolved PLGA is emulsified in an aqueous solution with a surfactant, and nanoprecipitation methods, where a water-miscible organic solvent containing dissolved PLGA is mixed with an aqueous solution [83, 84]. While these techniques allow for manipulation of the nanoparticle diameter by varying factors, such as the PLGA concentration and the surfactant concentration [84], the batch-to-batch reproducibility is low [85], and the nanoparticles are rarely below 100 nm [84].

Microfluidics, a technique that enables the manipulation of fluid streams through microscale fluidic channels, has emerged to overcome these problems, offering precise control of the nanoparticle diameter, greater batch-to-batch reproducibility, and a narrower particle size distribution [86]. Therefore, microfluidic methods seem to be the future of PLGA particle production.

Intradermal administration

The subcutaneous, intramuscular, and intradermal routes are among the most conventional vaccine administration routes. Among these, the dermis is more densely populated by different subsets of DCs compared to subcutaneous and muscle tissue, which contain fewer, less investigated DCs [87]. Therefore, intradermal delivery of a new TB vaccine could be of interest.

The BCG vaccine is already mainly administered intradermally. While the oral and respiratory administration routes seem to induce better mucosal and systemic responses compared to the subcutaneous and intradermal delivery (for BCG), they do not come without obstacles [56, 57]. The oral route is associated with cervical adenitis [56], and the efficacy of orally delivered BCG is lower in the developing world, where helminth and *Helicobacter Pylori* infections have been shown to decrease the effect [57]. For the respiratory route, intranasal vaccination (with *Escherichia coli* heat-labile toxin adjuvant) has been associated with facial nerve paralysis [56], intratracheal and endobronchial are challenging to deliver [56], and in aerosol delivery, it is hard to control the delivered dose and the uniformity of the distribution [57]. Therefore, the intradermal administration route remains a viable option.

Among the intradermal administration forms are dissolvable microneedle arrays (dMNAs). dMNAs are made of a dissolvable material, such as polymers or sugars. They are favourable, as they can: i) secure the stability of loaded drugs by keeping them in their dry form, ii) are possible to self-administer because of the easy application of the microneedle patch, which has needle lengths that would target the dermis, and iii) create zero needle waste as the needle dissolve leading to no spread of blood-borne pathogens [88].

DISSERTATION AIM AND OUTLINE

This dissertation describes how to design and optimise nanoparticulate vaccine formulations and dMNAs and assess if the formulations can induce $CD4^+$ and $CD8^+$ T-cell responses, which are deemed important in a vaccine against TB.

Chapter 2 reports on how the lipid composition of liposomes affects the immune system. AER-containing liposomal formulations were formulated with different cationic lipids and cholesterol contents, and their physicochemical characteristics and immunological potential in vitro were assessed. The formulations were added to DCs, and the uptake of the formulations and their ability to upregulate DC surface markers were evaluated. The most promising formulations were tested in a T-cell assay to test if the formulation-exposed DCs could upregulate T cells' activation markers and IFN-γ production.

Chapter 3 describes a novel modular microfluidic system to prepare PLGA nanoparticles. The system was set up to establish a low-cost method that circumvents bulk nanoparticle preparation methods, which are typically time-consuming and have high batch-to-batch variability. Parameters in the modular microfluidic system that affected physicochemical characteristics, such as the nanoparticle diameter, were determined, and it was possible to incorporate proteins into the PLGA nanoparticles. Furthermore, this microfluidics system was also used to prepare the lipid-PLGA hybrids used in **Chapter 4** and the PLGA nanoparticles incorporated in the dMNAs described in **Chapter 5**.

Chapter 4 describes the immunological responses of PLGA particles, lipid-composition-optimised liposomes, and lipid-PLGA hybrids. The three particulate adjuvant types formulated with AER were compared in vitro with and without the molecular adjuvants monophosphoryl lipid A and cytosine-phosphate-guanine motifs oligodeoxynucleotides (CpG ODN) 1826 to measure the uptake of the formulations in DCs and their ability to activate them. The three particulate formulations with AER and the molecular adjuvants' ability to induce protection against Mtb in mice are hereafter described.

Chapter 5 reports on the comparison of two administration forms: intradermal injection of an aqueous formulation and intradermal administration with dMNAs. The aqueous formulations and dMNAs contained the antigen ovalbumin and the molecular adjuvant CpG ODN 1826 with or without PLGA particles. These formulations were tested in mice to determine if the formulations could induce $CD4^+$ and $CD8^+$ T-cell responses.

Finally, **Chapter 6** contains the summary, general discussion, prospects, and conclusions learned from the research described in this dissertation.

References

1. Pier GB. On the greatly exaggerated reports of the death of infectious diseases. Clin Infect Dis. 2008;47(8):1113-4. https://doi.org/10.1086/592123.
2. Cohen ML. Changing patterns of infectious disease. Nature. 2000;406:762-7. https://doi.org/10.1038/35021206.
3. HIV.gov. A Timeline of HIV and AIDS [Internet]. https://www.hiv.gov/hiv-basics/overview/history/hiv-and-aids-timeline#year-1981. Accessed Nov 1 2024.
4. CDC. Ebola, Outbreak History [Internet]. https://www.cdc.gov/ebola/outbreaks/index.html. Accessed Nov 1 2024.
5. Baker O, Coqueugniot H, Dutour O, Chamel B, Coqueugniot É, Stordeur D, et al. Prehistory of human tuberculosis: Earliest evidence from the onset of animal husbandry in the Near East. Paléorient. 2017;43(2):35-51. https://doi.org/10.3406/paleo.2017.5765.
6. Coronavirus Death Toll [Internet]. 2022. https://www.worldometers.info/coronavirus/coronavirus-death-toll/. Accessed Mar 24 2022.
7. World Health Organization. Global tuberculosis report 2023: World Health Organization; 2023. https://www.who.int/teams/global-tuberculosis-programme/tb-reports/global-tuberculosis-report-2023.
8. Sinha P, Gupta A, Prakash P, Anupurba S, Tripathi R, Srivastava GN. Differentiation of Mycobacterium tuberculosis complex from non-tubercular mycobacteria by nested multiplex PCR targeting IS6110, MTP40 and 32kD alpha antigen encoding gene fragments. BMC Infect Dis. 2016;16:123. https://doi.org/10.1186/s12879-016-1450-1.
9. Brites D, Gagneux S. Co-evolution of Mycobacterium tuberculosis and Homo sapiens. Immunol Rev. 2015;264(1):6-24. https://doi.org/10.1111/imr.12264.
10. Dinkele R, Gessner S, McKerry A, Leonard B, Leukes J, Seldon R, et al. Aerosolisation of Mycobacterium tuberculosis by Tidal Breathing. Am J Respir Crit Care Med. 2022;206(2):206-16. https://doi.org/10.1164/rccm.202110-2378OC.
11. World Health Organization. Tuberculosis 2021. https://www.who.int/news-room/fact-sheets/detail/tuberculosis. Accessed Mar 23 2022.
12. Lerner TR, Borel S, Gutierrez MG. The innate immune response in human tuberculosis. Cell Microbiol. 2015;17(9):1277-85. https://doi.org/10.1111/cmi.12480.
13. Gengenbacher M, Kaufmann SH. Mycobacterium tuberculosis: success through dormancy. FEMS Microbiol Rev. 2012;36(3):514-32. https://doi.org/10.1111/j.1574-6976.2012.00331.x.
14. Connolly LE, Edelstein PH, Ramakrishnan L. Why is long-term therapy required to cure tuberculosis? PLoS Med. 2007;4(3):e120. https://doi.org/10.1371/journal.pmed.0040120.
15. Andersen P, Scriba TJ. Moving tuberculosis vaccines from theory to practice. Nat Rev Immunol. 2019;19(9):550-62. https://doi.org/10.1038/s41577-019-0174-z.
16. Lin C-H, Lin C-J, Kuo Y-W, Wang J-Y, Hsu C-L, Chen J-M, et al. Tuberculosis mortality: patient characteristics and causes. BMC Infect Dis. 2014;14(1):5. https://doi.org/10.1186/1471-2334-14-5.
17. Abayneh M, HaileMariam S, Asres A. Low Tuberculosis (TB) Case Detection: A Health Facility-Based Study of Possible Obstacles in Kaffa Zone, Southwest District of Ethiopia. Can J Infect Dis Med Microbiol. 2020;2020:7029458. https://doi.org/10.1155/2020/7029458.
18. Sazali MF, Rahim S, Mohammad AH, Kadir F, Payus AO, Avoi R, et al. Improving Tuberculosis Medication Adherence: The Potential of Integrating Digital Technology and Health Belief Model. Tuberc Respir Dis (Seoul). 2023;86(2):82-93. https://doi.org/10.4046/trd.2022.0148.
19. Bagchi S, Ambe G, Sathiakumar N. Determinants of poor adherence to anti-tuberculosis treatment in mumbai, India. Int J Prev Med. 2010;1(4):223-32.
20. Simbwa BN, Katamba A, Katana EB, Laker EAO, Nabatanzi S, Sendaula E, et al. The burden of drug resistant tuberculosis in a predominantly nomadic population in Uganda: a mixed methods study. BMC Infect Dis. 2021;21(1):950. https://doi.org/10.1186/s12879-021-06675-7.
21. Greenwood B. The contribution of vaccination to global health: past, present and future. Philos Trans R Soc Lond B Biol Sci. 2014;369(1645):20130433. https://doi.org/10.1098/rstb.2013.0433.
22. Hsu T, Hingley-Wilson SM, Chen B, Chen M, Dai AZ, Morin PM, et al. The primary mechanism of attenuation of bacillus Calmette-Guerin is a loss of secreted lytic function required for invasion of lung interstitial tissue. Proc Natl Acad Sci U S A. 2003;100(21):12420-5. https://doi.org/10.1073/pnas.1635213100.
23. Fine PEM. Variation in protection by BCG:

implications of and for heterologous immunity. Lancet. 1995;346(8986):1339-45. https://doi.org/10.1016/S0140-6736(95)92348-9.
24. Ottenhoff TH, Kaufmann SH. Vaccines against tuberculosis: where are we and where do we need to go? PLoS Pathog. 2012;8(5):e1002607. https://doi.org/10.1371/journal.ppat.1002607.
25. Sierra VG. Is a new tuberculosis vaccine necessary and feasible? A Cuban opinion. Tuberculosis. 2006;86(3):169-78. https://doi.org/10.1016/j.tube.2006.03.003.
26. Dockrell HM, Smith SG. What Have We Learnt about BCG Vaccination in the Last 20 Years? Front Immunol. 2017;8:1134. https://doi.org/10.3389/fimmu.2017.01134.
27. Ernst JD, Cornelius A, Bolz M, Sher A, Ehrt S, Edelstein P. Dynamics of Mycobacterium tuberculosis Ag85B Revealed by a Sensitive Enzyme-Linked Immunosorbent Assay. mBio. 2019;10(2):e00611-19. https://doi.org/10.1128/mBio.00611-19.
28. Wiker HG, Harboe M. The antigen 85 complex: a major secretion product of Mycobacterium tuberculosis. Microbiol Rev. 1992;56(4):648-61. https://doi.org/10.1128/mr.56.4.648-661.1992.
29. Gey van Pittius NC, Warren RM, van Helden PD. ESAT-6 and CFP-10: what is the diagnosis? Infect Immun. 2002;70(11):6509-10; author reply 11. https://doi.org/10.1128/IAI.70.11.6509-6511.2002-a.
30. Li W, Deng G, Li M, Zeng J, Zhao L, Liu X, et al. A recombinant adenovirus expressing CFP10, ESAT6, Ag85A and Ag85B of Mycobacterium tuberculosis elicits strong antigen-specific immune responses in mice. Mol Immunol. 2014;62(1):86-95. https://doi.org/10.1016/j.molimm.2014.06.007.
31. Andersen P, Andersen AB, Sørensen AL, Nagai S. Recall of long-lived immunity to Mycobacterium tuberculosis infection in mice. J Immunol. 1995;154(7):3359-72. https://doi.org/10.4049/jimmunol.154.7.3359.
32. Commandeur S, van Meijgaarden KE, Prins C, Pichugin AV, Dijkman K, van den Eeden SJF, et al. An Unbiased Genome-Wide *Mycobacterium tuberculosis* Gene Expression Approach To Discover Antigens Targeted by Human T Cells Expressed during Pulmonary Infection. J Immunol. 2013;190(4):1659-71. https://doi.org/10.4049/jimmunol.1201593.
33. Commandeur S, van den Eeden SJF, Dijkman K, Clark SO, van Meijgaarden KE, Wilson L, et al. The in vivo expressed Mycobacterium tuberculosis (IVE-TB) antigen Rv2034 induces CD4+ T-cells that protect against pulmonary infection in HLA-DR transgenic mice and guinea pigs. Vaccine. 2014;32(29):3580-8. https://doi.org/10.1016/j.vaccine.2014.05.005.
34. Bustamante-Marin XM, Ostrowski LE. Cilia and Mucociliary Clearance. Cold Spring Harb Perspect Biol. 2017;9(4). https://doi.org/10.1101/cshperspect.a028241.
35. Li W, Deng G, Li M, Liu X, Wang Y. Roles of Mucosal Immunity against Mycobacterium tuberculosis Infection. Tuberc Res Treat. 2012;2012:791728. https://doi.org/10.1155/2012/791728.
36. Mettelman RC, Allen EK, Thomas PG. Mucosal immune responses to infection and vaccination in the respiratory tract. Immunity. 2022;55(5):749-80. https://doi.org/10.1016/j.immuni.2022.04.013.
37. Britannica TeoE. Mucous membrane. Encyclopedia Britannica [Internet]. https://www.britannica.com/science/mucous-membrane. Accessed May 29 2024.
38. Tobin EH TD. Tuberculosis [Internet]. StatPearls Publishing. https://www.ncbi.nlm.nih.gov/books/NBK441916/. Accessed May 29 2024.
39. Cohen SB, Gern BH, Delahaye JL, Adams KN, Plumlee CR, Winkler JK, et al. Alveolar Macrophages Provide an Early Mycobacterium tuberculosis Niche and Initiate Dissemination. Cell Host Microbe. 2018;24(3):439-46.e4. https://doi.org/10.1016/j.chom.2018.08.001.
40. Chai Q, Wang L, Liu CH, Ge B. New insights into the evasion of host innate immunity by Mycobacterium tuberculosis. Cell Mol Immunol. 2020;17(9):901-13. https://doi.org/10.1038/s41423-020-0502-z.
41. Warner DF, Mizrahi V. The survival kit of Mycobacterium tuberculosis. Nat Med. 2007;13(3):282-4. https://doi.org/10.1038/nm0307-282.
42. Urdahl KB. Understanding and overcoming the barriers to T cell-mediated immunity against tuberculosis. Semin Immunol. 2014;26(6):578-87. https://doi.org/10.1016/j.smim.2014.10.003.
43. Dalod M, Chelbi R, Malissen B, Lawrence T. Dendritic cell maturation: functional specialisation through signaling specificity and transcriptional programming. EMBO J. 2014;33(10):1104-16. https://doi.org/10.1002/embj.201488027.
44. Worbs T, Hammerschmidt SI, Forster R. Dendritic cell migration in health and disease. Nat Rev Immunol. 2017;17(1):30-48. https://doi.org/10.1038/nri.2016.116.
45. Grommé M, Neefjes J. Antigen degradation or presentation by MHC class I molecules via classical and non-classical pathways. Mol Immunol. 2002;39(3-4):181-202. https://doi.org/10.1016/s0161-5890(02)00101-3.
46. Adams EJ, Luoma AM. The adaptable major histocompatibility complex (MHC) fold: structure and function of nonclassical and MHC class I-like molecules. Annu Rev Immunol. 2013;31:529-61. https://doi.org/10.1146/annurev-immunol-032712-095912.
47. Corthay A. A three-cell model for activation of naive T helper cells. Scand J Immunol. 2006;64(2):93-6. https://doi.org/10.1111/j.1365-3083.2006.01782.x.
48. Harrington LE, Hatton RD, Mangan PR, Turner H, Murphy TL, Murphy KM, et al. Interleukin 17-producing $CD4^+$ effector T cells develop via a lineage distinct from the T helper type 1 and 2 lineages. Nat Immunol. 2005;6(11):1123-32. https://doi.org/10.1038/ni1254.
49. Pelletier M, Maggi L, Micheletti A, Lazzeri E, Tamassia N, Costantini C, et al. Evidence for a cross-talk between human neutrophils and Th17 cells. Blood. 2010;115(2):335-43. https://doi.org/10.1182/blood-2009-04-216085.
50. Korn T, Bettelli E, Oukka M, Kuchroo VK. IL-17 and Th17 Cells. Annu Rev Immunol. 2009;27:485-517. https://doi.org/10.1146/annurev.immunol.021908.132710.
51. Ma CS, Deenick EK, Batten M, Tangye SG. The origins, function, and regulation of T follicular helper cells. J Exp Med. 2012;209(7):1241-53. https://doi.org/10.1084/jem.20120994.
52. Loser K, Beissert S. Regulatory T cells: banned cells for decades. J Invest Dermatol. 2012;132(3 Part 2):864-71. https://doi.org/10.1038/jid.2011.375.
53. 53. Cui W, Kaech SM. Generation of effector CD8+ T cells and their conversion to memory T cells. Immunol Rev. 2010;236:151-66. https://doi.org/10.1111/j.1600-065X.2010.00926.x.
54. Chang HF, Bzeih H, Schirra C, Chitirala P, Halimani M, Cordat E, et al. Endocytosis of Cytotoxic Granules Is Essential for Multiple Killing of Target Cells by T Lymphocytes. J Immunol. 2016;197(6):2473-84. https://doi.org/10.4049/jimmunol.1600828.
55. Silva Miranda M, Breiman A, Allain S, Deknuydt F, Altare F. The tuberculous granuloma: an unsuccessful host defence mechanism providing a safety shelter for the bacteria? Clin Dev Immunol. 2012;2012:139127. https://doi.org/10.1155/2012/139127.
56. Tanner R, Villarreal-Ramos B, Vordermeier HM, McShane H. The Humoral Immune Response to BCG Vaccination. Front Immunol. 2019;10. https://doi.org/10.3389/fimmu.2019.01317.
57. Singh S, Saavedra-Avila NA, Tiwari S, Porcelli SA. A century of BCG vaccination: Immune mechanisms, animal models, non-traditional routes and implications for COVID-19. Front Immunol. 2022;13. https://doi.org/10.3389/fimmu.2022.959656.
58. Kumar A. 7 - Different vaccination approach for vaccine development. In: Kumar A, editor. Visceral Leishmaniasis: Academic Press; 2021. p. 77-81. https://doi.org/10.1016/B978-0-323-91124-5.00006-0.
59. Zepp F. Principles of vaccine design-Lessons from nature. Vaccine. 2010;28(Supplement 3):C14-24. https://doi.org/10.1016/j.vaccine.2010.07.020.
60. Seo HS. Application of radiation technology in vaccines development. Clin Exp Vaccine Res. 2015;4(2):145-58. https://doi.org/10.7774/cevr.2015.4.2.145.
61. Di Pasquale A, Preiss S, Tavares Da Silva F, Garçon N. Vaccine Adjuvants: from 1920 to 2015 and Beyond. Vaccines (Basel). 2015;3(2):320-43. https://doi.org/10.3390/vaccines3020320.
62. Reyes C, Patarroyo MA. Adjuvants approved for human use: What do we know and what do we need to know for designing good adjuvants? Eur J Pharmacol. 2023;945:175632. https://doi.org/10.1016/j.ejphar.2023.175632.
63. Delany I, Rappuoli R, De Gregorio E. Vaccines for the 21st century. EMBO Mol Med. 2014;6(6):708-20. https://doi.org/10.1002/emmm.201403876.
64. Hafner AM, Corthésy B, Merkle HP. Particulate formulations for the delivery of poly(I:C) as vaccine adjuvant. Adv Drug Deliv Rev. 2013;65(10):1386-99. https://doi.org/10.1016/j.addr.2013.05.013.
65. Johnston D, Zaidi B, Bystryn JC. TLR7 imidazoquinoline ligand 3M-019 is a potent adjuvant for pure protein prototype vaccines. Cancer Immunol Immunother. 2007;56(8):1133-41. https://doi.org/10.1007/s00262-006-0262-3.
66. Tritto E, Mosca F, De Gregorio E. Mechanism of action of licensed vaccine adjuvants. Vaccine. 2009;27(25-26):3331-4. https://doi.org/10.1016/j.vaccine.2009.01.084.

67. O'Hagan DT, Ott GS, De Gregorio E, Seubert A. The mechanism of action of MF59 - an innately attractive adjuvant formulation. Vaccine. 2012;30(29):4341-8. https://doi.org/10.1016/j.vaccine.2011.09.061.
68. Ko EJ, Kang SM. Immunology and efficacy of MF59-adjuvanted vaccines. Hum Vaccin Immunother. 2018;14(12):3041-5. https://doi.org/10.1080/21645515.2018.1495301.
69. Lim JW, Na W, Kim HO, Yeom M, Kang A, Park G, et al. Co-delivery of antigens and immunostimulants via a polymersome for improvement of antigen-specific immune response. J Mater Chem B. 2020;8(26):5620-6. https://doi.org/10.1039/d0tb00892c.
70. Benne N, van Duijn J, Kuiper J, Jiskoot W, Slütter B. Orchestrating immune responses: How size, shape and rigidity affect the immunogenicity of particulate vaccines. J Control Release. 2016;234:124-34. https://doi.org/10.1016/j.jconrel.2016.05.033.
71. Baranov MV, Kumar M, Sacanna S, Thutupalli S, van den Bogaart G. Modulation of Immune Responses by Particle Size and Shape. Front Immunol. 2020;11:607945. https://doi.org/10.3389/fimmu.2020.607945.
72. Mant A, Chinnery F, Elliott T, Williams AP. The pathway of cross-presentation is influenced by the particle size of phagocytosed antigen. Immunology. 2012;136(2):163-75. https://doi.org/10.1111/j.1365-2567.2012.03558.x.
73. Rose F, Wern JE, Ingvarsson PT, van de Weert M, Andersen P, Follmann F, et al. Engineering of a novel adjuvant based on lipid-polymer hybrid nanoparticles: A quality-by-design approach. J Control Release. 2015;210:48-57. https://doi.org/10.1016/j.jconrel.2015.05.004.
74. Nakanishi T, Kunisawa J, Hayashi A, Tsutsumi Y, Kubo K, Nakagawa S, et al. Positively charged liposome functions as an efficient immunoadjuvant in inducing cell-mediated immune response to soluble proteins. J Control Release. 1999;61(1-2):233-40. https://doi.org/10.1016/s0168-3659(99)00097-8.
75. Benne N, Leboux RJT, Glandrup M, van Duijn J, Lozano Vigario F, Neustrup MA, et al. Atomic force microscopy measurements of anionic liposomes reveal the effect of liposomal rigidity on antigen-specific regulatory T cell responses. J Control Release. 2020;318:246-55. https://doi.org/10.1016/j.jconrel.2019.12.003.
76. Du G, Hathout RM, Nasr M, Nejadnik MR, Tu J, Koning RI, et al. Intradermal vaccination with hollow microneedles: A comparative study of various protein antigen and adjuvant encapsulated nanoparticles. J Control Release. 2017;266:109-18. https://doi.org/10.1016/j.jconrel.2017.09.021.
77. Barnier Quer C, Elsharkawy A, Romeijn S, Kros A, Jiskoot W. Cationic liposomes as adjuvants for influenza hemagglutinin: More than charge alone. Eur J Pharm Biopharm. 2012;81(2):294-302. https://doi.org/10.1016/j.ejpb.2012.03.013.
78. Karanth H, Murthy RS. pH-sensitive liposomes--principle and application in cancer therapy. J Pharm Pharmacol. 2007;59(4):469-83. https://doi.org/10.1211/jpp.59.4.0001.
79. Balamuralidhara V, Pramodkumar T, Srujana N, Venkatesh M, Gupta NV, Krishna K, et al. pH sensitive drug delivery systems: a review. Am J Drug Discov Dev. 2011;1(1):24-48.
80. Liu G, Zhu M, Zhao X, Nie G. Nanotechnology-empowered vaccine delivery for enhancing CD8+ T cells-mediated cellular immunity. Adv Drug Deliv Rev. 2021;176:113889. https://doi.org/10.1016/j.addr.2021.113889.
81. Anderson JM, Shive MS. Biodegradation and biocompatibility of PLA and PLGA microspheres. Adv Drug Deliv Rev. 2012;64:72-82. https://doi.org/10.1016/j.addr.2012.09.004.
82. Prabhu P, Patravale V. Potential of nanocarriers in antigen delivery: the path to successful vaccine delivery. Nanocarriers. 2014;1:10-45. https://doi.org/10.2478/nanca-2014-0001.
83. Operti MC, Bernhardt A, Grimm S, Engel A, Figdor CG, Tagit O. PLGA-based nanomedicines manufacturing: Technologies overview and challenges in industrial scale-up. Int J Pharm. 2021;605:120807. https://doi.org/10.1016/j.ijpharm.2021.120807.
84. Astete CE, Sabliov CM. Synthesis and characterisation of PLGA nanoparticles. J Biomater Sci Polym Ed. 2006;17(3):247-89. https://doi.org/10.1163/156856206775997322.
85. Streck S, Neumann H, Nielsen HM, Rades T, McDowell A. Comparison of bulk and microfluidics methods for the formulation of poly-lactic-co-glycolic acid (PLGA) nanoparticles modified with cell-penetrating peptides of different architectures. Int J Pharm X. 2019;1:100030. https://doi.org/10.1016/j.ijpx.2019.100030.
86. Valencia PM, Farokhzad OC, Karnik R, Langer R. Microfluidic technologies for accelerating the clinical translation of nanoparticles. Nat Nanotechnol. 2012;7(10):623-9. https://doi.org/10.1038/nnano.2012.168.
87. Romani N, Flacher V, Tripp CH, Sparber F, Ebner S, Stoitzner P. Targeting skin dendritic cells to improve intradermal vaccination. Curr Top Microbiol Immunol. 2012;351:113-38. https://doi.org/10.1007/82_2010_118.
88. Kim Y-C, Park J-H, Prausnitz MR. Microneedles for drug and vaccine delivery. Adv Drug Deliv Rev. 2012;64(14):1547-68. https://doi.org/10.1016/j.addr.2012.04.005.

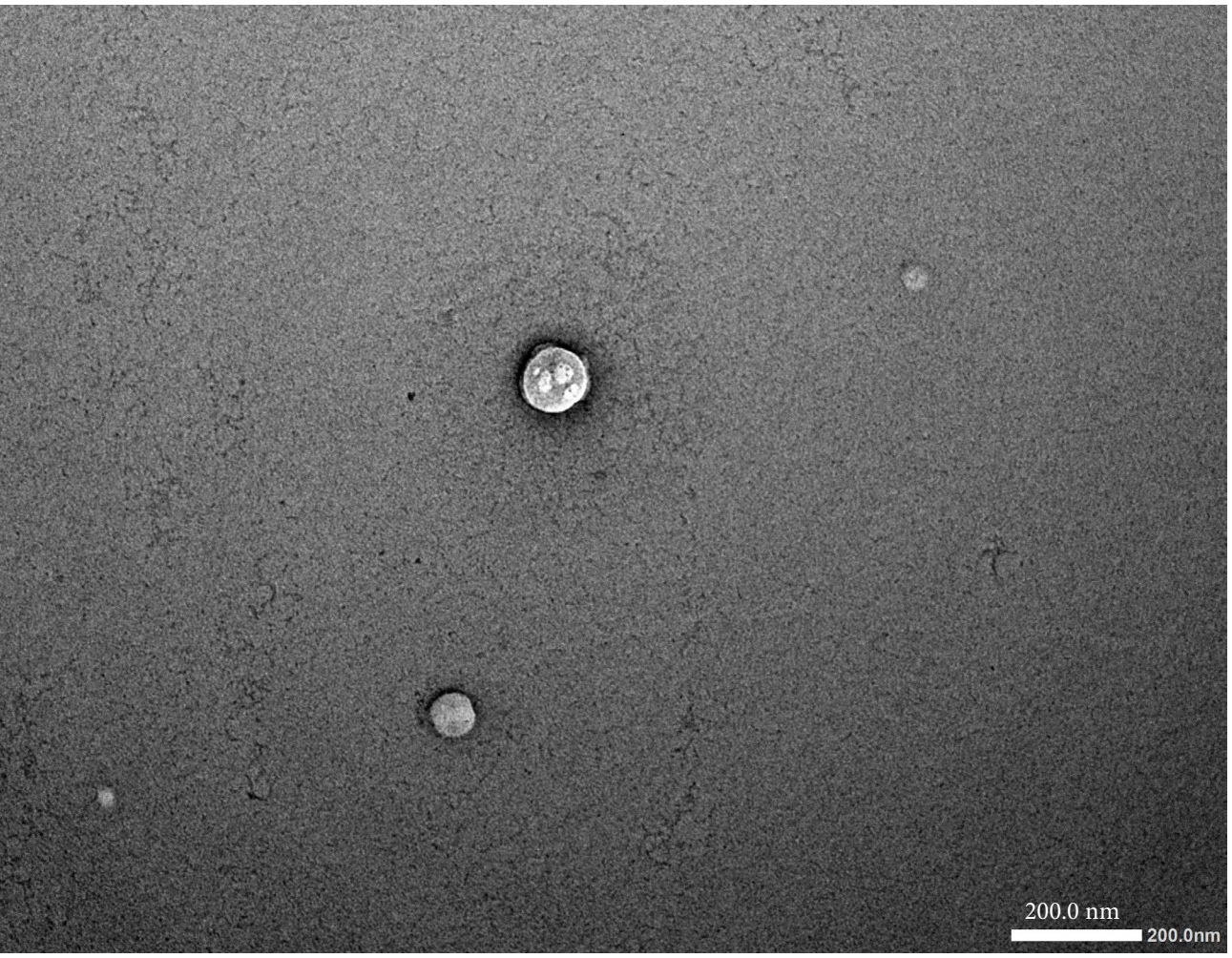

Liposomes produced with the modular microfluidic system, visualised with transmission electron microscopy.

CHAPTER 2

INTRINSIC IMMUNOGENICITY OF LIPOSOMES FOR TUBERCULOSIS VACCINES: EFFECT OF CATIONIC LIPID AND CHOLESTEROL

Adapted from Eur J Pharm Sci. 2024;195:106730

M.A. Neustrup[1,2*], M.M. Szachniewicz[1,2*], K.E. van Meijgaarden[2], W. Jiskoot[1], J.A. Bouwstra[1], M.C. Haks[2], A. Geluk[2], T.H.M. Ottenhoff[2]

[*] Authors contributed equally

[1] Division of BioTherapeutics, Leiden Academic Centre for Drug Research, Leiden University, Leiden, The Netherlands
[2] Department of Infectious Diseases, Leiden University Medical Center, Leiden, The Netherlands

ABSTRACT

Tuberculosis (TB) is still among the deadliest infectious diseases, hence there is a pressing need for more effective TB vaccines. Cationic liposome subunit vaccines are excellent vaccine candidates offering effective protection with a better safety profile than live vaccines. In this study, we aim to explore intrinsic adjuvant properties of cationic liposomes to maximize immune activation while minimizing aspecific cytotoxicity. To achieve this, we developed a rational strategy to select liposomal formulation compositions and assessed their physicochemical and immunological properties in *in vitro* models using human monocyte-derived dendritic cells (MDDCs). A broad selection of commercially available cationic compounds was tested to prepare liposomes containing Ag85B-ESAT6-Rv2034 (AER) fusion protein antigen. 1,2-Dioleoyl-*sn*-glycero-3-ethylphosphocholine (EPC)-based liposomes exhibited the most advantageous activation profile in MDDCs as assessed by cell surface activation markers, cellular uptake, antigen-specific T-cell activation, cytokine production, and cellular viability. The addition of cholesterol to 20 mol% improved the performance of the tested formulations compared to those without it; however, when its concentration was doubled there was no further benefit, resulting in reduced cell viability. This study provides new insights into the role of cationic lipids and cholesterol in liposomal subunit vaccines.

INTRODUCTION

Tuberculosis (TB) is among the top ten causes of lethality in low-income and lower-middle-income countries with an estimated 3.6 million undiagnosed individuals [1]. Approximately a quarter of the entire human population is (latently) infected with *Mycobacterium tuberculosis* (Mtb), and in 2021, 10.6 million people fell ill, and 1.6 million died from TB [2]. Moreover, the TB burden is aggravated by the increased occurrence of drug-resistant strains. Thus, TB continues to be a global problem that requires improved (early) diagnosis [3], treatment, and prevention [2, 4]. In this study, we aim to advance the knowledge of TB prevention by developing novel vaccine modalities.

Vaccines are commonly recognized as the most effective and inexpensive way of solving the burden of infectious diseases [5, 6]. The complete eradication of smallpox and rinderpest, and the more recent success of SARS-CoV2 vaccines, have proven the efficacy of vaccines in disease prevention [7]. Unfortunately, it is difficult to develop effective and safe vaccines against some infectious diseases, including TB. Currently, the only available vaccine against TB is *Mycobacterium bovis* Bacillus Calmette–Guérin (BCG) [8]. The BCG vaccine confers variable and often inadequate protection, especially against the pulmonary form in adults, which is accountable for Mtb transmission in adolescents and adults [9–11]. Therefore, there is still an urgent need for improved vaccines against TB [8]. The development of subunit vaccines can contribute to this demand.

Subunit vaccines are based either on synthesized or purified antigens, DNA, or RNA [12]. Being non-live, they are one of the safest vaccine types and as a result can potentially be administrated to a very broad population, including immunocompromised individuals [13, 14]. Hence, a subunit vaccine is a logical candidate for a TB vaccine, as the countries with the highest TB rates have a substantial incidence of HIV infection [2]. However, intrinsically subunit vaccines are often insufficiently immunogenic [14–16] as they lack immune-activating constituents, such as pathogen-associated molecular patterns (PAMPs), which are present in traditional (live-attenuated and inactivated) vaccines. Hence, this vaccine type often cannot induce proficient maturation of antigen-presenting cells (APCs), including dendritic cells (DCs). As a result, they fail to induce adequate protective immunity [17]. Thus, in order to overcome this inherent limitation, the development of subunit vaccine delivery systems is of utmost importance. This study addresses this issue.

Cationic liposomes are excellent subunit vaccine delivery systems that act as particulate adjuvants [12, 18–21]. Several liposome-based subunit vaccines have been approved for clinical use [22–24]. Liposomes can protect their antigenic cargo from degradation, and potentially co-deliver antigens with molecular adjuvants and PAMPs such as Toll-

like receptor (TLRs) ligands. In addition, such delivery systems facilitate and enhance antigen uptake by APCs allowing a reduction of the required dose of antigens as well as molecular adjuvants to induce the desired immune responses [12, 18, 25–28]. In particular, cationic liposomes can potently enhance antigen-specific immune responses as they have intrinsic immune-stimulatory properties to induce maturation of DCs and can trigger subsequent $CD4^+$–Th1 and $CD8^+$ T-cell responses [18, 28–32]. Therefore, cationic liposomes provide a powerful and versatile platform for vaccination.

The full potential of cationic liposomes as vaccine components has not been fully explored yet. It is known that the physicochemical properties of liposomes, like size and surface charge, affect the immunological outcomes, yet the role of the lipids forming the bilayer is still not fully understood [18, 33–36]. Several studies have compared cationic lipids and investigated their effect on immune responses; however, the available data is not conclusive [18, 34–39]. In many of these reports, the evaluated range of cationic lipids was limited. Therefore, it is challenging to draw definitive conclusions in the vaccine field. Moreover, the choice of biological systems, in which these liposomes were tested, varied greatly. Some of those studies used *in vitro* mouse or human models (using primary cells or cell lines) mainly looking at changes in (surface) activation markers of DCs. Others used *in vivo* models and focused on outcomes such as total Ig titers or neutralizing antibody titers. Similarly, the interplay of cationic lipids and liposome components with cholesterol has not been researched thoroughly. It is known that cholesterol can improve uptake of liposomes by APCs and phagocytes; however, the concentration required for this improvement and to what extent the immune response can be improved has not been clearly elucidated [15, 40–44]. Therefore, in this study, we have examined the effect of cholesterol incorporation into various liposomal compositions on the physicochemical properties of liposomes and on various biological outcomes in a systematic way.

The goal of this study was to formulate liposomes with different cationic lipids and cholesterol contents, investigate their effect on the physicochemical properties and assess human immune responses *in vitro*. The best-performing formulations were optimized to achieve the most potent immune stimulation while minimizing cellular toxicity. We compared several commercially available cationic lipids formulated in liposomal formulations containing the designed Mtb antigen AER, a hybrid antigen composed of three Mtb proteins with different functions. Previously, we showed that AER can reduce the bacterial load in HLA-DR3 transgenic mice as well as guinea pigs models of acute TB [45]. The formulations that fulfilled our predefined inclusion criteria were subsequently tested on primary human monocyte-derived DCs (MDDCs), cellular viability, antigen uptake, and cellular activation. The best-performing formulations were selected and optimized to maximize immune activation and minimize cytotoxicity. Since $CD4^+$ Th1-cell responses are an important correlate of immunity and protection against TB, the potential efficacy of the four best-performing vaccine formulations was further determined *in vitro* using the activation of Rv2034 and Ag85B antigen-specific reporter $CD4^+$ T-cell clones/lines.

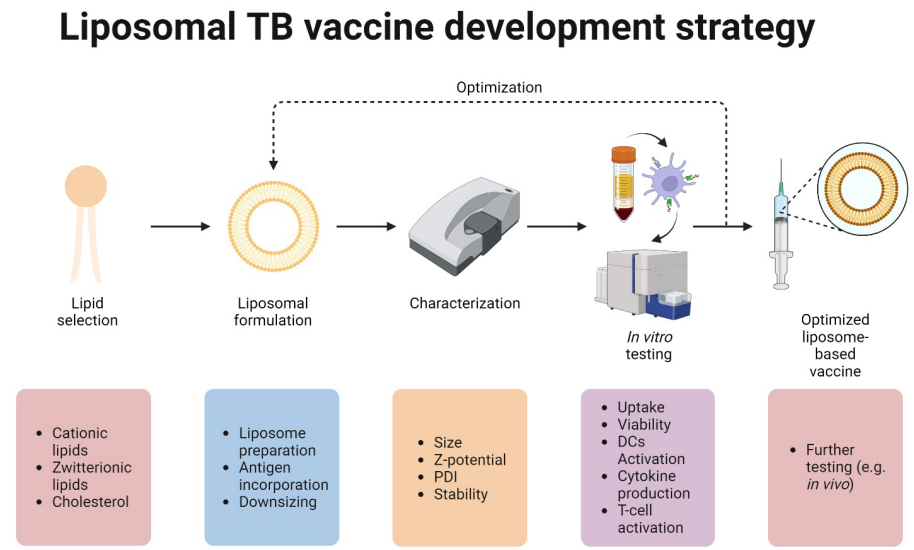

Figure 1. Schematic overview of the strategy used for the development and optimization of liposomal TB vaccines. Created with BioRender.com.

MATERIALS AND METHODS

Materials

1,2-dioleoyl-3-trimethylammonium-propane chloride salt (DOTAP), 3ß-[N-(N',N'-dimethylaminoethane)-carbamoyl]cholesterol hydrochloride (DC-chol), dimethyldioctadecylammonium bromide salt (DDA), 1,2-dioleoyl-*sn*-glycero-3-ethylphosphocholine chloride salt (EPC), N^4-cholesteryl-spermine hydrochloride (GL-67), 1,2-dioleyloxy-3-dimethylaminopropane (DODMA), N1-[2-((1S)-1-[(3-aminopropyl)amino]-4-[di(3-amino-propyl)amino]butylcarboxamido)ethyl]-3,4-di[oleyloxy]-benzamide (MVL5), 1,2-dioleoyl-*sn*-glycero-3-phosphocholine (DOPC), and 1,2-distearoyl-*sn*-glycero-3-phosphocholine (DSPC) were purchased from Avanti Polar Lipids, Inc. (USA). Cholesterol was obtained from Merck KGaA (Germany). Recombinant fusion protein AER was produced using the previously described method [46]. Briefly, MTB genes were amplified using polymerase chain reaction (PCR) from genomic DNA of lab strain H37Rv and cloned using Gateway technology (Invitrogen,

USA) in a bacterial expression vector containing an N-terminal hexahistidine (His) tag. Correct insertion of the products was confirmed using sequencing. The recombinant protein was expressed in *Escherichia coli* strain BL21 (DE3) and purified. The quality of the protein in terms of size and purity was evaluated by gel electrophoresis using Coomassie brilliant blue staining and Western blotting using an anti-His antibody (Invitrogen, USA). The endotoxin level in the protein was measured using a ToxinSensor™ Chromogenic Limulus Amebocyte Lysate (LAL) Endotoxin Assay Kit (GenScript, USA). The endotoxin contents were below 50 EU (endotoxin unit) per mg of a protein. Subsequently, AER was tested to exclude non-specific T-cell stimulation and cellular toxicity in the IFN-γ release assay. For this assay PBMCs of *in vitro* purified protein derivative (PPD) negative, healthy Dutch donors recruited at the Sanquin Blood Bank, Leiden, the Netherlands were used.

Preparation of liposomal formulations

The liposomal formulations were prepared using the thin-film hydration method. Lipids were dissolved in chloroform and added to round-bottom flasks. Various cationic lipids and zwitterionic lipids were used, and additionally, cholesterol was added to some formulations (Table 1). The lipids of choice were diluted in chloroform from 25 mg/ml stock solutions. The final total amount of lipids used per formulation was 5 mg (10 mg/ml) in chloroform. The lipid solution was transferred to a round-bottom flask, and the chloroform was evaporated using a rotary evaporator (Buchi rotavapor R210, Switzerland). Subsequently, the lipid film was rehydrated with 1 ml of 100 μg/ml AER in 10 mM phosphate buffer (PB) with 9.8% sucrose (pH = 7.4) to prepare AER-loaded liposomes. For the preparation of empty liposomes (without AER) and fluorescent-labelled liposomes (also without AER), only the buffer was used for rehydration. After the hydration, the liposomes were downsized using a tip sonicator (Branson Sonifier 250, US). The sonication program consisted of eight cycles; each cycle encompassed 30 s of sonication at a 10% amplitude, followed by a break of 60 s. Samples were submerged in ice during the sonication. Short sonication times at a low amplitude alongside submersion in ice allowed for the reduction of degradation of lipids. Hereafter, the liposomes were centrifuged (Allegra X-12R, US) at 524 g for 5 min to spin down the metal particles shed by the tip sonicator. To remove the metal-particle pellets, the supernatants containing liposomal formulations were transferred to new tubes, and the pellets were discarded.

To avoid the tip sonication would degrade the fluorophore, fluorescent-labelled liposomes (without AER) were downsized using a 10 ml extruder (LIPEX extruder, Northern Lipids, Canada). The liposomal formulations were extruded 5-6 times at room temperature, first through carbonate filters with a pore size of 400 nm and then through a 200 nm filter (Nucleopore Millipore, the Netherlands). Hereafter, the liposomes (5 mg/ml lipids) were stored at 4 °C. To assess the impact of tip sonication on biological results, we investigated the effect of pre-sonicated and non-sonicated solutions of AER as controls. We also studied the effects of AER-free, non-labeled liposomes that were not sonicated but extruded similarly to fluorescent-labeled liposomes.

Particle size and zeta-potential determination

The intensity-weighted average hydrodynamic diameter (Z-average size) and polydispersity index (PDI) of the liposomes were determined by dynamic light scattering, and the Zeta-potential was determined by laser Doppler electrophoresis. For the measurements, the formulations were diluted to 0.25 mg/mL lipid in 10 mM PB (pH = 7.4) and added to 1.5 ml VWR Two-Sided Disposable PS Cuvettes (VWR, the Netherlands). Measurements were conducted in technical triplicates with a minimum of ten runs for each measurement at 20 °C using a nano ZS Zetasizer coupled with a 633 nm laser and 173° optics (Malvern Instruments, Worcestershire, UK). The data were analysed with Zetasizer Software v7.13 (Malvern Instruments).

Generation of dendritic cells and macrophages from peripheral blood mononuclear cells

Peripheral blood mononuclear cells (PBMCs) were isolated from buffy coats obtained from healthy individuals after written informed consent (Sanquin Blood Bank, The Netherlands). PBMCs were separated from the blood using the Ficoll-based density gradient centrifugation method. Subsequently, $CD14^+$ cells were isolated from the PBMCs using the magnetic cell isolation (MACS) technique with an autoMACS Pro Separator (Miltenyi Biotec BV, the Netherlands). DCs, anti- (M2), and pro-inflammatory (M1) macrophages were generated from these $CD14^+$ cells by incubating them for six days in the presence of cytokines. To generate MDDCs, cells were incubated with 10 ng/ml recombinant human granulocyte-macrophage colony-stimulating factor (GM-CSF; Miltenyi Biotec BV, the Netherlands) and 10 ng/ml recombinant human interleukin 4 (IL-4; Peprotech, USA). M2 macrophages were differentiated in the presence of 50 ng/ml macrophage colony-stimulating factor (M-CSF; Miltenyi Biotec BV, the Netherlands), and M1 macrophages in the presence of 5 ng/ml GM-CSF (Miltenyi Biotec BV, the Netherlands) [47]. All cell types were cultured at 37 °C/5% CO_2 in a complete Roswell Park Memorial Institute (RPMI) 1640 medium that was supplemented with 10% fetal bovine serum (FBS), 100 units/ml penicillin and 100 μg/ml streptomycin, and 2 mM GlutaMAX (Gibco, Thermo Fisher Scientific, Belgium). MDDCs were harvested by pipetting the medium, and macrophages were harvested with trypsinization (Trypsin-EDTA 0.05%, phenol red, Gibco, Thermo Fisher Scientific, Belgium).

Activation and viability of MDDCs

To assess the potential cellular toxicity and the ability of the empty and AER-containing liposomal formulations to activate MDDCs, the formulations were added to round-bottom 96-well plates (CELLSTAR, Greiner Bio-One GmbH, Germany), seeded with 30,000

MDDCs/well (25 – 250 µg/ml lipids, in 200 µl medium) and incubated for 1 h at 37 ˚C/5% CO_2. Hereafter, the cells were washed with a complete RPMI medium to remove the free liposomes and cultured overnight at 37 °C/5% CO_2. The following day, the cells were spun down, and the supernatants were collected and stored at -20˚C till further use. To stain the cells for flow cytometry, the cells were first washed with FACS buffer (PBS containing 0.1% bovine serum albumin; Merck, Germany) and incubated for 5 min with 5% human serum (Sanquin Blood Bank, the Netherlands) in PBS to block non-specific Fc-receptor binding. Next, the cells were washed, and the cell surface markers on the MDDCs were stained for at least 30 min with monoclonal antibodies (CCR7-BB515 (clone 3D12), CD83-PE (clone HB15e), CD40-APC (clone 5C3), CD80-APC-R700 (clone L307.4), HLA-DR-V500 (clone G46-6) from BD Biosciences, Belgium, and CD86-BV421 (clone IT2.2) from BioLegend, the Netherlands) in FACS buffer. Subsequently, the cells were washed and stained with SYTOX AADvanced Dead Cell Stain (Invitrogen, Thermo Fisher Scientific, Belgium) in FACS buffer. Viability was calculated as a percentage of SYTOX AADvanced-negative cell population in relation to all recorded cells. Acquisition of flow cytometry data was performed using a BD FACSLyric Flow Cytometer (BD Biosciences, Belgium). Data were analyzed using FlowJo (version 10.6, FlowJo LLC, BD, USA) software.

Liposomal uptake study

MDDCs, M1, or M2 macrophages were seeded in round-bottom 96-well plates at a density of 30,000 cells/well. Afterwards, the cells were exposed to 1% v/v empty fluorescent-labeled liposomes (containing 0.1% mol% of 1,2-dioleoyl-*sn*-glycero-3-phosphoethanolamine-N-(Cyanine 5) (18:2 PE-Cy5) Avanti Polar Lipids, Inc., USA) for 1 h. Hereafter, the cells were washed with FACS buffer 3 times to remove free liposomes. The acquisition of flow cytometry data was performed using a BD FACSLyric Flow Cytometer. Data were analyzed using FlowJo (version 10.6) software.

T-cell activation

Similarly, heterozygous HLA-DR3$^+$ MDDCs were exposed for 1 h with liposomal formulations at 5 µg/ml AER and 250 µg/ml lipids in 200 µl of complete RPMI (Gibco, Thermo Fisher Scientific, Bleiswijk, the Netherlands) at 37 ˚C/5% CO_2. Cells were washed twice and $2x10^4$ pre-pulsed HLA-DR3$^+$ MDDCs were cocultured with either $1x10^5$ T-cells from the Rv2034 specific T-cell clone [48] (1B4 recognizing peptide 75-105) or an Ag85B-specific T-cell clone [49] (L10B4 recognizing peptide 56-65) in a 5 ml Falcon tube in a total volume of 400 µl of Iscove's Modified Dulbecco's Medium supplemented with Glutamax, 100 U/ml penicillin, 100 µg/ml streptomycin (Gibco, Thermo Fisher Scientific, Bleiswijk, the Netherlands) and 10% pooled human serum (Sigma, Merck, Darmstadt, Germany). After 6 h Brefeldin-A was added (3 µg/ml) (Sigma, Merck, Darmstadt, Germany) and cells were incubated for an additional 16 h at 37 ˚C/5% CO_2. Subsequently, cells were harvested and stained for flow cytometric analysis with the violet live/dead stain (ViViD, Invitrogen, Thermo Fisher Scientific, Bleiswijk, the Netherlands), surface markers CD3-HorizonV500 (UCHT1, BD Horizon, Belgium), CD4-AlexaFluor 700 (RPA-T4, BD Pharmingen, Belgium), CD8-FITC (HIT8a, BioLegend, the Netherlands) and after fixation and permeabilization with fix/perm reagents (Nordic MUbio, Susteren, the Netherlands) for IFN-γ-PerCP-Cy5.5 (4S.B3, Invitrogen, Thermo Fisher Scientific, the Netherlands) and CD154-PE (TRAP1, BD Pharmingen, Belgium).

Luminex assay

Supernatants from activation and viability experiments were tested in two Bio-Plex panels (Bio-Rad, Veenendaal, the Netherlands) according to the manufacturer's protocols. In total 16 analytes were measured. The chemokine panel consisted of CXCL9, CXCL11, CCL8, and CCL22. The cytokine panel included CCL11(Eotaxin), GM-CSF, IFN-α2, IL-1β, IL-1rα, IL-6, CXCL10, CCL2(MCP-1), CCL3, CCL4, RANTES and TNF-α. Samples were acquired on a Bio-Plex 200 system and analyzed with Bio-Plex manager software version 6.1.

Statistical analysis

Statistical analyses were performed in GraphPad Prism, version 8.01 (GraphPad Software, Prism, USA). The results were analyzed with the Kruskal-Wallis test followed by an uncorrected Dunn's post-hoc test when comparing non-parametric data sets of three or more groups to the control group, where $P < 0.05$ was considered as statistically significant (*$P < 0.05$, **$P < 0.01$, ***$P < 0.001$, ****$P < 0.0001$). Wilcoxon matched-pairs signed rank test was performed when comparing two non-parametric data groups.

RESULTS

Preparation and characterization of cationic liposomal formulations

A schematic overview of the development of our liposomal vaccine formulations is depicted in Fig. 1. In the first step, we tested the effect of the selected cationic lipids and cholesterol on the physicochemical properties of liposomes. We excluded formulations that were unstable or formed liposomes with Z-average size above 250 nm and PDI above 0.35 from further testing *in vitro*. Liposomal formulations with the various commercially available positively charged lipids (Fig. 2) at physiological pH were prepared. To test the effect of cholesterol (20 mol%), the zwitterionic phospholipid (either DOPC or DSPC) was replaced by cholesterol, while keeping the positively charged molar lipid content constant. The liposomal formulations had an antigen-to-lipid weight ratio of 1:50 and were prepared with the thin-film hydration method followed by tip sonication. The formulations are summarized in Table 1. Subsequently, all formulations were characterized in terms of their Z-average size, PDIs, and Zeta-potentials. The following selection criteria were included: no visible signs of aggregation or precipitation in the liposomal suspension, Z-average size < 250 nm, PDI < 0.33, and a Zeta-potential between 15

and 40 mV. These inclusion criteria were selected to assure the comparability of tested formulations by minimizing the effect of size differences. The physicochemical properties of the formulations that met these criteria are presented in Table 2. The results of the remaining formulations are presented in Table S1.

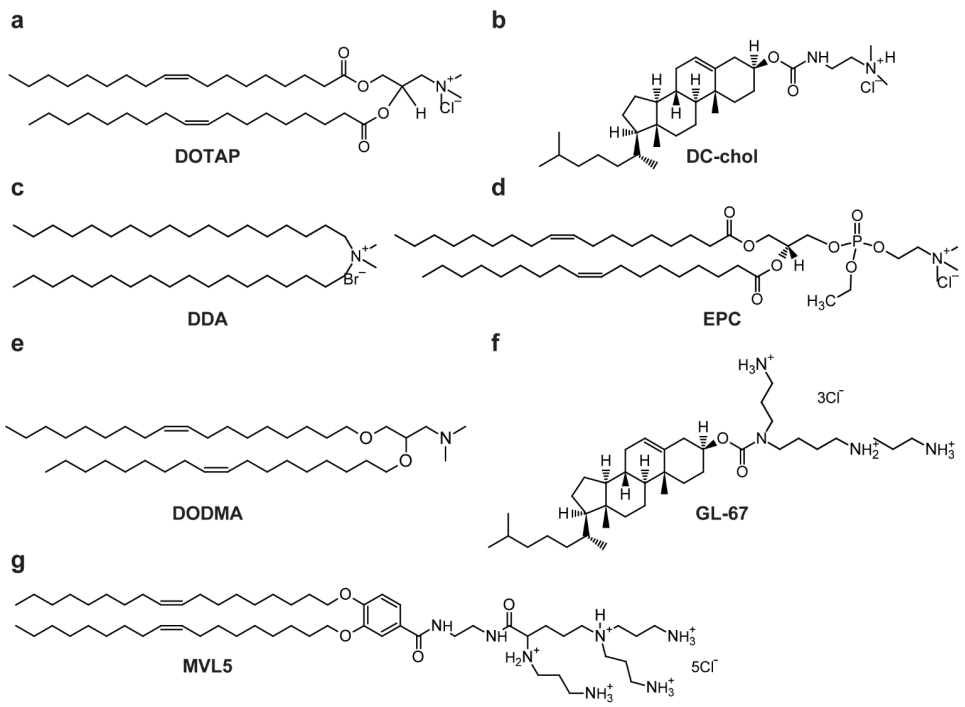

Figure 2. Molecular structures of cationic compounds. a) DOTAP: 1,2-dioleoyl-3-trimethylammonium-propane (chloride salt), b) DC-chol: 3ß-[N-(N',N'-dimethylaminoethane)-carbamoyl]cholesterol hydrochloride, c) DDA: dimethyldioctadecylammonium (bromide salt), d) EPC: 1,2-dioleoyl-*sn*-glycero-3-ethylphosphocholine (chloride salt), e) DODMA: 1,2-dioleyloxy-3-dimethylaminopropane, f) GL-67: N^4-cholesteryl-spermine hydrochloride, and g) MVL5: N1-[2-((1S)-1-[(3-aminopropyl)amino]-4-[di(3-amino-propyl)amino]butylcarboxamido)ethyl]-3,4-di[oleyloxy]-benzamide.

Table 1. List of investigated liposomal vaccine formulations.

Cationic lipid	Cholesterol	DOPC/DSPC	Molar lipid ratio
DOTAP	N.A.	DOPC	1:4
DC-chol	N.A.	DOPC	1:4
DDA	N.A.	DOPC	1:4
EPC	N.A.	DOPC	1:4
DOTAP	cholesterol	DOPC	1:1:3
DDA	cholesterol	DOPC	1:1:3
EPC	cholesterol	DOPC	1:1:3
DOTAP	N.A.	DSPC	1:4
DC-chol	N.A.	DSPC	1:4
DDA	N.A.	DSPC	1:4
EPC	N.A.	DSPC	1:4
DOTAP	cholesterol	DSPC	1:1:3
DDA	cholesterol	DSPC	1:1:3
EPC	cholesterol	DSPC	1:1:3
MVL5	N.A.	DSPC	1:4
MVL5	cholesterol	DSPC	1:1:3
GL-67	N.A.	DOPC	1:4
DODMA	N.A.	DOPC	1:4
DODMA	cholesterol	DOPC	1:1:3
GL-67	N.A.	DSPC	1:4
MVL5	cholesterol	DSPC	1:1:3
DODMA	cholesterol	DSPC	1:1:3

The physicochemical properties for most of the selected liposomal formulations were very similar with Z-average sizes between 80 and 100 nm, PDIs between 0.22 and 0.26, and Zeta-potentials between +15 and +24 mV. However, four formulations exceeded these ranges: AER/GL-67:DOPC, which had a PDI value of 0.32, and AER/DC-chol:DSPC, AER/DODMA:DOPC, and AER/DODMA:cholesterol:DOPC, which had Z-average sizes of 121, 182, and 230 nm, respectively. Although the physicochemical properties differed from the other formulations, we included them for further investigation as the liposome suspensions were stable and did not meet the exclusion criteria. The selected formulations remained stable for at least seven months during storage at 4 °C (remeasured after 4 or 7 months, Table S4). All the formulations were used within six weeks after preparation.

Table 2. Physicochemical properties of the selected formulations. The results represent mean ± SD. Number of batches n ≥ 3.

Formulation	Z-average size (nm)	PDI (-)	Zeta-potential (mV)
AER/DOTAP:DOPC	86 ± 1	0.25 ± 0.01	25.5 ± 0.4
AER/DC-chol:DOPC	102 ± 1	0.27 ± 0.01	24.1 ± 0.3
AER/DDA:DOPC	86 ± 1	0.23 ± 0.01	22.0 ± 0.5
AER/EPC:DOPC	92 ± 1	0.26 ± 0.01	26.4 ± 0.6
AER/DOTAP:cholesterol:DOPC	104 ± 6	0.23 ± 0.01	22.5 ± 2.5
AER/DDA:cholesterol:DOPC	106 ± 4	0.23 ± 0.01	27.0 ± 4.1
AER/EPC:cholesterol:DOPC	98 ± 3	0.26 ± 0.01	26.1 ± 4.3
AER/GL-67:DOPC	95 ± 3	0.32 ± 0.05	24.4 ± 0.4
AER/DC-chol:DSPC	121 ± 3	0.26 ± 0.02	20.2 ± 3.6
AER/DODMA:DOPC	182 ± 5	0.23 ± 0.02	16.1 ± 0.3
AER/DODMA:cholesterol:DOPC	230 ± 11	0.22 ± 0.03	17.3 ± 0.4

Effect of composition of liposomal vaccines on the activation of primary human dendritic cells

The selected liposomal formulations were examined on their ability to induce activation of human MDDCs. To assess DC activation, we measured the expression of cell surface DC activation markers. As shown in Fig. 3 and Fig. S1 a large variation in expression of activation markers was observed between cells derived from different donors. When compared to the control (medium only), many of the formulations induced a statistically significant upregulation of MDDC surface activation markers e.g., CD40, CD83, and CCR7, evident from both increased median fluorescence intensity values (Fig. 3) and histograms (using concatenation displaying the integrated results of all six donors; Fig. S1). Interestingly, the highest expression of surface activation markers was observed in response to formulations containing cholesterol, either as a component: AER/DDA:cholesterol:DOPC, AER/DOTAP:cholesterol:DOPC, and AER/EPC:cholesterol:DOPC, or as a structural part of the cationic constituent (GL-67): AER/GL-67:DOPC. The three latter induced similar or higher upregulation compared to the positive control LPS/TNFα. However, the remaining formulations containing cholesterol or its derivatives, AER/DC-chol:DOPC, AER/DC-chol:DSPC, and AER/DODMA:cholesterol:DOPC did not show the same potency to activate MDDCs, which also applied to the formulations without cholesterol: AER/DOTAP:DOPC, AER/DDA:DOPC, AER/EPC:DOPC, and AER/DODMA:DOPC. When comparing formulations containing the same cationic compound with their cognate formulations containing cholesterol, the cholesterol-containing formulations tended to increase the expression of the markers; however, only AER/DOTAP:cholesterol:DOPC induced a statistically significant increase of CD83 compared to AER/DOTAP:DOPC ($p < 0.05$) (Table S2). The most potent formulations were AER/DDA:cholesterol:DOPC, AER/EPC:cholesterol:DOPC, and AER/GL-67:DOPC. None of the formulations induced a statistically significant upregulation of CD80. Unadjuvanted AER did not increase the expression of any of the tested activation markers. The experiment was repeated, and similar results were obtained for batch 2 (Fig. S2 and S3). Furthermore, corresponding liposomal formulations without AER were tested and yielded similar results (Fig. S4), confirming that the upregulated cell surface expression levels were because of the liposomal constituents and not the loaded antigen. The DC-chol:DSPC formulations were excluded from the following studies because of suboptimal performance in the MDDC activation study. The effect of the sonication method was also investigated. In the repeated experiment (Fig. S3) in the AER control group pre-sonicated AER was used. Comparing the results from the original AER batch (batch 1, Fig. S3) and the sonicated batch (batch 2) revealed identical outcomes. Empty liposomal formulations (Fig. S4), which were downsized with the extrusion method instead of sonication, demonstrated no impact on MDDC activation. From these findings, we concluded that the sonication method did not have any measurable effects on our results.

In summary, these data indicate that DOPC formed more stable liposomes in these formulations compared to DSPC; the most effective cationic lipids were DDA, EPC, and GL-67. Moreover, the addition of cholesterol seemed to increase the DC activation capacity of cationic liposomes.

Effect of lipid composition on the uptake, viability, and cytokine production by MDDCs

Empty fluorescently labeled liposomes were used to evaluate the uptake of vaccine formulations by human MDDCs (Fig. 4a). The uptake depended on the composition of the formulations. The formulations that induced the highest uptake contained either cholesterol, DOTAP:cholesterol:DOPC and EPC:cholesterol:DOPC, or contained the cationic cholesterol-based derivative GL-67:DOPC. This correlated with the profile of the activation markers (Fig. 3). DC-chol:DOPC and DDA:cholesterol:DOPC were not taken up effectively, and neither were DODMA:cholesterol:DOPC liposomes. Therefore, the MDDCs do not take up all formulations equally, demonstrating clear selectivity. Compared to their cholesterol-free counterparts, EPC:cholesterol:DOPC and DOTAP:cholesterol:DOPC liposomes were taken up significantly better than the corresponding liposomes without cholesterol ($p < 0.05$). The full statistical comparison of the formulations is summarized in Table S3.

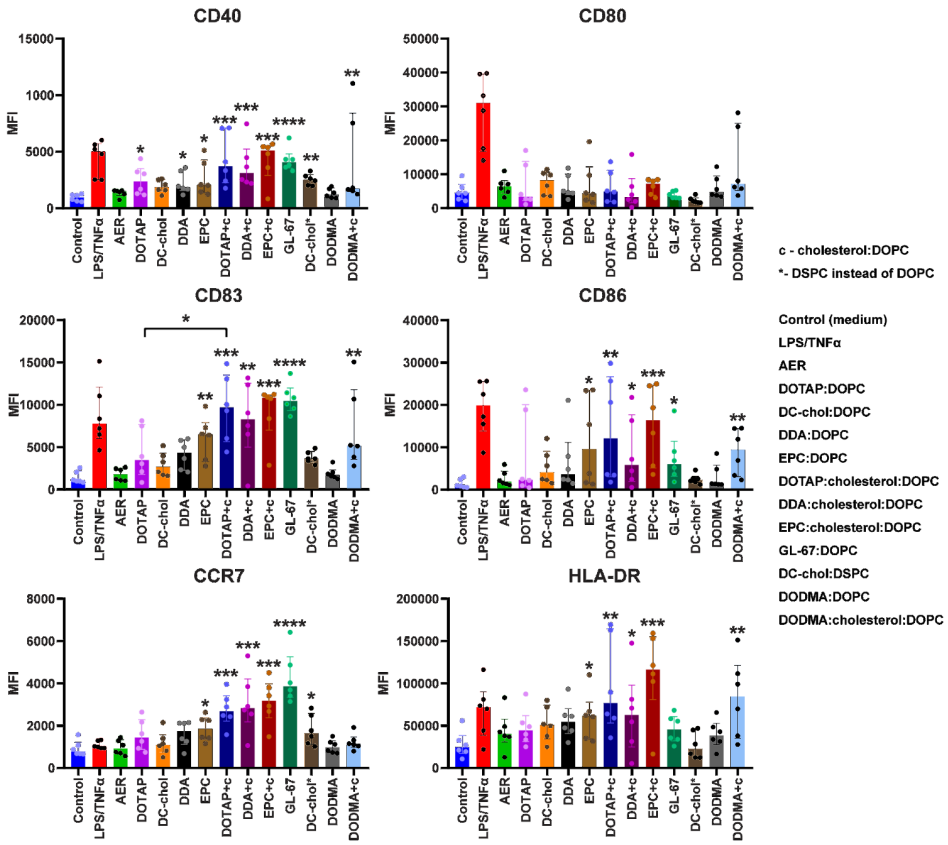

Figure 3. Cell surface activation marker expression levels in MDDCs after stimulation with medium (control), a combination of LPS and TNFα (100 and 5 ng/ml, respectively) as the positive control, unadjuvanted AER (5 μg/ml), and liposomal formulations (5 μg/ml AER, 250 μg/ml liposomes). Median fluorescence intensities related to the expression of indicated activation markers: CD40, CD80, CD83, CD86, CCR7, and HLA-DR. The formulations are compared to the control in the significance testing. The results represent median ± IQR. n = 6 (cell donors).

Liposome uptake was also studied for human macrophages. These were (GM-CSF differentiated) human (pro-inflammatory) M1 macrophages and (M-CSF differentiated) human (anti-inflammatory) M2 macrophages (Fig. S5), both of which are APCs and can locally play a role in processing and presenting antigens. Importantly, macrophages are the predominant habitat of Mtb and thus must be recognized by T-cells for bacterial control [8]. While sharing the same uptake pattern, both M1 and M2 macrophages had a higher liposome uptake than MDDCs, and GL-67:DOPC liposomes were taken up to the highest degree by the M1 and M2 macrophages.

Subsequently, the effect of the antigen-loaded liposomes on the viability of human MDDCs was tested. Each liposomal formulation was tested in three lipid concentrations: 25, 100, and 250 μg/mL with an AER-to-lipid weight ratio of 1:50. The viability of the cells depended substantially on the formulation added (Fig. 4b) as at the lowest concentration, none of the formulations reduced cellular viability. At the highest concentrations AER/DOTAP:cholesterol:DOPC, AER/DDA:cholesterol:DOPC, AER/EPC:cholesterol:DOPC caused intermediate cell death (between 25% and 35%) while also inducing the highest upregulation of the activation markers and the uptake in MDDCs and M1 and M2 macrophages. The formulations that increased the upregulation of the surface markers to a low degree also had a low impact on cellular viability (>85% viability). Only the AER/GL-67:DOPC liposomes caused an unacceptable reduction of viability as less than 20% of cells remained viable at the highest concentration. In general, cellular viability decreased as the concentration of AER and lipid concentration increased.

Antigen-specific T-cell responses

The three most promising liposomal formulations: AER/DOTAP:cholesterol:DOPC, AER/DDA:cholesterol:DOPC, AER/EPC:cholesterol:DOPC were selected to examine T-cell activation. GL-67-containing liposomes were highly toxic and did not improve the upregulation of surface markers in MDDCs substantially better than the other formulations, therefore we decided that these liposomes were not appropriate for further testing. Two HLA-DR3 restricted AER-specific T-cell clones were exposed to HLA-DR3$^+$ MDDCs from different donors, that had been incubated with the formulations. When MDDCs take up the liposomes, they will process the antigen and present it to T-cell clones that recognize the relevant peptide epitope presented via HLA-DR3 [48]. If the MDDCs receive costimulatory signals, they will mature and interact with the T cells, which will upregulate antigen-specific surface markers (CD154) and start producing cytokines (IFN-γ) as a result, which can be detected by flow cytometry using intracellular staining (Fig. 4c). Two of the AER-loaded formulations: DOTAP:cholesterol:DOPC and EPC:cholesterol:DOPC induced statistically significant increases in T-cell clone activation by an increase of the percentage of IFN-γ$^+$ CD154$^+$ double-positive cells compared to the empty liposomes. No statistical difference in the activation of T-cells was observed between the two AER-containing formulations. However, it has to be noted that variability in expression between different HLA-DR3$^+$ MDDCs donors was considerable.

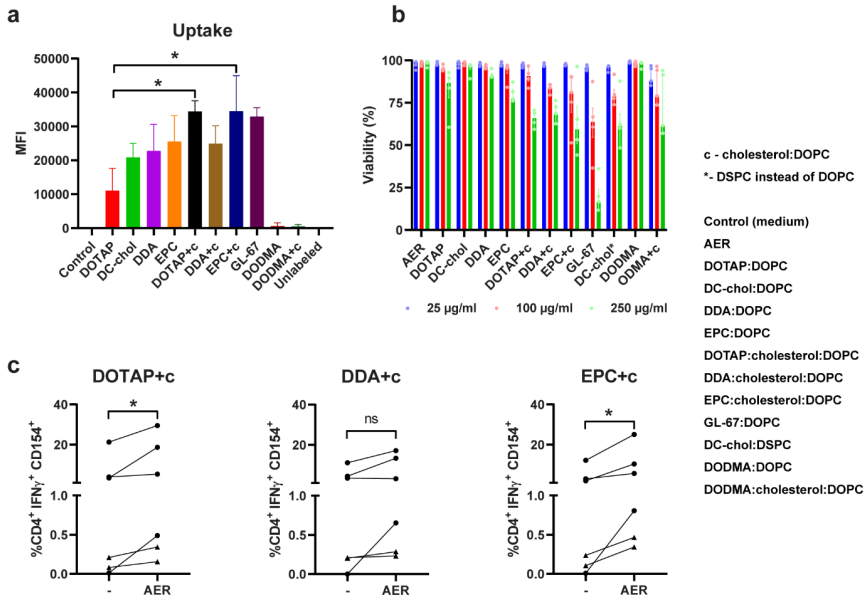

Figure 4. Effect of lipid composition on the uptake of liposomes, the viability of MDDCs, and the T-cell activation. a) Uptake of Cy5-labeled (empty) liposomes in MDDCs, n = 12, b) viability of MDDCs after exposure to AER-containing liposomal formulations, n = 6 (cell donors), c) T-cell activation as a percentage of $CD4^+$ T-cells that produce IFN-γ and express CD154. Comparison between empty (-) and AER-loaded (AER) liposomes (5 µg/ml AER, 250 µg/ml liposomes), exposure 1 h. Circles represent the L10B4 clone (Ag85B p56-65) and triangles the 1B4 clone (Rv2034 p75-105). The results in panels a and b represent median ± IQR.

Table 3. Physicochemical properties of optimized formulations. n≥3 (batches).

Formulation	Molar lipid ratio	Z-average size (nm)	PDI (-)	Zeta-potential (mV)
AER/DDA:cholesterol:DOPC*	2:1:2	141 ± 2	0.44 ± 0.01	33.5 ± 1.0
AER/DDA:cholesterol:DOPC*	1:2:2	136 ± 2	0.33 ± 0.01	30.1 ± 1.4
AER/DDA:cholesterol:DOPC*	2:2:1	156 ± 1	0.33 ± 0.01	31.7 ± 1.0
AER/EPC:cholesterol:DOPC	2:1:2	95 ± 6	0.28 ± 0.02	30.9 ± 0.8
AER/EPC:cholesterol:DOPC	1:2:2	109 ± 2	0.28 ± 0.01	31.6 ± 0.4
AER/EPC:cholesterol:DOPC	2:2:1	89 ± 1	0.26 ± 0.01	36.4 ± 3.6

*Visibly aggregated formulation. The sample for the measurement of the Z-average size, PDI, and Zeta-potential was taken from the upper part of the solution that was free of visible aggregates.

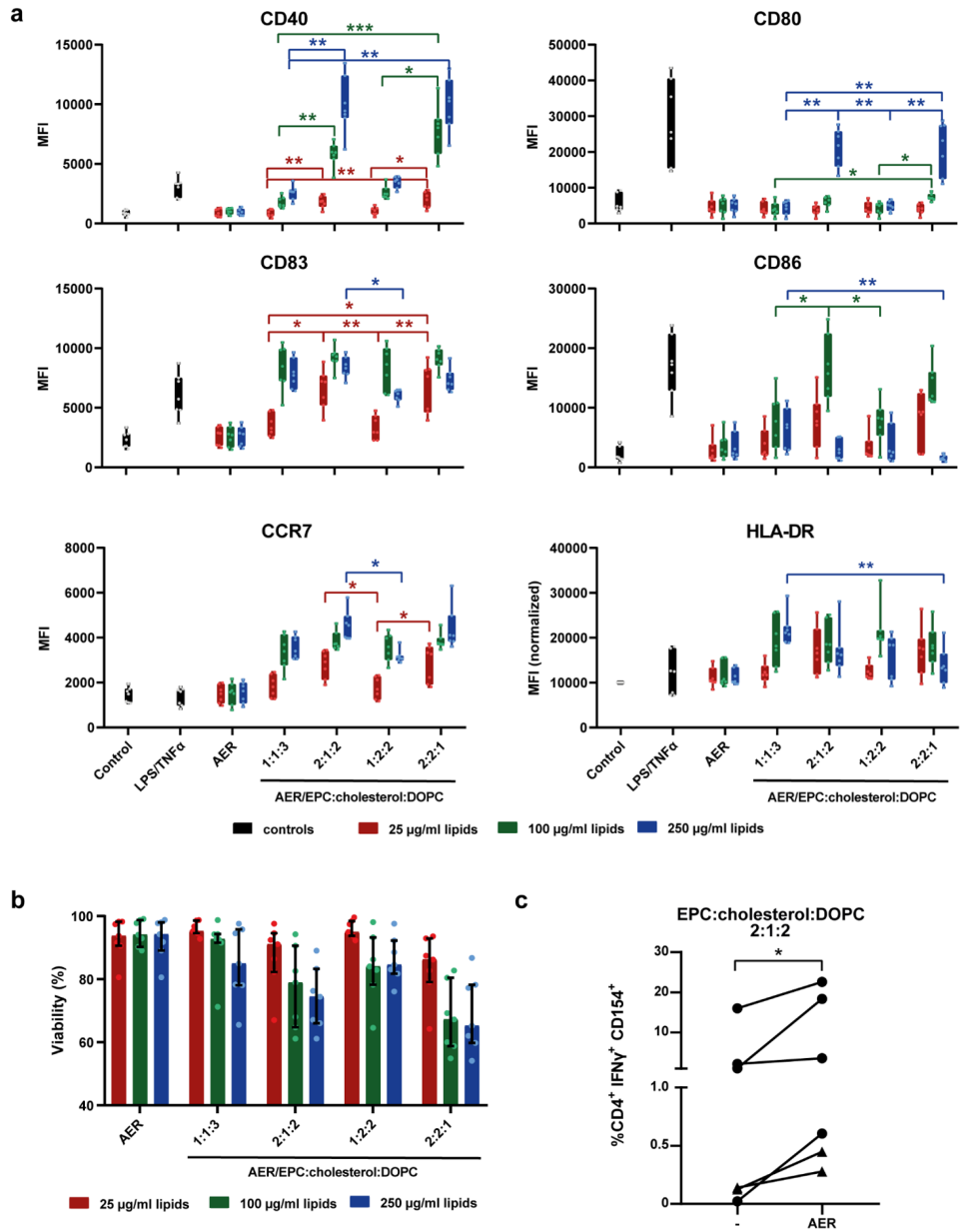

Figure 5. Upregulation of cell surface activation markers and the viability of MDDCs exposed to liposomal formulations containing AER/EPC:cholesterol:DOPC in different molar ratios. a) Median fluorescence intensities related to the expression of indicated activation markers: CD40, CD80, CD83, CD86, CCR7, and HLA-DR, n = 7 (cell donors). b) Viability of MDDCs after 1-h exposure to the liposomal formulations, n = 7 (cell donors). c) T-cell activation as a percentage of $CD4^+$ T-cells that produce IFN-γ and express CD154. Circles represent the L10B4 clone (Ag85B p56-65) and triangles the 1B4 clone (Rv2034 p), n = 6 (cell donors). The results represent median ± IQR.

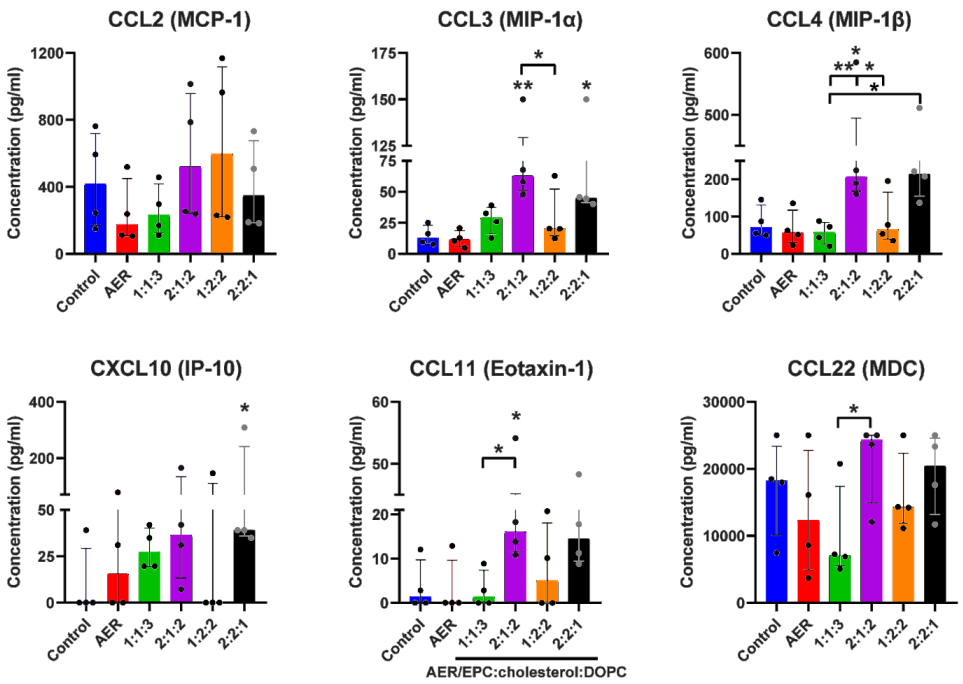

Figure 6. Production of cytokines by MDDCs exposed to liposomal formulations (5 μg/ml AER, 250 μg/ml liposomes, exposure 1 h), n = 4 (cell donors). The results represent median ± IQR.

Optimization of the best-performing formulations

The best-performing compositions in regard to cellular toxicity, uptake, and stimulatory capacities contained cholesterol and either DDA or EPC. DOTAP liposomes with cholesterol performed equally well. However, in a parallel unpublished work we saw that DOTAP liposomes were intrinsically less immunogenic, hence we did not include them. In the subsequent optimization step, we doubled the molar content of the cationic compound and/or cholesterol compared to formulations discussed above resulting in cationic lipid:cholesterol:DOPC molar ratios of 2:1:2, 1:2:2, and 2:2:1. The Z-average sizes, PDIs, and Zeta-potentials of the formulations are summarized in Table 3. We observed that the new variants of the AER/DDA:cholesterol:DOPC formulation did not meet our above-specified criteria in regard to the physicochemical properties and therefore were excluded from further analysis.

Effect of the increased cationic lipid and cholesterol contents on human DC activation, viability, T-cell activation, and cytokine production

The MDDCs were exposed to the best-performing formulation: AER/EPC:cholesterol:DOPC (molar lipid ratio 1:1:3 used in the first series of studies) and its three variations are reported in Table 3. The upregulation of the activation markers was evaluated (Fig. 5 and Fig. S6, statistical data is shown in Table S5). The initially developed AER/EPC:cholesterol:DOPC 1:1:3 liposomes induced all the evaluated activation markers, except for CD80 (Table S4). The two variations that contained a double amount of EPC induced a more robust activation indicated by increased Median Fluorescence Intensities values, e.g., CD40 and CCR7 (Fig. 5a), and histograms shifted towards high-intensity values (Fig. S6). At the highest tested concentration (5 μg/ml AER with 250 μg/ml total lipids), both the 2:1:2 and 2:2:1 formulations induced a statistically significant upregulation of CD80 when compared to the control. This was not achieved by any of the liposome formulations in the prior MDDC activation experiments. Interestingly, no difference was observed between 2:1:2 and 2:2:1 variants (that contain the double amount of EPC), and between 1:2:2 and 1:1:3 variants. We observed a decrease in cellular viability for these double-amount formulations, especially for 2:2:1.The formulation AER/EPC:cholesterol:DOPC 2:1:2 selected as the best upregulator of surface activation markers was tested again for T-cell recognition. Indeed, this formulation showed a significant increase in the percentage of IFN-γ^+ $CD154^+$ double-positive cells when compared to the empty liposomes.

Finally, we measured the levels of cytokines and chemokines with multiplex assays in the supernatants from MDDC cultures exposed to the original formulation of AER/EPC:cholesterol:DOPC and the three variations. We assessed the levels of several cytokines and chemokines (Fig. 6) and observed that formulations 2:1:2 and 2:2:1 induced significantly increased levels of CCL3, CCL4, CXCL10, and CCL11, compared to the AER alone and the 1:1:3 and 1:2:2 variants. For CCL2 and CCL22 we observed a (statistically non-significant) trend towards upregulation of the cytokine levels. For IL-12p40, IL-10, IL-1β, and TNF-α we did not observe changes in the concentration of detectable cytokines compared to the medium control.

DISCUSSION

Cationic liposomes are not only potent delivery systems for subunit vaccines but also exhibit intrinsic adjuvant properties. In this study, we explored these properties with an extensive list of commercially available cationic lipids and different cholesterol concentrations to evaluate their role in the physicochemical properties of liposomes and immunological outcomes as summarized in Fig. 1. In this way, we aim to fill the gap in publicly available data. We used a rationalized selection of assays that allowed us to perform a head-to-head comparison of multiple liposomes to identify the optimal formulation based on human in vitro immune responses.

The selection of lipids and stability of liposomes

The selected cationic lipids differ substantially in terms of their chemical structures, which can affect the stability of liposomes and, consequently, the interaction between the liposomes and APCs. We observed that the mean size of liposomes prepared with DODMA is larger compared to the other formulations, and this is likely because of its head group structure, which is smaller compared to quaternary ammonium cations. Liposomes prepared with MVL-5 and GL-67 were large and unstable in the presence of the AER. Their massive cationic head groups might interact with the antigen and cause aggregation, resulting in unstable suspensions.

The choice of lipids affects the stability, size, and PDI of the liposomes. We observed that liposomes that consisted of unsaturated lipids, e.g., AER/DOTAP:DOPC and AER/EPC:DOPC, were smaller than AER/DOTAP:DSPC and AER/EPC:DSPC liposomes that consisted of a mix of unsaturated and saturated lipids. Liposomes containing DDA, which is a saturated lipid, or cholesterol-based compounds like DC-chol and GL-67 should be stable. As expected, DC-chol formed stable liposomes when formulated with DOPC and DSPC. Surprisingly, AER/GL-67:DSPC and AER/DDA:DSPC formulations did not, this could be ascribed to the addition of the antigen.

The choice of lipid and consequent immunological response

The formulations that fulfilled our predefined selection criteria for further immunological evaluation were tested in several biological assays. We observed that liposomes containing cholesterol were taken up more efficiently by human MDDCs and also induced a higher expression of activation markers, but also increased cellular toxicity, which did not lead to massive cell death, compared to liposomes without cholesterol. This is likely because of the liquid-ordered organization of the bilayer of liposomes, which is more rigid than a liquid-disordered phase in liposomes without cholesterol [50–53]. This finding is in line with reports that more rigid liposomes with higher cholesterol content are more efficiently taken up by DCs [15] and macrophages [44, 54, 55].

When focusing on the cationic lipids, formulations containing DOTAP, DDA, EPC, and GL-67 induced the highest upregulation of surface activation markers. This might be a consequence of the higher uptake by MDDCs. We observed that liposomes containing DDA, EPC, and GL-67 tended to be more toxic as they reduced the viability of MDDCs more than those with DOTAP and DC-chol. Induction of cell death and activation of MDDCs can be mechanistically linked: apoptotic vesicles from dying cells can interact with TLRs on viable DCs, which can lead to cross-priming and induction of $CD8^+$ T-cells *in vivo* [56, 57]. The liposomal formulation with the cation GL-67 reduced the viability pronouncedly, even at lower concentrations. This is most probably caused by the induction of necrosis by the primary amines in GL-67 [58, 59]. It has been reported that liposomes containing cholesterol and eDPPC (ethyl dipalmitoylphosphatidylcholine), are taken up by APCs to a higher degree than liposomal formulations with both cholesterol and DDA or DC-chol [15]. This may suggest that cationic compounds having ethyl phosphocholine head groups, such as eDPPC and EPC, increased liposomal uptake. Vangasseri and colleagues reported that EPC-containing liposomes were superior in stimulating bone marrow-derived DCs (namely in upregulation of the surface expression of CD80) compared to liposomes containing other compounds e.g., DOTAP [60]. Based on these results, we selected three formulations for further evaluation: DOTAP:cholesterol:DOPC, DDA:cholesterol:DOPC and EPC:cholesterol:DOPC.

To gain more insights into the immunomodulatory capacity of these formulations, we used human T-cell activation assays, a step not commonly reported in adjuvant/delivery literature. The specific interaction of the liposome-treated DCs and T cells is essential to protective immunity against TB. We observed that all AER-loaded liposomes induced a higher activation of two different antigen-specific T-cell clones compared to the empty liposomes. This indicates that the AER-containing liposomal formulations were not only efficiently taken up by MDDCs, but were processed and their epitopes presented to activate the T-cell clones. DOTAP:cholesterol:DOPC and EPC:cholesterol:DOPC induced a statistically significant increase of antigen-specific T-cell activation compared to the empty counterparts, demonstrating clear antigen specificity. This was, however, not observed for DDA:cholesterol:DOPC, suggesting that this formulation was not as effective in delivering the antigen and activating MDDCs as the DOTAP- and EPC-based liposomes.

To further improve the quality of the immune response, we selected the cationic lipids DDA and EPC formulations and doubled the cationic lipid and/or cholesterol content. Because of the unfavorable physicochemical properties of the DDA formulation when increasing the cationic or cholesterol levels, we focused on the EPC formulations. Liposomes that contained a double amount of EPC, but not double cholesterol induced an increased upregulation of surface activation markers CD40 and CD80. This is in line with the literature showing that increasing the content of the cationic compound leads to stronger DC maturation [26] and increased IgG titers *in vivo* [18]. Similar to the initial set of formulations, the liposome variants that upregulated DCs activation markers induced also more cell death. Doubling the cholesterol content did not affect surface marker expression, however, there was reduced viability when a higher cholesterol content variant was used. We speculate that once a more rigid liquid-ordered organization occurs at 2:1:2 liposomal composition a further increase of cholesterol provides no additional beneficial effect. Therefore, we decided to only test the 2:1:2 liposome in the T-cell activation assay.

We observed a statistically significant increase of CD154 and IFN-γ double positive T cells when MDDCs were pre-treated with AER-containing liposome compared to the empty one. This indicates that increased EPC content did not negatively affect the ability of the liposome to activate T cells and it is likely to induce effective antigen presentation to T cells *in vivo*.

Lastly, the capacity of the AER-containing liposomes to induce cytokine production in MDDCs was assessed and we observed increased cytokine production for a few cytokines, especially CCL3 (MIP-1α), CCL4 (MIP-1β), CXCL10 (IP-10), and CCL11 (Eotaxin-1). CCL3 and CCL4 have been shown to actively chemoattract $CD8^+$ T cells [61], modulate the interactions between T cells and APCs in the draining lymph nodes after immunization, and enhance memory T-cell responses [62–64]. CXCL10 is reported as a specific chemoattractant for effector T cells [65] and is thought to be directly involved in the generation of antigen-specific $CD8^+$ T-cell responses after vaccination [66]. Moreover, it is a marker of trained immunity, mediating the inhibition of mycobacterial growth in human macrophages [67]. Therefore, this may indicate that liposomes containing 40 mol% EPC favor a microenvironment that is beneficial for TB vaccination, as both $CD4^+$ and $CD8^+$ T-cell responses are important to prevent TB [8]. CCL11 is an eosinophil-specific chemoattractant [68]. We observed a small increase in the CCL2 (MCP-1) production, which promotes the trafficking of effector cells including monocytes, memory T-cells, and natural killer cells from the circulation across the endothelium [69], and CCL22 (MDC). Expression of CCL22 induces cellular contacts of DCs with regulatory T cells through the CCR4 receptor [70] and inhibits the T-cell activation capacities of DCs by decreasing the expression of HLA molecules and CD80 [71]. Expression of CCL22 may therefore reduce T-cell activation *in vivo*. We did not detect any production of IL-12, IFN-α, which concurs with previous reports that cationic liposomes without molecular adjuvants do not induce IL-12 production in DCs [72]. The lack of these cytokines combined with the low production of pro-inflammatory cytokines (CCL3, CCL4, CXCL10) indicates that cationic liposomal formulations require additional adjuvants, e.g., TLR agonists, to achieve robust immune responses *in vivo*.

CONCLUSIONS

TB is still among the leading causes of death and it has been the deadliest infectious disease worldwide for decades. Therefore, additional measures that can control and combat this disease are highly needed. This study presents a strategy to compare, optimize, and select cationic liposomal compositions formulated with the multivalent Mtb antigen AER, based on a rational pipeline of in vitro testing and down-selecting using human cells, as a prelude further pre-clinical investigations, thus reducing animal experimentation. The best-performing formulation was comprised of an AER-containing formulation containing the lipids EPC:cholesterol:DOPC in a molar ratio of 2:1:2, as assessed by an increase in cell surface activation markers, cellular uptake, antigen-specific T-cell activation, cytokine production, and cellular viability. Moreover, the addition of cholesterol improved the performance of the formulations. The liposomal TB vaccine development strategy described in this paper can be used to elucidate which molecular adjuvants should be incorporated in the liposomal formulations before evaluating the effect of the composition in animal models and can be extended to other pathogens besides Mtb.

References

1. World Health Organization, 2020. The top 10 causes of death [WWW Document]. URL https://www.who.int/news-room/fact-sheets/detail/the-top-10-causes-of-death (accessed 10.25.22).
2. World Health Organization, 2022. Global Tuberculosis Report 2022. Geneva.
3. Pierneef, L., van Hooij, A., de Jong, D., Tjon Kon Fat, E.M., van Meijgaarden, K.E., Petruccioli, E., Vanini, V., Roukens, Anna H.E., Goletti, D., Corstjens, P.L.A.M., Joosten, Simone A., Geluk, Annemieke, Arbous, M.S., van den Berg, B.M., Cannegieter, S., Cobbaert, C.M., van der Does, A., van Dongen, J.J.M., Eikenboom, J., Feltkamp, M.C.M., Geluk, A., Goeman, J.J., Giera, M., Hankemeier, T., Heemskerk, M.H.M., Hiemstra, P.S., Hokke, C.H., Janse, J.J., Jochems, S.P., Joosten, S. A., Kikkert, M., Lamont, L., Manniën, J., Ottenhoff, T.H.M., del Prado, M.R., Queralt Rosinach, N., Roestenberg, M., Roos, M., Roukens, A. H.E., Smits, H.H., Snijder, E.J., Staal, F.J.T., Trouw, L.A., Tsonaka, R., Verhoeven, A., Visser, L.G., de Vries, J.J.C., van Westerloo, D.J., Wigbers, J., van der Wijk, H.J., van Wissen, R.C., Wuhrer, M., Yazdanbakhsh, M., Zlei, M., 2023. Host biomarker-based quantitative rapid tests for detection and treatment monitoring of tuberculosis and COVID-19. iScience 26, 105873. https://doi.org/10.1016/J.ISCI.2022.105873.
4. World Health Organization, 2018. UN General Assembly adopts Declaration of the first-ever United Nations High Level Meeting on TB. World Health Organization.
5. Pollard, A.J., Bijker, E.M., 2020. A guide to vaccinology: from basic principles to new developments. Nature Reviews Immunology 2020 21:2 21, 83–100. https://doi.org/10.1038/s41577-020-00479-7.
6. Rémy, V., Zöllner, Y., Heckmann, U., 2015. Vaccination: the cornerstone of an efficient healthcare system. J Mark Access Health Policy 3, 27041. https://doi.org/10.3402/JMAHP.V3.27041.
7. Woodland, D.L., 2017. Vaccine Development. Viral Immunol 30, 141. https://doi.org/10.1089/vim.2017.29017.dlw.
8. Ottenhoff, T.H.M., Kaufmann, S.H.E., 2012. Vaccines against Tuberculosis: Where Are We and Where Do We Need to Go? PLoS Pathog 8, e1002607. https://doi.org/10.1371/journal.ppat.1002607.
9. Fine, P.E.M., 1995. Variation in protection by BCG: implications of and for heterologous immunity. The Lancet 346, 1339–1345. https://doi.org/10.1016/S0140-6736(95)92348-9.
10. Rodrigues, L.C., Diwan, V.K., Wheeler, J.G., 1993. Protective effect of bcg against tuberculous meningitis and miliary tuberculosis: A meta-analysis. Int J Epidemiol 22, 1154–1158. https://doi.org/10.1093/ije/22.6.1154.
11. Trunz, B.B., Fine, P., Dye, C., 2006. Effect of BCG vaccination on childhood tuberculous meningitis and miliary tuberculosis worldwide: a meta-analysis and assessment of cost-effectiveness. Lancet 367, 1173–1180. https://doi.org/10.1016/S0140-6736(06)68507-3.
12. Christensen, D., Korsholm, K.S., Andersen, P., Agger, E.M., 2011. Cationic liposomes as vaccine adjuvants. Expert Rev Vaccines 10, 513–521. https://doi.org/10.1586/erv.11.17.
13. Moyle, P.M., Toth, I., 2013. Modern Subunit Vaccines: Development, Components, and Research Opportunities. ChemMedChem 8, 360–376. https://doi.org/10.1002/cmdc.201200487.
14. O'Hagan, D.T., MacKichan, M.L., Singh, M., 2001. Recent developments in adjuvants for vaccines against infectious diseases. Biomol Eng. https://doi.org/10.1016/S1389-0344(01)00101-0.
15. Barnier-Quer, C., Elsharkawy, A., Romeijn, S., Kros, A., Jiskoot, W., 2013. Adjuvant effect of cationic liposomes for subunit influenza vaccine: Influence of antigen loading method, cholesterol and immune modulators. Pharmaceutics 5, 392–410. https://doi.org/10.3390/pharmaceutics5030392.
16. Schmidt, S.T., Foged, C., Korsholm, K.S., Rades, T., Christensen, D., 2016. Liposome-based adjuvants for subunit vaccines: Formulation strategies for subunit antigens and immunostimulators. Pharmaceutics 8, 1–22. https://doi.org/10.3390/pharmaceutics8010007.
17. Moser, M., Leo, O., 2010. Key concepts in immunology. Vaccine. https://doi.org/10.1016/j.vaccine.2010.07.022.
18. Barnier Quer, C., Elsharkawy, A., Romeijn, S., Kros, A., Jiskoot, W., 2012. Cationic liposomes as adjuvants for influenza hemagglutinin: More than charge alone. European Journal of Pharmaceutics and Biopharmaceutics 81, 294–302. https://doi.org/10.1016/j.ejpb.2012.03.013.
19. Latif, N., Bachhawat, B.K., 1984. The effect of surface charges of liposomes in immunopotentiation. Biosci Rep 4, 99–107. https://doi.org/10.1007/BF01120305.
20. Liu, X., Da, Z., Wang, Yue, Niu, H., Li, R., Yu, H., He, S., Guo, M., Wang, Yong, Luo, Y., Ma, X., Zhu, B., 2016. A novel liposome adjuvant DPC mediates Mycobacterium tuberculosis subunit vaccine well to induce cell-mediated immunity and high protective efficacy in mice. Vaccine 34, 1370–1378. https://doi.org/10.1016/j.vaccine.2016.01.049.
21. Yan, W., Chen, W., Huang, L., 2007. Mechanism of adjuvant activity of cationic liposome: Phosphorylation of a MAP kinase, ERK and induction of chemokines. Mol Immunol 44, 3672–3681. https://doi.org/10.1016/j.molimm.2007.04.009.
22. Khademi, F., Taheri, R.A., Momtazi-Borojeni, A.A., Farnoosh, G., Johnston, T.P., Sahebkar, A., 2018. Potential of cationic liposomes as adjuvants/delivery systems for tuberculosis subunit vaccines, in: Reviews of Physiology, Biochemistry and Pharmacology. pp. 47–69. https://doi.org/10.1007/112_2018_9.
23. Luwi, N.E.M., Ahmad, S., Azlyna, A.S.N., Nordin, A., Sarmiento, M.E., Acosta, A., Azmi, M.N., Uskoković, V., Mohamud, R., Kadir, R., 2022. Liposomes as immunological adjuvants and delivery systems in the development of tuberculosis vaccine: A review. Asian Pac J Trop Med. https://doi.org/10.4103/1995-7645.332806.
24. Tretiakova, D.S., Vodovozova, E.L., 2022. Liposomes as Adjuvants and Vaccine Delivery Systems. Biochemistry (Moscow), Supplement Series A: Membrane and Cell Biology 2022 16:1 16, 1–20. https://doi.org/10.1134/S1990747822020076.
25. Heuts, J., Varypataki, E.M., van der Maaden, K., Romeijn, S., Drijfhout, J.W., van Scheltinga, A.T., Ossendorp, F., Jiskoot, W., 2018. Cationic Liposomes: A Flexible Vaccine Delivery System for Physicochemically Diverse Antigenic Peptides. Pharm Res 35, 1–9. https://doi.org/10.1007/s11095-018-2490-6.
26. Ma, Y., Zhuang, Y., Xie, X., Wang, C., Wang, F., Zhou, D., Zeng, J., Cai, L., 2011. The role of surface charge density in cationic liposome-promoted dendritic cell maturation and vaccine-induced immune responses. Nanoscale 3, 2307–2314. https://doi.org/10.1039/c1nr10166h.
27. Marasini, N., Ghaffar, K.A., Skwarczynski, M., Toth, I., 2017. Liposomes as a Vaccine Delivery System, in: Micro- and Nanotechnology in Vaccine Development. Elsevier Inc., pp. 221–239. https://doi.org/10.1016/B978-0-323-39981-4.00012-9.
28. Varypataki, E.M., van der Maaden, K., Bouwstra, J., Ossendorp, F., Jiskoot, W., 2015. Cationic Liposomes Loaded with a Synthetic Long Peptide and Poly(I:C): a Defined Adjuvanted Vaccine for Induction of Antigen-Specific T Cell Cytotoxicity. AAPS Journal 17, 216–226. https://doi.org/10.1208/s12248-014-9686-4.
29. Brgles, M., Habjanec, L., Halassy, B., Tomašić, J., 2009. Liposome fusogenicity and entrapment efficiency of antigen determine the Th1/Th2 bias of antigen-specific immune response. Vaccine 27, 5435–5442. https://doi.org/10.1016/j.vaccine.2009.07.012.
30. Du, G., Hathout, R.M., Nasr, M., Nejadnik, M.R., Tu, J., Koning, R.I., Koster, A.J., Slütter, B., Kros, A., Jiskoot, W., Bouwstra, J.A., Mönkäre, J., 2017. Intradermal vaccination with hollow microneedles: A comparative study of various protein antigen and adjuvant encapsulated nanoparticles. Journal of Controlled Release 266, 109–118. https://doi.org/10.1016/j.jconrel.2017.09.021.
31. Henriksen-Lacey, M., Bramwell, V.W., Christensen, D., Agger, E.M., Andersen, P., Perrie, Y., 2010. Liposomes based on dimethyldioctadecylammonium promote a depot effect and enhance immunogenicity of soluble antigen. Journal of Controlled Release 142, 180–186. https://doi.org/10.1016/j.jconrel.2009.10.022.
32. Nakanishi, T., Kunisawa, J., Hayashi, A., Tsutsumi, Y., Kubo, K., Nakagawa, S., Nakanishi, M., Tanaka, K., Mayumi, T., 1999. Positively charged liposome functions as an efficient immunoadjuvant in inducing cell-mediated immune response to soluble proteins. Journal of Controlled Release 61, 233–240. https://doi.org/10.1016/S0168-3659(99)00097-8.
33. Benne, N., Van Duijn, J., Kuiper, J., Jiskoot, W., Slütter, B., 2016. Orchestrating immune responses: How size, shape and rigidity affect the immunogenicity of particulate vaccines. https://doi.org/10.1016/j.jconrel.2016.05.033
34. Even-Or, O., Joseph, A., Itskovitz-Cooper, N., Samira, S., Rochlin, E., Eliyahu, H., Goldwaser, I., Balasingam, S., Mann, A.J., Lambkin-Williams, R., Kedar, E., Barenholz, Y., 2011. A new intranasal influenza vaccine based on a novel polycationic lipid-ceramide carbamoyl-spermine (CCS). II. Studies in mice and ferrets and mechanism of adjuvanticity. Vaccine 29, 2474–2486. https://doi.org/10.1016/j.vaccine.2011.01.009.

35. Rosenkrands, I., Agger, E.M., Olsen, A.W., Korsholm, K.S., Andersen, C.S., Jensen, K.T., Andersen, P., 2005. Cationic liposomes containing mycobacterial lipids: A new powerful Th1 adjuvant system. Infect Immun 73, 5817–5826. https://doi.org/10.1128/IAI.73.9.5817-5826.2005.
36. Soema, P.C., Willems, G.J., Jiskoot, W., Amorij, J.P., Kersten, G.F., 2015. Predicting the influence of liposomal lipid composition on liposome size, zeta potential and liposome-induced dendritic cell maturation using a design of experiments approach. European Journal of Pharmaceutics and Biopharmaceutics 94, 427–435. https://doi.org/10.1016/j.ejpb.2015.06.026.
37. Chen, W., Yan, W., Huang, L., 2008. A simple but effective cancer vaccine consisting of an antigen and a cationic lipid. Cancer Immunology, Immunotherapy 57, 517–530. https://doi.org/10.1007/s00262-007-0390-4.
38. Guy, B., Pascal, N., Françon, A., Bonnin, A., Gimenez, S., Lafay-Vialon, E., Trannoy, E., Haensler, J., 2001. Design, characterization and preclinical efficacy of a cationic lipid adjuvant for influenza split vaccine. Vaccine 19, 1794–1805. https://doi.org/10.1016/S0264-410X(00)00386-8.
39. Jiao, X., 2003. Modulation of cellular immune response against hepatitis C virus nonstructural protein 3 by cationic liposome encapsulated DNA immunization. Hepatology 37, 452–460. https://doi.org/10.1053/jhep.2003.50051.
40. Aramaki, K., Watanabe, Y., Takahashi, J., Tsuji, Y., Ogata, A., Konno, Y., 2016. Charge boosting effect of cholesterol on cationic liposomes. Colloids Surf A Physicochem Eng Asp 506, 732–738. https://doi.org/10.1016/j.colsurfa.2016.07.040.
41. Bakouche, O., Gerlier, D., 1986. Enhancement of immunogenicity of tumour virus antigen by liposomes: the effect of lipid composition. Immunology 58, 507–13.
42. Batenjany, M.M., Boni, L.T., Guo, Y., Neville, M.E., Bansal, S., Robb, R.J., Popescu, M.C., 2001. The effect of cholesterol in a liposomal Muc1 vaccine. Biochim Biophys Acta Biomembr 1514, 280–290. https://doi.org/10.1016/S0005-2736(01)00383-2.
43. Ishida, T., Yasukawa, K., Kojima, H., Harashima, H., Kiwada, H., 2001. Effect of cholesterol content in activation of the classical versus the alternative pathway of rat complement system induced by hydrogenated egg phosphatidylcholine-based liposomes. Int J Pharm 224, 69–79. https://doi.org/10.1016/S0378-5173(01)00737-2.
44. Kaur, R., Henriksen-Lacey, M., Wilkhu, J., Devitt, A., Christensen, D., Perrie, Y., 2014. Effect of incorporating cholesterol into DDA:TDB liposomal adjuvants on bilayer properties, biodistribution, and immune responses. Mol Pharm 11, 197–207. https://doi.org/10.1021/mp400372j.
45. Commandeur, S., van den Eeden, S.J.F., Dijkman, K., Clark, S.O., van Meijgaarden, K.E., Wilson, L., Franken, K.L.M.C., Williams, A., Christensen, D., Ottenhoff, T.H.M., Geluk, A., 2014. The in vivo expressed Mycobacterium tuberculosis (IVE-TB) antigen Rv2034 induces CD4+ T-cells that protect against pulmonary infection in HLA-DR transgenic mice and guinea pigs. Vaccine 32, 3580–3588. https://doi.org/10.1016/j.vaccine.2014.05.005.
46. Franken, K.L.M.C., Hiemstra, H.S., Van Meijgaarden, K.E., Subronto, Y., Den Hartigh, J., Ottenhoff, T.H.M., Drijfhout, J.W., 2000. Purification of His-Tagged Proteins by Immobilized Chelate Affinity Chromatography: The Benefits from the Use of Organic Solvent. Protein Expr Purif 18, 95–99. https://doi.org/10.1006/PREP.1999.1162.
47. Verreck, F.A.W., Boer, T. de, Langenberg, D.M.L., Zanden, L. van der, Ottenhoff, T.H.M., 2006. Phenotypic and functional profiling of human proinflammatory type-1 and anti-inflammatory type-2 macrophages in response to microbial antigens and IFN-γ- and CD40L-mediated costimulation. J Leukoc Biol 79, 285–293. https://doi.org/10.1189/JLB.0105015.
48. Commandeur, S., Coppola, M., Dijkman, K., Friggen, A.H., Meijgaarden, K.E. van, Eeden, S.J.F. van den, Wilson, L., Schip, J.J. van der P., Franken, K.L.M.C., Geluk, A., Ottenhoff, T.H.M., 2014a. Clonal Analysis of the T-Cell Response to In Vivo Expressed Mycobacterium tuberculosis Protein Rv2034, Using a CD154 Expression Based T-Cell Cloning Method. PLoS One 9, e99203. https://doi.org/10.1371/JOURNAL.PONE.0099203.
49. Geluk, A., Van Meijgaarden, K.E., De Vries, R.R.P., Sette, A., Ottenhoff, T.H.M., 1997. A DR17-restricted T cell epitope from a secreted Mycobacterium tuberculosis antigen only binds to DR17 molecules at neutral pH. Eur J Immunol 27, 842–847. https://doi.org/10.1002/EJI.1830270406.
50. Benne, N., Leboux, R.J.T., Glandrup, M., van Duijn, J., Lozano Vigario, F., Neustrup, M.A., Romeijn, S., Galli, F., Kuiper, J., Jiskoot, W., Slütter, B., 2020. Atomic force microscopy measurements of anionic liposomes reveal the effect of liposomal rigidity on antigen-specific regulatory T cell responses. Journal of Controlled Release 318, 246–255. https://doi.org/10.1016/j.jconrel.2019.12.003.
51. Krause, M.R., Regen, S.L., 2014. The structural role of cholesterol in cell membranes: From condensed bilayers to lipid rafts. Acc Chem Res 47, 3512–3521. https://doi.org/10.1021/ar500260t.
52. Martinez-Seara, H., Ró G, T., Karttunen, M., Vattulainen, I., Reigada, R., n.d. Cholesterol Induces Specific Spatial and Orientational Order in Cholesterol/Phospholipid Membranes. https://doi.org/10.1371/journal.pone.0011162.
53. Takechi-Haraya, Y., Sakai-Kato, K., Abe, Y., Kawanishi, T., Okuda, H., Goda, Y., 2016. Atomic Force Microscopic Analysis of the Effect of Lipid Composition on Liposome Membrane Rigidity. Langmuir 32, 6074–6082. https://doi.org/10.1021/acs.langmuir.6b00741.
54. Christensen, D., Henriksen-Lacey, M., Kamath, A.T., Lindenstrøm, T., Korsholm, K.S., Christensen, J.P., Rochat, A.F., Lambert, P.H., Andersen, P., Siegrist, C.A., Perrie, Y., Agger, E.M., 2012. A cationic vaccine adjuvant based on a saturated quaternary ammonium lipid have different in vivo distribution kinetics and display a distinct CD4 T cell-inducing capacity compared to its unsaturated analog. Journal of Controlled Release 160, 468–476. https://doi.org/10.1016/j.jconrel.2012.03.016.
55. Takano, S., Aramaki, Y., Tsuchiya, S., 2003. Physicochemical properties of liposomes affecting apoptosis induced by cationic liposomes in macrophages. Pharm Res 20, 962–968. https://doi.org/10.1023/A:1024441702398.
56. Caruso, S., Poon, I.K.H., 2018. Apoptotic cell-derived extracellular vesicles: More than just debris. Front Immunol. https://doi.org/10.3389/fimmu.2018.01486.
57. Winau, F., Weber, S., Sad, S., De Diego, J., Hoops, S.L., Breiden, B., Sandhoff, K., Brinkmann, V., Kaufmann, S.H.E., Schaible, U.E., 2006. Apoptotic vesicles crossprime CD8 T cells and protect against tuberculosis. Immunity 24, 105–117. https://doi.org/10.1016/j.immuni.2005.12.001.
58. Arisaka, M., Nakamura, T., Yamada, A., Negishi, Y., Aramaki, Y., 2010. Involvement of protein kinase Cδ in induction of apoptosis by cationic liposomes in macrophage-like RAW264.7 cells. FEBS Lett 584, 1016–1020. https://doi.org/10.1016/j.febslet.2010.01.055.
59. Mayhew, E., Ito, M., Lazo, R., 1987. Toxicity of non-drug-containing liposomes for cultured human cells. Exp Cell Res 171, 195–202. https://doi.org/10.1016/0014-4827(87)90262-X.
60. Vangasseri, D.P., Cui, Z., Chen, W., Hokey, D.A., Falo, L.D., Huang, L., 2006. Immunostimulation of dendritic cells by cationic liposomes. Mol Membr Biol 23, 385–395. https://doi.org/10.1080/09687860600790537.
61. Honey, K., 2006. CCL3 and CCL4 actively recruit CD8+ T cells. Nat Rev Immunol 6, 427. https://doi.org/10.1038/nri1862.
62. Askew, D., Su, C.A., Barkauskas, D.S., Dorand, R.D., Myers, J., Liou, R., Nthale, J., Huang, A.Y., 2016. Transient Surface CCR5 Expression by Naive CD8 + T Cells within Inflamed Lymph Nodes Is Dependent on High Endothelial Venule Interaction and Augments Th Cell–Dependent Memory Response. The Journal of Immunology 196, 3653–3664. https://doi.org/10.4049/jimmunol.1501176.
63. Castellino, F., Huang, A.Y., Altan-Bonnet, G., Stoll, S., Scheinecker, C., Germain, R.N., 2006. Chemokines enhance immunity by guiding naive CD8+ T cells to sites of CD4+ T cell-dendritic cell interaction. Nature 440, 890–895. https://doi.org/10.1038/nature04651.
64. Hugues, S., Scholer, A., Boissonnas, A., Nussbaum, A., Combadière, C., Amigorena, S., Fetler, L., 2007. Dynamic imaging of chemokine-dependent CD8+ T cell help for CD8+ T cell responses. Nat Immunol 8, 921–930. https://doi.org/10.1038/ni1495.
65. Khan, I.A., MacLean, J.A., Lee, F.S., Casciotti, L., DeHaan, E., Schwartzman, J.D., Luster, A.D., 2000. IP-10 is critical for effector T cell trafficking and host survival in Toxoplasma gondii infection. Immunity 12, 483–494. https://doi.org/10.1016/S1074-7613(00)80200-9.
66. Majumder, S., Bhattacharjee, S., Paul Chowdhury, B., Majumdar, S., 2012. CXCL10 Is Critical for the Generation of Protective CD8 T Cell Response Induced by Antigen Pulsed CpG-ODN Activated Dendritic Cells. PLoS One 7, e48727. https://doi.org/10.1371/journal.pone.0048727.
67. Joosten, S.A., Van Meijgaarden, K.E., Arend, S.M., Prins, C., Oftung, F., Korsvold, G.E., Kik, S. V., Arts, R.J.W., Van Crevel, R., Netea, M.G., Ottenhoff, T.H.M., 2018. Mycobacterial growth inhibition is associated with trained innate immunity. J Clin Invest 128, 1837–1851. https://doi.org/10.1172/JCI97508.

68. Lacy, P., 2017. Eosinophil Cytokines in Allergy, in: Cytokine Effector Functions in Tissues. Elsevier Inc., pp. 173–218. https://doi.org/10.1016/B978-0-12-804214-4.00011-7.
69. Deshmane, S.L., Kremlev, S., Amini, S., Sawaya, B.E., 2009. Monocyte chemoattractant protein-1 (MCP-1): An overview. Journal of Interferon and Cytokine Research 29, 313–325. https://doi.org/10.1089/jir.2008.0027.
70. Rapp, M., Wintergerst, M.W.M., Kunz, W.G., Vetter, V.K., Knott, M.M.L., Lisowski, D., Haubner, S., Moder, S., Thaler, R., Eiber, S., Meyer, B., Röhrle, N., Piseddu, I., Grassmann, S., Layritz, P., Kühnemuth, B., Stutte, S., Bourquin, C., von Andrian, U.H., Endres, S., Anz, D., 2019. CCL22 controls immunity by promoting regulatory T cell communication with dendritic cells in lymph nodes. Journal of Experimental Medicine 216, 1170–1181. https://doi.org/10.1084/jem.20170277.
71. Kühnemuth, B., Piseddu, I., Knott, M., Vetter, V., Layritz, P., Endres, S., Anz, D., 2017. CCL22 impedes T cell activation capacities of dendritic cells by reducing membrane expression of MHC molecules and CD80. The Journal of Immunology 198.
72. Varypataki, E.M., van der Maaden, K., Bouwstra, J., Ossendorp, F., Jiskoot, W., 2015. Cationic Liposomes Loaded with a Synthetic Long Peptide and Poly(I:C): a Defined Adjuvanted Vaccine for Induction of Antigen-Specific T Cell Cytotoxicity. AAPS Journal 17, 216–226. https://doi.org/10.1208/s12248-014-9686-4.

SUPPLEMENTARY MATERIAL

Table S1. Physicochemical properties of the formulations that did not meet the inclusion criteria. The listed formulations had visible aggregation. The results represent mean ± SD.

Formulation	Z-average size (nm)	PDI (-)	Z-potential (mV)
AER/DOTAP:DSPC	>1000 (± 85)	0.84 ± 0.60	23.4 ± 1.8
AER/DDA:DSPC	>1000 (± 644)	1.00 ± 0.01	21.2 ± 0.5
AER/EPC:DSPC	402 ± 20	0.87 ± 0.10	18.2 ± 0.2
AER/DOTAP:chol:DSPC	215 ± 5	0.37 ± 0.01	33.6 ± 0.4
AER/DDA:chol:DSPC	143 ± 4	0.23 ± 0.03	32.0 ± 0.3
AER/EPC:chol:DSPC	741 ± 24	0.63 ± 0.01	30.3 ± 0.8
AER/GL-67:DSPC	>1000 (± 525)	0.27 ± 0.08	10.4 ± 5.4
AER/MVL5:DOPC	>1000 (± 980)	0.23 ± 0.11	6.7 ± 0.8
AER/MVL5:chol:DOPC	>1000 (± 655)	0.74 ± 0.40	0.7 ± 0.6
AER/MVL5:chol:DSPC	>1000 (± 1268)	1.00 ± 0.01	4.1 ± 0.1
AER/DODMA:chol:DSPC	258 ± 16	0.65 ± 0.31	10.9 ± 0.3

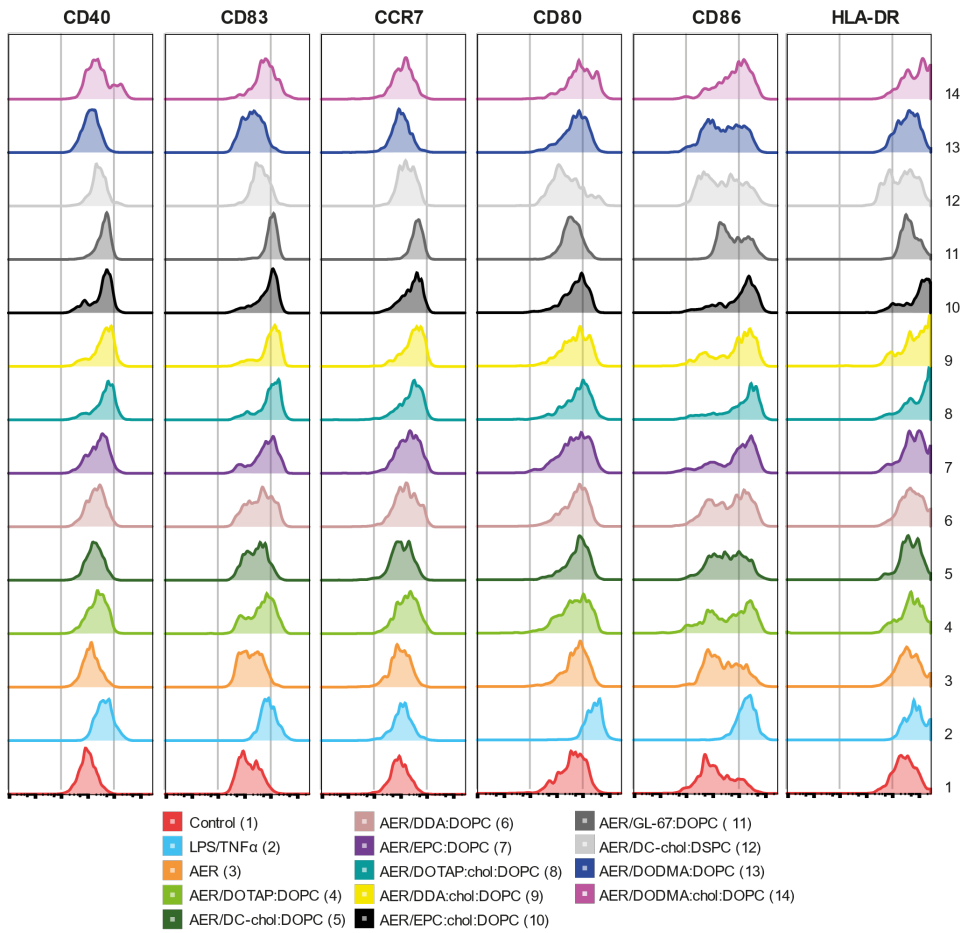

Figure S1. Upregulation of surface activation markers in MDDCs (GM-CSF/IL-4 differentiated) after stimulation with medium (negative control), a combination of LPS/TNFα (100 and 5 ng/ml, respectively), AER (5 μg/ml) and liposomal formulations (5 μg/ml AER, 250 μg/ml liposomes, exposure 1 h). The upregulation of the surface activation markers is presented as concatenated flow cytometry data of all donors, n = 6.

Table S2. Statistical comparisons between different groups as measured by Kruskal-Wallis and Uncorrected Dunn's test (Figure 2a). Medium (negative control), a combination of LPS/TNFα (100 and 5 ng/ml, respectively), AER (5 μg/ml) and liposomal formulations (5 μg/ml AER, 250 μg/ml liposomes, exposure 1 h) ns $p > 0.05$, * $p < 0.05$, ** $p < 0.01$, *** $p < 0.001$, **** $p < 0.0001$.

Uncorrected Dunn's test	Significance					
	CD40	CD80	CD83	CD86	CCR7	HLA-DR
Control vs. LPS/TNFα	****	**	***	****	ns	*
Control vs. AER	ns	ns	ns	ns	ns	ns

Uncorrected Dunn's test	Significance					
	CD40	CD80	CD83	CD86	CCR7	HLA-DR
Control vs. AER/DOTAP:DOPC	*	ns	ns	ns	ns	ns
Control vs. AER/DC-chol:DOPC	ns	ns	ns	ns	ns	ns
Control vs. AER/DDA:DOPC	*	ns	ns	ns	ns	ns
Control vs. AER/EPC:DOPC	*	ns	**	*	*	*
Control vs. AER/DOTAP:chol:DOPC	***	ns	***	**	***	**
Control vs. AER/DDA:chol:DOPC	***	ns	**	*	***	*
Control vs. AER/EPC:chol:DOPC	***	ns	***	***	***	***
Control vs. AER/GL-67:DOPC	****	ns	****	*	****	ns
Control vs. AER/DC-chol:DSPC	**	ns	ns	ns	*	ns
Control vs. AER/DODMA:DOPC	ns	ns	ns	ns	ns	ns
Control vs. AER/DODMA:chol:DOPC	**	ns	**	**	ns	**
LPS/TNFα vs. AER	***	*	***	**	ns	ns
LPS/TNFα vs. AER/DOTAP:DOPC	ns	**	ns	*	ns	ns
LPS/TNFα vs. AER/DC-chol:DOPC	*	*	*	*	ns	ns
LPS/TNFα vs. AER/DDA:DOPC	*	*	ns	*	ns	ns
LPS/TNFα vs. AER/EPC:DOPC	ns	**	ns	ns	ns	ns
LPS/TNFα vs. AER/DOTAP:chol:DOPC	ns	**	ns	ns	**	ns
LPS/TNFα vs. AER/DDA:chol:DOPC	ns	***	ns	ns	**	ns
LPS/TNFα vs. AER/EPC:chol:DOPC	ns	*	ns	ns	**	ns
LPS/TNFα vs. AER/GL-67:DOPC	ns	***	ns	ns	***	ns
LPS/TNFα vs. AER/DC-chol:DSPC	ns	****	ns	**	ns	*
LPS/TNFα vs. AER/DODMA:DOPC	***	**	**	**	ns	ns
LPS/TNFα vs. AER/DODMA:chol:DOPC	ns	ns	ns	ns	ns	ns
AER vs. AER/DOTAP:DOPC	ns	ns	ns	ns	ns	ns
AER vs. AER/DC-chol:DOPC	ns	ns	ns	ns	ns	ns
AER vs. AER/DDA:DOPC	ns	ns	ns	ns	ns	ns
AER vs. AER/EPC:DOPC	ns	ns	*	ns	*	ns
AER vs. AER/DOTAP:chol:DOPC	**	ns	***	*	**	ns
AER vs. AER/DDA:chol:DOPC	**	ns	**	ns	**	ns
AER vs. AER/EPC:chol:DOPC	**	ns	***	**	***	*
AER vs. AER/GL-67:DOPC	***	ns	****	ns	****	ns
AER vs. AER/DC-chol:DSPC	*	**	ns	ns	ns	ns
AER vs. AER/DODMA:DOPC	ns	ns	ns	ns	ns	ns

Uncorrected Dunn's test	Significance					
	CD40	CD80	CD83	CD86	CCR7	HLA-DR
AER vs. AER/DODMA:chol:DOPC	ns	ns	**	ns	ns	ns
AER/DOTAP:DOPC vs. AER/DC-chol:DOPC	ns	ns	ns	ns	ns	ns
AER/DOTAP:DOPC vs. AER/DDA:DOPC	ns	ns	ns	ns	ns	ns
AER/DOTAP:DOPC vs. AER/EPC:DOPC	ns	ns	ns	ns	ns	ns
AER/DOTAP:DOPC vs. AER/ DOTAP:chol:DOPC	ns	ns	*	ns	ns	ns
AER/DOTAP:DOPC vs. AER/ DDA:chol:DOPC	ns	ns	ns	ns	ns	ns
AER/DOTAP:DOPC vs. AER/EPC:chol:DOPC	ns	ns	*	*	*	*
AER/DOTAP:DOPC vs. AER/GL-67:DOPC	ns	ns	**	ns	**	ns
AER/DOTAP:DOPC vs. AER/DC-chol:DSPC	ns	ns	ns	ns	ns	ns
AER/DOTAP:DOPC vs. AER/DODMA:DOPC	ns	ns	ns	ns	ns	ns
AER/DOTAP:DOPC vs. AER/ DODMA:chol:DOPC	ns	ns	ns	ns	ns	ns
AER/DC-chol:DOPC vs. AER/DDA:DOPC	ns	ns	ns	ns	ns	ns
AER/DC-chol:DOPC vs. AER/EPC:DOPC	ns	ns	ns	ns	ns	ns
AER/DC-chol:DOPC vs. AER/ DOTAP:chol:DOPC	ns	ns	**	ns	**	ns
AER/DC-chol:DOPC vs. AER/ DDA:chol:DOPC	ns	ns	*	ns	**	ns
AER/DC-chol:DOPC vs. AER/EPC:chol:DOPC	ns	ns	**	ns	**	ns
AER/DC-chol:DOPC vs. AER/GL-67:DOPC	*	ns	**	ns	***	ns
AER/DC-chol:DOPC vs. AER/DC-chol:DSPC	ns	**	ns	ns	ns	ns
AER/DC-chol:DOPC vs. AER/ DODMA:DOPC	ns	ns	ns	ns	ns	ns
AER/DC-chol:DOPC vs. AER/ DODMA:chol:DOPC	ns	ns	ns	ns	ns	ns
AER/DDA:DOPC vs. AER/EPC:DOPC	ns	ns	ns	ns	ns	ns
AER/DDA:DOPC vs. AER/ DOTAP:chol:DOPC	ns	ns	*	ns	ns	ns
AER/DDA:DOPC vs. AER/DDA:chol:DOPC	ns	ns	ns	ns	ns	ns
AER/DDA:DOPC vs. AER/EPC:chol:DOPC	ns	ns	ns	ns	*	ns
AER/DDA:DOPC vs. AER/GL-67:DOPC	*	ns	*	ns	**	ns
AER/DDA:DOPC vs. AER/DC-chol:DSPC	ns	*	ns	ns	ns	ns
AER/DDA:DOPC vs. AER/DODMA:DOPC	ns	ns	ns	ns	ns	ns
AER/DDA:DOPC vs. AER/ DODMA:chol:DOPC	ns	ns	ns	ns	ns	ns

Uncorrected Dunn's test	Significance					
	CD40	CD80	CD83	CD86	CCR7	HLA-DR
AER/EPC:DOPC vs. AER/DOTAP:chol:DOPC	ns	ns	ns	ns	ns	ns
AER/EPC:DOPC vs. AER/DDA:chol:DOPC	ns	ns	ns	ns	ns	ns
AER/EPC:DOPC vs. AER/EPC:chol:DOPC	ns	ns	ns	ns	ns	ns
AER/EPC:DOPC vs. AER/GL-67:DOPC	ns	ns	ns	ns	*	ns
AER/EPC:DOPC vs. AER/DC-chol:DSPC	ns	ns	ns	ns	ns	*
AER/EPC:DOPC vs. AER/DODMA:DOPC	ns	ns	*	ns	ns	ns
AER/EPC:DOPC vs. AER/ DODMA:chol:DOPC	ns	ns	ns	ns	ns	ns
AER/DOTAP:chol:DOPC vs. AER/ DDA:chol:DOPC	ns	ns	ns	ns	ns	ns
AER/DOTAP:chol:DOPC vs. AER/ EPC:chol:DOPC	ns	ns	ns	ns	ns	ns
AER/DOTAP:chol:DOPC vs. AER/GL-67:DOPC	ns	ns	ns	ns	ns	ns
AER/DOTAP:chol:DOPC vs. AER/DC-chol:DSPC	ns	ns	*	*	ns	**
AER/DOTAP:chol:DOPC vs. AER/ DODMA:DOPC	**	ns	***	*	**	*
AER/DOTAP:chol:DOPC vs. AER/ DODMA:chol:DOPC	ns	ns	ns	ns	*	ns
AER/DDA:chol:DOPC vs. AER/ EPC:chol:DOPC	ns	ns	ns	ns	ns	ns
AER/DDA:chol:DOPC vs. AER/GL-67:DOPC	ns	ns	ns	ns	ns	ns
AER/DDA:chol:DOPC vs. AER/DC-chol:DSPC	ns	ns	ns	ns	ns	*
AER/DDA:chol:DOPC vs. AER/ DODMA:DOPC	**	ns	**	ns	**	ns
AER/DDA:chol:DOPC vs. AER/ DODMA:chol:DOPC	ns	ns	ns	ns	*	ns
AER/EPC:chol:DOPC vs. AER/GL-67:DOPC	ns	ns	ns	ns	ns	*
AER/EPC:chol:DOPC vs. AER/DC-chol:DSPC	ns	*	*	*	ns	***
AER/EPC:chol:DOPC vs. AER/ DODMA:DOPC	**	ns	***	**	**	*
AER/EPC:chol:DOPC vs. AER/ DODMA:chol:DOPC	ns	ns	ns	ns	**	ns
AER/GL-67:DOPC vs. AER/DC-chol:DSPC	ns	ns	*	ns	*	ns
AER/GL-67:DOPC vs. AER/DODMA:DOPC	***	ns	****	ns	****	ns
AER/GL-67:DOPC vs. AER/ DODMA:chol:DOPC	ns	ns	ns	ns	***	ns

Uncorrected Dunn's test	Significance					
	CD40	CD80	CD83	CD86	CCR7	HLA-DR
AER/DC-chol:DSPC vs. AER/DODMA:DOPC	*	*	ns	ns	ns	ns
AER/DC-chol:DSPC vs. AER/DODMA:chol:DOPC	ns	**	ns	ns	ns	**
AER/DODMA:DOPC vs. AER/DODMA:chol:DOPC	ns	ns	*	ns	ns	ns

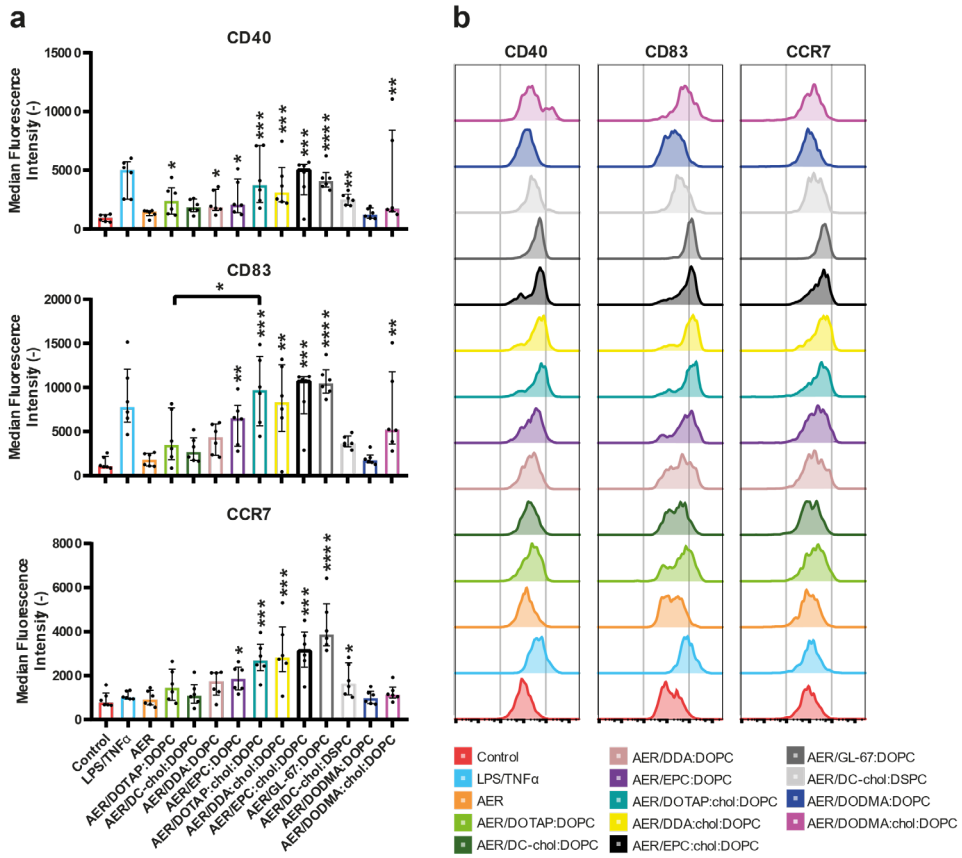

Figure S2. Upregulation of surface activation markers in MDDCs in the second experiment with selected liposomal formulations. A) Median fluorescence intensities related to expression of indicated (selected) activation markers: CD40, CD83 and CCR7. B) Upregulation of the surface activation markers as concatenated flow cytometry data of all donors, n = 7. The statistical significance was measured by the Kruskal-Wallis and Uncorrected Dunn's test, and the formulations were compared to the control.

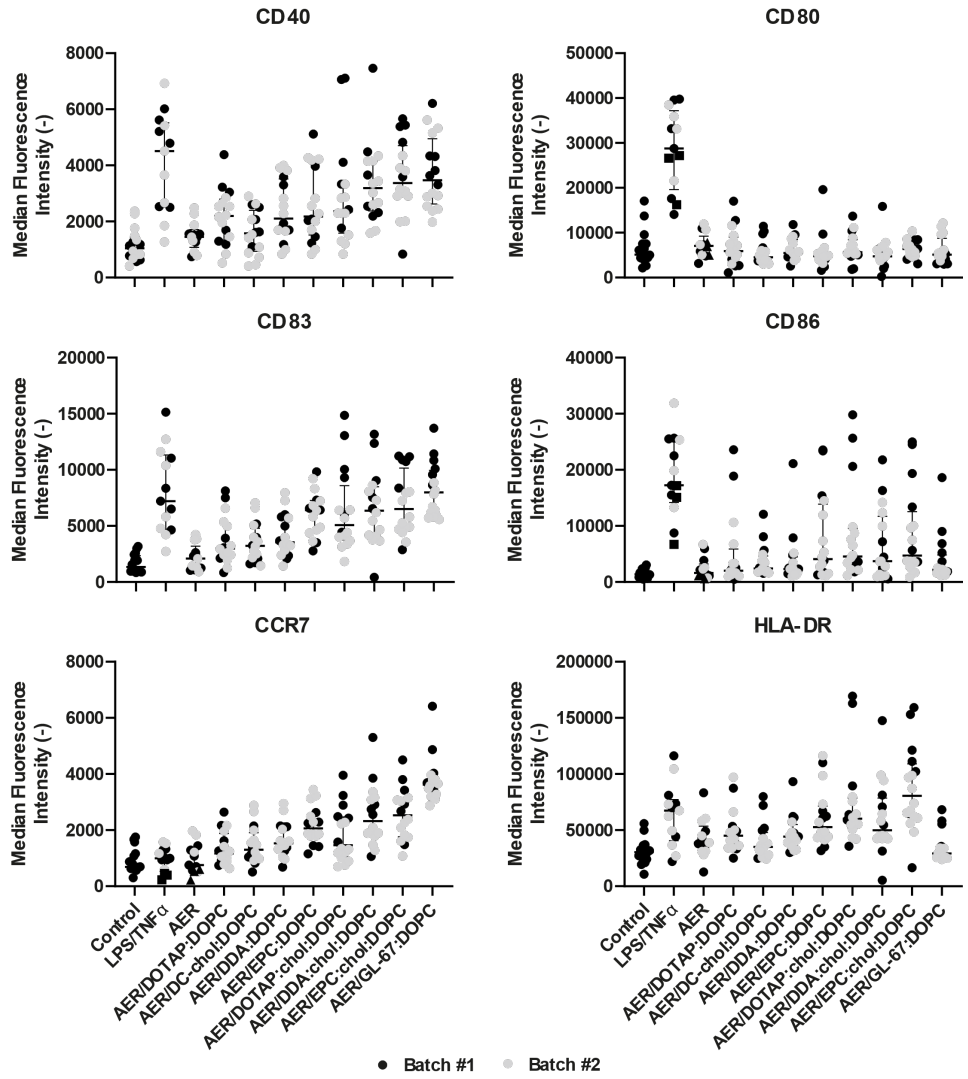

Figure S3. Upregulation of surface activation markers in two experiments using MDDCs (the black dots are from the first experiment reported in the main manuscript, and the grey dots are the repeat of this experiment). Median fluorescence intensities related to the expression of the indicated activation markers. The statistical significance is not shown.

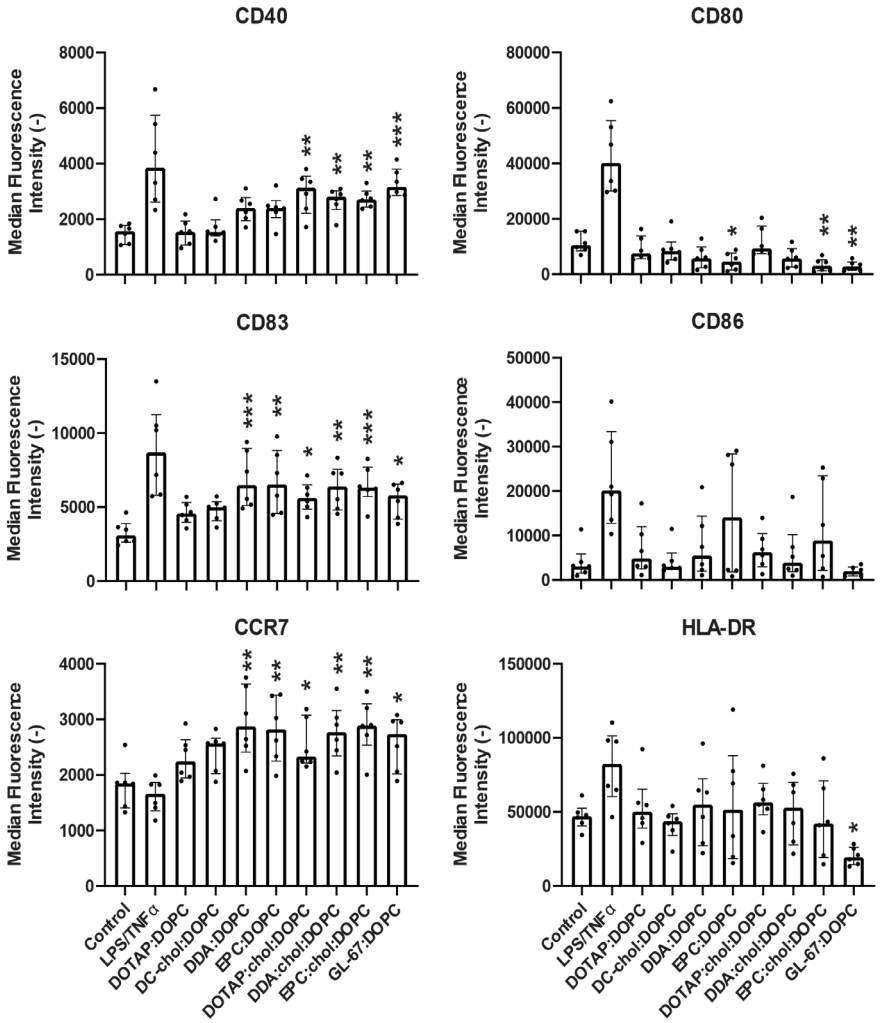

Figure S4. Upregulation of surface activation markers in MDDCs after stimulation with empty (antigen-free) liposomal formulations. Median fluorescence intensities related to the expression of indicated activation markers, n = 5. The statistical significance was measured by Kruskal-Wallis and Uncorrected Dunn's test, and the formulations were compared to the control.

Table S3. Statistical comparisons between different groups (uptake) as measured by Kruskal-Wallis and Uncorrected Dunn's test (Figure 3a). ns $p > 0.05$, * $p < 0.05$, ** $p < 0.01$, *** $p < 0.001$, **** $p < 0.0001$.

Uncorrected Dunn's test	p-value
Control vs. DOTAP:DOPC	***
Control vs. DC-chol:DOPC	****
Control vs. DDA:DOPC	****
Control vs. EPC:DOPC	****
Control vs. DOTAP:chol:DOPC	****
Control vs. DDA:chol:DOPC	****
Control vs. EPC:chol:DOPC	****
Control vs. GL-67:DOPC	****
Control vs. DODMA:DOPC	ns
Control vs. DODMA:chol:DOPC	ns
Control vs. Unlabeled liposomes	ns
DOTAP:DOPC vs. DC-chol:DOPC	ns
DOTAP:DOPC vs. DDA:DOPC	ns
DOTAP:DOPC vs. EPC:DOPC	ns
DOTAP:DOPC vs. DOTAP:chol:DOPC	*
DOTAP:DOPC vs. DDA:chol:DOPC	ns
DOTAP:DOPC vs. EPC:chol:DOPC	*
DOTAP:DOPC vs. GL-67:DOPC	ns
DOTAP:DOPC vs. DODMA:DOPC	*
DOTAP:DOPC vs. DODMA:chol:DOPC	*
DOTAP:DOPC vs. Unlabeled liposomes	***
DC-chol:DOPC vs. DDA:DOPC	ns
DC-chol:DOPC vs. EPC:DOPC	ns
DC-chol:DOPC vs. DOTAP:chol:DOPC	ns
DC-chol:DOPC vs. DDA:chol:DOPC	ns
DC-chol:DOPC vs. EPC:chol:DOPC	ns
DC-chol:DOPC vs. GL-67:DOPC	ns
DC-chol:DOPC vs. DODMA:DOPC	**
DC-chol:DOPC vs. DODMA:chol:DOPC	**
DC-chol:DOPC vs. Unlabeled liposomes	****
DDA:DOPC vs. EPC:DOPC	ns
DDA:DOPC vs. DOTAP:chol:DOPC	ns
DDA:DOPC vs. DDA:chol:DOPC	ns
DDA:DOPC vs. EPC:chol:DOPC	ns

Uncorrected Dunn's test	p-value
DDA:DOPC vs. GL-67:DOPC	ns
DDA:DOPC vs. DODMA:DOPC	***
DDA:DOPC vs. DODMA:chol:DOPC	***
DDA:DOPC vs. Unlabeled liposomes	****
EPC:DOPC vs. DOTAP:chol:DOPC	ns
EPC:DOPC vs. DDA:chol:DOPC	ns
EPC:DOPC vs. EPC:chol:DOPC	ns
EPC:DOPC vs. GL-67:DOPC	ns
EPC:DOPC vs. DODMA:DOPC	***
EPC:DOPC vs. DODMA:chol:DOPC	***
EPC:DOPC vs. Unlabeled liposomes	****
DOTAP:chol:DOPC vs. DDA:chol:DOPC	ns
DOTAP:chol:DOPC vs. EPC:chol:DOPC	ns
DOTAP:chol:DOPC vs. GL-67:DOPC	ns
DOTAP:chol:DOPC vs. DODMA:DOPC	****
DOTAP:chol:DOPC vs. DODMA:chol:DOPC	****
DOTAP:chol:DOPC vs. Unlabeled liposomes	****
DDA:chol:DOPC vs. EPC:chol:DOPC	ns
DDA:chol:DOPC vs. GL-67:DOPC	ns
DDA:chol:DOPC vs. DODMA:DOPC	***
DDA:chol:DOPC vs. DODMA:chol:DOPC	***
DDA:chol:DOPC vs. Unlabeled liposomes	****
EPC:chol:DOPC vs. GL-67:DOPC	ns
EPC:chol:DOPC vs. DODMA:DOPC	****
EPC:chol:DOPC vs. DODMA:chol:DOPC	****
EPC:chol:DOPC vs. Unlabeled liposomes	****
GL-67:DOPC vs. DODMA:DOPC	****
GL-67:DOPC vs. DODMA:chol:DOPC	****
GL-67:DOPC vs. Unlabeled liposomes	****
DODMA:DOPC vs. DODMA:chol:DOPC	ns
DODMA:DOPC vs. Unlabeled liposomes	ns
DODMA:chol:DOPC vs. Unlabeled liposomes	ns

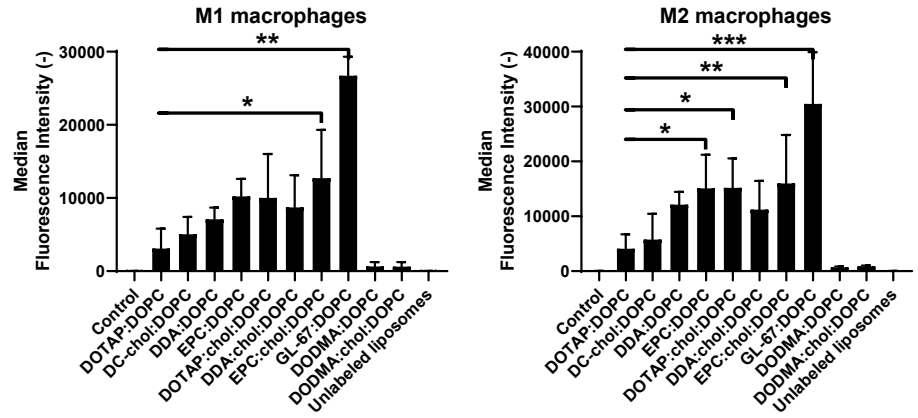

Figure S5. Uptake in monocyte-derived macrophages of pro-inflammatory M1 (GM-CSF differentiated) and anti-inflammatory M2 (M-CSF differentiated) macrophages. The statistical significance was measured by the Kruskal-Wallis and Uncorrected Dunn's test, and the formulations were compared to the DOTAP:DOPC formulation.

Table S4. Physicochemical properties of selected formulations after preparation and 4 or 7 months after. n = 1 (batches)

DOPC:DOTAP/AER			
Time (months)	PDI	Z-average size (nm)	Z-potential (mV)
0	0.15 ± 0.01	128.1 ± 0.6	30.8 ± 0.5
7	0.16 ± 0.01	129.7 ± 0.5	30.5 ± 0.6
DOPC-DOTAP (empty)			
Time (months)	PDI	Z-average size (nm)	Z-potential (mV)
0	0.12 ± 0.02	157.8 ± 0.5	33.4 ± 0.4
7	0.14 ± 0.01	156.9 ± 0.3	30.2 ± 0.3
DOPC -DC-Chol/AER			
Time (months)	PDI	Z-average size (nm)	Z-potential (mV)
0	0.26 ± 0.01	90.5 ± 0.1	29.2 ± 0.5
4	0.28 ± 0.01	97.8 ± 1.0	30.4 ± 0.3

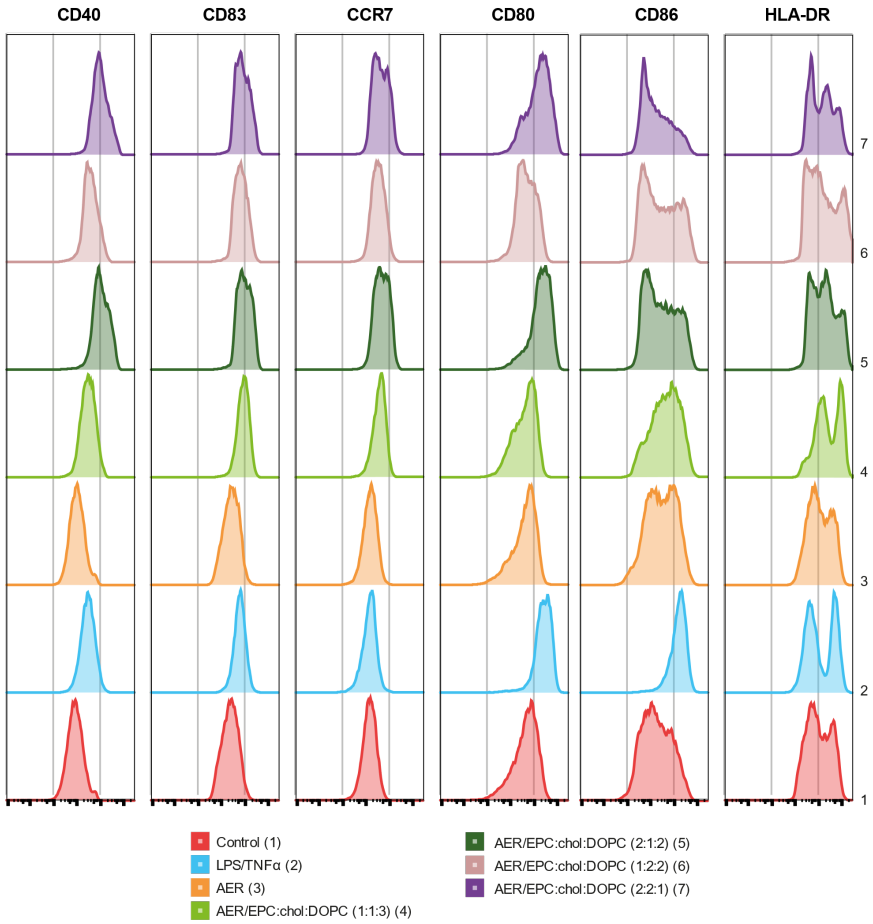

Figure S6. Upregulation of surface activation markers in MDDCs after stimulation with medium (control), LPS/TNFα cocktail (100 and 5 ng/ml, respectively), AER (5 µg/ml) and liposomal formulations (5 µg/ml AER, 250 µg/ml liposomes, exposure 1 hour). Upregulation of the surface activation markers is presented as concatenated flow cytometry data of all donors, n = 7.

Table S5. Statistical comparisons between different groups as measured by Kruskal-Wallis and Uncorrected Dunn's test (Figure 4a). ns $p > 0.05$, * $p < 0.05$, ** $p < 0.01$, *** $p < 0.001$, **** $p < 0.0001$.

Uncorrected Dunn's test	Significance					
0.5 µg/ml AER / 25 µg/ml lipids	CD40	CD80	CD83	CD86	CCR7	HLA-DR
Control vs. LPS/TNFα	****	*	***	****	ns	ns
Control vs. AER	ns	ns	ns	ns	ns	ns
Control vs. AER/EPC:chol:DOPC 1:1:3	ns	ns	ns	ns	ns	ns
Control vs. AER/EPC:chol:DOPC 2:1:2	**	ns	****	**	**	***
Control vs. AER/EPC:chol:DOPC 1:2:2	ns	ns	ns	ns	ns	*
Control vs. AER/EPC:chol:DOPC 2:2:1	**	ns	****	**	**	***
LPS/TNFα vs. AER	***	**	**	***	ns	ns
LPS/TNFα vs. AER/EPC:chol:DOPC 1:1:3	****	***	*	**	ns	ns
LPS/TNFα vs. AER/EPC:chol:DOPC 2:1:2	ns	***	ns	ns	***	*
LPS/TNFα vs. AER/EPC:chol:DOPC 1:2:2	**	**	*	**	ns	ns
LPS/TNFα vs. AER/EPC:chol:DOPC 2:2:1	ns	***	ns	ns	***	ns
AER vs. AER/EPC:chol:DOPC 1:1:3	ns	ns	ns	ns	ns	ns
AER vs. AER/EPC:chol:DOPC 2:1:2	*	ns	***	*	**	*
AER vs. AER/EPC:chol:DOPC 1:2:2	ns	ns	ns	ns	ns	ns
AER vs. AER/EPC:chol:DOPC 2:2:1	**	ns	***	*	**	*
AER/EPC:chol:DOPC 1:1:3 vs. AER/EPC:chol:DOPC 2:1:2	**	ns	*	ns	ns	ns
AER/EPC:chol:DOPC 1:1:3 vs. AER/EPC:chol:DOPC 1:2:2	ns	ns	ns	ns	ns	ns
AER/EPC:chol:DOPC 1:1:3 vs. AER/EPC:chol:DOPC 2:2:1	**	ns	*	ns	ns	ns
AER/EPC:chol:DOPC 2:1:2 vs. AER/EPC:chol:DOPC 1:2:2	ns	ns	**	ns	*	ns
AER/EPC:chol:DOPC 2:1:2 vs. AER/EPC:chol:DOPC 2:2:1	ns	ns	ns	ns	ns	ns
AER/EPC:chol:DOPC 1:2:2 vs. AER/EPC:chol:DOPC 2:2:1	*	ns	**	ns	*	ns

Uncorrected Dunn's test	Significance					
2 µg/ml AER / 100 µg/ml lipids	CD40	CD80	CD83	CD86	CCR7	HLA-DR
Control vs. LPS/TNFα	**	**	ns	****	ns	ns
Control vs. AER	ns	ns	ns	ns	ns	ns
Control vs. AER/EPC:chol:DOPC 1:1:3	ns	ns	***	ns	**	**
Control vs. AER/EPC:chol:DOPC 2:1:2	****	ns	****	****	***	**
Control vs. AER/EPC:chol:DOPC 1:2:2	**	ns	***	ns	**	****
Control vs. AER/EPC:chol:DOPC 2:2:1	****	ns	***	***	***	**
LPS/TNFα vs. AER	**	***	ns	***	ns	ns
LPS/TNFα vs. AER/EPC:chol:DOPC 1:1:3	ns	****	ns	*	**	*
LPS/TNFα vs. AER/EPC:chol:DOPC 2:1:2	ns	*	*	ns	***	*
LPS/TNFα vs. AER/EPC:chol:DOPC 1:2:2	ns	****	ns	*	**	**
LPS/TNFα vs. AER/EPC:chol:DOPC 2:2:1	*	ns	*	ns	***	*
AER vs. AER/EPC:chol:DOPC 1:1:3	ns	ns	**	ns	**	*
AER vs. AER/EPC:chol:DOPC 2:1:2	****	ns	***	***	***	*
AER vs. AER/EPC:chol:DOPC 1:2:2	*	ns	***	ns	**	**
AER vs. AER/EPC:chol:DOPC 2:2:1	****	ns	***	**	***	*
AER/EPC:chol:DOPC 1:1:3 vs. AER/ EPC:chol:DOPC 2:1:2	**	ns	ns	*	ns	ns
AER/EPC:chol:DOPC 1:1:3 vs. AER/ EPC:chol:DOPC 1:2:2	ns	ns	ns	ns	ns	ns
AER/EPC:chol:DOPC 1:1:3 vs. AER/ EPC:chol:DOPC 2:2:1	***	*	ns	ns	ns	ns
AER/EPC:chol:DOPC 2:1:2 vs. AER/ EPC:chol:DOPC 1:2:2	ns	ns	ns	*	ns	ns
AER/EPC:chol:DOPC 2:1:2 vs. AER/ EPC:chol:DOPC 2:2:1	ns	ns	ns	ns	ns	ns
AER/EPC:chol:DOPC 1:2:2 vs. AER/ EPC:chol:DOPC 2:2:1	*	*	ns	ns	ns	ns

Uncorrected Dunn's test	Significance					
5 µg/ml AER / 250 µg/ml lipids	CD40	CD80	CD83	CD86	CCR7	HLA-DR
Control vs. LPS/TNFα	*	***	*	***	ns	ns
Control vs. AER	ns	ns	ns	ns	ns	ns
Control vs. AER/EPC:chol:DOPC 1:1:3	ns	ns	****	*	**	****
Control vs. AER/EPC:chol:DOPC 2:1:2	****	**	****	ns	****	**
Control vs. AER/EPC:chol:DOPC 1:2:2	**	ns	*	ns	*	*
Control vs. AER/EPC:chol:DOPC 2:2:1	****	**	***	ns	***	ns
LPS/TNFα vs. AER	*	***	*	**	ns	ns
LPS/TNFα vs. AER/EPC:chol:DOPC 1:1:3	ns	***	ns	ns	**	***
LPS/TNFα vs. AER/EPC:chol:DOPC 2:1:2	*	ns	*	**	****	ns
LPS/TNFα vs. AER/EPC:chol:DOPC 1:2:2	ns	***	ns	**	*	ns
LPS/TNFα vs. AER/EPC:chol:DOPC 2:2:1	*	ns	ns	****	****	ns
AER vs. AER/EPC:chol:DOPC 1:1:3	ns	ns	***	ns	**	***
AER vs. AER/EPC:chol:DOPC 2:1:2	****	**	****	ns	****	ns
AER vs. AER/EPC:chol:DOPC 1:2:2	**	ns	ns	ns	ns	ns
AER vs. AER/EPC:chol:DOPC 2:2:1	****	**	**	ns	***	ns
AER/EPC:chol:DOPC 1:1:3 vs. AER/ EPC:chol:DOPC 2:1:2	**	**	ns	ns	ns	ns
AER/EPC:chol:DOPC 1:1:3 vs. AER/ EPC:chol:DOPC 1:2:2	ns	ns	ns	ns	ns	ns
AER/EPC:chol:DOPC 1:1:3 vs. AER/ EPC:chol:DOPC 2:2:1	**	**	ns	**	ns	**
AER/EPC:chol:DOPC 2:1:2 vs. AER/ EPC:chol:DOPC 1:2:2	ns	**	*	ns	*	ns
AER/EPC:chol:DOPC 2:1:2 vs. AER/ EPC:chol:DOPC 2:2:1	ns	ns	ns	ns	ns	ns
AER/EPC:chol:DOPC 1:2:2 vs. AER/ EPC:chol:DOPC 2:2:1	ns	**	ns	ns	ns	ns

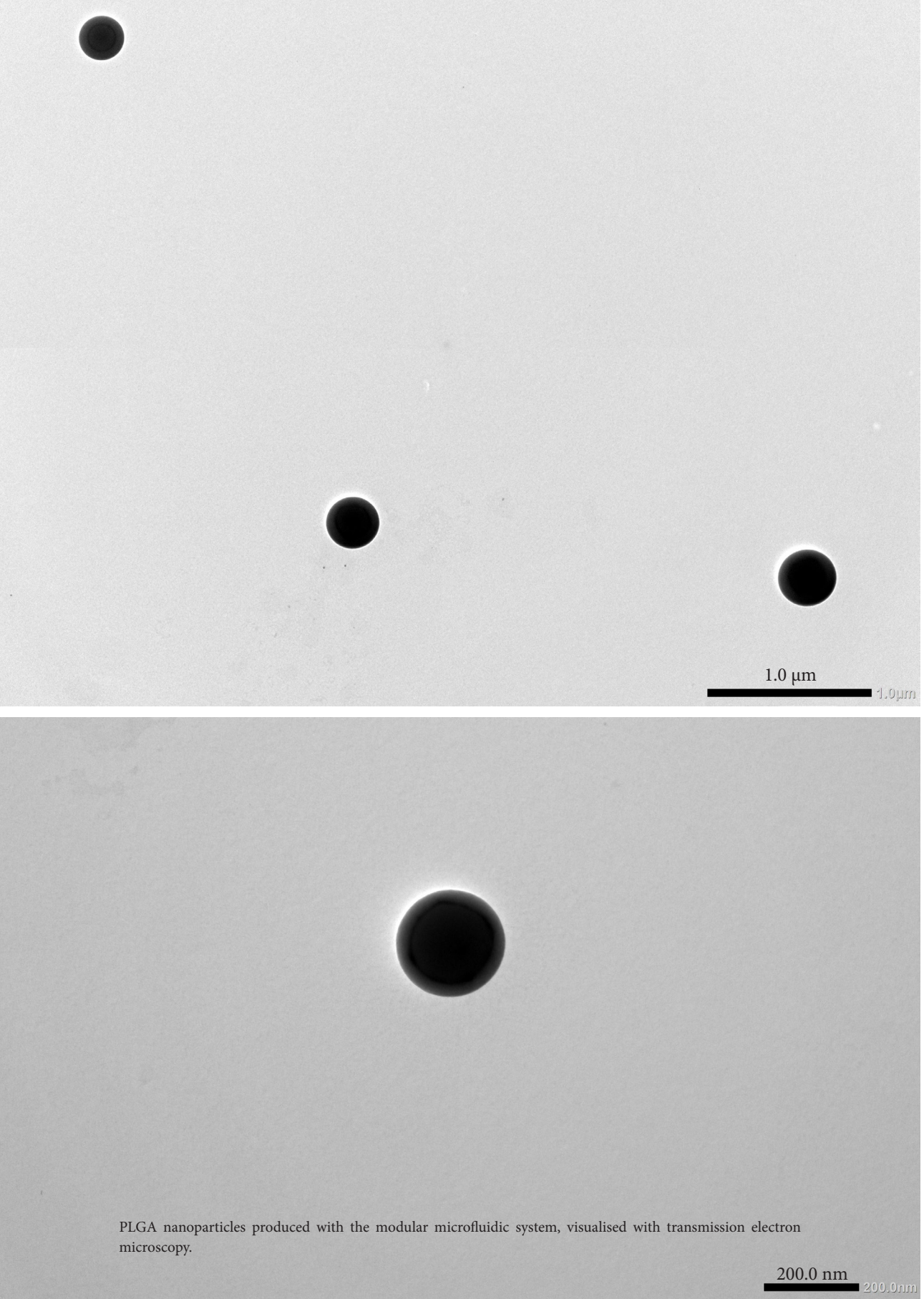

PLGA nanoparticles produced with the modular microfluidic system, visualised with transmission electron microscopy.

CHAPTER 3

A VERSATILE, LOW-COST MODULAR MICROFLUIDIC SYSTEM TO PREPARE POLY(LACTIC-*CO*-GLYCOLIC ACID) NANOPARTICLES WITH ENCAPSULATED PROTEIN

Adapted from Pharm Res. 2024;41(12):2347-61

M.A. Neustrup[1,2], T.H.M. Ottenhoff[2], W. Jiskoot[1], J.A. Bouwstra[1], K. van der Maaden[1,3]

[1] Division of BioTherapeutics, Leiden Academic Centre for Drug Research, Leiden University, Leiden, The Netherlands
[2] Department of Infectious Diseases, Leiden University Medical Center, Leiden, The Netherlands
[3] Tumor Immunology Group, Department of Immunology, Leiden University Medical Center, Leiden, The Netherlands

ABSTRACT

Microfluidics has emerged as a promising technique to prepare nanoparticles. However, the current microfluidic devices are mainly chip-based and are often integrated into expensive systems that lack on-the-spot versatility. The aim of this study was to set up a modular microfluidic system based on low-cost capillaries and reusable, easy-to-clean building blocks that can prepare poly(D,L-lactic-*co*-glycolic acid) (PLGA) nanoparticles with and without incorporated water-soluble biomacromolecules. A two-syringe system variant of the microfluidic system was set up to prepare PLGA particles and to investigate how the flow rates, solvents, and PLGA concentrations impacted the PLGA nanoparticle formation. A three-syringe system was designed to examine the incorporation of proteins into the PLGA particles. The formation of the nanoparticles was affected by the PLGA concentration in the organic solvent, where an increasing concentration led to larger particle diameters (33–180 nm), and by the total flow rate, where an increase in the total flow rate led to smaller nanoparticles (197–77 nm). Using ultrapure water as the aqueous solvent resulted in precipitation at the outlet at higher PLGA concentrations. Aqueous poly(vinyl alcohol) created neutral particles in contrast to the negatively charged particles obtained with ultrapure water or an ethanol-water mixture. Incorporation of the proteins ovalbumin or lysozyme with a three-syringe system resulted in encapsulation efficiencies above 40%. A cheap and easily adjustable modular microfluidic system was developed to prepare PLGA nanoparticles with highly reproducible particle diameters that can effectively be loaded with proteins for drug and vaccine delivery.

INTRODUCTION

Poly(D,L-lactic-*co*-glycolic acid) (PLGA) nanoparticles fall in the size range of 10–1,000 nm [1] an are suitable for a wide range of biomedical applications, as reviewed elsewhere [2]. They have an excellent safety profile, being both biodegradable and biocompatible [3], and their properties are adjustable, allowing for the customisation of their properties to fit specific applications. For instance, the degradation rate of the particles, and thereby the release of the encapsulated drug or contrast agent, is tunable, as particles made with a PLGA polymer with higher hydrophilicity, lower crystallinity, or lower molecular weight tend to degrade faster [3]. PLGA nanoparticles are widely used in preclinical studies where they, among others, have been used in imaging [4], cancer therapies [5], as well as (subunit) vaccines with peptides [6] and proteins [7]. PLGA polymer is already approved as an excipient for human parenteral use by the U.S. Food and Drug Administration, mainly as a microparticle component of depot formulations in antibiotics, antipsychotics, diabetes, plus medications against cancer and hormonal diseases [8]. As PLGA-based products are already approved, it signifies a promising future for PLGA nanoparticles, making them an attractive option for the development of next-generation drug delivery systems with their great tunability and safety.

PLGA nanoparticles are mainly produced by two methods: emulsion-based methods, where a water-immiscible or partly water-immiscible organic solvent containing dissolved PLGA is emulsified in an aqueous solution with a surfactant, and nanoprecipitation methods, where a water-miscible organic solvent containing dissolved PLGA is mixed with an aqueous solution [9, 10]. The emulsification process is conventionally carried out with techniques such as sonication, high-shear mixing, or high-pressure homogenisation, while nanoprecipitation usually is carried out by adding an organic solvent with dissolved PLGA drop-wise to an aqueous formulation under mechanical stirring [9, 10]. While these techniques allow for manipulation of the nanoparticle diameter by varying factors, such as the PLGA concentration and the surfactant concentration [10], the batch-to-batch reproducibility is low [11], and the nanoparticles are rarely below 100 nm [10]. Microfluidics, a technique that enables the manipulation of fluid streams through microscale fluidic channels, has emerged to overcome these problems, offering precise control of the nanoparticle diameter, greater batch-to-batch reproducibility, and a narrower particle size distribution [12]. While emulsion-based microfluidics, also called droplet-based microfluidics, tend to generate micrometre-sized particles, nanoprecipitation microfluidics, also called continuous microfluidics, tend to generate nano-sized particles [13]. This particle diameter control is particularly important in vaccination, where the particle diameter and other factors, such as surface charge and rigidity, affect the cellular uptake and influence the immune response [14–16]. In addition to size control, microfluidics can reduce solvent waste during production and result in shorter preparation times, as it allows for one-step nanoparticle assembly [10].

Incorporation of active pharmaceutical ingredients into PLGA micro- and nanoparticles using microfluidic systems has mainly been applied for small hydrophobic drugs, such as bupivacaine, risperidone, ibuprofen, and paclitaxel, and small hydrophilic drugs such as doxorubicin hydrochloride [13]. Only very few research groups study the incorporation of large water-soluble biomacromolecules, such as proteins, with microfluidic systems. Recently, the proteins ovalbumin, bovine serum albumin, and a fusion protein have been incorporated into PLGA nanoparticles (with different lactide-to-glycolide ratios) with encapsulation efficiencies ranging from 7 to 38% with loading capacities of 0.5 to 3.1 wt% with a microfluidic system [17]. That study used a microfluidic system called Nanoassemblr®, which combines two fluids via a herringbone [17]. Although the Nanoassemblr® system can incorporate various compounds into PLGA nanoparticles, the system is quite expensive and cannot easily be rebuilt for formulations requiring more optimisation.

In this research, we developed a versatile, low-cost modular microfluidic system that enables the combination of multiple fluid flows. As a starting point, a two-syringe system, whose fluids meet in a co-flow, was set up to determine critical parameters for the preparation of the PLGA nanoparticles. Different solvents, PLGA concentrations, and solvent flows were used to delimit how these factors affect nanoparticle formation. Based on these results, a three-syringe system was designed to incorporate two water-soluble proteins with different physicochemical properties: i) ovalbumin, a protein with a molecular size of 42.7 kDa [18] which is negatively charged at pH 7.4 [19], and ii) lysozyme, a protein with a molecular size of 14.3 kDa [20], which is positively charged at pH 7.4 [21]. Using our novel nanoparticle preparation system, we obtained PLGA nanoparticles with tunable nanoparticle diameters and well-defined physicochemical properties. Moreover, we show that proteins with different properties are effectively loaded into PLGA nanoparticles using this modular microfluidics system.

MATERIALS AND METHODS

Materials

NE300 syringe pumps were purchased from ProSense B.V. (Oosterhout, The Netherlands). Pierce Micro bicinchoninic acid protein assay kit, 500 µL Hamilton® Gastight® syringes from the 1700 series with polytetrafluoroethylene (PTFE) Luer-lock terminations, disposable polystyrene BRAND® Macro cuvettes, and polyether ether ketone (PEEK) capillary tubing with an inner diameter (ID) of 0.02" (0.5 mm) and an outer diameter (OD) of 1/16" (1.6 mm), were bought from Fisher Emergo B.V. (Landsmeer, the Netherlands). 10 mL Hamilton® Gastight® syringes from the 1000 series with PTFE Luer-lock termination were purchased from Brunschwig Chemie B.V (Amsterdam, the Netherlands). A PTFE tube with an ID of 1.6 mm was purchased from Waters Chromatography B.V. (Etten-Leur, the Netherlands). The following CapTite™ microfluidic components were purchased from Mengel Engineering (Virum, Denmark): one-piece fittings in PEEK for tubes with an ID of 1/16" (1.6-mm fittings), one-piece fittings in PEEK for capillaries with an ID of 360 µm (360-µm fittings), female fitting Luer-lock adapters in PEEK for capillaries with an ID of 360 µm (Luer-lock adapters), 360 µm to 1/16" two-piece adapters in PEEK (360-µm-to-1.6-mm adapters), 1/16" to 360 µm two-piece adapters in PEEK (1.6-mm-to-360-µm adapters), interconnect tee in Ultem® 1000 resin (untreated polyetherimide) for tubes with an ID of 1/16" (1.6-mm-interconnect tee) and interconnect tee in Ultem® 1000 polyetherimide for capillaries with an ID of 360 µm (360-µm-interconnect tee). Polyimide-coated fused silica capillary tubing with IDs of 75 ± 3 µm and 250 ± 6 µm with IDs of 363 ± 10 µm and 360 ± 10 µm, respectively, were purchased from BGB Analytic Benelux B.V. (Harderwijk, the Netherlands). Poly(D,L-lactic-*co*-glycolic acid) (PLGA) (acid terminated, lactide:glycolide 50:50, Mw 24,000-38,000), sodium dodecyl sulphate with a minimum purity of 99.0%, sodium phosphate dibasic dihydrate with a purity of 99.5%, sodium phosphate monobasic dihydrate with a minimum purity of 99.0%, and pure sodium hydroxide pellets were purchased from Merck Chemicals B.V. (Amsterdam, the Netherlands). Lysozyme from chicken egg white with a protein content not less than 90% (measured with UV absorbance) (pI 11.35, electrophoretic analyses were performed in buffers of ionic strength of 0.1 [21]) and poly(vinyl alcohol) (Mw ~31,000) (PVA) were purchased from Sigma-Aldrich Chemie B.V. (Zwijndrecht, the Netherlands). Analytical grade dimethyl sulfoxide (DMSO) with a purity over 99% and HPLC-R grade acetonitrile with a purity over 99.9% were purchased from Biossolve B.V. (Valkenswaard, the Netherlands). EndoFit™ Ovalbumin (chicken egg albumin for in-vivo use) (pI 4.4, measured in 10 mM phosphate buffer at a concentration of 1 mg/mL [19]) with a minimum purity of 98% was purchased from InvivoGen®, Bio-Connect B.V. (Huissen, the Netherlands). Ethyl acetate with a minimum purity of 99.9 vol%, 96 vol% ethanol, and acetone with a minimum purity of 99.8 vol% were purchased from Boom B.V. (Meppel, the Netherlands). Spectra-Por® Milli-Q® water (ultrapure water), with a resistivity of 18.2 MΩ/cm at 25°C, was tapped from a Milli-Q® Advantage A10 water purification system (Merck).

Setup of the microfluidic system

The PLGA nanoparticles were prepared with a modular microfluidic system assembled as either a two-syringe system or a three-syringe system, as depicted in Fig. 1. To assemble the core component, a 1.6-mm-interconnect tee with three ports in a T shape designated Port 1, Port 2, and Port 3, where Port 1 and 3 were opposite of each other, and Port 2 was positioned at an angle of 90°, was connected through Port 3 to a 7 cm long piece of PEEK tube with a 1.6-mm fitting. A 360-µm-to-1.6-mm adapter was attached to a Luer-lock adapter and screwed on Syringe 1 (a 10-mL syringe). Hereafter, a 20 cm long PTFE tube with an ID of 1.6 mm was attached to it with a 1.6-mm fitting. The other end of the PTFE tube was connected to Port 2 with a 1.6-mm fitting. When the tubes were attached, they were first pushed fully into the 1.6-mm-interconnect tee before the 1.6-mm fitting was screwed on. A 1.6-mm-to-360-µm adapter was connected to Port 1.

As the first step of assembling the attachment of the two-syringe system, a Luer-lock adapter was screwed on Syringe 2 (a 10-mL syringe). A 14 cm long capillary with an ID of 250 µm was attached to the Luer-lock adapter with a 360-µm fitting. When the capillary was attached to the Luer-lock adapter, the capillary was pushed to the end of the 360-µm fitting tip before insertion. The other end of the capillary was attached to the core component by inserting it through a 360-µm fitting and pushing it through the 1.6-mm-interconnect tee and PEEK tube till it reached 1 cm through the PEEK tube, after which the 360-µm fitting was screwed on the 1.6-mm-to-360-µm adapter.

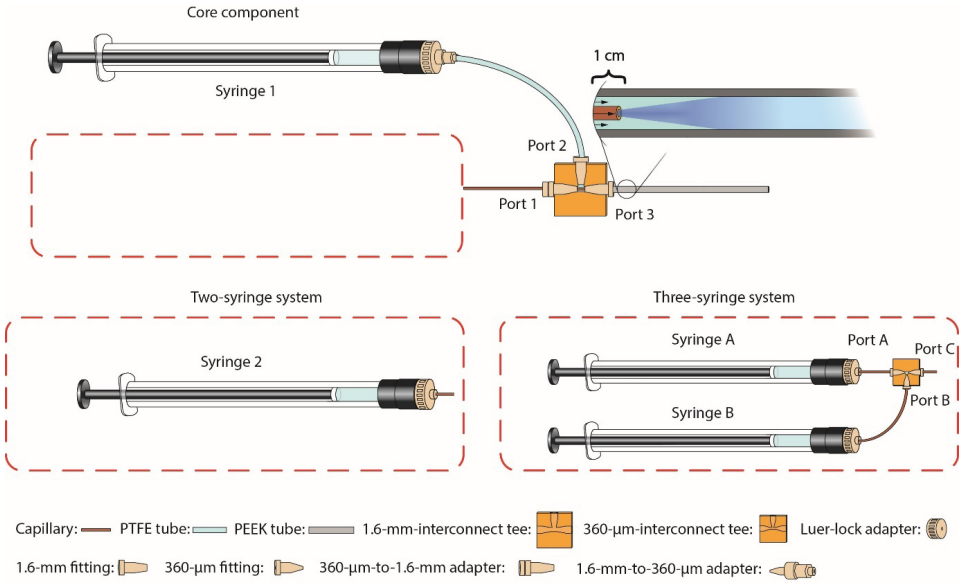

Figure 1. Schematic representation of the modular microfluidic system. The core component consists of Syringe 1 that is connected through a clear tube to an interconnect tee (yellow). A capillary (brown) passes laterally through the interconnect tee (via Ports 1 and 3) and extends 1 cm into the PEEK tube (grey). This allows for a co-flow, where the fluid from Syringe 1 constitutes the outer flow. The fluid from the capillary constitutes the inner flow and comes either from Syringe 2, making it a two-syringe system, or the combined fluid from Syringe A and Syringe B, making it a three-syringe system. PTFE: polytetrafluoroethylene, PEEK: polyether ether ketone.

As the first step of assembling the attachment for the three-syringe system, Luer-lock adapters were screwed on Syringe A (a 500-µL syringe) and Syringe B (a 10-mL syringe). Two 14 cm long capillaries with IDs of 75 µm and 250 µm were attached to the Luer-lock adapters with 360-µm fittings on Syringe A and Syringe B, respectively. A 360-µm-interconnect tee with three ports in a T shape designated Port A, Port B, and Port C, where Port A and C were opposite of each other, and Port B was positioned at an angle of 90° from Port A and B, was connected through Port A to the capillary from Syringe A with a 360-µm fitting. The capillary from Syringe B was connected to Port B with a 360-µm fitting. Port C was connected to a 14 cm long capillary with an ID of 250 µm using a 360-µm fitting. The other end of the capillary attached to Port C was attached to the core component, as explained in the setup of the two-syringe system.

To complete the setup, the syringes were mounted on syringe pumps. When the formulations were collected from the end of the PEEK tube, the tube was held perpendicular to the sample collectors, and an initial volume of approximately 150 µL was discarded before the sample was tapped.

Preparation of PLGA nanoparticles

Effect of solvent and PLGA concentration on nanoparticle formation

The solvents and the concentration of PLGA used in the microfluidic system may play a role in the formation and properties of the formed PLGA nanoparticles. A two-syringe system was employed to investigate how six different solvents and nine PLGA concentrations influence the formation and characteristics of the resulting nanoparticles. The total flow rate (TFR) and the flow rate ratio (FRR) were held constant at values of 5.00 mL/min and 1:3 between Syringe 2 and 1, respectively. The organic solvent in Syringe 2, where PLGA was dissolved, was acetone or acetonitrile. The aqueous solvent in Syringe 1 was ultrapure water, 20 mg/mL PVA filtered through a 0.22 µm filter, or 96 vol% ethanol mixed 1:1 (v/v) with ultrapure water (ethanol-water mixture). In total, six solvent combinations were tested: 1) acetone and ultrapure water, 2) acetone and ethanol-water mixture, 3) acetone and 20 mg/mL PVA, 4) acetonitrile and ultrapure water, 5) acetonitrile and ethanol-water mixture, and 6) acetonitrile and 20 mg/mL PVA. For each solvent combination, nine concentrations of PLGA in the organic phase were tested (0.25, 0.5, 1, 3, 5, 7, 10, 15, and 20 mg/mL). All samples were prepared in triplicate on different days, and each sample was measured three times.

Effect of flow rate on nanoparticle formation

The flow rates of the organic and aqueous fluids in the modular microfluidic system may affect the formation and properties of the formed PLGA nanoparticles. The effect of five different FRRs and eight TFRs variations on the particle formation and characteristics was investigated with the two-syringe system. A PLGA concentration of 3 mg/mL in acetonitrile was selected in combination with an ethanol-water mixture as the aqueous phase (as optimised in section 2.3.1.). To test the effect of the FRR, the TFR was held constant at 5.00 mL/min and the FRRs between the fluid in Syringe 2 and Syringe 1 were set to either 1:1, 1:2, 1:3, 1:4, or 1:5. To test the effect of the TFR, the FRR between the fluid in Syringe 1 and Syringe 2 was held constant at 1:3, and the TFRs were set to either 0.100, 0.500, 1.00, 2.00, 3.00, 4.00, 5.00, or 6.00 mL/min. All samples were prepared in triplicate on different days, and each sample was measured in triplicate. The various variables are summarised in Table 1.

Table 1. Different variables were examined in this work with the two-syringe system.

Examined	Variables	Constants
Section 2.3.1.	**Solvent in Syringe 1**	**FRR**
	Ultrapure water	1:3 between Syringe 2 and 1
	20 mg/mL PVA in ultrapure water	
PLGA concentrations and solvents	Ethanol-water mixture	
	Solvent in Syringe 2	**TFR**
	Acetone	5,000 µL/min
	Acetonitrile	
	PLGA concentration	
	0.25, 0.5, 1, 3, 5, 7, 10, 15, or 20 mg/mL	
Section 2.3.2.	**FRR between Syringe 2 and 1**	**Solvent in syringe 1**
	1:1, 1:2, 1:3, 1:4, or 1:5	10 mg/mL PVA in ultrapure water
		Solvent in Syringe 2
FRR		Acetonitrile
		PLGA concentration
		3 mg/mL
		TFR
		5,000 µL/min
Section 2.3.2.	**TFR**	**Solvent in syringe 1**
	0.100, 0.500, 1.00, 2.00, 3.00, 4.00, 5.00, or 6.00 mL/min	10 mg/mL PVA in ultrapure water
		Solvent in Syringe 2
TFR		Acetonitrile
		PLGA concentration
		3 mg/mL
		FRR
		1:3 between Syringe 2 and 1

FRR: flow rate ratio, TFR: total flow rate, PVA: poly(vinyl alcohol), PLGA: Poly(D,L-lactic-*co*-glycolic acid).

Encapsulation of proteins in PLGA nanoparticles

To study the incorporation of biomacromolecules in PLGA nanoparticles with the modular microfluidic system, two differently charged proteins were investigated in the three-syringe system (see Fig. 1) at different concentrations. Ovalbumin and lysozyme, the selected proteins, have a negative and a positive charge at physiological pH, respectively. The flow rates used for incorporating both proteins were 3.700, 0.050, and 1.250 mL/min for Syringes 1, A, and B, respectively, and the content of Syringe 1 was 10 mg/mL PVA. For incorporating ovalbumin into the PLGA nanoparticles, the content of Syringe B was 5 mg/mL PLGA in acetonitrile, and the content of Syringe A was ovalbumin in ultrapure water where seven ovalbumin concentrations were tested: 0, 1.25, 2.5, 5.0, 7.5, 10.0, 12.5 mg/mL.

For incorporating lysozyme into the PLGA nanoparticles, the content of Syringe B was 2 mg/mL PLGA in acetonitrile, and the content of Syringe A was lysozyme in ultrapure water where seven lysozyme concentrations were tested: 0, 0.5, 1.0, 2.0, 3.0, 4.0, 5.0 mg/mL. All samples were prepared in triplicate. After preparation, the organic solvents in the formulations were evaporated under a stream of nitrogen, and the nanoparticle diameters and zeta potentials were measured. For the encapsulation efficiency measurements, the obtained formulations were added to 2 mL Eppendorf vials and diluted with ultrapure water to obtain formulations with a PLGA concentration of 0.5 mg/mL.

Characterisation of the PLGA nanoparticles

Determination of the encapsulation efficiencies of ovalbumin and lysozyme

The encapsulation efficiencies of ovalbumin and lysozyme in the protein-loaded PLGA nanoparticles were determined. To determine the encapsulation efficiencies, samples were taken before centrifugation and from the supernatant after centrifugation in a Microfuge® 18 centrifuge (14,000 g, 30 min, Beckman Coulter Nederland B.V., Woerden, the Netherlands).

The samples were mixed in the volume ratio 1:1 with a mixture of 30 vol% DMSO, 0.1 M NaOH, and 10 mg/mL sodium dodecyl sulphate to disrupt the PLGA nanoparticles and incubated at 37 °C for 2 h. The standard curve was prepared with either ovalbumin or lysozyme in 15 vol% DMSO, 0.05 M NaOH, and 5 mg/mL sodium dodecyl sulphate. Each sample was prepared in triplicate and plated on a transparent flat-bottom 96-well plate (Greiner Bio-One B.V., Alphen aan den Rijn, The Netherlands). The amounts of ovalbumin or lysozyme were quantified with a micro bicinchoninic acid assay following the manufacturer's instructions. The absorbance was measured at 562 nm with a plate reader (Tecan Spark®, Männedorf, Switzerland) with the software SparkControl v3.1.
The encapsulation efficiency (EE%) was calculated using the following equation:

$$\mathrm{EE\%} = \frac{C(\textit{total protein}) - C(\textit{protein in the supernatant})}{C(\textit{total protein})} \cdot 100\%$$

Where *C(total protein)* is the concentration of either ovalbumin or lysozyme measured in the sample before it was spun down, and *C(protein in the supernatant)* is the concentration of either ovalbumin or lysozyme in the supernatant after the nanoparticles were spun down.

Determination of the particle's diameter and the zeta potential

The empty PLGA nanoparticles and the nanoparticles with proteins incorporated were measured on a Zetasizer Nano ZS equipped with a helium-neon laser (Malvern Panalytical B.V., Almelo, the Netherlands) with Zetasizer Software v7.13 to determine the intensity-weighted mean hydrodynamic particle diameters (particle diameters) and polydispersity indexes (PDIs) with dynamic light scattering (measured at a detection angle of 173°), and the zeta potentials with laser Doppler electrophoresis. Before the measurements, the

formulations were diluted in 10 mM phosphate buffer (7.5 mM Na_2HPO_4, 2.5 mM NaH_2PO_4, pH 7.4) and added to disposable BRAND™ Macro cuvettes. The zeta potential was measured with a universal dip cell (Malvern Panalytical B.V.). The measurements were performed in technical triplicates.

Statistical analyses

The data were analysed in GraphPad Prism® version 8.0.1 (GraphPad Software, CA, USA). The data were analysed with the correlation tool to investigate the relationship between the PLGA concentration, TFR, or FRR and the particle diameter, PDI, or zeta potential. Each batch was treated as an individual value, adding to the degrees of freedom. The Pearson correlation coefficient was used to determine if the correlation between the variables was positive, negative, or if there was no correlation. The significances of the correlation coefficients were determined with two-tailed tests where a p-value of < 0.05 was considered significant. A one-way analysis of variance, followed by Tukey's multiple comparisons test, was performed to compare the means where $p < 0.05$ was considered statistically significant. To determine if the solvents impacted the relationship between the PLGA concentrations and particle diameters, the significance of the difference between two slopes was calculated where $p < 0.05$ was considered statistically significant.

RESULTS

Increasing the PLGA concentration in the organic phase results in larger nanoparticles

Empty PLGA nanoparticles were prepared using the modular microfluidic system with different solvents and PLGA concentrations. Independent of the organic phase (acetone or acetonitrile) and aqueous phase (ultrapure water, 20 mg/mL PVA in ultrapure water, or an ethanol-water mixture), an increased PLGA concentration resulted in an increased particle diameter of the formed nanoparticles (see Fig. 2). The solvent choice and the PLGA concentration affected the zeta potential. At higher PLGA concentrations, the formed nanoparticles became more monodisperse (as indicated by a lower PDI).

When the aqueous phase consisted of ultrapure water, a PLGA deposit at the tip of the PEEK tube was observed at higher PLGA concentrations. The deposit was observed from 3 mg/mL when PLGA was dissolved in acetone and from 7 mg/mL when PLGA was dissolved in acetonitrile. No deposits were observed when the solvent in the aqueous phase was the ethanol-water mixture or 20 mg/mL PVA in ultrapure water. The largest particle diameter was generated in the system with 20 mg/mL PLGA in acetone as the organic phase and 20 mg/mL PVA in ultrapure water as the aqueous phase, where the particle diameter reached 181 nm, and the smallest with 0.5 mg/mL acetone as an organic phase with 20 mg/mL PVA in ultrapure water, where the particle diameter reached 33 nm. The PDIs were below 0.3 for all the formulations except those prepared with PLGA concentrations below 1 mg/mL PLGA and 20 mg/mL PVA in ultrapure water in the aqueous phase. The zeta potentials were below -16 mV when the formulations were prepared with ultrapure water or ethanol-water mixture in the aqueous phase (Fig. 3). When the formulations were prepared with 20 mg/mL PVA in ultrapure water in the aqueous phase, the nanoparticles were hardly not charged (zeta potentials between -5 to 0 mV).

Correlation statistics were performed to see if there were positive or negative correlations between the PLGA concentration and the particle diameters (see Table 2) (see Table S1 for the PDIs and zeta potentials). There were statistically significant positive correlations between the PLGA concentrations and particle diameter for all the solvent combinations (see Table 1 for the solvent combinations), meaning that increasing PLGA concentrations resulted in larger particles. Significant negative correlations existed between the PLGA concentration and the zeta potential for the solvent combinations without PVA, which instead had significant positive correlations, and the PLGA concentrations and the PDIs for all solvent combinations except for acetone and the ethanol-water mixture.

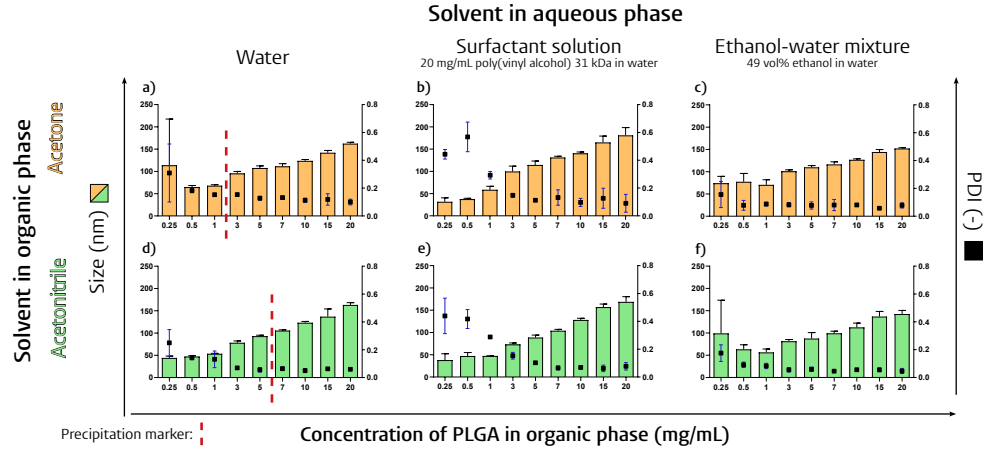

Figure 2. The influence of the PLGA concentration in the organic phase on the particle diameter and PDI of the formed PLGA nanoparticles, where the organic and aqueous phase consisted of a) acetone and ultrapure water, b) acetone and PVA in ultrapure water, c) acetone and an ethanol-water mixture d) acetonitrile and ultrapure water, e) acetonitrile and PVA in ultrapure water, f) and acetonitrile and an ethanol-water mixture, respectively. The TFR was 5,000 µL/min, and the FRR between the organic and the aqueous phase was 1:3. The precipitation marker indicates where the PLGA started to precipitate at the tip of the PEEK tube. Mean ± SD, n = 3. PDI: polydispersity index.

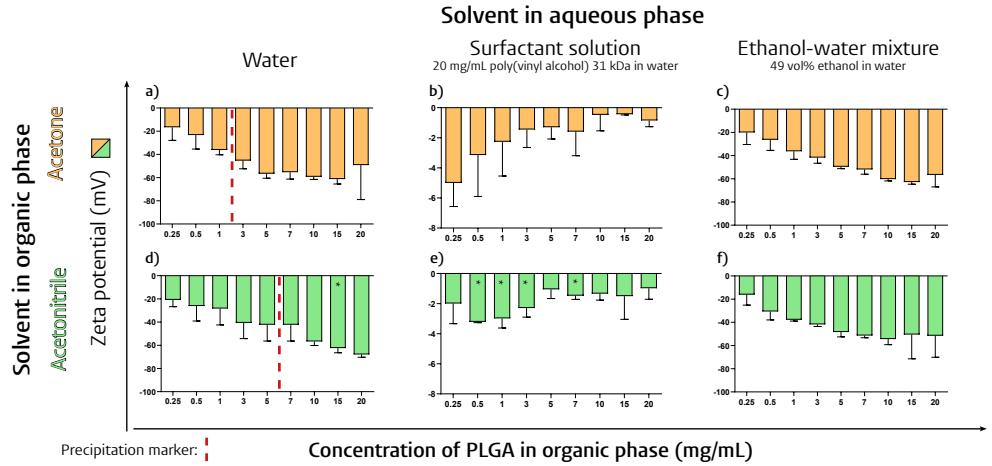

Figure 3. The influence of the PLGA concentration in the organic phase on the zeta potential of the formed PLGA nanoparticles, where the organic and aqueous phase consisted of a) acetone and ultrapure water, b) acetone and PVA in ultrapure water, c) acetone and an ethanol-water mixture d) acetonitrile and ultrapure water, e) acetonitrile and PVA in ultrapure water, f) and acetonitrile and an ethanol-water mixture, respectively. The TFR was 5,000 µL/min, and the FRR between the organic and the aqueous phase was 1:3. The precipitation marker indicates where the PLGA started to precipitate at the tip of the PEEK tube. Mean ± SD, n = 3 (*n = 2).

We compared the influence of the PLGA concentration on the formation of size-controlled nanoparticles in the microfluidic system for the different solvent combinations. The PLGA concentrations 0.25 and 0.5 mg/mL were excluded, as they had large standard deviations for some solvent combinations. A one-way analysis of variance with Tukey's multiple comparisons was performed to see if the PLGA particle diameters prepared with 1 mg/mL with different solvent combinations varied. The particles generated with the solvent combination "acetonitrile and PVA in ultrapure water" at a PLGA concentration of 1 mg/mL were significantly smaller than the ones generated with "acetone and ultrapure water" ($p = .022$) and "acetone and an ethanol-water mixture" ($p = .010$). To see if the particle formation followed different patterns after a PLGA concentration of 1 mg/mL, the slopes between the particle diameter and the PLGA concentration for the different solvent combinations were compared (Table 3).

The trend among the solvents was that the solvent combinations with acetone had lower slopes than the ones with acetonitrile, meaning that the particle diameter increases more with the increment of the PLGA concentration for the particles created with acetonitrile compared to the particles created with acetone. This was statistically corroborated by the slope of "acetone and ultrapure water" being statistically lower than its counterpart "acetonitrile and ultrapure water". The groups with PVA in ultrapure water (both with acetone and acetonitrile) had statistically higher slopes than the ones with ultrapure water and the ethanol-water mixture. This was shown by "acetone and PVA in ultrapure water" being significantly higher than the other groups with acetone and "acetonitrile and PVA in ultrapure water" being significantly higher than all the other groups, except for "acetone and PVA in ultrapure water". There was a trend of the groups with the ultrapure water having a slightly lower slope than the groups with the ethanol-water mixture.

Table 2. Pearson correlation coefficients showing the influence of the PLGA concentration on the particle diameter for the different solvent combinations and the influence of FRR or TFR on the particle diameter (see Table 1 for the combinations). A Pearson correlation coefficient shows the relationship between two variables; a value closer to +1 indicates a strong positive correlation, and a value closer to -1 indicates a strong inverse correlation. A two-tailed test measured the significance of the correlation coefficients. Not significant: $p > 0.05$, significant: $p < 0.05$. When performing the correlation statistics, the values for the flow rate ratios were set as the flow rate percentage from Syringe 2 (containing PLGA dissolved in organic solvent) out of the total flow, e.g., FRR 1:3 between Syringes 2 and 1 = 25%.

	Pearson correlation coefficient	P-value	Significant
Relationship between the PLGA concentration and the particle diameter for the solvents:			
Acetone and ultrapure water	0.64	$3.0 \cdot 10^{-4}$	Yes
Acetone and PVA in ultrapure water	0.91	$< 1.0 \cdot 10^{-10}$	Yes
Acetone and an ethanol-water mixture	0.92	$< 1.0 \cdot 10^{-10}$	Yes
Acetonitrile and ultrapure water	0.97	$< 1.0 \cdot 10^{-10}$	Yes
Acetonitrile and PVA in ultrapure water	0.97	$< 1.0 \cdot 10^{-10}$	Yes
Acetonitrile and an ethanol-water mixture	0.72	$2.6 \cdot 10^{-5}$	Yes
Relationship between the FRR or the TFR and particle diameter:			
FRR (percentage of the organic phase)	0.50	$5.9 \cdot 10^{-2}$	No
TFR	-0.85	$1.5 \cdot 10^{-7}$	Yes

The PLGA particle diameter is influenced by the TFR but not the FRR

Empty PLGA nanoparticles were prepared using the modular microfluidic system with different FRRs and TFRs. During the evaluation of the effect of FRR and TFR on the formation of nanoparticles, the PLGA concentration was maintained at 3 mg/mL, the organic solvent was acetonitrile, and the aqueous solvent was an ethanol-water mixture. Five FRRs (flow of the organic phase vs. flow of the aqueous phase) were tested (Table 1), while the TFR was kept constant (5 mL/min). When performing the correlation statistics, the values for the flow rate ratios were set as the flow rate percentage from Syringe 2 (containing the PLGA dissolved in the organic solvent) out of the total flow, e.g., FRR 1:3 between Syringes 2 and 1 = 25%. When testing the TFR, the FRR between the flow of the organic phase and the aqueous phase was kept constant (1:3). Eight TFRs were tested (see Table 1). The particle diameters and PDIs are summarised in Fig. 4a-b and the zeta potential data in Fig. 5a-b.

Table 3. Statistical comparisons of the formation of size-controlled nanoparticles via alteration of PLGA concentrations in the microfluidic system (linear regression curves) when using different solvents. The concentrations from 1 mg/mL to 20 mg/mL for the different solvent types were compared. Above the diagonal grey line: the p-values for the slope. Not significant: $p > 0.05$ (red), significant: $p < 0.05$ (green).

	Acetone and ultrapure water	Acetone and PVA in ultrapure water	Acetone and an ethanol-water mixture	Acetonitrile and ultrapure water	Acetonitrile and PVA in ultrapure water	Acetonitrile and an ethanol-water mixture
Equation	$y = 4.4 \cdot x + 77.4$	$y = 5.7 \cdot x + 77.4$	$y = 3.8 \cdot x + 84.0$	$y = 5.3 \cdot x + 61.4$	$y = 6.4 \cdot x + 54.2$	$y = 4.4 \cdot x + 64.1$
Acetone and ultrapure water		$3.9 \cdot 10^{-2}$	$1.9 \cdot 10^{-1}$	$4.6 \cdot 10^{-2}$	$1.2 \cdot 10^{-4}$	$9.7 \cdot 10^{-1}$
Acetone and PVA in ultrapure water			$5.8 \cdot 10^{-3}$	$5.2 \cdot 10^{-1}$	$3.4 \cdot 10^{-1}$	$5.1 \cdot 10^{-2}$
Acetone and an ethanol-water mixture				$4.2 \cdot 10^{-3}$	$1.3 \cdot 10^{-5}$	$2.7 \cdot 10^{-1}$
Acetonitrile and ultrapure water					$4.1 \cdot 10^{-2}$	$7.5 \cdot 10^{-2}$
Acetonitrile and PVA in ultrapure water						$5.1 \cdot 10^{-4}$
Acetonitrile and an ethanol-water mixture						

Correlation statistics were performed to see how the FRR or TFR affected the particle diameter (Table 2) (see Table S1 for the PDIs and zeta potentials). There was a significant inverse correlation between the TFR and the particle diameter, i.e., increasing the TFR led to smaller nanoparticles. In contrast, there was no correlation between the FRR (flow rate percentage of the organic phase) and the particle diameter. Both the PDI and zeta potential increased with a decrease in the organic phase flow rate percentage, and the zeta potentials increased at higher TFRs ($p < 0.05$). The PDI was not statistically significantly influenced by altering the TFR ($p > 0.05$).

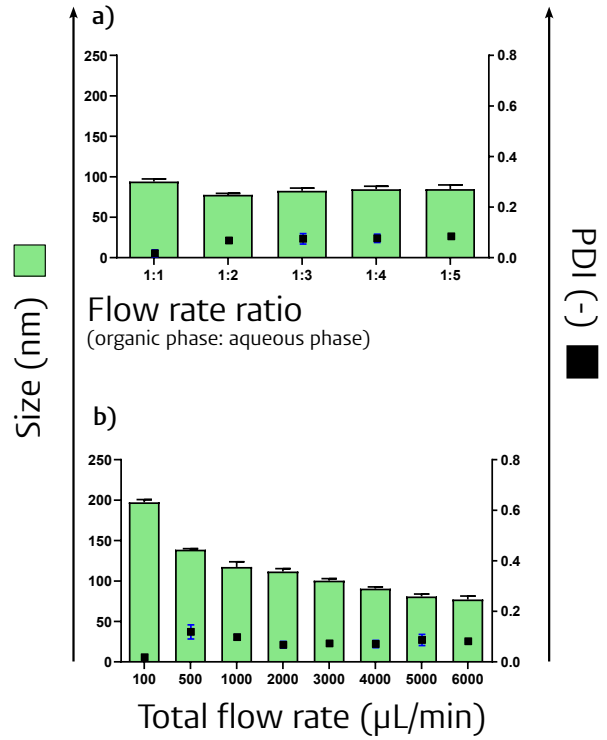

Figure 4. The influence of a) the FRR and b) the TFR on the nanoparticle diameter and PDI. The PLGA concentration was set to 3 mg/mL, the organic phase was acetonitrile, and the aqueous phase consisted of the ethanol-water mixture. The FRR between the organic and the aqueous phase for a) the TFR was 1:3, and the TFR for b) FRR was set to 5,000 µL/min. Mean ± SD, n = 3. PDI: polydispersity index.

The PLGA particle diameters increase with increasing amounts of lysozyme, while the diameter for ovalbumin-containing nanoparticles only changes slightly

Based on the results of the two-syringe system, a three-syringe system was designed to incorporate two water-soluble proteins with different physicochemical properties: i) ovalbumin, a 42.7 kDa protein [18] which is negatively charged at pH 7.4 [19], and ii) lysozyme, a 14.3 kDa protein [20], which is positively charged at pH 7.4 [21].

The particle diameters, PDIs, and encapsulation efficiencies of the proteins in the PLGA nanoparticles are reported in Fig. 6. For lysozyme, the particle diameter increases with the lysozyme-to-PLGA weight ratio until the particle diameter reaches 180 nm at a ratio of 1:16.7 ($p = .02$ between the ratio 1:50 and 1:16.7), whereafter, it reaches a plateau (Fig. 6a). The PDI is above 0.1 until the lysozyme-to-PLGA weight ratio reaches 1:16.7, whereafter it stays below 0.1 (PDI 1:12.5 compared to 1:100 $p = .006$, compared to 1:50 $p = .03$, compared to 1:25 $p = .0002$) (Fig. 6a). The encapsulation efficiency for lysozyme increases

until it reaches a lysozyme-to-PLGA weight ratio of 1:12.5 with an encapsulation efficiency of 85.2 ± 2.6%, whereafter it decreases to 67.4 ± 7.9% at the 1:10 weight ratio ($p = .01$ between 1:50 and 1:16.7, $p = .002$ between 1:25 and 1:12.5, and $p = .005$ between 1:12.5 and 1:10) (Fig. 6c). For ovalbumin, the particle diameter increases from the ovalbumin-to-PLGA weight ratio of 1:100 to 1:50, from 104.4 ± 1.0 nm to 112.8 ± 0.9 nm ($p = .02$), whereafter it decreases slightly from 101.2 ± 4.7 nm at 1:25 to 90.7 ± 1.6 nm at 1:10 ($p = .003$)((Fig. 6b). The PDI stays around 0.1 until an ovalbumin-to-PLGA weight ratio of 1:10 (Fig. 6b). The general trend is that the encapsulation efficiency for ovalbumin decreases with the increasing ovalbumin-to-PLGA weight ratio (Fig. 6d).

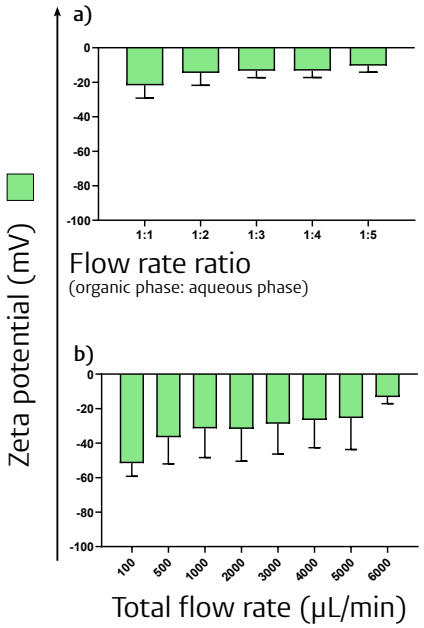

Figure 5. The influence of a)the FRR and b) the TFR on the zeta potential. The PLGA concentration was set to 3 mg/mL, the organic phase was acetonitrile, and the aqueous phase consisted of the ethanol-water mixture. The FRR between the organic and the aqueous phase for a) the TFR was 1:3, and the TFR for b) FRR was set to 5,000 µL/min. Mean ± SD, n = 3.

DISCUSSION

Traditional bulk processes for producing PLGA nanoparticles often have limitations as they are regularly associated with low throughput and lack of batch-to-batch consistency [11]. In comparison, microfluidics is a system of small channels, which allows for one-step assembly of the particles in a continuous manner [10, 12]. This leads to increased scalability, reduced production times, and precise control of the mixing, which makes it possible to tune the particle diameter [10, 12]. In summary, microfluidics have the potential to revolutionise drug delivery by offering more control over critical nanoparticulate formulation parameters.

In this study, we pursued three objectives: first, to set up a low-cost microfluidic system that does not rely on a microfluidic chip. Second, to investigate the parameters that affect the physicochemical properties of the PLGA nanoparticles using the microfluidic system. Lastly, to incorporate hydrophilic proteins into the PLGA nanoparticles.

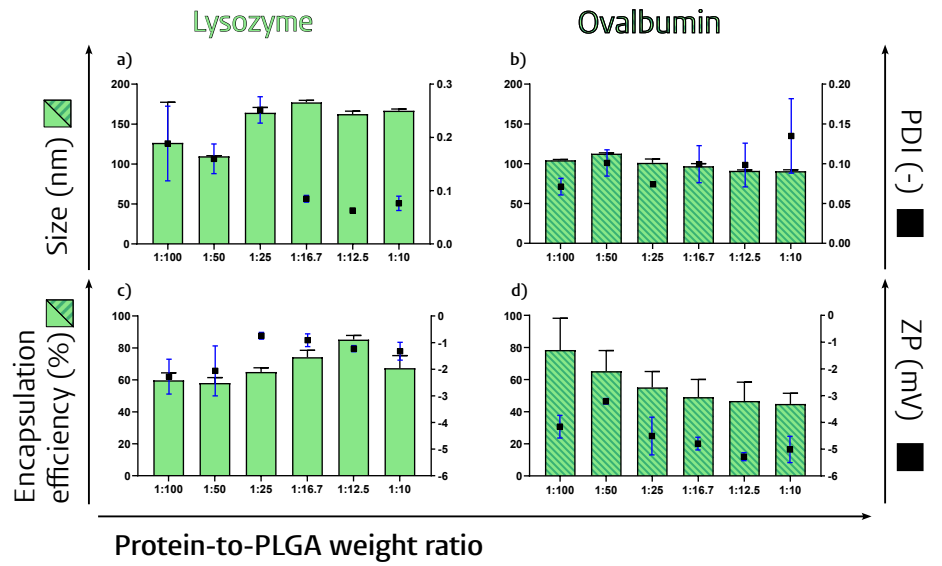

Figure 6. The influence of the protein-to-PLGA ratio for the protein lysozyme a) and ovalbumin b) on the size and PDI, and the encapsulation efficiency and zeta potential of lysozyme c) and ovalbumin d). Values represent mean ± SD, n = 3. ZP = zeta potential, PDI = polydispersity index.

We managed to set up a modular microfluidic system that produced nanoparticles with highly reproducible particle diameters, where an increasing particle diameter was obtained by increasing the PLGA concentration in the organic phase (increased the particle diameter from 33 to 180 nm) or by decreasing the TFR (increased particle diameters from 77 to 197 nm). In addition, the hydrophilic proteins ovalbumin and lysozyme were incorporated at different protein-to-PLGA weight ratios, resulting in encapsulation efficiencies above 40%.

Incorporation of proteins

The modular microfluidic system described in this paper can be adapted for multi-step processes. We decided to use a three-syringe setup for the incorporation of the proteins as we previously tested a two-syringe system versus a three-syringe system to prepare drug-loaded liposomes, where the three-syringe setup was advantageous (unpublished data). We chose

to incorporate the antigens ovalbumin and lysozyme into PLGA nanoparticles. Ovalbumin, a negatively charged protein at physiological pH, is readily available and is often used as a model antigen to study antigen-specific immune responses in mice [22]. In opting for a protein possessing distinct attributes from ovalbumin, we selected lysozyme for its low cost and positive charge at physiological pH [20, 21]. The aqueous solvent PVA in ultrapure water was chosen for both proteins as the proteins aggregated visibly with higher concentrations of ovalbumin, when the solvent combination of the ethanol-water mixture was used, and because PLGA precipitated at higher concentrations, when ultrapure water was used.

The PLGA concentration for creating the PLGA nanoparticles with incorporated proteins was set to 3 mg/mL for lysozyme and 5 mg/mL for ovalbumin. These concentrations were chosen to create particles of around 100 nm. While the particle diameter stayed around 100 nm for ovalbumin, it increased with the lysozyme-to-PLGA weight ratio from 110 nm (1:100) to 177 nm (1:16.7), whereafter it dropped slightly. This is likely due to the positive charge of lysozyme that attracts the negatively charged PLGA. We measured the encapsulation efficiencies of ovalbumin and lysozyme. Ovalbumin had an encapsulation efficiency of 44–78% where the encapsulation efficiency decreased with increasing amounts of ovalbumin. The encapsulation efficiency for lysozyme was 58–85%, where the highest encapsulation efficiency was at the lysozyme-to-PLGA weight ratio of 1:12.5. While our focus remained on a lactide:glycolide 50:50 polymer, other investigations have explored the impact of various PLGA polymers on encapsulation efficiency and particle diameter. They found that lactide:glycolide 85:15 polymer demonstrated higher encapsulation efficiency of ovalbumin [17], this aspect could be a worthwhile avenue for future exploration.

The modular microfluidic system used in this study has also been used to prepare PLGA particles for opalescence studies [23] and to incorporate the lipid dye (2*Z*)-2-[(*E*)-3-(3,3-dimethyl-1-octadecylindol-1-ium-2-yl)prop-2-enylidene]-3,3-dimethyl-1-octadecylindole; perchlorate into PLGA particles of various sizes with the two-syringe system, where the lipid was dissolved in the organic phase, to visualise the uptake of PLGA particles of different sizes in zebrafish [24]. Furthermore, ovalbumin and oligonucleotide 1826 (a Class B CpG oligonucleotide; a murine TLR9 ligand) into PLGA nanoparticles for incorporation into dissolving nanoparticles [25]. If another lipophilic substance should be incorporated into the PLGA nanoparticles, it could be dissolved in the organic solvent together with the PLGA. If a compound that is not dissolvable in the organic phase or water should be incorporated, it could possibly be dissolved in another solvent and be incorporated with the three-syringe system. The modular microfluidic system has also been used to prepare polymer-lipid hybrids, which are particles with a PLGA core surrounded by a lipid layer(s) (submitted manuscript by Mikolaj Szachniewicz et al.), by adding an extra attachment to the system, making it a four-syringe system.

The choice of the microfluidic settings

The chosen materials (polymers, drugs, surfactants) and settings (flow rates, channel geometries) used in microfluidic systems affect the physicochemical characteristics of the formed empty PLGA particles. Therefore, we tested how PLGA concentrations, solvents, FRR, and TFR affected the particle formation in this system. The nanoparticle diameters in our study ranged from 32 to 197 nm. The sizes are normally larger with conventional methods, as double-emulsion and nanoprecipitation methods lead to PLGA nanoparticles with a minimum particle diameter of around 150 nm [7, 26]. According to some existing literature, FRR influences the PLGA particle diameter where an increase in the rate of the aqueous solvent correlates with a reduction in particle diameter [17, 27]. However, this is not always the case, as the FRR did not affect the particle diameter in another study [28]. The FRR did not significantly affect the particle diameter in our system; however, there was a trend towards smaller particles with an increased rate of the aqueous solvent (i.e., decreased rate of organic solvent). An increase in TFR correlated with a reduction in PLGA particle diameter, similar to the literature [17, 28].

Our study revealed that the choice of solvent affects the PLGA particle diameter. We tested two organic solvents and three aqueous solvents in our microfluidic system. The particle diameter increased with an increasing PLGA concentration in the organic solvent for all the solvent combinations.

The organic solvents acetone and acetonitrile were chosen as they are both miscible with water [29] because we were aiming for nanoprecipitation microfluidics, also called continuous microfluidics, which tend to generate nano-sized particles [13]. The organic solvent acetone generated larger particle diameters than acetonitrile (at a PLGA concentration of 1 mg/mL), which is also shown in another microfluidic setup [30]. This is likely due to the diffusion coefficient of acetonitrile in water being higher than the diffusion coefficient of acetone in water which favours the formation of smaller nanoparticles [31]. However, we observed that the size difference was reduced when the PLGA concentration was increased. Adding PVA to ultrapure water generated smaller nanoparticles than the ethanol-water mixture and ultrapure water at low PLGA concentrations. However, smaller particle diameters at low concentrations could be due to the formation of PVA micelles, as acetonitrile without PLGA with 20 mg/mL PVA in ultrapure water led to particle diameters of 19.7 ± 8.7 nm. The knowledge of how the solvent affects the particle diameter can be used to generate nanoparticles with a specific particle diameter, e.g., if the goal is to prepare small nanoparticles, the combination of a low concentration of PLGA in acetonitrile together with PVA in ultrapure water could be used.

Using ultrapure water as the aqueous phase led to PLGA precipitation on the PEEK tube at concentrations higher than 1 mg/mL PLGA in acetone and 5 mg/mL in acetonitrile. This is probably due to the lack of PLGA particle stabilisation in ultrapure water, whereas PVA can stabilise the particle formation [32]. The nanoparticle formulations prepared with PVA

in ultrapure water had neutral zeta potentials (-5 to 0 mV). In comparison, nanoparticles prepared with ultrapure water or the ethanol-water mixture had negative zeta potentials (-16 to -68 mV). This is likely due to the PVA layer on the surface of the NPs that shields the charge [33]. The different aqueous solvents have pros and cons. By using the ultrapure water, no ethanol or excess PVA is added, which, depending on the application, possibly would need to be removed. However, using ultrapure water did not stabilise the particles over a certain PLGA concentration. This led to a lower PLGA concentration in the produced formulation, as the PLGA precipitated in the PEEK tube. The PVA stabilises the particle formation but leads to a neutral charge and a possible surplus of surfactant in the formulation. However, this can be advantageous as PVA can stabilise the PLGA particles during freeze-drying [34]. The PVA concentration can be adjusted to determine the optimal concentration to stabilise the particles while creating a minimal PVA surplus in the formulation. The ethanol-water mixture leads to a negative charge while creating a surplus of ethanol that, dependent on the application, needs to be removed. However, it seems to stabilise the production of empty PLGA particles.

The modular microfluidic system: technical aspects

Initially, a microfluidic setup with two syringes was established. The components within the microfluidic system were thoughtfully selected to ensure cost-effectiveness. The pumps were low-cost (NE300 (single) syringe pumps (ProSense B.V.)) while it still was possible to adjust the speed by using syringes with different IDs. Syringes with a larger ID were able to generate higher flow rates as the turning screw that pushed on the syringe plunger flange had a maximum speed. Therefore, 10 mL syringes were used to contain the aqueous and organic phases to ensure a high flow rate while still being able to fit within the clamp. A 500-µL syringe was used to contain the aqueous proteins as i) it was possible to see the piston move when starting the pump (to ensure that the block pushing on the piston was installed correctly). And ii) because it would lead to less solvent loss, thereby ensuring less protein loss, as there was a dead volume in the plain tip, and also because the pump needed to be stopped before the plunger hit the plain tip, the end of the syringe, to not damage it.

For our microfluidics system, we selected components with excellent chemical stability against the used solvents at room temperature. The fluid path of the syringes consisted of a PTFE-tipped plunger and a borosilicate glass syringe with PTFE Luer-lock terminations [35–37], which are made of highly chemically inert materials [38, 39]. Gastight® syringes are leak-free, ensuring a flow without the risk of air intake [37]. The PEEK tube, the CapTite™ Luer-lock adapters, fittings, and adapters were made of PEEK, which is commonly used in chromatography and is also an inert material [40]. PTFE and PEEK are resistant to acetone, acetonitrile, ethyl acetate, water, and ethanol [41]. The interconnect tees were crafted from polyetherimide, which has good chemical resistance; however, it is not recommended for use with acetone and ethyl acetate at elevated temperatures (>50°C) [42, 43]. Despite the chemical resistance of the selected microfluidic-system components, we carefully inspected the different components before and after each nanoparticle preparation run. We did not notice damage on the interconnect tee's screwing mechanism after the use of acetone, however, it did lead to a slightly shiny surface after extended immersion in acetone. If an interconnect tee in PEEK or PTFE could be found that would be preferable.

Polyimide-coated fused silica capillary tubing with IDs of 75 µm and 250 µm and ODs of approximately 360 µm had polyimide coatings of 20 µm and 18 µm, respectively [44]. This meant that the capillary with an ID of 250 µm had a silica layer of approximately 30 µm, while the capillary with an ID of 75 µm had a silica layer of approximately 110 µm. While the capillary with an ID of 75 µm kept its integrity for days, the capillary with an ID of 250 µm tended to break after a few minutes due to its thin silica layer. Unfortunately, it was not possible to use a capillary with an ID of 75 µm for the syringe containing the organic phase, as the syringe pump could not generate the required amount of force required for the high flow rate on the syringe plunger without the drive-screw malfunctioning. Therefore, it is advisable to pre-test capillaries with large IDs to determine the retainment of their integrity at high flow rates/pressures.

CONCLUSION

We successfully developed a modular microfluidic system based on easily cleanable block components, ensuring minimal clogging and on-the-spot modifications. Through our investigations, we identified critical process parameters in the production that could affect the physicochemical properties of the PLGA nanoparticles.

The formation of the nanoparticles was affected by the PLGA concentration in the organic solvent and the total flow rate. The solvent in the aqueous phase affected the stability of the PLGA nanoparticles and the zeta potential. We effectively achieved the incorporation of the biomacromolecules ovalbumin and lysozyme with encapsulation efficiencies above 40%, showing the potential to formulate subunit vaccines and therapeutic proteins for controlled release utilising this method. Altogether, our system is a low-cost and highly versatile modular microfluidic platform that can produce PLGA nanoparticles in a highly reproducible manner with and without encapsulated protein.

References

1. Rao JP, Geckeler KE. Polymer nanoparticles: Preparation techniques and size-control parameters. Prog Polym Sci. 2011;36(7):887-913. https://doi.org/10.1016/j.progpolymsci.2011.01.001.
2. Danhier F, Ansorena E, Silva JM, Coco R, Le Breton A, Préat V. PLGA-based nanoparticles: an overview of biomedical applications. J Control Release. 2012;161(2):505-22. https://doi.org/10.1016/j.jconrel.2012.01.043.
3. Prabhu P, Patravale V. Potential of nanocarriers in antigen delivery: the path to successful vaccine delivery. Nanocarriers. 2014;1:10-45. https://doi.org/10.2478/nanca-2014-0001.
4. Zhang Y, García-Gabilondo M, Grayston A, Feiner IVJ, Anton-Sales I, Loiola RA, et al. PLGA protein nanocarriers with tailor-made fluorescence/MRI/PET imaging modalities. Nanoscale. 2020;12(8):4988-5002. https://doi.org/10.1039/C9NR10620K.
5. Acharya S, Sahoo SK. PLGA nanoparticles containing various anticancer agents and tumour delivery by EPR effect. Adv Drug Deliv Rev. 2011;63(3):170-83. https://doi.org/10.1016/j.addr.2010.10.00.
6. Varypataki EM, Silva AL, Barnier-Quer C, Collin N, Ossendorp F, Jiskoot W. Synthetic long peptide-based vaccine formulations for induction of cell mediated immunity: A comparative study of cationic liposomes and PLGA nanoparticles. J Control Release. 2016;226:98-106. https://doi.org/10.1016/j.jconrel.2016.02.018.
7. Mönkäre J, Pontier M, van Kampen EEM, Du G, Leone M, Romeijn S, et al. Development of PLGA nanoparticle loaded dissolving microneedles and comparison with hollow microneedles in intradermal vaccine delivery. Eur J Pharm Biopharm. 2018;129:111-21. https://doi.org/10.1016/j.ejpb.2018.05.031.
8. Ghitman J, Biru EI, Stan R, Iovu H. Review of hybrid PLGA nanoparticles: Future of smart drug delivery and theranostics medicine. Mater Des. 2020;193:108805. https://doi.org/10.1016/j.matdes.2020.108805.
9. Operti MC, Bernhardt A, Grimm S, Engel A, Figdor CG, Tagit O. PLGA-based nanomedicines manufacturing: Technologies overview and challenges in industrial scale-up. Int J Pharm. 2021;605:120807. https://doi.org/10.1016/j.ijpharm.2021.120807.
10. Astete CE, Sabliov CM. Synthesis and characterization of PLGA nanoparticles. J Biomater Sci Polym Ed. 2006;17(3):247-89. https://doi.org/10.1163/156856206775997322.
11. Streck S, Neumann H, Nielsen HM, Rades T, McDowell A. Comparison of bulk and microfluidics methods for the formulation of poly-lactic-co-glycolic acid (PLGA) nanoparticles modified with cell-penetrating peptides of different architectures. Int J Pharm X. 2019;1:100030. https://doi.org/10.1016/j.ijpx.2019.100030.
12. Valencia PM, Farokhzad OC, Karnik R, Langer R. Microfluidic technologies for accelerating the clinical translation of nanoparticles. Nat Nanotechnol. 2012;7(10):623-9. https://doi.org/10.1038/nnano.2012.168.
13. Rezvantalab S, Keshavarz Moraveji M. Microfluidic assisted synthesis of PLGA drug delivery systems. RSC Adv. 2019;9(4):2055-72. https://doi.org/10.1039/c8ra08972h.
14. Benne N, van Duijn J, Kuiper J, Jiskoot W, Slütter B. Orchestrating immune responses: How size, shape and rigidity affect the immunogenicity of particulate vaccines. J Control Release. 2016;234:124-34. https://doi.org/10.1016/j.jconrel.2016.05.033.
15. Silva AL, Soema PC, Slütter B, Ossendorp F, Jiskoot W. PLGA particulate delivery systems for subunit vaccines: Linking particle properties to immunogenicity. Hum Vaccin Immunother. 2016;12(4):1056-69. https://doi.org/10.1080/21645515.2015.1117714.
16. Albanese A, Tang PS, Chan WC. The effect of nanoparticle size, shape, and surface chemistry on biological systems. Annu Rev Biomed Eng. 2012;14:1-16. https://doi.org/10.1146/annurev-bioeng-071811-150124.
17. Roces CB, Christensen D, Perrie Y. Translating the fabrication of protein-loaded poly(lactic-co-glycolic acid) nanoparticles from bench to scale-independent production using microfluidics. Drug Deliv Transl Res. 2020;10(3):582-93. https://doi.org/10.1007/s13346-019-00699-y.
18. Nisbet AD, Saundry RH, Moir AJ, Fothergill LA, Fothergill JE. The complete amino-acid sequence of hen ovalbumin. Eur J Biochem. 1981;115(2):335-45. https://doi.org/10.1111/j.1432-1033.1981.tb05243.x.
19. van der Maaden K, Yu H, Sliedregt K, Zwier R, Leboux R, Oguri M, et al. Nanolayered chemical modification of silicon surfaces with ionizable surface groups for pH-triggered protein adsorption and release: application to microneedles. J Mater Chem B. 2013;1(35):4466-77. https://doi.org/10.1039/c3tb20786b.
20. Canfield RE. The Amino Acid Sequence of Egg White Lysozyme. J Biol Chem. 1963;238(8):2698-707. https://doi.org/10.1016/S0021-9258(18)67888-3.
21. Wetter L, Deutsch H. Immunological studies on egg white proteins: IV. Immunochemical and physical studies of lysozyme. J Biol Chem. 1951;192(1):237-42. https://doi.org/10.1016/S0021-9258(18)55926-3.
22. Taconic Biosciences. Immunology: Ovalbumin (OVA) Challenge [Internet]. https://www.taconic.com/find-your-model/gems/cryopreserved-models/knockout-repository/phenotypic-data-packages/comprehensive/ovalbumin-challenge.html. Accessed 04 Mar 2024.
23. Kunz P, Stuckenberger E, Hausmann K, Gentiluomo L, Neustrup M, Michalakis S, et al. Understanding opalescence measurements of biologics - A comparison study of methods, standards, and molecules. Int J Pharm. 2022;628:122321. https://doi.org/10.1016/j.ijpharm.2022.122321.
24. Arias-Alpizar G, Koch B, Hamelmann NM, Neustrup MA, Paulusse JMJ, Jiskoot W, et al. Stabilin-1 is required for the endothelial clearance of small anionic nanoparticles. Nanomedicine : nanotechnology, biology, and medicine. 2021;34:102395. https://doi.org/10.1016/j.nano.2021.102395.
25. Lee J, Neustrup MA, Slütter B, O'Mahony C, Bouwstra JA, van der Maaden K. Intradermal Vaccination with PLGA Nanoparticles via Dissolving Microneedles and Classical Injection Needles. Pharm Res. 2024;41(2):305-19. https://doi.org/10.1007/s11095-024-03665-7.
26. Hajavi J, Ebrahimian M, Sankian M, Khakzad MR, Hashemi M. Optimization of PLGA formulation containing protein or peptide-based antigen: Recent advances. J Biomed Mater Res A. 2018;106(9):2540-51. https://doi.org/10.1002/jbm.a.36423.
27. Karnik R, Gu F, Basto P, Cannizzaro C, Dean L, Kyei-Manu W, et al. Microfluidic Platform for Controlled Synthesis of Polymeric Nanoparticles. Nano Lett. 2008;8(9):2906-12. https://doi.org/10.1021/nl801736q.
28. Bao Y, Maeki M, Ishida A, Tani H, Tokeshi M. Preparation of size-tunable sub-200 nm PLGA-based nanoparticles with a wide size range using a microfluidic platform. PLoS One. 2022;17(8):e0271050. https://doi.org/10.1371/journal.pone.0271050.
29. Merck. Solvent Miscibility Table [Internet]. https://www.sigmaaldrich.com/NL/en/technical-documents/technical-article/analytical-chemistry/purification/solvent-miscibility-table. Accessed 18 Sep 2024.
30. Lababidi N, Sigal V, Koenneke A, Schwarzkopf K, Manz A, Schneider M. Microfluidics as tool to prepare size-tunable PLGA nanoparticles with high curcumin encapsulation for efficient mucus penetration. Beilstein J Nanotechnol. 2019;10:2280-93. https://doi.org/10.3762/bjnano.10.220.
31. Huang W, Zhang C. Tuning the Size of Poly(lactic-co-glycolic Acid) (PLGA) Nanoparticles Fabricated by Nanoprecipitation. Biotechnol J. 2018;13(1). https://doi.org/10.1002/biot.201700203.
32. Stromberg ZR, Lisa Phipps M, Magurudeniya HD, Pedersen CA, Rajale T, Sheehan CJ, et al. Formulation of stabilizer-free, nontoxic PLGA and elastin-PLGA nanoparticle delivery systems. Int J Pharm. 2021;597:120340. https://doi.org/10.1016/j.ijpharm.2021.120340.
33. Sahoo SK, Panyam J, Prabha S, Labhasetwar V. Residual polyvinyl alcohol associated with poly (D,L-lactide-co-glycolide) nanoparticles affects their physical properties and cellular uptake. J Control Release. 2002;82(1):105-14. https://doi.org/10.1016/s0168-3659(02)00127-x.
34. Andreana I, Bincoletto V, Manzoli M, Rodà F, Giarraputo V, Milla P, et al. Freeze Drying of Polymer Nanoparticles and Liposomes Exploiting Different Saccharide-Based Approaches. Materials (Basel). 2023;16(3). https://doi.org/10.3390/ma16031212.
35. Fischer Scientific. Hamilton™ 1000 Series Gastight™ Syringes: Luer Lock Syringes, TLL Termination [Internet]. https://www.fishersci.nl/shop/products/hamilton-1000-series-gastight-syringes-luer-lock-syringes-tll-termination-14/10374902. Accessed 25 Mar 2024.
36. Hamilton Company. 500 µL Gastight Syringe Model 1750 TLL, PTFE Luer Lock, Needle Sold Separately [Internet]. https://www.hamiltoncompany.com/laboratory-products/syringes/81220. Accessed 25 Mar 2024.
37. Hamilton Company. Hamilton Reference Guide SYRINGES & NEEDLES 2023. Lit. No. L20097 Rev. D — 09/2023. https://assets-labs.

hamiltoncompany.com/File-Uploads/Syringe_Needle_Reference-Guide.pdf?v=1696888429.
38. Nag A, Baksi A, Ghosh J, Kumar V, Bag S, Mondal B, et al. Tribochemical Degradation of Polytetrafluoroethylene in Water and Generation of Nanoplastics. ACS Sustain Chem Eng. 2019;7(21):17554-8. https://doi.org/10.1021/acssuschemeng.9b03573.
39. CP Lab Safety. PTFE and Teflon Chemical Compatibility [Internet]. https://www.calpaclab.com/teflon-ptfe-compatibility/. Accessed 26 Mar 2024.
40. CP Lab Safety. PEEK Chemical Compatibility [Internet]. https://www.calpaclab.com/polyetherether-ketone-peek-chemical-compatibility-chart/. Accessed 26 Mar 2024.
41. VICI AG International. Chromatography Fluid/Gas Transfer 2009. Catalog 10 Int. p. 108-9. https://www.greyhoundchrom.com/Content/Images/uploaded/files/Vici%20Jour/Vici%20Jour.pdf.
42. Advanced Sensor Technologies I. ULTEM - PEI (Poly-Ether-Imide) Chemical Resistance Chart. https://www.astisensor.com/ultem.pdf.
43. Thermo Fischer Scientific. Labware Chemical Resistance Table. https://tools.thermofisher.com/content/sfs/brochures/D20480.pdf.
44. BGB. TSP - Standard Polyimide Coating [Internet]. https://www.bgb-info.com/home.php?cat=303. Accessed 26 Mar 2024.

SUPPLEMENTARY MATERIAL

Table S1. Pearson correlation coefficient showing the influence of the PLGA concentration on the PDI or zeta potential for the different solvent combinations, FRR or TFR (see Table 1 for the combinations). The Pearson correlation coefficient shows the relationship between two variables, a value closer to +1 indicates a strong positive correlation, and a value closer to -1 indicates a strong inverse correlation. The significance of the correlation coefficients was measured by a two-tailed test. Not significant: $p > .05$, significant: $p < .05$. When performing the correlation statistics, the values for the flow rate ratios were set as the flow rate percentage from Syringe 2 (containing PLGA dissolved in organic solvent) out of the total flow, e.g., FRR 1:3 between Syringes 2 and 1 = 25%.

	Pearson correlation coefficient	p-value	Significant
PDI			
Acetone and ultrapure water	-0.46	$1.5 \cdot 10^{-2}$	Yes
Acetone and PVA in ultrapure water	-0.65	$2.4 \cdot 10^{-4}$	Yes
Acetone and an ethanol-water mixture	-0.31	$1.1 \cdot 10^{-1}$	No
Acetonitrile and ultrapure water	-0.54	$3.4 \cdot 10^{-3}$	Yes
Acetonitrile and PVA in ultrapure water	-0.70	$4.3 \cdot 10^{-5}$	Yes
Acetonitrile and an ethanol-water mixture	-0.50	$6.9 \cdot 10^{-3}$	Yes
FRR	-0.87	$2.2 \cdot 10^{-5}$	Yes
TFR	0.12	$5.6 \cdot 10^{-1}$	No
Zeta potential			
Acetone and ultrapure water	-0.55	$2.8 \cdot 10^{-3}$	Yes
Acetone and PVA in ultrapure water	0.53	$4.7 \cdot 10^{-3}$	Yes
Acetone and an ethanol-water mixture	-0.77	$3.2 \cdot 10^{-6}$	Yes
Acetonitrile and ultrapure water	-0.83	$1.7 \cdot 10^{-7}$	Yes
Acetonitrile and PVA in ultrapure water	0.50	$1.5 \cdot 10^{-2}$	Yes
Acetonitrile and an ethanol-water mixture	-0.58	$1.7 \cdot 10^{-3}$	Yes
FRR	-0.63	$1.3 \cdot 10^{-2}$	Yes
TFR	0.56	$4.9 \cdot 10^{-3}$	Yes

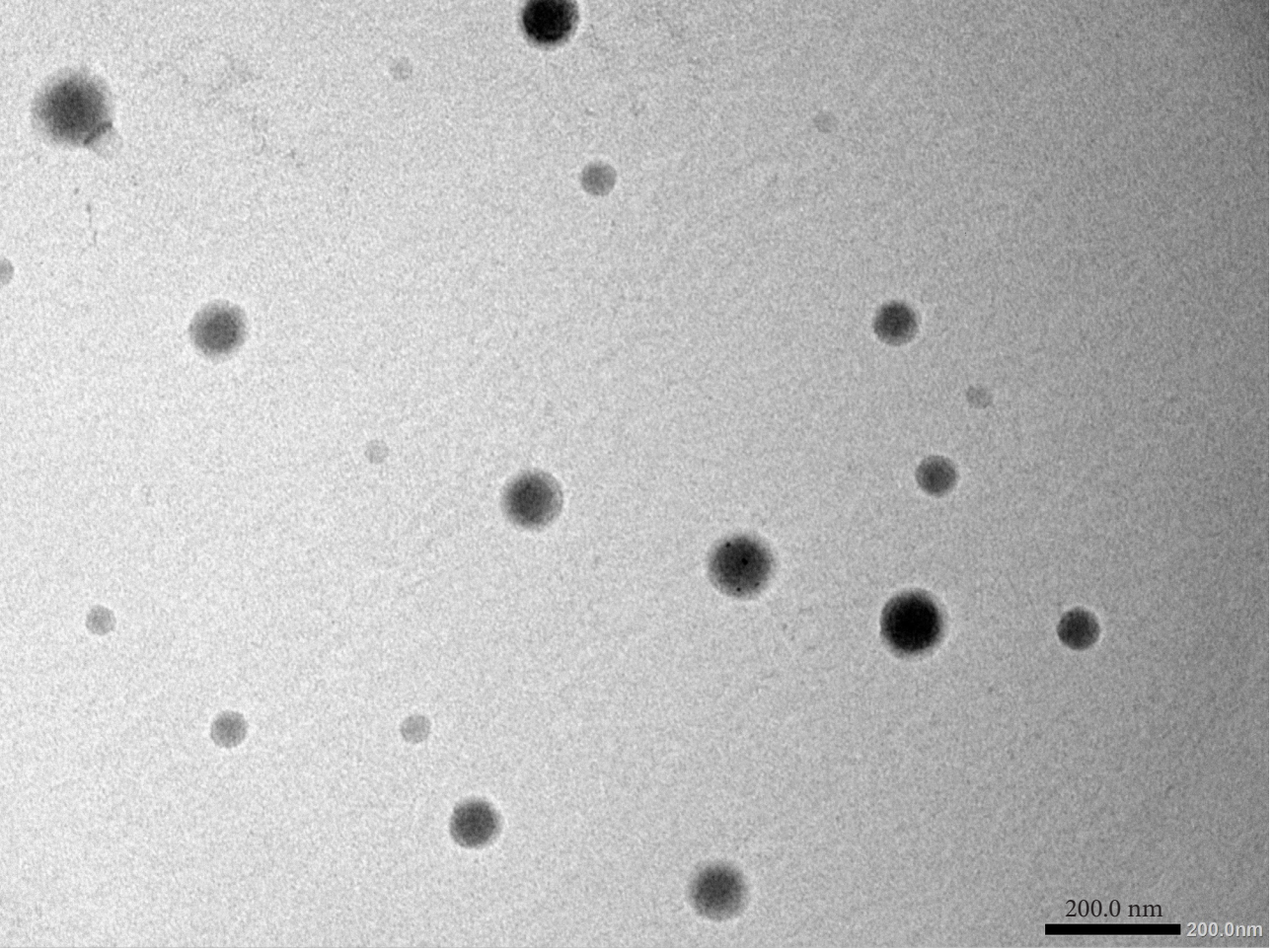

CHAPTER 4

EVALUATION OF PLGA, LIPID-PLGA HYBRID NANOPARTICLES, AND CATIONIC PH-SENSITIVE LIPOSOMES AS TUBERCULOSIS VACCINE DELIVERY SYSTEMS IN A *MYCOBACTERIUM TUBERCULOSIS* CHALLENGE MOUSE MODEL – A COMPARISON

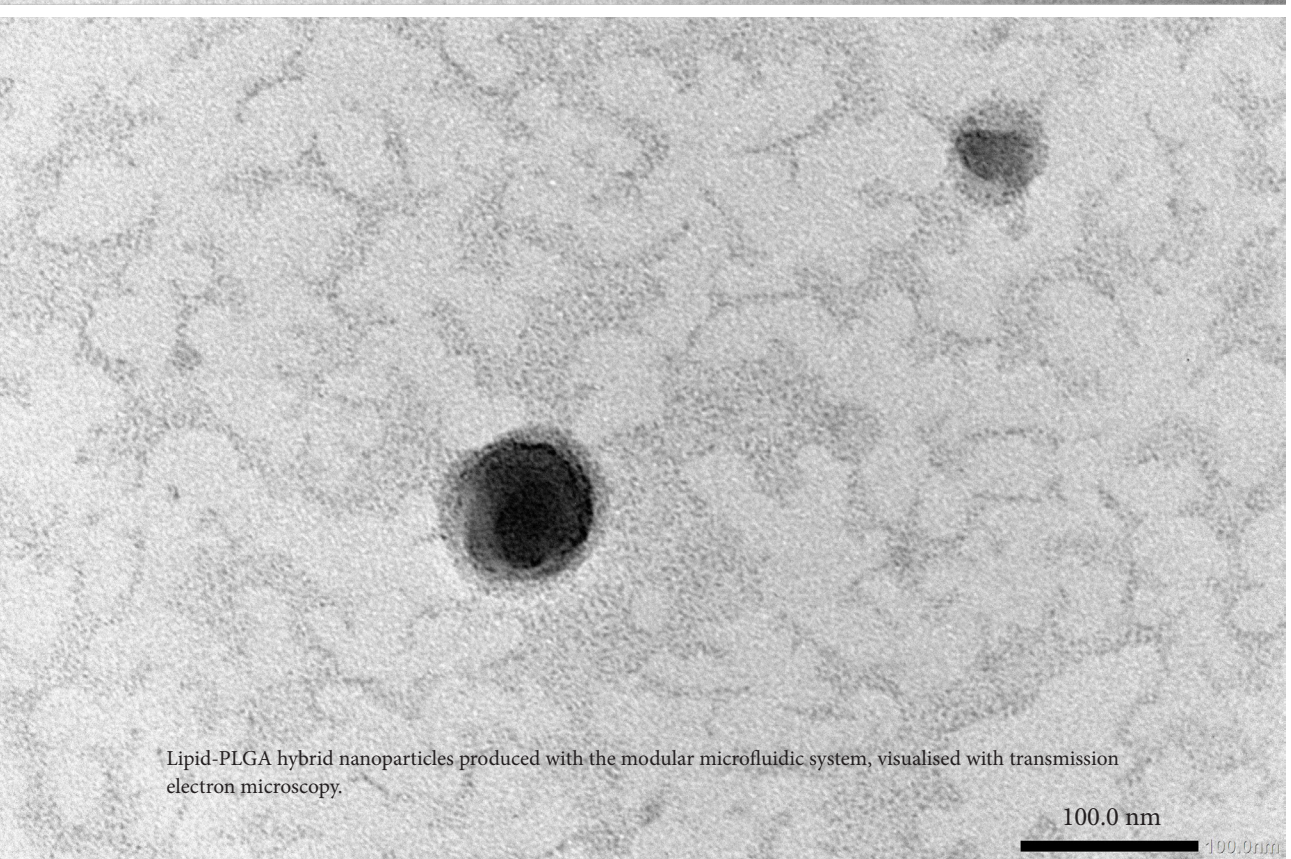

Lipid-PLGA hybrid nanoparticles produced with the modular microfluidic system, visualised with transmission electron microscopy.

Adapted from Int J Pharm. 2024;666:124842

M.M. Szachniewicz[1], M.A. Neustrup[2], S.J.F. van den Eeden[1], K.E. van Meijgaarden[1], K.L.M.C. Franken[1], S. van Veen[1], R.I. Koning[3], R.W.A.L. Limpens[3], A. Geluk[1], J.A. Bouwstra[2], T.H.M. Ottenhoff[1]

[1] Department of Infectious Diseases and LUCID, Leiden University Medical Center, Leiden, The Netherlands
[2] Division of BioTherapeutics, Leiden Academic Centre for Drug Research, Leiden University, Leiden, The Netherlands
[3] Electron Microscopy Facility, Leiden University Medical Center, Leiden, The Netherlands

ABSTRACT

Tuberculosis (TB) continues to pose a global threat for millennia, currently affecting over 2 billion people and causing 10.6 million new cases and 1.3 million deaths annually. The only existing vaccine, *Mycobacterium Bovis* Bacillus Calmette-Guérin (BCG), provides highly variable and inadequate protection in adults and adolescents. This study explores newly developed subunit tuberculosis vaccines that use a multistage protein fusion antigen Ag85b-ESAT6-Rv2034 (AER). The protection efficacy, as well as *in vivo* induced immune responses, were compared for five vaccines: BCG; AER-CpG/MPLA mix; poly(D,L-lactic-co-glycolic acid) (PLGA); lipid-PLGA hybrid nanoparticles (NPs); and cationic pH-sensitive liposomes (the latter three delivering AER together with CpG and MPLA). All vaccines, except the AER-adjuvant mix, induced protection in *Mycobacterium tuberculosis* (Mtb)-challenged C57/Bl6 mice as indicated by a significant reduction in bacterial burden in lungs and spleens of the animals. Four AER-based vaccines significantly increased the number of circulating multifunctional $CD4^+$ and $CD8^+$ T-cells producing IL-2, IFN-γ, and TNFα, exhibiting a central memory phenotype. Furthermore, AER-based vaccines induced an increase in $CD69^+$ B-cell counts as well as high antigen-specific antibody titers. Unexpectedly, none of the observed immune responses were associated with the bacterial burden outcome, such that the mechanism responsible for the observed vaccine-induced protection of these vaccines remains unclear. These findings suggest the existence of non-classical protective mechanisms for Mtb infection, which could, once identified, provide interesting targets for novel vaccines.

INTRODUCTION

The WHO estimates that approximately one quarter of the world's human population is latently infected with TB [1]. Dubbed the 'white plague', pulmonary TB is the primary transmissible form caused by *Mycobacterium tuberculosis* (Mtb) [2]. In 2022, 1.3 million died from TB, including 167,000 with HIV, making it a leading cause of death in this group of patients, and the second leading infectious disease killer after COVID-19, with the major cause of death due to antibiotic resistance [1]. TB is curable and preventable, but multidrug-resistant TB (MDR-TB) is an increasing public health threat [1]. The WHO aims to end the TB epidemic by 2030 as part of the United Nations' Sustainable Development Goals (SDGs) [3, 4]. As outlined by the End TB Strategy and the Western Pacific regional framework to end TB: 2021–2030 [5], the main tools to achieve this goal involve point-of-care approaches, early and easily accessible diagnostics, shorter and more effective treatment regiments, comprehensive treatment of all people with TB, including those with MDR-TB, management of co-morbidities, preventative treatment, and vaccination [3, 5].

Vaccination is indispensable for preventing infectious diseases like TB. Vaccines have enabled the eradication of smallpox and rinderpest and, more recently, have been essential in the fight against SARS-CoV-2 [6–8]. The only licensed TB vaccine *Mycobacterium Bovis* Bacillus Calmette-Guérin (BCG), unfortunately offers highly variable and often insufficient protection [9–11]. Therefore, there is an unmet demand for better vaccines against TB [10].

Subunit vaccines, produced with synthesized or purified antigens, DNA, or RNA, are safe and suitable for use in wide populations, including those with compromised immunity [12, 13]. This broad applicability is especially important for TB in countries with high HIV rates [5]. However, they often lack immunogenicity, making further improved delivery system development essential for subunit vaccines [14, 15]. Vaccine delivery systems use biocompatible nanoparticles (NPs) that prevent or limit antigen degradation and elimination, allow co-encapsulation of antigens with (molecular) adjuvants, and enhance uptake by antigen-presenting cells (APCs) [16–18]. The work presented in this paper investigates and compares the immunological and biological effects of poly(D,L-lactic-*co*-glycolic acid) (PLGA), lipid-PLGA hybrid NPs, and cationic pH-sensitive liposomes as particulate delivery systems for protein-based TB vaccines.

PLGA is one of the most extensively studied polymers for numerous biomedical applications. It is available in varied compositions and molecular weights. Its versatile characteristics make it suitable for tissue engineering and sustained-release drug and vaccine delivery systems. PLGA has excellent safety records, tunable degradation, release properties, and high versatility. This has led to its wide adoption in several biomedical applications and longstanding approval by the US Food and Drug Administration for human use including drug delivery, and various biomedical products ranging from sutures

to implants [17, 19–24]. It biodegrades through hydrolysis into non-toxic metabolic by-products lactic and glycolic acid [23]. Previous studies have demonstrated the efficacy of antigen- and adjuvant-loaded PLGA nanoparticles in enhancing cell-mediated immune response in mice [25–32].

Cationic liposomes are potent delivery systems that serve as particulate adjuvants [12, 16, 33–35]. Several liposome-based vaccines have been approved for clinical use [36–38]. Specifically, cationic liposomes can enhance immune responses, inducing the maturation of DCs and triggering T-cell responses, making them a versatile vaccination platform [39–41].

pH-sensitive liposomes are a subclass of (cationic) liposomes that respond to pH changes by altering their molecular bilayer organization upon a decrease in pH. When exposed to an acidic environment, bilayers destabilize, which results in a fusion of the liposome with the endosomal membrane, thus releasing their cargo. This allows them to deliver antigens and adjuvants into a cell's cytosol, avoiding endosomal degradation [42–46]. This unique ability to escape rapid degradation has potential vaccination benefits [47]. Unlike non-pH-sensitive liposomes that degrade inside the endosome [48, 49] pH-sensitive liposomes can protect antigens and facilitate cross-priming [49, 50], which could significantly impact the type of immune responses induced by a vaccine [51].

Lipid-PLGA hybrid NPs are complex nanostructures that have been successfully used in drug and vaccine delivery in preclinical research [52–56]. These hybrid NPs comprise a biodegradable PLGA core enveloped in a lipid shell that encapsulates drugs or antigens. They combine the properties of both PLGA NPs and liposomes. PLGA provides a rigid and solid core that allows sustained controlled release of antigens and adjuvants whereas the (cationic) lipid shell overcomes the lack of the immunogenicity of PLGA, facilitates uptake by APCs, reduces the degradation rate of the PLGA core by limiting water diffusion into the particle, thus ensuring controlled release kinetics [52, 54, 57, 58]. In vaccine applications, cationic lipid-PLGA hybrid NPs have demonstrated enhanced immunogenicity and induced humoral and cellular immune responses [58–64].

In this study, the immunogenicity and effectiveness of tuberculosis vaccines prepared with NP-based delivery systems were compared to the antigen-adjuvant mixture in mice. The fusion protein antigen Ag85B-ESAT6-Rv2034 (AER) combined with adjuvants monophosphoryl lipid A (MPLA), cytosine-phosphate-guanine motifs oligodeoxynucleotides (CpG ODN) were used in the formulation. AER consists of Ag85B, an immunodominant antigen rich in epitopes offering enhanced protection when combined with other antigens [65]; ESAT6 which is a potent immunomodulatory antigen that is not expressed by BCG [21, 66]; both used in vaccines currently in clinical trials: H1:IC31 [67], and H56:IC31 [68]; and Rv2034 which is a potent *in vivo* expressed Mtb antigen [69]. AER mixed with CAF09 adjuvant induced protection in HLA-DR3 transgenic mice and in guinea pigs [70]. CpG is a Toll-like receptor (TLR) 9 ligand that induces robust Th1 responses, and MPLA, a TLR4 agonist, induces Th1 and Th17 responses [71–73]. A combination of both has been successfully used in several phase II and III clinical trials, and it was demonstrated safe and effective in the induction of robust T-cell and antibody responses [74–78]. The novel tuberculosis subunit vaccines developed in this research were tested *in vitro* on primary human APCs for immunogenicity and *in vivo* on C57Bl/6 mice with intranasal H37Rv Mtb infection to quantify protection, specifically CFU reduction in lungs and spleens. Immune responses in vaccinated, non-Mtb challenged mice were analyzed using a 27-marker spectral flow cytometry for $CD4^+$, $CD8^+$ T-cells, and B-cell responses. Additionally, serum antigen-specific antibody titers were measured.

MATERIALS AND METHODS

Materials

1,2-dioleoyl-sn-glycero-3-phosphocholine (DOPC), 1,2-dioleoyl-sn-glycero-3-ethyl-phosphocholinechloride salt (EPC), 1,2-dioleoyl-sn-glycero-3-phosphoethanolamine (DOPE), N-(4-carboxybenzyl)-N,N-dimethyl-2,3-bis(oleoyloxy)propan-1-aminium (DOBAQ), and monophosphoryl lipid A, PHAD (MPLA) were purchased from Avanti Polar Lipids, Inc. in the USA. Fig. S1 illustrates the chemical structures of these lipids. Class B CpG oligonucleotide ODN1826 was acquired from InvivoGen (the Netherlands). PLGA (acid terminated, lactide:glycolide 50:50, Mw 24,000-38,000) was purchased from Merck Chemicals B.V. (the Netherlands). Interconnect tees for use with 360 µm outer diameter capillaries, one-piece fittings (for 360 µm capillaries and for 1/16" tubings), two-piece adapters (360-µm-to-1.6-mm and 1.6-mm-to-360-µm), and Luer-lock adapters (for use with 360 µm capillaries and 1/16" tubings), were obtained from Mengel Engineering (Denmark). Polyether ether ketone capillary tubing (inner diameter of 0.02" and outer diameter of 1/16"), was bought from Fisher Emergo B.V. (the Netherlands). A Teflon tube (1/16") was sourced from Waters Chromatography B.V. (the Netherlands). TSP Standard polyimide-coated fused silica tubings, (75 µm and 250 µm inner diameters, and 360 µm outer diameter) were obtained from BGB Analytik Benelux B.V. (the Netherlands). Polytetrafluoroethylene Luer-lock Hamilton gastight (1710TLL 100 µL, 1001TLL 1 ml, and 1010TLL 10 ml) syringes were purchased from Merck (Germany). Recombinant fusion protein AER was produced as described by Franken et al. [79]. Briefly, genes from Mtb (lab strain H37Rv) were amplified using PCR with genomic DNA. The amplified genes were cloned into bacteria using an N-terminal hexa-histidine (His) tag utilizing Gateway technology (Invitrogen, USA), and their successful insertion was confirmed through sequencing. The antigen AER was then expressed in *Escherichia coli* strain BL21 (DE3) and purified. Its quality was assessed through gel electrophoresis followed by Coomassie brilliant blue staining and with an anti-His antibody (Invitrogen, USA) Western blotting, which evaluated the size and purity of the protein. The ToxinSensor

Chromogenic Limulus Amebocyte Lysate (LAL) Endotoxin Assay Kit (GenScript, USA) was employed to determine the endotoxin contamination level in the protein, revealing levels below 50 endotoxin units per 1 mg of protein.

Liposome production

Liposomes were made using the thin-film hydration method, as described previously [80]. Lipids were dissolved in chloroform and diluted from 25 mg/ml stocks to 10 mg per batch. The composition used was DOPC:DOPE:DOBAQ:EPC in a molar ratio 3:5:2:4. The lipid solution was placed in a flask and chloroform was removed using a Buchi rotavapor R210 (Switzerland). The lipid film was then rehydrated with 1 ml of 200 µg/ml AER in 10 mM phosphate buffer (PB) at pH 7.4 to create AER-containing liposomes. These were downsized with Branson sonifier 250 (US) using an eight-cycle sonication program comprising 30 s of sonication at 10% amplitude, followed by a 60-s break, and centrifuged (at 500 g for 3 min) to remove metal particles. The liposomal suspensions (5 mg/ml lipids) were transferred to new tubes and stored at 4 °C overnight. The final product contained 40 µg/ml AER and 2 mg/ml lipids after dilution with 10 mM PB.

PLGA NP preparation

The PLGA NPs were produced using a modular microfluidic system. A three-component system was used for PLGA NPs. Briefly, the contents of two syringes, Syringe 1 and 2, met each other in a T-flow, subsequently, the combined fluid met the contents of a third syringe, Syringe 3, in a co-flow, where the combined fluid constitutes the inner flow and the content of Syringe 3 constitutes the outer flow. The three syringes contained: 1) 3.33 mg/ml AER solution and 1 mg/ml CpG in water for injection, 2) 5 mg/ml PLGA and 12.5 µg/ml MPLA in acetonitrile, and 3) water for injection. The flow rates for the fluids in Syringe 1, 2, and 3 were set to 37.5, 1250, and 4955 µl/min, respectively, obtaining a total flow rate of 6242.5 µl/min, and final concentrations of 20 µg/ml AER, 6 µg/ml CpG, 2 mg/ml PLGA, and 2.5 µg/ml MPLA. The suspensions were set under a stream of nitrogen to evaporate the acetonitrile and concentrate the formulations. Before the characterization of particles and further use *in vitro* and *in vivo*, a concentrated solution of PB was added to obtain a concentration of 10 mM PB in the final product (40 µg/ml AER, 12 µg/ml CpG, 2 mg/ml PLGA, and 5 µg/ml MPLA).

Lipid-PLGA hybrid NP preparation

The lipid-PLGA NPs were produced using the same method as PLGA NPs with modifications. A four-component system was used in this case. As described above, AER solution with CpG was combined with PLGA (without MPLA) solution in an interconnected tee. The combined flow (1287.5 µl/min) was then directed into another tee, where it was combined with water for injection (at 3712 µl/min), and 5 mg/ml lipid solution of DOPC:DOPE:DOBAQ:EPC (3:5:2:4) containing 12.5 µg/ml MPLA in ethanol at a flow rate of 1250 µl/min. The total flow rate was 6249.5 µl/min. The produced suspension was then evaporated and twice up-concentrated under nitrogen flow. The final product contained 40 µg/ml AER, 12 µg/ml CpG, 2 mg/ml PLGA, 2 mg/ml lipids, 5 µg/ml MPLA, and 10 mM PB.

Determination of size and zeta-potential

The hydrodynamic diameter (Z-average size) and polydispersity index (PDI) of the liposomal formulations were determined with dynamic light scattering (DLS), and zeta potential was measured using laser Doppler electrophoresis as described previously [80]. Liposomes were diluted to 0.25 mg/ml lipid in 10 mM PB at pH 7.4 and added to 1.5 ml VWR Two-Sided Disposable PS Cuvettes (VWR, the Netherlands). Measurements, conducted in triplicates with at least ten runs at 20 °C, were performed using a Nano ZS Zetasizer with 633 nm laser and 173° optics (Malvern Instruments, UK). The data were analyzed with Zetasizer Software v7.13 (Malvern Instruments).

Differentiation of human monocyte-derived dendritic cells (MDDCs) and macrophages (MDMFs)

After written informed consent, PBMCs were obtained from healthy donors' buffy coats (Sanquin Blood Bank, Netherlands) as described previously [80]. Using the Ficoll-based density gradient centrifugation method, PBMCs were separated, and $CD14^+$ cells were isolated via the magnetic cell isolation method (MACS) with an autoMACS Pro Separator (Miltenyi Biotec BV, the Netherlands). These cells were then differentiated into DCs, and type 1 and 2 (M1 and M2, respectively) macrophages over six days using cytokines. MDDCs were generated with 10 ng/ml recombinant human granulocyte-macrophage colony-stimulating factor (GM-CSF; Miltenyi Biotec BV, the Netherlands) and 10 ng/ml recombinant human interleukin 4 (IL-4; Peprotech, USA). For M1 macrophages we used 5 ng/ml GM-CSF, and for M2 macrophages we used 50 ng/ml macrophage colony-stimulating factor (M-CSF; Miltenyi Biotec BV, the Netherlands) [81]. Cells were cultured at 37 °C/5% CO_2 in Roswell Park Memorial Institute (RPMI) 1640 medium, supplemented with 10% fetal bovine serum (FBS), penicillin (100 units/ml), streptomycin (100 µg/ml), and 2 mM GlutaMAX (Gibco, Belgium). MDDCs were harvested through pipetting, while for macrophages, we used trypsinization (Gibco, Belgium).

Uptake study

To assess the uptake of liposome, MDDCs, M1, and M2 MDMFs were cultured in 96-well plates with round bottoms (CELLSTAR, Greiner Bio-One GmbH, Germany), each well containing 30,000 cells. These cells were then treated with 1% (v/v) empty fluorescent liposomes containing 0.1% mol% of 1,2-dioleoyl-*sn*-glycero-3-phosphoethanolamine-N-(Cyanine 5) (18:2 PE-Cy5) sourced from Avanti Polar Lipids, Inc., USA, for 1 h. Following exposure, the cells were washed three times with FACS buffer to eliminate any free liposomes. Flow cytometry data collection was collected using a BD FACSLyric Flow Cytometer (BD Biosciences, Belgium), and the analysis of this data was conducted using the FlowJo software, version 10.6 (FlowJo LLC, BD, USA) [80].

Activation study

The adjuvant properties of formulations loaded with AER were investigated using MDDCs as described previously [82]. To 30,000 cells/well in MDDCs seeded in 96-well plates with round bottoms (CELLSTAR, Greiner Bio-One GmbH, Germany), at a density of 30,000 cells per well, with lipid concentrations ranging from 25 to 250 µg/ml in 200 µl of medium. The cells were incubated for 1 h at 37 °C/5% CO_2. Subsequent to this incubation, cells were rinsed with a complete RPMI medium and then cultured overnight. The following day, cells were centrifuged, the supernatants collected and stored at -20 °C for later use. For flow cytometry, cells were washed with FACS buffer (PBS with 0.1% bovine serum albumin; Merck, Germany) and blocked for 5 min with 5% human serum (Sanquin Blood Bank, the Netherlands) in PBS to prevent non-specific Fc-receptor binding. After blocking, cells were stained for 30 min with monoclonal antibodies targeting various cell surface markers: CCR7-BB515 (clone 3D12, catalog 565870), CD83-PE (clone HB15e, catalog 556855), CD40-APC (clone 5C3, 555591), CD80-APC-R700 (clone L307.4, catalog 565157), HLA-DR-V500 (clone G46-6, 561225) from BD Biosciences, Belgium, and CD86-BV421 (clone IT2.2, 305426) from BioLegend, the Netherlands, all at a dilution of 1:200 in FACS buffer. Post-staining, cells were again washed three times and resuspended in FACS buffer. Flow cytometry data was acquired using a BD FACSLyric Flow Cytometer and analyzed with FlowJo software.

Luminex assay

According to the manufacturer's protocols, supernatants were tested in two Bio-Plex panels (Bio-Rad, Veenendaal, the Netherlands). In total, 16 analytes were measured. The chemokine panel consisted of CXCL9, CXCL11, CCL8, and CCL22. The cytokine panel included CCL11 (Eotaxin), GM-CSF, IFN-α2, IL-1β, IL-1rα, IL-6, CXCL10, CCL2(MCP-1), CCL3, CCL4, RANTES and TNF-α. Samples were acquired on a Bio-Plex 200 system and analyzed with Bio-Plex manager software version 6.1.

Mice

All mouse experiments were individually designed, reviewed, ethically approved, and registered by the institutional Animal Welfare Body of the Leiden University Medical Center (LUMC). The study was conducted under project license AVD116002017856, issued by the Netherlands's Central Authority for Scientific Procedures on Animals (CCD). The experiments adhered to the Dutch Act on Animal Experimentation and EU Directive 2010/63/EU for animal experiments.

The Jackson Laboratory (USA) provided C57Bl/6 mice (stock number SC1300004), which were housed in the LUMC animal facility. Female mice, aged 6–8 weeks and matched for age (17–18 g weight), were utilized for each experiment. Mice were housed in a specific pathogen-free, temperature-controlled environment (20 °C ± 1 °C; humidity 55% ± 15%,) including a controlled day-night cycle (12 h per day; 60-300 lux), in individually ventilated cages containing bedding and nesting materials and as enrichment a tunnel and gnawing wood with no more than six mice per cage. Food and drinking water *ad libitum*. Mice were acclimatized for one week following transport before the experiments began.

Two independent experiments were performed. The experimental groups, summarized in Table 1, included naïve (unimmunized) mice as a negative control and a BCG immunized group as a control group using the licensed TB vaccine. Each mouse was considered an experimental unit, and mice in the same experimental group were housed together in one cage. Each group consisted of six mice, and a total of 36 mice were used per experiment. The results from the two experiments were combined for statistical analysis, increasing the number of mice to 12 per group and 72 in total.

Immunizations

C57Bl/6 mice were randomly allocated to six groups (6 mice per group). The naïve group served as the unimmunized control. Mice in the remaining groups were vaccinated with either BCG or AER combined with CpG (ODN1826) and MPLA (PHAD) or with AER together with CpG and MPLA delivered in PLGA NPs, cationic pH-sensitive liposomes or pH-sensitive lipid PLGA hybrid NPs. For immunizations that involved nanoparticle-based delivery systems, mice were given 3 subcutaneous (s.c.) injections in the right flank every 2 weeks with appropriate formulations (Table 1). Four weeks post-final immunization, mice were either sacrificed or infected with live Mtb. When AER was mixed with adjuvants, mice received 3 injections every 2 weeks with a solution of 25 µg AER, 50 µg CpG, and 1 µg MPLA in 200 µl PBS. For BCG vaccination, mice were given a single s.c. injection with 10^6 CFU live BCG (Danish strain 1331) 12 weeks prior to sacrifice or Mtb infection. BCG bacterial counts were determined by placing the suspension on 7H10 agar plates (Difco, BD, Franklin Lakes, NJ USA) supplemented with BBL Middlebrook OADC enrichment (BD, Franklin Lakes, NJ USA) and counting colonies after a 3-week incubation at 37 °C. Doses, frequency, and routes of administration were selected based on previous research [70, 80, 83].

Table 1. Summary of vaccination groups and doses of vaccine constituents administrated to a mouse in a single immunization. Each group consists of 6 mice per experiment. All adjuvanted systems also contained CpG and MPLA. NA: not applicable.

Group	Description	AER (µg)	Lipid (µg)	PLGA (µg)	CpG (µg)	MPLA (µg)
Naïve	Unimmunized	NA	NA	NA	NA	NA
BCG	Approved vaccine	NA	NA	NA	NA	NA
Ag	Antigen-adjuvant mix	25	NA	NA	50	1
PLGA	PLGA NPs	8	NA	400	2.5	1
Hybrid	Lipid-PLGA hybrid NPs	8	400	400	2.5	1
pH	pH-sensitive liposome	8	400	NA	2.5	1

Intranasal infection with H37Rv Mtb

Unimmunized and immunized mice were infected with live Mtb H37Rv either 4 weeks post-AER vaccination or 12 weeks after BCG vaccination. Mice were sedated using isoflurane (Pharmachemie BV, The Netherlands) and received an intranasal dose of 10^5 CFU Mtb sourced from glycerol stocks kept at at -80 °C [84]. The bacterial count was measured using 7H10 agar plates. The bacterial colonies were counted after incubation for 3 weeks at 37 °C. Six weeks following the Mtb infection, the mice were humanely euthanized using CO_2. Their spleens and lungs were aseptically extracted. These tissues were then processed using 70 µM mesh strainers (Corning, USA) in a sterile PBS solution. The counts of bacteria were evaluated by serial dilutions on 7H11 agar plates (procured from BD Bioscience, USA), which were supplemented with OADC and PANTA (sourced from BD, Franklin Lakes, NJ USA).

Splenocyte cultures

Splenocytes from immunized uninfected mice were resuspended at 3×10^6 cells/ml in Iscove's Modified Dulbecco's Medium (IMDM; Lonza, Switzerland) with 2 mM GlutaMAX™, 100 U/100 µg/ml penicillin-streptomycin (both purchased from Gibco, Paisley, UK), and 8% heat-inactivated fetal bovine serum (FBS; Greiner, Frickenhausen, Deutschland), and stimulated *in vitro* with 5 µg/ml of AER or its single components at 37 °C and 5% CO_2. After 6 days, the splenocytes were restimulated with the same protein for 5 h, and 2.5 µg/ml Brefeldin A (Sigma, Merck, Darmstadt, Germany) was added overnight. They were then harvested and stained for intracellular cytokines and surface markers the next day, as described previously [83].

Antibody enzyme-linked immunosorbent assay (ELISA)

Blood was drawn from immunized, uninfected mice via heart puncture and cooled on ice. It was then centrifuged at 15,000 rpm for 10 min to obtain sera. ELISA was used to determine antibodies against proteins in sera, as described previously [83]. Plates were coated overnight with AER (5 µg/ml) or PBS/0.4% BSA (Sigma, Merck, Darmstadt, Germany) at 4 °C and blocked for 2 h with PBS/1% BSA/1% Tween-20. Serum dilutions (100 µl/well) were kept at 37 °C for 2 h, followed by a wash (PBS, 0.05% Tween-20) and incubation with horse radish peroxide (HRP)-labeled rabbit-anti-mouse antibodies: total IgG, IgG1, IgG2a, IgG2b, IgG2c, IgG3, and IgM (Dako, Denmark). After a 2-h incubation at 37 °C, plates were washed and treated with 100 µl/well tetramethylbenzidine substrate (TMB; Sigma) for 15 min. Then H_2SO_4 was added, and OD450 was measured using a Spectramax i3x spectrometer Molecular Devices, CA, USA).

Antibody staining and flow cytometry

Surface and intracellular staining procedures were described elsewhere [83]. In short, splenocytes were transferred to 96-well plates and washed with PBS. They were stained with Zombie UV Fixable Viability Kit (BioLegend, the Netherlands), diluted 1:250 in PBS, and incubated with 100 µl of dye per well for 30 min. The cells were washed twice with FACS buffer (PBS with 0.1% BSA), blocked with 20 µl of 5% normal mouse serum (Thermo Fisher Scientific Inc., Bleiswijk, the Netherlands) in FACS buffer, then washed and stained with CCR7 for 30 min at 37 °C. The full list of antibodies used is summarized in Table S1. Lastly, the cells were washed twice and stained with a 50 µl/well antibody mix containing 10 µl/well of BD Horizon Brilliant Stain Buffer Plus (BD Biosciences, Belgium). Cells were incubated at 4 °C for 30 min, washed twice with FACS buffer, and then fixated and permeabilized with eBioscience Foxp3/Transcription Factor Staining Buffer Set (Invitrogen, Thermo Fisher Scientific, Belgium) at 4 °C for 60 min.

Following a wash, intracellular staining was performed using a diluted antibody mix in permeabilization buffer. Cells were incubated with 50 µl/well antibody mix for 45 min, washed twice with FACS buffer, and resuspended in 100 µl/well FACS buffer. They were then stored at 4 °C until measured with a Cytek Aurora spectral flow cytometer (Cytek Biosciences, Fremont, CA, USA) at the Flow Cytometry Core Facility of Leiden University Medical Center in the Netherlands.

Flow cytometry data analysis

Data were analyzed with FlowJo v10.8.0 and OMIQ (www.omiq.ai) software, as described previously [83]. The analysis strategy is shown in Fig. S2. In brief, data were first manually gated in FlowJo to remove debris, doublets, and acquisition-disturbed cells. Cells were then gated on CD3 vs CD19, and T-cells ($CD3^+CD19^-$) and B-cells ($CD3^-CD19^+$) were separately exported (min. 20,000 events each) to OMIQ. The imported data were further cleaned with FlowAI in OMIQ, and single marker gates were created. Using Boolean gating, gate combinations were made. Counts for all Boolean gates were exported, and statistical analysis was conducted. Uniform manifold approximation and projection (UMAP) was performed on digitally concatenated cells from all mice in each group.

Cryo-electron microscopy

Cryo-electron microscopy was performed as described previously [85]. Quantifoil 2/2 electron microscopy grids were glow discharged in 0.2 mbar air, at 25 mA, and for 30 s using an Easyglow (Pelco). A 3 µl droplet of the sample was added to the glow discharged grids, and blotted away using filter paper (Whatman no.4) for 3 s at 85–95% humidity and room temperature, using an EM GP (Leica). The grid was subsequently plunged into liquid ethane/propane (2:1) at -196 °C. Grids were transferred into a Talos Arctica (Thermo Fisher Scientific) and images were acquired using EPU (Thermo Fisher Scientific) in multi-grid mode, at 0.55 nm/pixel, 15000x nominal magnification. Images were recorded on a K3 direct electron detector (Gatan) in counting mode and ZLP imaging in movie mode, a defocus of -5 µm, and an electron dose of ~ 4 e/A2/s with 8 s exposure time (corresponding to a total dose of 35 e/A2). Using this magnification/pixel size and electron dose, the full 2-µm hole is visible in one image, and the vesicle bilayer (at 4 nm) can be discerned. Movies (80 frames in total) were aligned using MotionCor2 and converted to tiff using EMAN2.

Statistical analysis

Mann-Whitney statistical test with Benjamini Hochberg FDR correction was carried out using R [86] and RStudio [87], to identify differentially abundant populations of cells. Statistical analyses to compare vaccination groups were performed in GraphPad Prism, version 8.01 (GraphPad Software, Prism, USA), using the Kruskal-Wallis test and an uncorrected Dunn's posthoc test for non-parametric comparisons of three or more groups to the control group, where cutoff of $P < 0.05$ was selected as statistically significant (*$P < 0.05$, **$P < 0.01$, ***$P < 0.001$, ****$P < 0.0001$). Bar values represent the median and error bars the interquartile range (IQR) unless indicated otherwise.

RESULTS

In vitro testing of vaccine formulations

Formulations were prepared using three types of nanoparticle-based vaccine delivery systems: PLGA NPs, lipid-PLGA hybrid NPs, and cationic pH-sensitive liposomes. Both hybrid NPs and liposomes shared the same lipid composition DOPC:DOPE:DOBAQ:EPC (3:5:2:4). We performed the initial immunogenicity tests in primary human MDDCs, including the performance of PLGA NPs.

First, we examined the uptake of PLGA NPs (Fig. S2). The uptake was assessed using primary human MDDCs (IL-4 and GM-CSF-induced), as well as pro-inflammatory M1 (GM-CSF-induced) and anti-inflammatory (M-CSF-induced) MDMFs. The uptake of empty PLGA NPs in MDDCs was much lower compared to the uptake observed in type 1 and 2 MDMFs (Fig. S2a). Because the PLGA NPs were not positively charged and no targeting moieties were used, it was expected that the uptake in DCs would be low.

Subsequently, the uptake of empty PLGA and empty cationic lipid-PLGA hybrid NPs was compared in MDDCs only (the primary APCs of our interest) (Fig. S2b). A significantly higher uptake was measured for the lipid-PLGA hybrid NPs compared to the PLGA NPs. Similarly to our previous work, pH-sensitive liposomes were efficiently taken up by all three types of APCs (manuscript submitted). These results thus show that professional APCs relatively poorly take up PLGA NPs without any adjuvants.

Subsequently, we examined the activation of primary human MDDCs in terms of the expression of cell-surface activation markers and cytokine production (Fig. S3 and S4). Unadjuvanted PLGA, lipid-PLGA NPs, and pH-sensitive liposomes were tested, as well as their counterparts formulated with CpG and MPLA adjuvants. Unadjuvanted PLGA NPs, as expected, were weakly immunogenic, failed to increase activation marker expression, and induced weak or non-detectable cytokine production. Unadjuvanted lipid-PLGA hybrid NPs were more efficient in activating MDDCs in terms of cell surface markers and cytokine production than the PLGA NPs. Cationic pH-sensitive liposomes induced CD40, CD83, and CCR7 expression but did not induce cytokine production. However, PLGA and lipid-PLGA NPs adjuvanted with CpG and MPLA induced both cell-surface markers expression and cytokine production. These results indicated that inert PLGA NPs, when formulated with potent adjuvants, can induce robust immune responses in vitro and, therefore, are promising delivery systems.

Physicochemical characterization of vaccine formulations and mouse study design

PLGA, lipid-PLGA hybrid NPs, and cationic pH-sensitive liposomes formulated with AER antigen, CpG, and MPLA adjuvants were prepared and characterized (Table 2). PLGA NPs had the smallest size about 85 nm, and very low Zeta-potential of about -50 mV. Lipid-PLGA hybrid NPs and liposomes had higher sizes of about 140 nm and 170 nm, respectively, as well as Zeta-potential between 20 ÷ 25 mV. Cryo-electron microscopy (Fig. S5A) revealed spherical PLGA NPs in the size range between 50 and 100 nm with unsharp edges. Cryo-electron images of lipid-PLGA hybrid NPs (Fig. S5B) revealed spherical NPs with clear lipid bilayer-resembling features. Subsequently, formulations were administrated subcutaneously to mice three times two weeks apart. Naïve (unimmunized) mice and BCG and AER mixed with CpG and MPLA were used as control groups. The immunization groups are summarized in Table 1. In the AER-adjuvant mix group, higher doses of antigen (25 µg compared to 8 µg) and CpG (50 µg compared to 2.5 µg) were used.

Table 2. Physicochemical properties of liposomes used for immunization of mice. Results represent a mean of n = 6 batches (3 batches used in 2 experiments, each batch value is a mean of a triplicate) and standard deviation.

Formulation	Z-average size (nm)	PDI (-)	Zeta-potential (mV)
AER/PLGA	83.9 ± 17.8	0.25 ± 0.10	-49.6 ± 11.2
AER/DOPC:DOPE:DOBAQ:EPC/PLGA	139.7 ± 8.0	0.19 ± 0.03	25.1 ± 1.8
AER/DOPC:DOPE:DOBAQ:EPC	166.9 ± 41.6	0.34 ± 0.09	21.5 ± 3.2

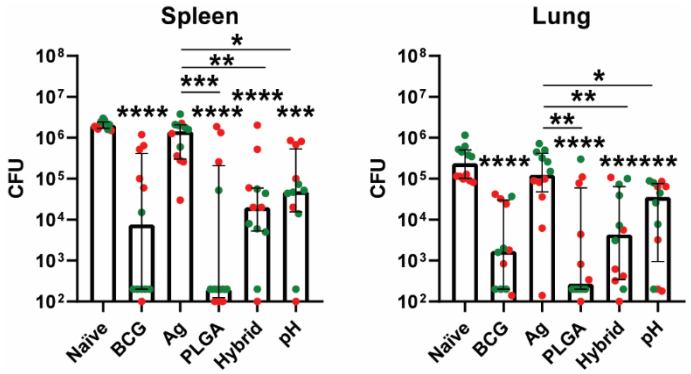

Figure 1. Bacterial burden in spleens (a) and lungs (b) of challenged mice represented by colony forming units (CFU) of Mtb. Each point represents CFU obtained from a single mouse. Colors indicate mice used in the same experiment. Groups: naïve – unimmunized mice; BCG – live BCG; Ag –antigen (25 μg Ag85B-ESAT6-Rv2034, AER) adjuvant mix (50 μg CpG, 1 μg MPLA), NP-free; PLGA – antigen (8 μg AER) and adjuvants (2.5 μg CpG, 1 μg MPLA) delivered in PLGA (400 μg) NPs; Hybrid – antigen (8 μg AER) and adjuvants (2.5 μg CpG, 1 μg MPLA) delivered in lipid (400 μg DOPC:DOPE:DOBAQ:EPC, 3:5:2:4)-PLGA (400 μg) NPs; pH – (8 μg AER) antigen and adjuvants (2.5 μg CpG, 1 μg MPLA) delivered in cationic pH-sensitive liposomes (400 μg DOPC:DOPE:DOBAQ:EPC, 3:5:2:4). n = 12. Bars represent median ± IQR. *$p < 0.05$, **$p < 0.01$, ***$p < 0.001$, ****$p < 0.0001$ (Kruskal-Wallis with an uncorrected Dunn's posthoc test).

Nanoparticle-based subunit vaccines induce protection against Mtb in mice

The bacterial burden in lungs and spleens of infected mice was examined six weeks after the infection, which corresponds to ten weeks after the last immunizations (Fig. 1). Bacterial counts from mice vaccinated with PLGA, lipid-PLGA, and pH-sensitive liposomal formulations as well as BCG were all significantly reduced compared to unimmunized mice and mice vaccinated with AER-adjuvant mix both in lungs and spleens, mounting to 2–3 log differences. Mice vaccinated with PLGA NPs had lower median CFUs, both in spleens and lungs, compared to BCG and the other two NP-based vaccines; however, the difference was not statistically significant between these groups. Noteworthy, NP-based vaccines used much lower doses of the antigen (8 μg vs 25 μg) and CpG (2.5 μg vs 50 μg) compared to the antigen-adjuvant mix.

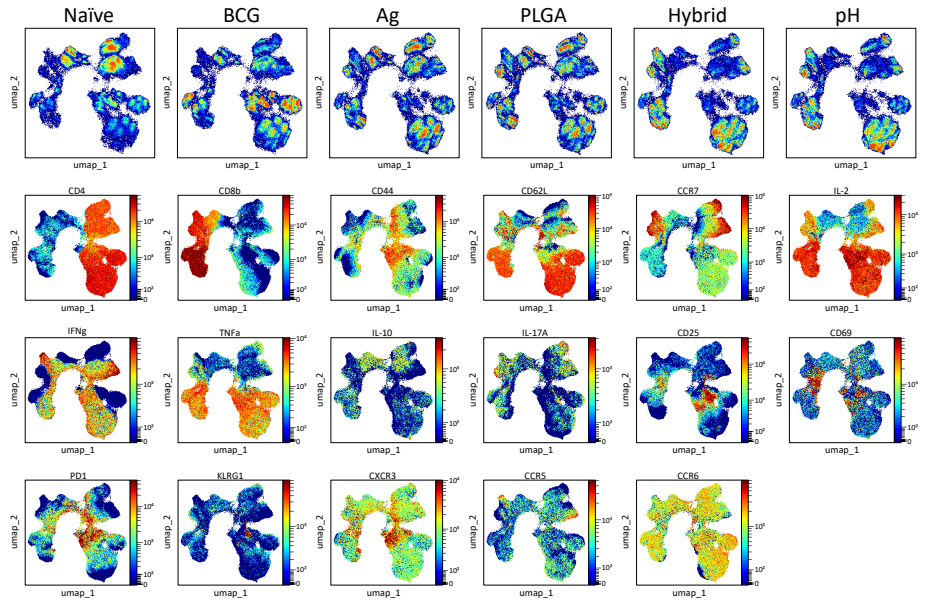

Figure 2. UMAP visualization of concatenated, AER-restimulated spleen-derived $CD4^+$, and $CD8^+$ T cells ($CD3^+$ $CD19^-$) from all tested mice (per group) showing differential abundances of various populations of cells followed by color-continuous plots depicting phenotypical markers distribution. Groups: naïve – unimmunized mice; BCG – live BCG; Ag –antigen (25 μg Ag85B-ESAT6-Rv2034, AER) adjuvant mix (50 μg CpG, 1 μg MPLA), NP-free; PLGA – antigen (8 μg AER) and adjuvants (2.5 μg CpG, 1 μg MPLA) delivered in PLGA (400 μg) NPs; Hybrid – antigen (8 μg AER) and adjuvants (2.5 μg CpG, 1 μg MPLA) delivered in lipid (400 μg DOPC:DOPE:DOBAQ:EPC, 3:5:2:4)-PLGA (400 μg) NPs; pH – (8 μg AER) antigen and adjuvants (2.5 μg CpG, 1 μg MPLA) delivered in cationic pH-sensitive liposomes (400 μg DOPC:DOPE:DOBAQ:EPC, 3:5:2:4).

AER-specific $CD4^+$ and $CD8^+$ T-cell responses in splenocytes ex vivo

Splenocytes from immunized (but non-Mtb-challenged mice) were collected and restimulated with AER. The cells were then stained with a 27-color panel and analyzed using spectral flow cytometry to evaluate the immune responses. Concatenated flow cytometry events of $CD3^+$ $CD19^-$ T-cells were examined following uniform manifold approximation and projection (UMAP) dimensionality reduction (Fig. 2). UMAP was employed to evaluate global qualitative changes across experimental groups, utilizing all $CD3^+$ $CD19^-$ events simultaneously. The visual inspection of the data revealed differences in the abundance of T cells between the groups. Major differences in the abundances of $CD4^+$ and $CD8^+$ cells, especially cells expressing IL-2, IFN-γ, and TNF-α, were observed when comparing UMAPs of vaccinated mice compared to naïve mice. Subsequently, differential subset abundance analysis was performed to identify populations of interest and perform quantitative comparisons. We then selected sufficiently large cell populations (>100 events) and exhibited specific phenotypic markers that not only differentiated them from other cell subsets but also provided insights into their functional role. If several subsets were characterized by overlapping marker expression patterns, we selected one

that was defined by more markers and was still large enough. We observed several CD4⁺ T-cell subpopulations that were differentially abundant (Fig. 3). The largest population was a polyfunctional population defined as CD4⁺ IL-2⁺ IFN-γ⁺ TNF-α⁺ IL-17A⁻ IL-10⁻ CD44⁻ CD62L⁺ CCR7⁻ T cells. All AER-based vaccination groups increased this population, displaying a central memory phenotype, but interestingly, this was not the case for BCG. Similarly, a monofunctional Th1 cell subset defined as CD4⁺ IL-2⁻ IFN-γ⁺ TNF-α⁻ IL-17A⁻ IL-10⁻ CD44⁻ CD62L⁻ CCR7⁺ T cells displaying an effector memory phenotype was also differentially enriched. On the other hand, two subpopulations of CD4⁺ T cells were increased following BCG vaccination but not AER-based vaccines: a monofunctional central memory population of CD4⁺ IL-2⁺ IFN-γ⁻ TNF-α⁻ IL-17A⁻ IL-10⁻ CD44⁻ CD62L⁺ CCR7⁻ T cells as well as a population CD4⁺ IL-2⁺ TNF-α⁺ CD25⁺ CD69⁺. Th17 responses were not observed in this study.

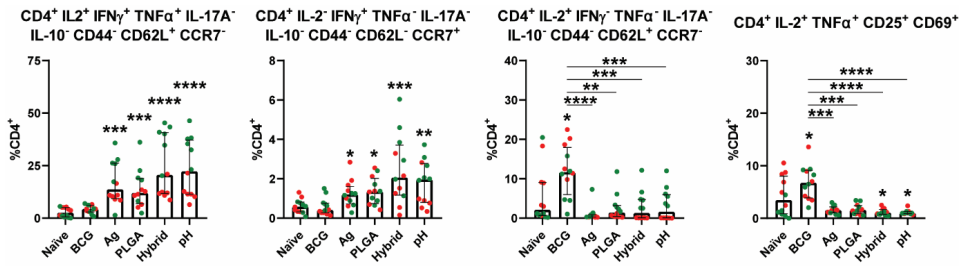

Figure 3. Differential abundance of CD4⁺ T-cells present in AER restimulated splenocytes from immunized non-Mtb-challenged mice. Markers defining each population are indicated above each graph. Graph values depict percentages of the population as a part of the CD3⁺ CD19⁻ CD4⁺ CD8⁻ cell subset. Each dot represents a single mouse and results from the same experiment are shown in one color. Groups: naïve – unimmunized mice; BCG – live BCG; Ag –antigen (25 μg Ag85B-ESAT6-Rv2034, AER) adjuvant mix (50 μg CpG, 1 μg MPLA), NP-free; PLGA – antigen (8 μg AER) and adjuvants (2.5 μg CpG, 1 μg MPLA) delivered in PLGA (400 μg) NPs; Hybrid – antigen (8 μg AER) and adjuvants (2.5 μg CpG, 1 μg MPLA) delivered in lipid (400 μg DOPC:DOPE:DOBAQ:EPC, 3:5:2:4)-PLGA (400 μg) NPs; pH – (8 μg AER) antigen and adjuvants (2.5 μg CpG, 1 μg MPLA) delivered in cationic pH-sensitive liposomes (400 μg DOPC:DOPE:DOBAQ:EPC, 3:5:2:4). n = 12 (mice). The minimal number of events used in the analysis was 20,000. Bars represent median ± IQR. *p < 0.05, **p< 0.01, ***p < 0.001, ****p < 0.0001 (Kruskal-Wallis with an uncorrected Dunn's posthoc test).

Similarly, we analyzed CD8⁺ T-cell populations (Fig. 4). The largest population was a polyfunctional central memory T-cell subset defined as CD8⁺ IL-2⁺ IFN-γ⁺ TNF-α⁺ IL-17A⁻ IL-10⁻ CD44⁻ CD62L⁺ CCR7⁻ T-cells. It was significantly increased in all groups immunized with AER-based vaccines but not in the case of BCG. We also observed two other subsets that were increased by AER-based vaccines: a monofunctional central memory CD4⁺ IL-2⁻ IFN-γ⁺ TNF-α⁻ IL-17A⁻ IL-10⁻ CD62L⁺ CCR7⁺ T-cells and T-cells defined as CD8⁺ IL-17A⁺ IFN-γ⁺. One population increased following BCG immunization, but none of the AER-based vaccines defined as CD8⁺ IL-2⁺ TNF-α⁺ CD44⁺ CD62L⁻ CCR7⁻ displayed predominantly an effector memory phenotype.

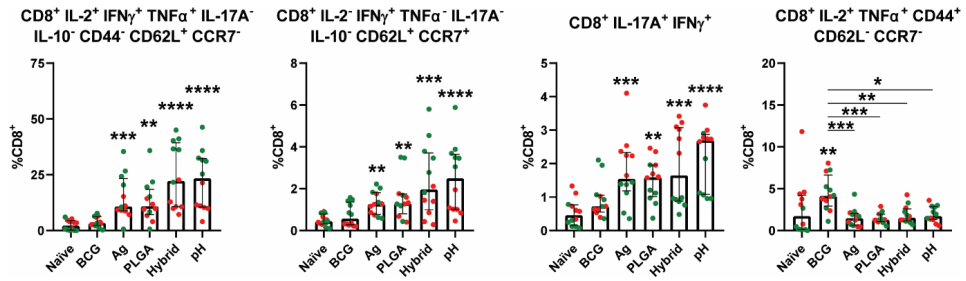

Figure 4. Differential abundance of CD8⁺ T-cell populations present in AER restimulated splenocytes from immunized non-Mtb-challenged mice. Markers defining each population are indicated above each graph. Graph values depict percentages of the population as a part of the CD3⁺ CD19⁻ CD4⁻ CD8⁺ cell subset. Each dot represents a percentage value from a single mouse and results from the same experiment are shown in one color. Groups: naïve – unimmunized mice; BCG – live BCG; Ag –antigen (25 μg Ag85B-ESAT6-Rv2034, AER) adjuvant mix (50 μg CpG, 1 μg MPLA), NP-free; PLGA – antigen (8 μg AER) and adjuvants (2.5 μg CpG, 1 μg MPLA) delivered in PLGA (400 μg) NPs; Hybrid – antigen (8 μg AER) and adjuvants (2.5 μg CpG, 1 μg MPLA) delivered in lipid (400 μg DOPC:DOPE:DOBAQ:EPC, 3:5:2:4)-PLGA (400 μg) NPs; pH – (8 μg AER) antigen and adjuvants (2.5 μg CpG, 1 μg MPLA) delivered in cationic pH-sensitive liposomes (400 μg DOPC:DOPE:DOBAQ:EPC, 3:5:2:4). n = 12 (mice). The minimal number of events used in the analysis was 20,000. Bars represent median ± IQR. *p < 0.05, **p< 0.01, ***p < 0.001, ****p < 0.0001 (Kruskal-Wallis with an uncorrected Dunn's posthoc test).

Differentially abundant B-cell populations

Similar to the analysis of T-cell responses, B-cell data were dimensionally reduced and UMAPs were analyzed (Fig. 5). The UMAPs revealed the presence of differentially abundant populations of cells between different groups. Subsequently, differential subset abundance analysis was carried out, and statistically significant subsets were analyzed using univariate plots (Fig. 6). Three B-cell populations expressing activation marker CD69 were found in AER-restimulated splenocytes. The largest population was a subset identified as MHCII⁺ IgM⁻ IgD⁻ B220⁺ CD69⁺ B cells corresponding to germinal center B cells, followed by MHCII⁺ IgM⁻ IgD⁺ B220⁺ CD69⁺ (follicular B/B2 cells), and MHCII⁺ IgM⁺ IgD⁻ B220⁺ CD69⁺ (marginal zone B-cell, transitional 1 B cells) follicular B/B2) [88, 89]. All three B-cell subsets were more abundant in mouse groups vaccinated with AER-based vaccines compared to naïve mice. Moreover, mice vaccinated with lipid-PLGA hybrid NPs as well as pH-sensitive liposomes had higher counts of these B cells compared to mice vaccinated with AER mixed with CpG and MPLA. B cells defined as IL-17A⁺ B220⁺ MHCII⁺ B cells were increased in mice vaccinated with BCG compared to naïve mice and mice vaccinated with AER-based vaccines.

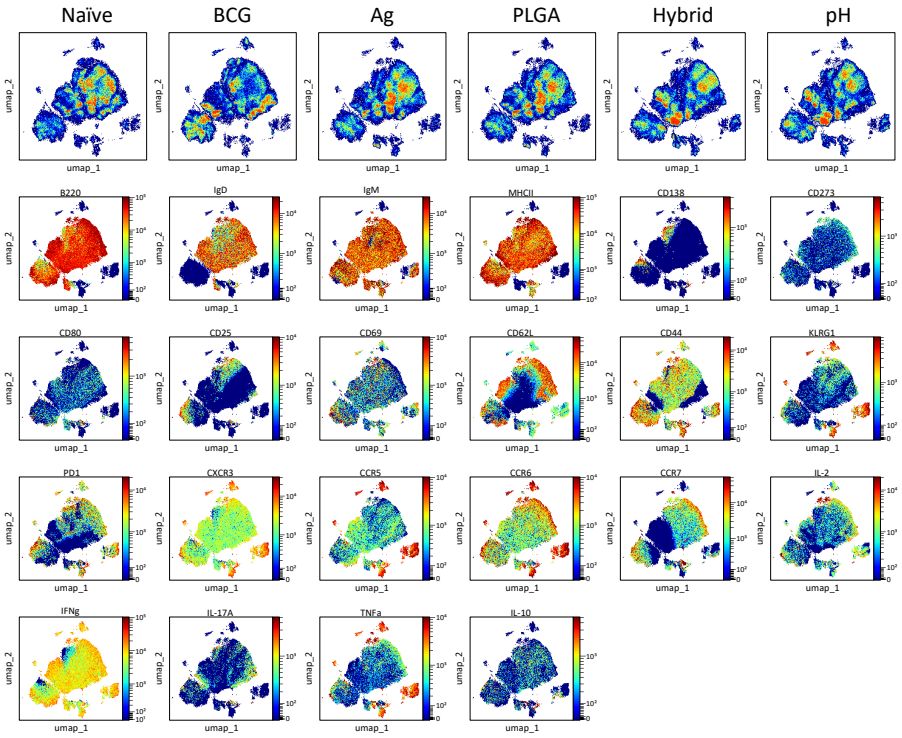

Figure 5. UMAP visualization of concatenated, AER-restimulated spleen-derived B-cells ($CD3^-$ $CD19^+$) from all tested mice (per group) showing differential abundances of various populations of cells followed by color-continuous plots depicting phenotypical markers distribution. Groups: naïve – unimmunized mice; BCG – live BCG; Ag –antigen (25 μg Ag85B-ESAT6-Rv2034, AER) adjuvant mix (50 μg CpG, 1 μg MPLA), NP-free; PLGA – antigen (8 μg AER) and adjuvants (2.5 μg CpG, 1 μg MPLA) delivered in PLGA (400 μg) NPs; Hybrid – antigen (8 μg AER) and adjuvants (2.5 μg CpG, 1 μg MPLA) delivered in lipid (400 μg DOPC:DOPE:DOBAQ:EPC, 3:5:2:4)-PLGA (400 μg) NPs; pH – (8 μg AER) antigen and adjuvants (2.5 μg CpG, 1 μg MPLA) delivered in cationic pH-sensitive liposomes (400 μg DOPC:DOPE:DOBAQ:EPC, 3:5:2:4).

AER-specific antibody production

AER-specific antibody titers were investigated to explore humoral immune responses after vaccination. All four AER-based vaccines resulted in high antibody titers (Fig. 7). However, in sera from naïve and BCG-vaccinated mice, AER-specific total Ig titers were below the detection limit. The highest total as well as IgG1 and IgG2 antibody titers were observed in mice vaccinated with cationic pH-sensitive liposomes and the lowest in mice immunized with the AER-adjuvant mix. Moreover, we also observed titers of other subtypes: high IgG2b and IgG2c as well as moderate-low levels of IgG3 and IgM (Fig. S6).

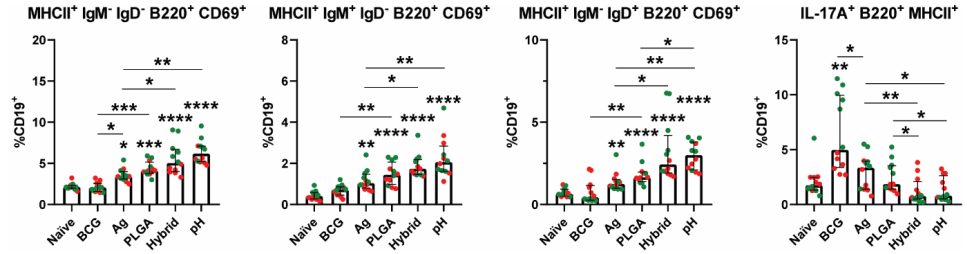

Figure 6. Differential abundance of $CD19^+$ B-cell populations present in AER restimulated splenocytes from immunized non-Mtb-challenged mice. Markers defining each population are indicated above each graph. Graph values depict percentages of the population as a part of the $CD3^-$ $CD19^+$ cell subset. Each dot represents a percentage value from a single mouse and results from the same experiment are shown in one color. Groups: naïve – unimmunized mice; BCG – live BCG; Ag –antigen (25 μg Ag85B-ESAT6-Rv2034, AER) adjuvant mix (50 μg CpG, 1 μg MPLA), NP-free; PLGA – antigen (8 μg AER) and adjuvants (2.5 μg CpG, 1 μg MPLA) delivered in PLGA (400 μg) NPs; Hybrid – antigen (8 μg AER) and adjuvants (2.5 μg CpG, 1 μg MPLA) delivered in lipid (400 μg DOPC:DOPE:DOBAQ:EPC, 3:5:2:4)-PLGA (400 μg) NPs; pH – (8 μg AER) antigen and adjuvants (2.5 μg CpG, 1 μg MPLA) delivered in cationic pH-sensitive liposomes (400 μg DOPC:DOPE:DOBAQ:EPC, 3:5:2:4). n = 12 (mice). The minimal number of events used in the analysis was 20,000. Bars represent median ± IQR. *$p < 0.05$, **$p < 0.01$, ***$p < 0.001$, ****$p < 0.0001$. (Kruskal-Wallis with an uncorrected Dunn's posthoc test).

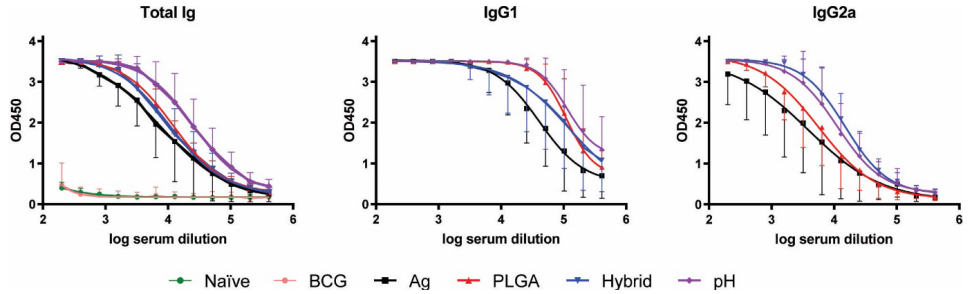

Figure 7. Quantification of AER-specific antibodies in sera. The type of antibody measured is indicated above each graph. Values represent OD450 ELISA, and serum dilutions are shown on the x-axis. Groups are indicated in the legend. Groups: naïve – unimmunized mice; BCG – live BCG; Ag –antigen (25 μg Ag85B-ESAT6-Rv2034, AER) adjuvant mix (50 μg CpG, 1 μg MPLA), NP-free; PLGA – antigen (8 μg AER) and adjuvants (2.5 μg CpG, 1 μg MPLA) delivered in PLGA (400 μg) NPs; Hybrid – antigen (8 μg AER) and adjuvants (2.5 μg CpG, 1 μg MPLA) delivered in lipid (400 μg DOPC:DOPE:DOBAQ:EPC, 3:5:2:4)-PLGA (400 μg) NPs; pH – (8 μg AER) antigen and adjuvants (2.5 μg CpG, 1 μg MPLA) delivered in cationic pH-sensitive liposomes (400 μg DOPC:DOPE:DOBAQ:EPC, 3:5:2:4). n = 6 (mice). Values represent mean ± standard deviation.

DISCUSSION

TB remains a global epidemic, as a highly contagious airborne infectious disease that remains one of the foremost causes of death worldwide for centuries. According to the 2022 WHO Global Tuberculosis Report, approximately a quarter of the global population is latently infected with Mtb. Between 2000 and 2021, TB claimed the lives of 1.4 to 2 million individuals

annually, with a peak mortality between 2000 and 2010. In 2022 alone, TB was responsible for over one million deaths, surpassing fatalities from any other single infectious agent before the COVID-19 pandemic. Despite intense research efforts, the world still lacks a licensed effective TB vaccine, especially for adolescents and adults. The only licensed vaccine, BCG, offers moderate protection to infants and children but falls short for adult populations with the highest TB incidence, emphasizing the urgent need for a new vaccine [1].

NPs are very effective delivery systems for subunit vaccines, offering several advantages in enhancing their efficacy. Firstly, NPs function as adjuvants, enhancing the antigenicity of associated antigens, and can mimic some properties of pathogens like viruses. Secondly, NPs can trigger both innate and adaptive immune responses, acting as effective antigen carriers that enhance antigen processing and presentation. Their nanoscale size promotes efficient uptake by phagocytic cells and facilitates robust innate immune responses. This positions NPs as pivotal tools in next-generation vaccine development [90–92].

The physicochemical properties of NPs dictate their recognition, uptake, and immune responses [93–95]. Key properties such as size, charge, hydrophobicity, and rigidity affect interactions with interstitial matrix and antigen-presenting cells (APCs) [96, 97]. Small particles (<20 nm) drain to blood capillaries and are eliminated, while particles 20–100 nm drain into lymph nodes (LNs) and are taken up by LN-resident APCs. Larger NPs (>100 nm) remain at the injection site (SOI) until transported to LNs by resident APCs [98, 99]. Surface charge affects interactions with the interstitial matrix and cellular membranes [95]. Neutral and negatively charged NPs drain more easily into LNs [100, 101], while positively charged particles are more efficiently taken up by APCs [102, 103] and form depots, facilitating immune responses [40]. The depot effect allows precise targeting of APCs, controlled antigen release, and antigens retention at the SOI. This leads to prolonged exposure to the immune system and continuous stimulation of the APCs in the vicinity of the SOI. Rigid NPs are more efficiently taken up by APCs and facilitate depot formation at the SOI [104, 105] compared to soft NPs [106, 107]. Hydrophilic NPs may accumulate more in LNs than hydrophobic ones of similar size [108, 109].

In this study, PLGA NPs (85 nm, -50 mV) with a hydrophilic, acid-terminated surface likely exhibited short retention at the SOI and efficient transport to LNs, which resulted in strong immune responses possibly due to slow release of antigens and adjuvants from the NP core. Hybrid lipid-PLGA NPs and liposomes (140–170 nm, 20–25 mV) with hydrophilic surfaces formed palpable depots at the SOI, likely resulting in extended antigen presentation. Although hybrid NPs most likely offered a slow release of antigens and adjuvants compared to the expected burst release from liposomes, both types of NPs induced comparable protection and immune response.

To date, no clear immune correlates of protection against tuberculosis have been established. Therefore, it remains a challenge to identify types of immune responses that should be induced by a vaccine that would result in protection against Mtb. Historically, T-helper-1 responses were deemed essential for a successful TB vaccination, and this notion was supported by ample evidence [10, 110–112]. However, over time a conventional strategy aiming to induce predominant Th1/Th17 responses and minimize Th2/Treg immunity is being complemented by a more balanced approach that would lead to the interplay between Th1 and Th2 responses as well as B-cell responses. Such a diverse immune response repertoire is supposed to be more beneficial for the host.

All of the AER-containing vaccines induced primarily polyfunctional $CD4^+$ and $CD8^+$ T-cells that produced IL-2, IFN-γ, and TNF-α, as well as monofunctional IFN-γ-producing T-cells, which both displayed a central memory phenotype [113]. The observed polyfunctional T-cells expressed CD62L but not CD44 or CCR7, which could mean that they belong to a separate central memory T-cell subset that has lost CD44, as shown by Henao-Tamayo et al. [113]. $CD4^+$ T cells with such a phenotype were observed to possess a significant expansion potential and induced excellent protection when transferred to $Rag^{-/-}$ mice challenged with Mtb H37Rv but not $CD4^+$ $CD44^{hi}$ $CD62L^{lo}$ cells [114]. $CD44^{lo}$ $CD62L^{hi}$ T-cells could significantly contribute to the protective responses like T cells with $CD62L^{hi}$ $CCR7^{hi}$ central memory phenotype. Central memory $CD4^+$ T cells rather than effector memory T cells mediate long-term protection, and it has been suggested that inadequate protection conferred by BCG in adults and adolescents may be (partially) attributed to insufficient central memory T-cell responses [115].

Noteworthy, we observed a significant increase in $CD8^+$ T cells compared to naïve mice, especially in mice vaccinated with lipid-PLGA hybrid NPs, and cationic pH-sensitive liposomes. The significance of cytotoxic $CD8^+$ T cells in Mtb protection is debated. Beyond directly killing infected cells, they produce cytokines, modulate the immune response, and work together with Th1 cells [116, 117]. Recent research suggests $CD8^+$ T cells, alongside Th1 cells, are promising vaccine targets against Mtb [10, 118, 119]. Mouse studies support their importance in controlling Mtb [120–123]. Specifically, $CD8^+$ T-cell depletion increases bacterial load during latent phases in both mice [124] and non-human primates [125]. Interestingly, we observed elevated counts of IL-17A-producing $CD8^+$ T cells but not $CD4^+$ T cells. These $CD8^+$ T cells, referred to as Tc17, are postulated to exhibit functions comparable to Th17 cells [126, 127]. Th17 cells contribute to protective responses in the early stages of Mtb infection by engaging neutrophils and Th1 cells to infection sites and play a role in the formation of mature granuloma, which is crucial for the control of the disease [10, 128]. However, further investigations are necessary to elucidate the specific role of Tc17 cells in immune responses against Mtb infection.

An increase in three subsets of CD69-expressing B cells and high total AER-specific and Ig subtypes were observed in mice immunized with AER-based vaccines, which could contribute to the protection. B cell and antibody responses are believed to contribute to TB immunity, but their exact role remains ambiguous [129, 130]. Evidence for B-cell involvement is substantiated by increased vulnerability to Mtb in B-cell-depleted subjects restored post-B-cell transfer [131–133] and B-cell dysfunction in active TB patients rectifying post-treatment [134]. However, some genetic knockout studies and Mtb infection models challenge this perspective [135–137]. The protective role of antibody responses is supported by research on sera transfers from LTBI patients showing protective effects in mice [138] as well as treatment with monoclonal antibodies against Mtb antigens has been shown to improve survival, reduce spread, decrease tissue damage, and decrease mycobacterial load in animals [139–142]. Differential antibody responses between LTBI and ATB patients have also been shown. Antibodies from LTBI patients exhibited enhanced FC receptor profiles and enhanced macrophage killing of intracellular Mtb [143].

All delivery-system-based AER vaccines (PLGA, lipid-PLGA hybrid NPs, and pH-sensitive liposomes) induced protection in intranasal Mtb challenge mouse model but not AER-adjuvant mix, despite overall similar immune responses induced by all AER vaccines. Importantly, the immunological effects induced by the NP-based vaccine were achieved at significantly lower doses of the antigen and adjuvants. This highlights the substantial advantage of using these nanoparticles for vaccine delivery, as they lead to better immunological outcomes and can reduce costs associated with antigens. $CD4^+$, $CD8^+$ T-cell, and B-cell responses that we observed have been previously linked with protective outcomes by others; however, they do not explain the induced protection by these vaccines. The protection mechanism remains unknown because there are no established correlates of Mtb protection, and none of the immune responses observed in this study were associated with bacterial burden outcomes. This knowledge gap is a major hurdle in developing effective TB vaccines, and this issue has been raised in the literature before [144, 145].

The study's primary limitation is its single time point assessment, missing dynamic immune responses, and potential long-term effects. Future research should investigate multiple time points and explore various doses of the antigen, NPs, and adjuvants. The 7-day lymphocyte restimulation limited early immune responses study. The lack of immune response data from Mtb-challenged mice limits direct protection correlation. However, the study's strength lies in linking human innate responses with adaptive immune responses in vaccinated mice, finding NP-based vaccines that outperform BCG, hinting at broader applicability to other models and human use.

CONCLUSION

In this study, three types of NP-based potential TB vaccines were compared *in vivo*: PLGA, lipid-PLGA hybrid NPs, and cationic pH-sensitive liposomes. The formulations used Ag85B-ESAT6-Rv2034 AER fusion antigen, and two adjuvants (CpG and MPLA). Lipids used in the production of the hybrid NPs and liposomes comprised of DOPC:DOPE:DOBAQ:EPC at 3:5:2:4 molar ratio. This study describes the side-by-side comparison of three types of delivery systems in terms of protection (Mtb burden reduction in lungs and spleens) as well as a comprehensive exploration of immune responses: $CD4^+$/$CD8^+$ T-cell, B-cell, and antigen-specific antibody production. Vaccines that used NP-based delivery systems induced protection in intranasal Mtb-challenged mice as indicated by a significant CFU reduction compared to NP-free vaccination (AER mixed with CpG and MPLA). Moreover, NP-based vaccines induced a significant increase in polyfunctional $CD4^+$, and $CD8^+$ T-cells, as well as $CD69^+$ B-cell subsets, and high antigen-specific antibody titers. NP-based vaccines induced protection and protective immune responses at much lower doses of the antigen and molecular adjuvants than the NP-free vaccine. Our study's strength lies in linking human innate with adaptive immune responses in immunized mice, thereby identifying NP-based vaccines that outperform BCG. PLGA, lipid-PLGA hybrid NPs, and cationic pH-sensitive liposomes are excellent promising vaccine delivery candidates, and their application should be further explored.

References

1. World Health Organization, 2023. Global Tuberculosis Report 2023. Geneva. https://iris.who.int/handle/10665/373828.
2. Coppola, M., Ottenhoff, T.H., 2018. Genome wide approaches discover novel Mycobacterium tuberculosis antigens as correlates of infection, disease, immunity and targets for vaccination. Semin. Immunol. 39, 88–101. https://doi.org/10.1016/J.SMIM.2018.07.001.
3. World Health Organization, 2015. The end TB strategy. World Health Organization, https://iris.who.int/handle/10665/331326.
4. World Health Organization, 2015. Implementing the end TB strategy: the essentials. World Health Organization, https://iris.who.int/handle/10665/206499.
5. World Health Organization, 2022a. Western Pacific regional framework to end TB: 2021-2030. WHO Regional Office for the Western Pacific, https://iris.who.int/handle/10665/352278.
6. Pérez-Alós, L., Armenteros, J.J.A., Madsen, J.R., Hansen, C.B., Jarlhelt, I., Hamm, S.R., Heftdal, L.D., Pries-Heje, M.M., Møller, D.L., Fogh, K., Hasselbalch, R.B., Rosbjerg, A., Brunak, S., Sørensen, E., Larsen, M.A.H., Ostrowski, S.R., Frikke-Schmidt, R., Bayarri-Olmos, R., Hilsted, L.M., Iversen, K.K., Bundgaard, H., Nielsen, S.D., Garred, P., 2022. Modeling of waning immunity after SARS-CoV-2 vaccination and influencing factors. Nat. Commun. 2022 13:1 13, 1–11. https://doi.org/10.1038/s41467-022-29225-4.
7. Pollard, A.J., Bijker, E.M., 2020. A guide to vaccinology: from basic principles to new developments. Nat. Rev. Immunol. 2020 21:2 21, 83–100. https://doi.org/10.1038/s41577-020-00479-7.
8. Rémy, V., Zöllner, Y., Heckmann, U., 2015. Vaccination: the cornerstone of an efficient healthcare system. J. Mark. Access Health Policy 3, 27041. https://doi.org/10.3402/JMAHP.V3.27041.
9. Brewer, T.F., 2000. Preventing Tuberculosis with Bacillus Calmette-Guérin Vaccine: A Meta-Analysis of the Literature. Clin. Infect. Dis. 31, S64–S67. https://doi.org/10.1086/314072.
10. Ottenhoff, T.H.M., Kaufmann, S.H.E., 2012. Vaccines against Tuberculosis: Where Are We and Where Do We Need to Go? PLoS Pathog. 8, e1002607. https://doi.org/10.1371/journal.ppat.1002607.
11. Trunz, B.B., Fine, P., Dye, C., 2006. Effect of BCG vaccination on childhood tuberculous meningitis and miliary tuberculosis worldwide: a meta-analysis and assessment of cost-effectiveness. Lancet 367, 1173–1180. https://doi.org/10.1016/S0140-6736(06)68507-3.
12. Christensen, D., Korsholm, K.S., Andersen, P., Agger, E.M., 2011. Cationic liposomes as vaccine adjuvants. Expert Rev. Vaccines 10, 513–521. https://doi.org/10.1586/erv.11.17.
13. Moyle, P.M., Toth, I., 2013. Modern Subunit Vaccines: Development, Components, and Research Opportunities. ChemMedChem 8, 360–376. https://doi.org/10.1002/cmdc.201200487.
14. Barnier-Quer, C., Elsharkawy, A., Romeijn, S., Kros, A., Jiskoot, W., 2013. Adjuvant Effect of Cationic Liposomes for Subunit Influenza Vaccine: Influence of Antigen Loading Method, Cholesterol and Immune Modulators. Pharmaceutics 5, 392–410. https://doi.org/10.3390/pharmaceutics5030392.
15. Tandrup Schmidt, S., Foged, C., Smith Korsholm, K., Rades, T., Christensen, D., 2016. Liposome-Based Adjuvants for Subunit Vaccines: Formulation Strategies for Subunit Antigens and Immunostimulators. Pharmaceutics 8, 7. https://doi.org/10.3390/pharmaceutics8010007.
16. Marasini, N., Ghaffar, K.A., Skwarczynski, M., Toth, I., 2017. Liposomes as a Vaccine Delivery System, in: Micro- and Nanotechnology in Vaccine Development, 221–239. https://doi.org/10.1016/B978-0-323-39981-4.00012-9.
17. Silva, A.L., Soema, P.C., Slütter, B., Ossendorp, F., Jiskoot, W., 2016. PLGA particulate delivery systems for subunit vaccines: Linking particle properties to immunogenicity. Hum. Vaccin. Immunother. 12, 1056–1069. https://doi.org/10.1080/21645515.2015.1117714.
18. Storni, T., Kündig, T.M., Senti, G., Johansen, P., 2005. Immunity in response to particulate antigen-delivery systems. Adv. Drug Deliv. Rev. 57, 333–355. https://doi.org/10.1016/J.ADDR.2004.09.008.
19. Allahyari, M., Mohit, E., 2016. Peptide/protein vaccine delivery system based on PLGA particles. Hum. Vaccin. Immunother. 12, 806–828. https://doi.org/10.1080/21645515.2015.1102804.
20. Danhier, F., Ansorena, E., Silva, J.M., Coco, R., Le Breton, A., Préat, V., 2012. PLGA-based nanoparticles: An overview of biomedical applications. J. Control. Release 161, 505–522. https://doi.org/10.1016/J.JCONREL.2012.01.043.
21. Duong, V.T., Skwarczynski, M., Toth, I., 2023. Towards the development of subunit vaccines against tuberculosis: The key role of adjuvant. Tuberculosis 139, 102307. https://doi.org/10.1016/J.TUBE.2023.102307.
22. Ignjatovic, N.L., Ajdukovic, Z.R., Savic, V.P., Uskokovic, D.P., 2010. Size effect of calcium phosphate coated with poly-DL-lactide-co-glycolide on healing processes in bone reconstruction. J. Biomed. Mater. Res. B. Appl. Biomater. 94B, 108–117. https://doi.org/10.1002/JBM.B.31630.
23. Jain, R.A., 2000. The manufacturing techniques of various drug loaded biodegradable poly(lactide-co-glycolide) (PLGA) devices. Biomaterials 21, 2475–2490. https://doi.org/10.1016/S0142-9612(00)00115-0.
24. Lü, J.M., Wang, X., Marin-Muller, C., Wang, H., Lin, P.H., Yao, Q., Chen, C., 2014. Current advances in research and clinical applications of PLGA-based nanotechnology. Expert Rev. Mol. Diagn. 9, 325–341. https://doi.org/10.1586/ERM.09.15.
25. Akagi, T., Baba, M., Akashi, M., 2012. Biodegradable nanoparticles as vaccine adjuvants and delivery systems: Regulation of immune responses by nanoparticle-based vaccine. Adv. Polym. Sci. 247, 31–64. https://doi.org/10.1007/12_2011_150.
26. Ashhurst, A.S., Parumasivam, T., Chan, J.G.Y., Lin, L.C.W., Flórido, M., West, N.P., Chan, H.K., Britton, W.J., 2018. PLGA particulate subunit tuberculosis vaccines promote humoral and Th17 responses but do not enhance control of Mycobacterium tuberculosis infection. PLoS One 13, e0194620. https://doi.org/10.1371/JOURNAL.PONE.0194620.
27. Chong, C.S.W., Cao, M., Wong, W.W., Fischer, K.P., Addison, W.R., Kwon, G.S., Tyrrell, D.L., Samuel, J., 2005. Enhancement of T helper type 1 immune responses against hepatitis B virus core antigen by PLGA nanoparticle vaccine delivery. J. Control. Release 102, 85–99. https://doi.org/10.1016/J.JCONREL.2004.09.014.
28. Hamdy, S., Molavi, O., Ma, Z., Haddadi, A., Alshamsan, A., Gobti, Z., Elhasi, S., Samuel, J., Lavasanifar, A., 2008. Co-delivery of cancer-associated antigen and Toll-like receptor 4 ligand in PLGA nanoparticles induces potent CD8+ T cell-mediated anti-tumor immunity. Vaccine 26, 5046–5057. https://doi.org/10.1016/J.VACCINE.2008.07.035.
29. Liang, Z., Li, M., Ni, J., Hussain, T., Yao, J., Song, Y., Liu, Y., Wang, H., Zhou, X., 2022. CFP10–loaded PLGA nanoparticles as a booster vaccine confer protective immunity against Mycobacterium bovis. Bioimpacts 12, 395. https://doi.org/10.34172/BI.2022.23645.
30. Malik, A., Gupta, M., Mani, R., Bhatnagar, R., 2019. Single-dose Ag85b-ESAT6–loaded poly(Lactic-co-glycolic acid) nanoparticles confer protective immunity against tuberculosis. Int. J. Nanomedicine 14, 3129–3143. https://doi.org/10.2147/IJN.S172391.
31. Ni, J., Liu, Y., Hussain, T., Li, M., Liang, Z., Liu, T., Zhou, X., 2021. Recombinant ArgF PLGA nanoparticles enhances BCG induced immune responses against Mycobacterium bovis infection. Biomed. Pharmacother.137, 111341. https://doi.org/10.1016/J.BIOPHA.2021.111341.
32. Schlosser, E., Mueller, M., Fischer, S., Basta, S., Busch, D.H., Gander, B., Groettrup, M., 2008. TLR ligands and antigen need to be coencapsulated into the same biodegradable microsphere for the generation of potent cytotoxic T lymphocyte responses. Vaccine 26, 1626–1637. https://doi.org/10.1016/J.VACCINE.2008.01.030.
33. Heuts, J., Varypataki, E.M., van der Maaden, K., Romeijn, S., Drijfhout, J.W., van Scheltinga, A.T., Ossendorp, F., Jiskoot, W., 2018. Cationic Liposomes: A Flexible Vaccine Delivery System for Physicochemically Diverse Antigenic Peptides. Pharm. Res. 35, 1–9. https://doi.org/10.1007/s11095-018-2490-6.
34. Latif, N., Bachhawat, B.K., 1984. The effect of surface charges of liposomes in immunopotentiation. Biosci. Rep. 4, 99–107. https://doi.org/10.1007/BF01120305.
35. Liu, X., Da, Z., Wang, Yue, Niu, H., Li, R., Yu, H., He, S., Guo, M., Wang, Yong, Luo, Y., Ma, X., Zhu, B., 2016. A novel liposome adjuvant DPC mediates Mycobacterium tuberculosis subunit vaccine well to induce cell-mediated immunity and high protective efficacy in mice. Vaccine 34, 1370–1378. https://doi.org/10.1016/j.vaccine.2016.01.049.
36. Khademi, F., Taheri, R.A., Momtazi-Borojeni, A.A., Farnoosh, G., Johnston, T.P., Sahebkar, A., 2018. Potential of cationic liposomes as adjuvants/delivery systems for tuberculosis subunit vaccines, in: Reviews of Physiology, Biochemistry and Pharmacology, 47–69. https://doi.org/10.1007/112_2018_9.
37. Luwi, N.E.M., Ahmad, S., Azlyna, A.S.N., Nordin, A., Sarmiento, M.E., Acosta, A., Azmi, M.N., Uskoković, V., Mohamud, R., Kadir, R.,

2022. Liposomes as immunological adjuvants and delivery systems in the development of tuberculosis vaccine: A review. Asian Pac. J. Trop. Med. https://doi.org/10.4103/1995-7645.332806.
38. Tretiakova, D.S., Vodovozova, E.L., 2022. Liposomes as Adjuvants and Vaccine Delivery Systems. Biochem. (Mosc.) Suppl. Ser. A Membr. Cell Biol. 16:1 16, 1–20. https://doi.org/10.1134/S1990747822020076.
39. Du, G., Hathout, R.M., Nasr, M., Nejadnik, M.R., Tu, J., Koning, R.I., Koster, A.J., Slütter, B., Kros, A., Jiskoot, W., Bouwstra, J.A., Mönkäre, J., 2017. Intradermal vaccination with hollow figure needles: A comparative study of various protein antigen and adjuvant encapsulated nanoparticles. J. Control. Release 266, 109–118. https://doi.org/10.1016/j.jconrel.2017.09.021.
40. Henriksen-Lacey, M., Bramwell, V.W., Christensen, D., Agger, E.M., Andersen, P., Perrie, Y., 2010. Liposomes based on dimethyldioctadecylammonium promote a depot effect and enhance immunogenicity of soluble antigen. J. Control. Release 142, 180–186. https://doi.org/10.1016/j.jconrel.2009.10.022.
41. Nakanishi, T., Kunisawa, J., Hayashi, A., Tsutsumi, Y., Kubo, K., Nakagawa, S., Nakanishi, M., Tanaka, K., Mayumi, T., 1999. Positively charged liposome functions as an efficient immunoadjuvant in inducing cell-mediated immune response to soluble proteins. J. Control. Release 61, 233–240. https://doi.org/10.1016/S0168-3659(99)00097-8.
42. Balamurali, V., Pramodkuma, T.M., Srujana, N., Venkatesh, M.P., Gupta, N.V., Krishna, K.L., Gangadhara, H.V., 2010. pH Sensitive Drug Delivery Systems: A Review. Am. J. Drug Discov. Dev. 1, 24–48. https://doi.org/10.3923/AJDD.2011.24.48.
43. Karanth, H., Murthy, R.S.R., 2007. pH-Sensitive liposomes-principle and application in cancer therapy. J. Pharm. Pharmacol. 59, 469–483. https://doi.org/10.1211/JPP.59.4.0001.
44. Liu, X., Huang, G., 2013. Formation strategies, mechanism of intracellular delivery and potential clinical applications of pH-sensitive liposomes. Asian J. Pharm. Sci. 8, 319–328. https://doi.org/10.1016/J.AJPS.2013.11.002.
45. Mu, Y., Gong, L., Peng, T., Yao, J., Lin, Z., 2021. Advances in pH-responsive drug delivery systems. OpenNano 5, 100031. https://doi.org/10.1016/J.ONANO.2021.100031.
46. Zhuo, S., Zhang, F., Yu, J., Zhang, X., Yang, G., Liu, X., 2020. pH-Sensitive Biomaterials for Drug Delivery. Molecules 25. https://doi.org/10.3390/MOLECULES25235649.
47. Chang, J.S., Choi, M.J., Cheong, H.S., Kim, K., 2001. Development of Th1-mediated CD8+ effector T cells by vaccination with epitope peptides encapsulated in pH-sensitive liposomes. Vaccine 19, 3608–3614. https://doi.org/10.1016/S0264-410X(01)00104-9.
48. Andersen, B.M., Ohlfest, J.R., 2012. Increasing the efficacy of tumor cell vaccines by enhancing cross priming. Cancer Lett. 325, 155–164. https://doi.org/10.1016/J.CANLET.2012.07.012.
49. Fehres, C.M., Unger, W.W.J., Garcia-Vallejo, J.J., van Kooyk, Y., 2014. Understanding the biology of antigen cross-presentation for the design of vaccines against cancer. Front. Immunol. 5, 149. https://doi.org/10.3389/FIMMU.2014.00149.
50. Melero, I., Gaudernack, G., Gerritsen, W., Huber, C., Parmiani, G., Scholl, S., Thatcher, N., Wagstaff, J., Zielinski, C., Faulkner, I., Mellstedt, H., 2014. Therapeutic vaccines for cancer: an overview of clinical trials. Nat. Rev. Clin. Oncol. 11:9, 509–524. https://doi.org/10.1038/nrclinonc.2014.111.
51. Wang, C., Li, P., Liu, L., Pan, H., Li, H., Cai, L., Ma, Y., 2016. Self-adjuvanted nanovaccine for cancer immunotherapy: Role of lysosomal rupture-induced ROS in MHC class I antigen presentation. Biomaterials 79, 88–100. https://doi.org/10.1016/J.BIOMATERIALS.2015.11.040.
52. Alsaab, H.O., Alharbi, F.D., Alhibs, A.S., Alanazi, N.B., Alshehri, B.Y., Saleh, M.A., Alshehri, F.S., Algarni, M.A., Almugaiteeb, T., Uddin, M.N., Alzhrani, R.M., 2022. PLGA-Based Nanomedicine: History of Advancement and Development in Clinical Applications of Multiple Diseases. Pharmaceutics 14:12, 2728. https://doi.org/10.3390/PHARMACEUTICS14122728.
53. Hadinoto, K., Sundaresan, A., Cheow, W.S., 2013. Lipid–polymer hybrid nanoparticles as a new generation therapeutic delivery platform: A review. Eur. J. Pharm. Biopharm. 85, 427–443. https://doi.org/10.1016/J.EJPB.2013.07.002.
54. Pandita, D., Kumar, S., Lather, V., 2015. Hybrid poly(lactic-co-glycolic acid) nanoparticles: design and delivery prospectives. Drug Discov. Today 20, 95–104. https://doi.org/10.1016/J.DRUDIS.2014.09.018.
55. Sah, H., Thoma, L.A., Desu, H.R., Sah, E., Wood, G.C., 2013. Concepts and practices used to develop functional PLGA-based nanoparticulate systems. Int. J. Nanomedicine 8, 747–765. https://doi.org/10.2147/IJN.S40579.
56. Tan, S., Li, X., Guo, Y., Zhang, Z., 2013. Lipid-enveloped hybrid nanoparticles for drug delivery. Nanoscale 5, 860–872. https://doi.org/10.1039/C2NR32880A.
57. Ghitman, J., Biru, E.I., Stan, R., Iovu, H., 2020. Review of hybrid PLGA nanoparticles: Future of smart drug delivery and theranostics medicine. Mater. Des. 193, 108805. https://doi.org/10.1016/J.MATDES.2020.108805.
58. Rose, F., Wern, J.E., Ingvarsson, P.T., Van De Weert, M., Andersen, P., Follmann, F., Foged, C., 2015. Engineering of a novel adjuvant based on lipid-polymer hybrid nanoparticles: A quality-by-design approach. J. Control. Release 210, 48–57. https://doi.org/10.1016/J.JCONREL.2015.05.004.
59. Khademi, F., Derakhshan, M., Yousefi-Avarvand, A., Najafi, A., Tafaghodi, M., 2018. A novel antigen of Mycobacterium tuberculosis and MPLA adjuvant co-entrapped into PLGA:DDA hybrid nanoparticles stimulates mucosal and systemic immunity. Microb. Pathog. 125, 507–513. https://doi.org/10.1016/J.MICPATH.2018.10.023.
60. Khademi, F., Sahebkar, A., Fasihi-Ramandi, M., Taheri, R.A., 2018. Induction of strong immune response against a multicomponent antigen of Mycobacterium tuberculosis in BALB/c mice using PLGA and DOTAP adjuvant. APMIS 126, 509–514. https://doi.org/10.1111/APM.12851.
61. Liu, L., Cao, F., Liu, X., Wang, H., Zhang, C., Sun, H., Wang, C., Leng, X., Song, C., Kong, D., Ma, G., 2016. Hyaluronic Acid-Modified Cationic Lipid-PLGA Hybrid Nanoparticles as a Nanovaccine Induce Robust Humoral and Cellular Immune Responses. ACS Appl. Mater. Interfaces 8, 11969–11979. https://doi.org/https://doi.org/10.1021/acsami.6b01135.
62. Liu, L., Ma, P., Wang, H., Zhang, C., Sun, H., Wang, C., Song, C., Leng, X., Kong, D., Ma, G., 2016. Immune responses to vaccines delivered by encapsulation into and/or adsorption onto cationic lipid-PLGA hybrid nanoparticles. J. Control. Release 225, 230–239. https://doi.org/10.1016/J.JCONREL.2016.01.050.
63. Moon, J.J., Suh, H., Polhemus, M.E., Ockenhouse, C.F., Yadava, A., Irvine, D.J., 2012. Antigen-Displaying Lipid-Enveloped PLGA Nanoparticles as Delivery Agents for a Plasmodium vivax Malaria Vaccine. PLoS One 7, e31472. https://doi.org/10.1371/JOURNAL.PONE.0031472.
64. Rose, F., Wern, J.E., Gavins, F., Andersen, P., Follmann, F., Foged, C., 2018. A strong adjuvant based on glycol-chitosan-coated lipid-polymer hybrid nanoparticles potentiates mucosal immune responses against the recombinant Chlamydia trachomatis fusion antigen CTH522. J. Control. Release 271, 88–97. https://doi.org/10.1016/J.JCONREL.2017.12.003.
65. Karbalaei Zadeh Babaki, M., Soleimanpour, S., Rezaee, S.A., 2017. Antigen 85 complex as a powerful Mycobacterium tuberculosis immunogene: Biology, immune-pathogenicity, applications in diagnosis, and vaccine design. Microb. Pathog. 112, 20–29. https://doi.org/10.1016/J.MICPATH.2017.08.040.
66. Li, W., Deng, G., Li, M., Zeng, J., Zhao, L., Liu, X., Wang, Y., 2014. A recombinant adenovirus expressing CFP10, ESAT6, Ag85A and Ag85B of Mycobacterium tuberculosis elicits strong antigen-specific immune responses in mice. Mol. Immunol. 62, 86–95. https://doi.org/10.1016/J.MOLIMM.2014.06.007.
67. Mearns, H., Geldenhuys, H.D., Kagina, B.M., Musvosvi, M., Little, F., Ratangee, F., Mahomed, H., Hanekom, W.A., Hoff, S.T., Ruhwald, M., Kromann, I., Bang, P., Hatherill, M., Andersen, P., Scriba, T.J., Rozot, V., Abrahams, D.A., Mauff, K., Smit, E., Brown, Y., Hughes, E.J., Makgotlho, E., Keyser, A., Erasmus, M., Makhethe, L., Africa, H., Hopley, C., Steyn, M., 2017. H1:IC31 vaccination is safe and induces long-lived TNF-α+IL-2+CD4 T cell responses in M. tuberculosis infected and uninfected adolescents: A randomized trial. Vaccine 35, 132–141. https://doi.org/10.1016/J.VACCINE.2016.11.023.
68. Luabeya, A.K.K., Kagina, B.M.N., Tameris, M.D., Geldenhuys, H., Hoff, S.T., Shi, Z., Kromann, I., Hatherill, M., Mahomed, H., Hanekom, W.A., Andersen, P., Scriba, T.J., Schoeman, E., Krohn, C., Day, C.L., Africa, H., Makhethe, L., Smit, E., Brown, Y., Suliman, S., Hughes, E.J., Bang, P., Snowden, M.A., McClain, B., Hussey, G.D., 2015. First-in-human trial of the post-exposure tuberculosis vaccine H56:IC31 in Mycobacterium tuberculosis infected and non-infected healthy adults. Vaccine 33, 4130–4140. https://doi.org/10.1016/J.VACCINE.2015.06.051.
69. Commandeur, S., van Meijgaarden, K.E., Prins, C., Pichugin, A. V., Dijkman, K., van den Eeden, S.J.F., Friggen, A.H., Franken, K.L.M.C., Dolganov, G., Kramnik, I., Schoolnik, G.K., Oftung, F., Korsvold, G.E., Geluk, A., Ottenhoff, T.H.M., 2013. An Unbiased Genome-Wide Mycobacterium tuberculosis Gene Expression Approach To Discover Antigens Targeted by

Human T Cells Expressed during Pulmonary Infection. J. Immunol. 190, 1659–1671. https://doi.org/10.4049/JIMMUNOL.1201593.
70. Commandeur, S., van den Eeden, S.J.F., Dijkman, K., Clark, S.O., van Meijgaarden, K.E., Wilson, L., Franken, K.L.M.C., Williams, A., Christensen, D., Ottenhoff, T.H.M., Geluk, A., 2014. The in vivo expressed Mycobacterium tuberculosis (IVE-TB) antigen Rv2034 induces CD4+ T-cells that protect against pulmonary infection in HLA-DR transgenic mice and guinea pigs. Vaccine 32, 3580–3588. https://doi.org/10.1016/j.vaccine.2014.05.005.
71. Ko, E.J., Lee, Y., Lee, Y.T., Kim, Y.J., Kim, K.H., Kang, S.M., 2018. MPL and CpG combination adjuvants promote homologous and heterosubtypic cross protection of inactivated split influenza virus vaccine. Antiviral Res. 156, 107–115. https://doi.org/10.1016/J.ANTIVIRAL.2018.06.004.
72. Meraz, I.M., Savage, D.J., Segura-Ibarra, V., Li, J., Rhudy, J., Gu, J., Serda, R.E., 2014. Adjuvant cationic liposomes presenting MPL and IL-12 induce cell death, suppress tumor growth, and alter the cellular phenotype of tumors in a murine model of breast cancer. Mol. Pharm. 11, 3484–3491. https://doi.org/10.1021/mp5002697.
73. Todoroff, J., Lemaire, M.M., Fillee, C., Jurion, F., Renauld, J.C., Huygen, K., Vanbever, R., 2013. Mucosal and Systemic Immune Responses to Mycobacterium tuberculosis Antigen 85A following Its Co-Delivery with CpG, MPLA or LTB to the Lungs in Mice. PLoS One 8, e63344. https://doi.org/10.1371/JOURNAL.PONE.0063344.
74. Dreno, B., Thompson, J.F., Smithers, B.M., Santinami, M., Jouary, T., Gutzmer, R., Levchenko, E., Rutkowski, P., Grob, J.J., Korovin, S., Drucis, K., Grange, F., Machet, L., Hersey, P., Krajsova, I., Testori, A., Conry, R., Guillot, B., Kruit, W.H.J., Demidov, L., Thompson, J.A., Bondarenko, I., Jaroszek, J., Puig, S., Cinat, G., Hauschild, A., Goeman, J.J., van Houwelingen, H.C., Ulloa-Montoya, F., Callegaro, A., Dizier, B., Spiessens, B., Debois, M., Brichard, V.G., Louahed, J., Therasse, P., Debruyne, C., Kirkwood, J.M., 2018. MAGE-A3 immunotherapeutic as adjuvant therapy for patients with resected, MAGE-A3-positive, stage III melanoma (DERMA): a double-blind, randomised, placebo-controlled, phase 3 trial. Lancet Oncol. 19, 916–929. https://doi.org/10.1016/S1470-2045(18)30254-7.
75. Gutzmer, R., Rivoltini, L., Levchenko, E., Testori, A., Utikal, J., Ascierto, P.A., Demidov, L., Grob, J.J., Ridolfi, R., Schadendorf, D., Queirolo, P., Santoro, A., Loquai, C., Dreno, B., Hauschild, A., Schultz, E., Lesimple, T.P., Vanhoutte, N., Salaun, B., Gillet, M., Jarnjak, S., De Sousa Alves, P.M., Louahed, J., Brichard, V.G., Lehmann, F.F., 2016. Safety and immunogenicity of the PRAME cancer immunotherapeutic in metastatic melanoma: results of a phase I dose escalation study. ESMO Open 1, e000068. https://doi.org/10.1136/ESMOOPEN-2016-000068.
76. Kruit, W.H., Suciu, S., Dreno, B., Chiarion-Sileni, V., Mortier, L., Robert, C., Maio, M., Brichard, V.G., Lehmann, F., Keilholz, U., 2008. Immunization with recombinant MAGE-A3 protein combined with adjuvant systems AS15 or AS02B in patients with unresectable and progressive metastatic cutaneous melanoma: A randomized open-label phase II study of the EORTC Melanoma Group (16032- 18031). J. Clin. Oncol. 26, 9065–9065. https://doi.org/10.1200/JCO.2008.26.15_SUPPL.9065.
77. Kruit, W.H.J., Suciu, S., Dreno, B., Mortier, L., Robert, C., Chiarion-Sileni, V., Maio, M., Testori, A., Dorval, T., Grob, J.J., Becker, J.C., Spatz, A., Eggermont, A.M.M., Louahed, J., Lehmann, F.F., Brichard, V.G., Keilholz, U., 2013. Selection of immunostimulant AS15 for active immunization with MAGE-A3 protein: results of a randomized phase II study of the European Organisation for Research and Treatment of Cancer Melanoma Group in Metastatic Melanoma. J. Clin. Oncol. 31, 2413–2420. https://doi.org/10.1200/JCO.2012.43.7111.
78. Vansteenkiste, J.F., Cho, B.C., Vanakesa, T., De Pas, T., Zielinski, M., Kim, M.S., Jassem, J., Yoshimura, M., Dahabreh, J., Nakayama, H., Havel, L., Kondo, H., Mitsudomi, T., Zarogoulidis, K., Gladkov, O.A., Udud, K., Tada, H., Hoffman, H., Bugge, A., Taylor, P., Gonzalez, E.E., Liao, M.L., He, J., Pujol, J.L., Louahed, J., Debois, M., Brichard, V., Debruyne, C., Therasse, P., Altorki, N., 2016. Efficacy of the MAGE-A3 cancer immunotherapeutic as adjuvant therapy in patients with resected MAGE-A3-positive non-small-cell lung cancer (MAGRIT): a randomised, double-blind, placebo-controlled, phase 3 trial. Lancet Oncol. 17, 822–835. https://doi.org/10.1016/S1470-2045(16)00099-1.
79. Franken, K.L.M.C., Hiemstra, H.S., Van Meijgaarden, K.E., Subronto, Y., Den Hartigh, J., Ottenhoff, T.H.M., Drijfhout, J.W., 2000. Purification of His-Tagged Proteins by Immobilized Chelate Affinity Chromatography: The Benefits from the Use of Organic Solvent. Protein Expr. Purif. 18, 95–99. https://doi.org/10.1006/PREP.1999.1162.
80. Szachniewicz, M.M., Neustrup, M.A., van Meijgaarden, K.E., Jiskoot, W., Bouwstra, J.A., Haks, M.C., Geluk, A., Ottenhoff, T.H.M., 2024. Intrinsic immunogenicity of liposomes for tuberculosis vaccines: Effect of cationic lipid and cholesterol. Eur. J. Pharm. Sci. 195, 106730. https://doi.org/10.1016/J.EJPS.2024.106730.
81. Verreck, F.A.W., Boer, T. de, Langenberg, D.M.L., Zanden, L. van der, Ottenhoff, T.H.M., 2006. Phenotypic and functional profiling of human proinflammatory type-1 and anti-inflammatory type-2 macrophages in response to microbial antigens and IFN-γ- and CD40L-mediated costimulation. J. Leukoc. Biol. 79, 285–293. https://doi.org/10.1189/JLB.0105015.
82. Szachniewicz, M.M., van Meijgaarden, K.E., Kavrik, E., Jiskoot, W., Bouwstra, J.A., Haks, M.C., Geluk, A., Ottenhoff, T.H.M., 2024. Cationic pH-sensitive liposomes as subunit vaccine delivery systems against tuberculosis: effect of liposome composition on cellular innate immune responses. Int. Immunopharmacol. Manuscript submitted for publication.
83. Szachniewicz, M.M., van den Eeden, S.J.F., van Meijgaarden, K.E., Franken, K.L.M.C., van Veen, S., Geluk, A., Bouwstra, J.A., Ottenhoff, T.H.M., 2024. Cationic pH-sensitive liposome-based subunit tuberculosis vaccine induces protection in mice challenged with Mycobacterium tuberculosis. Eur. J. Pharm. Biopharm. 203, 114437. https://doi.org/10.1016/J.EJPB.2024.114437.
84. Geluk, A., van den Eeden, S.J.F., van Meijgaarden, K.E., Dijkman, K., Franken, K.L.M.C., Ottenhoff, T.H.M., 2012. A multistage-polyepitope vaccine protects against Mycobacterium tuberculosis infection in HLA-DR3 transgenic mice. Vaccine 30, 7513–7521. https://doi.org/10.1016/J.VACCINE.2012.10.045.
85. Ali, M., van Gent, M.E., de Waal, A.M., van Doodewaerd, B.R., Bos, E., Koning, R.I., Cordfunke, R.A., Drijfhout, J.W., Nibbering, P.H., 2023. Physical and Functional Characterization of PLGA Nanoparticles Containing the Antimicrobial Peptide SAAP-148. Int. J. Mol. Sci. 24, 2867. https://doi.org/10.3390/IJMS24032867/S1.
86. R Core Team, 2023. R: A language and environment for statistical computing.
87. RStudio Team, 2023. RStudio: Integrated Development Environment for R.
88. Kleiman, E., Salyakina, D., De Heusch, M., Hoek, K.L., Llanes, J.M., Castro, I., Wright, J.A., Clark, E.S., Dykxhoorn, D.M., Capobianco, E., Takeda, A., Renauld, J.C., Khan, W.N., 2015. Distinct transcriptomic features are associated with transitional and mature B-cell populations in the mouse spleen. Front. Immunol. 6, 126060. https://doi.org/10.3389/FIMMU.2015.00030/ABSTRACT.
89. Pillai, S., Cariappa, A., 2009. The follicular versus marginal zone B lymphocyte cell fate decision. Nat. Rev. Immunol. 2009 9:11 9, 767–777. https://doi.org/10.1038/nri2656.
90. Demento, S.L., Cui, W., Criscione, J.M., Stern, E., Tulipan, J., Kaech, S.M., Fahmy, T.M., 2012. Role of sustained antigen release from nanoparticle vaccines in shaping the T cell memory phenotype. Biomaterials 33, 4957–4964. https://doi.org/10.1016/J.BIOMATERIALS.2012.03.041.
91. Reed, S.G., Orr, M.T., Fox, C.B., 2013. Key roles of adjuvants in modern vaccines. Nat. Med. 19:12, 1597–1608. https://doi.org/10.1038/nm.3409.
92. Zhao, L., Seth, A., Wibowo, N., Zhao, C.X., Mitter, N., Yu, C., Middelberg, A.P.J., 2014. Nanoparticle vaccines. Vaccine 32, 327–337. https://doi.org/10.1016/J.VACCINE.2013.11.069.
93. Jia, J., Zhang, Y., Xin, Y., Jiang, C., Yan, B., Zhai, S., 2018. Interactions Between Nanoparticles and Dendritic Cells: From the Perspective of Cancer Immunotherapy. Front. Oncol. 8, 410678. https://doi.org/10.3389/FONC.2018.00404/BIBTEX.
94. Liu, J., Miao, L., Sui, J., Hao, Y., Huang, G., 2020. Nanoparticle cancer vaccines: Design considerations and recent advances. Asian J. Pharm. Sci. 15, 576–590. https://doi.org/10.1016/J.AJPS.2019.10.006.
95. Wang, Yongchao, Wang, J., Zhu, D., Wang, Yufei, Qing, G., Zhang, Y., Liu, X., Liang, X.J., 2021. Effect of physicochemical properties on in vivo fate of nanoparticle-based cancer immunotherapies. Acta Pharm. Sin. B 11, 886–902. https://doi.org/10.1016/J.APSB.2021.03.007
96. Getts, D.R., Shea, L.D., Miller, S.D., King, N.J.C., 2015. Harnessing nanoparticles for immune modulation. Trends Immunol. 36, 419–427. https://doi.org/10.1016/J.IT.2015.05.007.
97. Moyano, D.F., Liu, Y., Peer, D., Rotello, V.M., 2016. Modulation of Immune Response Using

Engineered Nanoparticle Surfaces. Small 12, 76–82. https://doi.org/10.1002/SMLL.201502273.
98. Correia-Pinto, J.F., Csaba, N., Alonso, M.J., 2013. Vaccine delivery carriers: Insights and future perspectives. Int. J. Pharm. 440, 27–38. https://doi.org/10.1016/J.IJPHARM.2012.04.047.
99. Fan, Y., Moon, J.J., 2015. Nanoparticle Drug Delivery Systems Designed to Improve Cancer Vaccines and Immunotherapy. Vaccines 3, 662-685. https://doi.org/10.3390/VACCINES3030662.
100. Doddapaneni, B.S., Kyryachenko, S., Chagani, S.E., Alany, R.G., Rao, D.A., Indra, A.K., Alani, A.W.G., 2015. A three-drug nanoscale drug delivery system designed for preferential lymphatic uptake for the treatment of metastatic melanoma. J. Control. Release 220, 503–514. https://doi.org/10.1016/J.JCONREL.2015.11.013.
101. Min, Y., Roche, K.C., Tian, S., Eblan, M.J., McKinnon, K.P., Caster, J.M., Chai, S., Herring, L.E., Zhang, L., Zhang, T., Desimone, J.M., Tepper, J.E., Vincent, B.G., Serody, J.S., Wang, A.Z., 2017. Antigen-capturing nanoparticles improve the abscopal effect and cancer immunotherapy. Nat. Nanotechnol. 2017 12:9 12, 877–882. https://doi.org/10.1038/nnano.2017.113.
102. Foged, C., Brodin, B., Frokjaer, S., Sundblad, A., 2005. Particle size and surface charge affect particle uptake by human dendritic cells in an in vitro model. Int. J. Pharm. 298, 315–322. https://doi.org/10.1016/J.IJPHARM.2005.03.035.
103. Henriksen-Lacey, M., Christensen, D., Bramwell, V.W., Lindenstrøm, T., Agger, E.M., Andersen, P., Perrie, Y., 2010b. Liposomal cationic charge and antigen adsorption are important properties for the efficient deposition of antigen at the injection site and ability of the vaccine to induce a CMI response. J. Control. Release 145, 102–108. https://doi.org/10.1016/J.JCONREL.2010.03.027.
104. Christensen, D., Henriksen-Lacey, M., Kamath, A.T., Lindenstrøm, T., Korsholm, K.S., Christensen, J.P., Rochat, A.F., Lambert, P.H., Andersen, P., Siegrist, C.A., Perrie, Y., Agger, E.M., 2012. A cationic vaccine adjuvant based on a saturated quaternary ammonium lipid have different in vivo distribution kinetics and display a distinct CD4 T cell-inducing capacity compared to its unsaturated analog. J. Control. Release 160, 468–476. https://doi.org/10.1016/j.jconrel.2012.03.016.
105. Merkel, T.J., Jones, S.W., Herlihy, K.P., Kersey, F.R., Shields, A.R., Napier, M., Luft, J.C., Wu, H., Zamboni, W.C., Wang, A.Z., Bear, J.E., DeSimone, J.M., 2011. Using mechanobiological mimicry of red blood cells to extend circulation times of hydrogel microparticles. Proc. Nat. Acad. Sci. 108, 586–591. https://doi.org/10.1073/PNAS.1010013108.
106. Anselmo, A.C., Zhang, M., Kumar, S., Vogus, D.R., Menegatti, S., Helgeson, M.E., Mitragotri, S., 2015. Elasticity of nanoparticles influences their blood circulation, phagocytosis, endocytosis, and targeting. ACS Nano 9, 3169–3177. https://doi.org/10.1021/acsnano.5b00147.
107. Sun, J., Zhang, L., Wang, J., Feng, Q., Liu, D., Yin, Q., Xu, D., Wei, Y., Ding, B., Shi, X., Jiang, X., 2015. Tunable Rigidity of (Polymeric Core)–(Lipid Shell) Nanoparticles for Regulated Cellular Uptake. Adv. Mater. 27, 1402–1407. https://doi.org/10.1002/ADMA.201404788.
108. Moyano, D.F., Goldsmith, M., Solfiell, D.J., Landesman-Milo, D., Miranda, O.R., Peer, D., Rotello, V.M., 2012. Nanoparticle hydrophobicity dictates immune response. J. Am. Chem. Soc. 134, 3965–3967. https://doi.org/10.1021/JA2108905.
109. Rao, D.A., Forrest, M.L., Alani, A.W.G., Kwon, G.S., Robinson, J.R., 2010. Biodegradable PLGA based nanoparticles for sustained regional lymphatic drug delivery. J. Pharm. Sci. 99, 2018–2031. https://doi.org/10.1002/JPS.21970.
110. Flynn, J.A.L., 2004. Immunology of tuberculosis and implications in vaccine development. Tuberculosis 84, 93–101. https://doi.org/10.1016/J.TUBE.2003.08.010.
111. Griffiths, K.L., Khader, S.A., 2014. Novel vaccine approaches for protection against intracellular pathogens. Curr. Opin. Immunol. 28, 58–63. https://doi.org/10.1016/J.COI.2014.02.003.
112. Ottenhoff, T.H.M., Lewinsohn, D.A., Lewinsohn, D.M., 2008. Human CD4 and CD8 T Cell Responses to Mycobacterium tuberculosis: Antigen Specificity, Function, Implications and Applications, in: Handbook of Tuberculosis, 119–155. https://doi.org/10.1002/9783527611614.CH23.
113. Henao-Tamayo, M.I., Ordway, D.J., Irwin, S.M., Shang, S., Shanley, C., Orme, I.M., 2010. Phenotypic definition of effector and memory T-lymphocyte subsets in mice chronically infected with mycobacterium tuberculosis. Clin. Vaccine Immunol. 17, 618–625. https://doi.org/10.1128/CVI.00368-09.
114. Kipnis, A., Irwin, S., Izzo, A.A., Basaraba, R.J., Orme, I.M., 2005. Memory T Lymphocytes Generated by Mycobacterium bovis BCG Vaccination Reside within a CD4 CD44lo CD62 Ligandhi Population. Infect. Immun. 73, 7759. https://doi.org/10.1128/IAI.73.11.7759-7764.2005.
115. Orme, I.M., 2010. The Achilles heel of BCG. Tuberculosis 90, 329–332. https://doi.org/10.1016/J.TUBE.2010.06.002.
116. Lu, Y.J., Barreira-Silva, P., Boyce, S., Powers, J., Cavallo, K., Behar, S.M., 2021. CD4 T cell help prevents CD8 T cell exhaustion and promotes control of Mycobacterium tuberculosis infection. Cell Rep. 36, 109696. https://doi.org/10.1016/J.CELREP.2021.109696.
117. Prezzemolo, T., Guggino, G., La Manna, M.P., Di Liberto, D. Di, Dieli, F., Caccamo, N., 2014. Functional signatures of human CD4 and CD8 T cell responses to Mycobacterium tuberculosis. Front. Immunol. 5, 83298. https://doi.org/10.3389/FIMMU.2014.00180/BIBTEX.
118. Behar, S.M., Woodworth, J.S.M., Wu, Y., 2007. Next generation: tuberculosis vaccines that elicit protective CD8+ T cells. Expert Rev. Vaccines 6, 441–456. https://doi.org/10.1586/14760584.6.3.441.
119. Boom, W.H., 2007. New TB vaccines: is there a requirement for CD8+ T cells? J. Clin. Invest. 117, 2092–2094. https://doi.org/10.1172/JCI32933.
120. Behar, S.M., Dascher, C.C., Grusby, M.J., Wang, C.R., Brenner, M.B., 1999. Susceptibility of Mice Deficient in CD1D or TAP1 to Infection with Mycobacterium tuberculosis. J. Exp. Med. 189, 1973–1980. https://doi.org/10.1084/JEM.189.12.1973.
121. Flynn, J.L., Goldstein, M.M., Triebold, K.J., Koller, B., Bloom, B.R., 1992. Major histocompatibility complex class I-restricted T cells are required for resistance to Mycobacterium tuberculosis infection. Proc. Nat. Acad. Sci. 89, 12013–12017. https://doi.org/10.1073/PNAS.89.24.12013.
122. Orme, I.M., 1987. The kinetics of emergence and loss of mediator T lymphocytes acquired in response to infection with Mycobacterium tuberculosis. J. Immunol. 138, 293–298. https://doi.org/10.4049/JIMMUNOL.138.1.293.
123. Sousa, A.O., Mazzaccaro, R.J., Russell, R.G., Lee, F.K., Turner, O.C., Hong, S., Van Kaer, L., Bloom, B.R., 2000. Relative contributions of distinct MHC class I-dependent cell populations in protection to tuberculosis infection in mice. Proc. Nat. Acad. Sci. 97, 4204–4208. https://doi.org/10.1073/PNAS.97.8.4204.
124. Van Pinxteren, L.A.H., Cassidy, J.P., Smedegaard, B.H.C., Agger, E.M., Andersen, P., 2000. Control of latent Mycobacterium tuberculosis infection is dependent on CD8 T cells. Eur. J. Immunol. 30, 3689–3698. https://doi.org/10.1002/1521-4141.
125. Lin, P.L., Rutledge, T., Green, A.M., Bigbee, M., Fuhrman, C., Klein, E., Flynn, J.L., 2012. CD4 T Cell Depletion Exacerbates Acute Mycobacterium tuberculosis While Reactivation of Latent Infection Is Dependent on Severity of Tissue Depletion in Cynomolgus Macaques. AIDS Res. Hum. Retroviruses 28, 1693–1702. https://doi.org/10.1089/AID.2012.0028.
126. Ciric, B., El-behi, M., Cabrera, R., Zhang, G.-X., Rostami, A., 2009. IL-23 Drives Pathogenic IL-17-Producing CD8+ T Cells. J. Immunol. 182, 5296–5305. https://doi.org/10.4049/JIMMUNOL.0900036.
127. Mills, K.H.G., 2022. IL-17 and IL-17-producing cells in protection versus pathology. Nat. Rev. Immunol. 2022 23:1 23, 38–54. https://doi.org/10.1038/s41577-022-00746-9.
128. Ernst, J.D., 2012. The immunological life cycle of tuberculosis. Nat. Rev. Immunol. 2012 12:8 12, 581–591. https://doi.org/10.1038/nri3259.
129. Duong, V.T., Skwarczynski, M., Toth, I., 2023b. Towards the development of subunit vaccines against tuberculosis: The key role of adjuvant. Tuberculosis 139, 102307. https://doi.org/10.1016/J.TUBE.2023.102307.
130. Rijnink, W.F., Ottenhoff, T.H.M., Joosten, S.A., 2021. B-Cells and Antibodies as Contributors to Effector Immune Responses in Tuberculosis. Front. Immunol. 12, 640168. https://doi.org/10.3389/FIMMU.2021.640168/BIBTEX
131. Maglione, P.J., Xu, J., Chan, J., 2007. B Cells Moderate Inflammatory Progression and Enhance Bacterial Containment upon Pulmonary Challenge with Mycobacterium tuberculosis. J. Immunol. 178, 7222–7234. https://doi.org/10.4049/JIMMUNOL.178.11.7222.
132. Phuah, J., Wong, E.A., Gideon, H.P., Maiello, P., Coleman, M.T., Hendricks, M.R., Ruden, R., Cirrincione, L.R., Chan, J., Lin, P.L., Flynn, J.A.L., 2016. Effects of B cell depletion on early Mycobacterium tuberculosis infection in cynomolgus macaques. Infect. Immun. 84, 1301–1311. https://doi.org/10.1128/iai.00083-16.
133. Vordermeier, H.M., Venkataprasad, N., Harris, D.P., Ivanyi, J., 2003. Increase of tuberculous infection in the organs of B cell-deficient mice. Clin. Exp. Immunol. 106, 312–316. https://doi.org/10.1046/J.1365-2249.1996.D01-845.X.

134. Joosten, S.A., van Meijgaarden, K.E., del Nonno, F., Baiocchini, A., Petrone, L., Vanini, V., Smits, H.H., Palmieri, F., Goletti, D., Ottenhoff, T.H.M., 2016. Patients with Tuberculosis Have a Dysfunctional Circulating B-Cell Compartment, Which Normalizes following Successful Treatment. PLoS Pathog. 12, e1005687. https://doi.org/10.1371/JOURNAL.PPAT.1005687.
135. Bosio, C.M., Gardner, D., Elkins, K.L., 2000. Infection of B Cell-Deficient Mice with CDC 1551, a Clinical Isolate of Mycobacterium tuberculosis: Delay in Dissemination and Development of Lung Pathology. J. Immunol. 164, 6417–6425. https://doi.org/10.4049/JIMMUNOL.164.12.6417.
136. Johnson, C.M., Cooper, A.M., Frank, A.A., Bonorino, C.B.C., Wysoki, L.J., Orme, I.M., 1997. Mycobacterium tuberculosis aerogenic rechallenge infections in B cell-deficient mice. Tuberc. Lung Dis. 78, 257–261. https://doi.org/10.1016/S0962-8479(97)90006-X.
137. Turner, J., Frank, A.A., Brooks, J. V., Gonzalez-Juarrero, M., Orme, I.M., 2001. The progression of chronic tuberculosis in the mouse does not require the participation of B lymphocytes or interleukin-4. Exp. Gerontol. 36, 537–545. https://doi.org/10.1016/S0531-5565(00)00257-6.
138. Li, H., Wang, X.X., Wang, B., Fu, L., Liu, G., Lu, Y., Cao, M., Huang, H., Javid, B., 2017. Latently and uninfected healthcare workers exposed to TB make protective antibodies against Mycobacterium tuberculosis. Proc. Nat. Acad. Sci. 114, 5023–5028. https://doi.org/10.1073/pnas.1611776114.
139. Balu, S., Reljic, R., Lewis, M.J., Pleass, R.J., McIntosh, R., van Kooten, C., van Egmond, M., Challacombe, S., Woof, J.M., Ivanyi, J., 2011. A Novel Human IgA Monoclonal Antibody Protects against Tuberculosis. J. Immunol. 186, 3113–3119. https://doi.org/10.4049/JIMMUNOL.1003189.
140. Hamasur, B., Haile, M., Pawlowski, A., Schröder, U., Källenius, G., Svenson, S.B., 2004. A mycobacterial lipoarabinomannan specific monoclonal antibody and its F(ab´)2 fragment prolong survival of mice infected with Mycobacterium tuberculosis. Clin. Exp. Immunol. 138, 30–38. https://doi.org/10.1111/J.1365-2249.2004.02593.X.
141. López, Y., Yero, D., Falero-Diaz, G., Olivares, N., Sarmiento, M.E., Sifontes, S., Solis, R.L., Barrios, J.A., Aguilar, D., Hernández-Pando, R., Acosta, A., 2009. Induction of a protective response with an IgA monoclonal antibody against Mycobacterium tuberculosis 16 kDa protein in a model of progressive pulmonary infection. Int. J. Med. Microbiol. 299, 447–452. https://doi.org/10.1016/J.IJMM.2008.10.007.
142. Zimmermann, N., Thormann, V., Hu, B., Köhler, A., Imai-Matsushima, A., Locht, C., Arnett, E., Schlesinger, L.S., Zoller, T., Schürmann, M., Kaufmann, S.H., Wardemann, H., 2016. Human isotype-dependent inhibitory antibody responses against Mycobacterium tuberculosis. EMBO Mol. Med. 8, 1325–1339. https://doi.org/10.15252/EMMM.201606330.
143. Lu, L.L., Chung, A.W., Rosebrock, T.R., Ghebremichael, M., Yu, W.H., Grace, P.S., Schoen, M.K., Tafesse, F., Martin, C., Leung, V., Mahan, A.E., Sips, M., Kumar, M.P., Tedesco, J., Robinson, H., Tkachenko, E., Draghi, M., Freedberg, K.J., Streeck, H., Suscovich, T.J., Lauffenburger, D.A., Restrepo, B.I., Day, C., Fortune, S.M., Alter, G., 2016. A Functional Role for Antibodies in Tuberculosis. Cell 167, 433-443.e14. https://doi.org/10.1016/J.CELL.2016.08.072.
144. Kagina, B.M.N., Abel, B., Scriba, T.J., Hughes, E.J., Keyser, A., Soares, A., Gamieldien, H., Sidibana, M., Hatherill, M., Gelderbloem, S., Mahomed, H., Hawkridge, A., Hussey, G., Kaplan, G., Hanekom, W.A., 2012. Specific T Cell Frequency and Cytokine Expression Profile Do Not Correlate with Protection against Tuberculosis after Bacillus Calmette-Guérin Vaccination of Newborns. Am. J. Respir. Crit. Care Med. 182, 1073–1079. https://doi.org/10.1164/RCCM.201003-0334OC.
145. Mittrücker, H.W., Steinhoff, U., Köhler, A., Krause, M., Lazar, D., Mex, P., Miekley, D., Kaufmann, S.H.E., 2007. Poor correlation between BCG vaccination-induced T cell responses and protection against tuberculosis. Proc. Nat. Acad. Sci. 104, 12434–12439. https://doi.org/10.1073/pnas.0703510104.

SUPPLEMENTARY MATERIAL

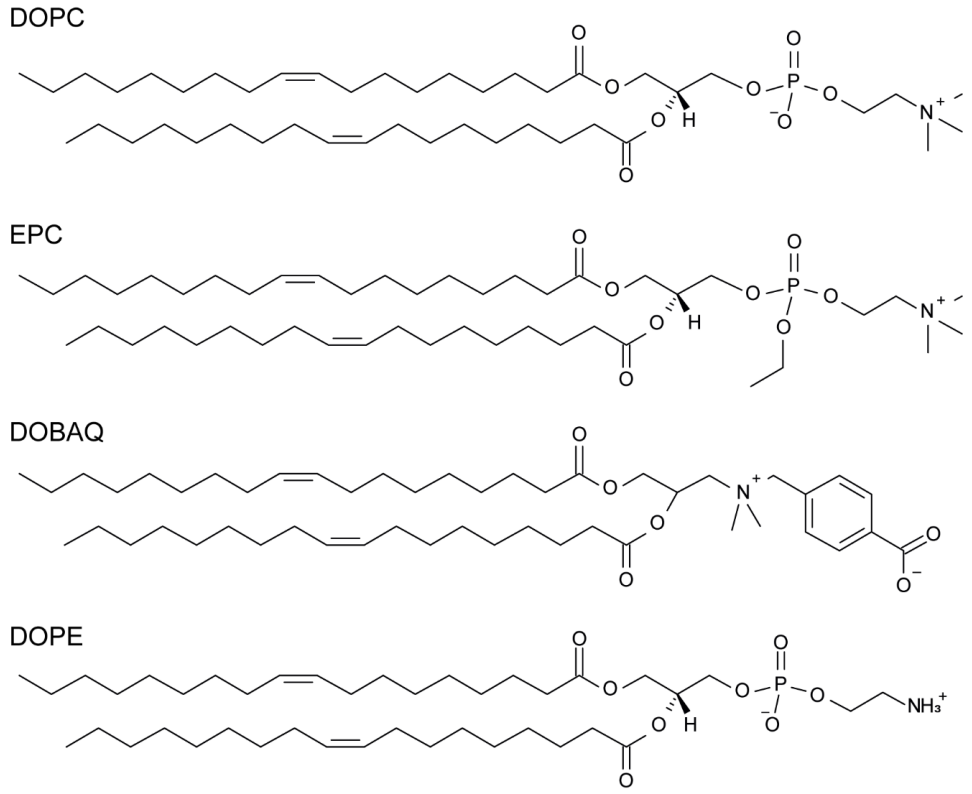

Figure S1. Chemical structures of lipids used in production of pH-sensitive liposomes and lipid-PLGA hybrid NPs.

Table S1. List of antibodies used for spectral flow cytometry analysis of $CD4^+$, $CD8^+$, and $CD3^-$ $CD19^+$ cells.

Marker	Fluorochrome	Clone	Catalog	Manufacturer
CCR7 (CD197)	PE/Cyanine5	4B12	120113	BioLegend
CD273	Brilliant Ultra Violet (BUV) 395	TY25	565102	BD Biosciences
CD8b.2	BUV 496	53-5.8	741049	BD Biosciences
CD80	BUV 661	16-10A1	741515	BD Biosciences
CD69	BUV 737	H1.2F3	612793	BD Biosciences
CD25	Brilliant Violet (BV) 480	PC61	566120	BD Biosciences
CD154	Super Bright 436	MR1	62-1541-82	Thermo Fisher
IgD	Pacific Blue	11-26c.2a	405711	BioLegend
I-A/I-E (MHC II)	BV 510	M5/114.15.2	107636	BioLegend
CD44	BV 570	IM7	103037	BioLegend
PD-1 (CD279)	BV 605	29F.1A12	135220	BioLegend
CXCR3 (CD183)	BV 650	CXCR3-173	126531	BioLegend
KLRG1 (MAFA)	BV 711	2F1/KLRG1	138427	BioLegend
CCR6 (CD196)	BV 785	29-2L17	129823	BioLegend
CD4	Spark Blue 550	GK1.5	100474	BioLegend
CCR5 (CD195)	PerCP/Cyanine5.5	HM-CCR5	107015	BioLegend
CD19	PE Fire 640	6D5	115574	BioLegend
CD138	APC	281-2	142505	BioLegend
B220 (CD45R)	Spark NIR 685	RA3-6B2	103267	BioLegend
CD62L (L-selectin)	APC/Fire 750	MEL-14	104449	BioLegend
CD3	APC/Fire 810	17A2	100267	BioLegend
IL-2	APC-R700	JES6-5H4	565186	BD Biosciences
IL-17A	PE	eBio17B7	12-7177-81	Thermo Fisher
IgM	FITC	RMM-1	406505	BioLegend
IL-10	PE/Dazzle 594	JES5-16E3	505033	BioLegend
TNFα	PE/Cyanine7	MP6-XT22	506323	BioLegend
IFNγ	Alexa Fluor 647	XMG1.2	505816	BioLegend

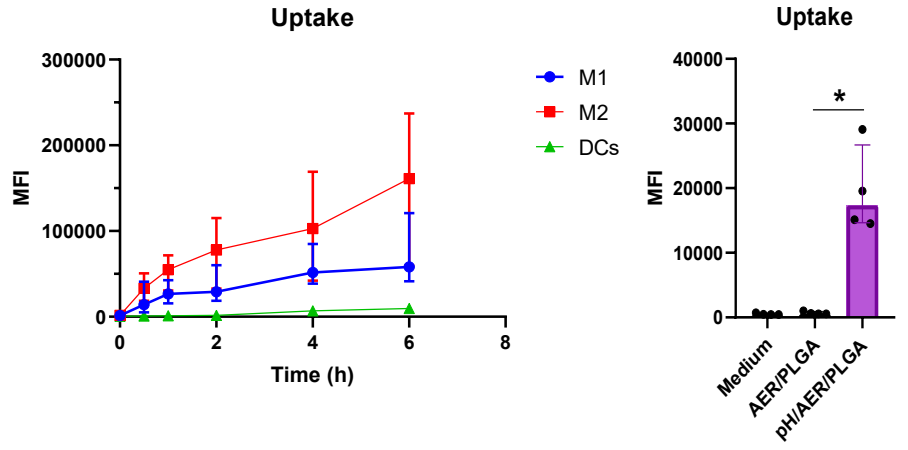

Figure S2. Uptake of (DiI-stained) PLGA NPs and lipid-PLGA hybrid NPs. A) Uptake kinetics of PLGA NPs by MDDCs, pro-inflammatory (M1), and anti-inflammatory M2 MDMFs between 1 and 6 hours of exposure. n = 4 (MDMFs), n =2 (MDDCs) donors. B) Uptake of PLGA NPs and lipid-PLGA hybrid NPs by MDDCs after 1 h of exposure. n = 4 donors. Results represent median fluorescence intensity (MFI) ± IQR.

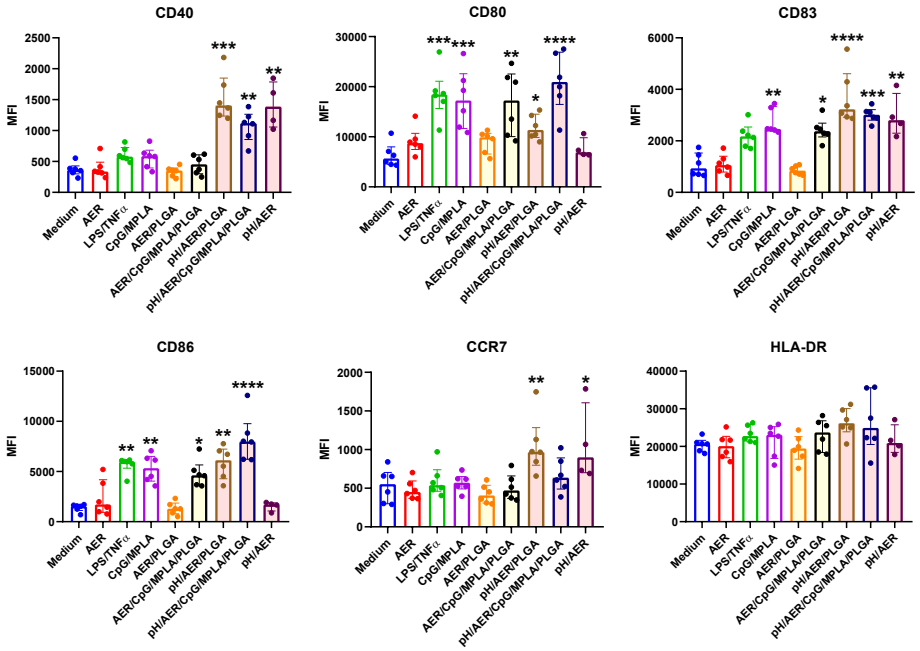

Figure S3. Cell surface activation marker expression levels in MDDCs after stimulation with medium, unadjuvanted AER (5 μg/ml), a combination of LPS and TNFα (100 and 5 ng/ml, respectively), CpG and MPLA (1.56 and 0.625 μg/ml, respectively) as the positive controls, and vaccine formulations: PLGA NPs (5 μg/ml AER, 250 μg/ml PLGA), lipid-PLGA hybrid NPs (5 μg/ml AER, 250 μg/ml lipids, 250 μg/ml PLGA), and (pH) liposomal formulation (5 μg/ml AER, 250 μg/ml liposomes), and their adjuvanted counterparts (containing additionally 1.56 and 0.625 μg/ml CpG and MPLA, respectively). Median fluorescence intensities (MFI) related to the expression of indicated activation markers. The formulations are compared to the medium in the significance testing. The results represent median ± IQR. n = 4 or 6 (cell donors).

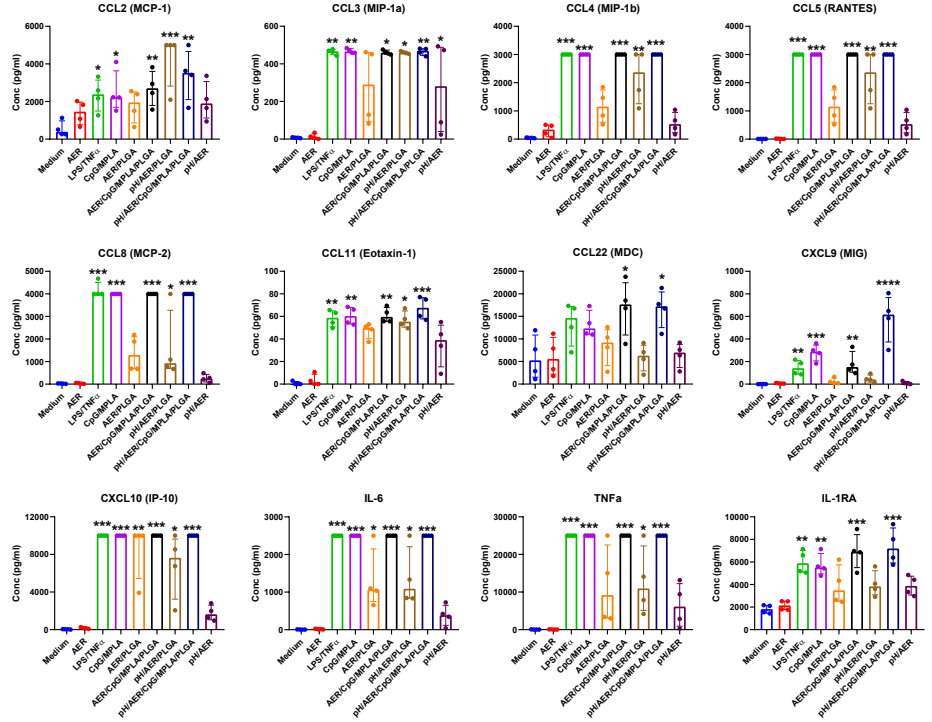

Figure S4. Production of cytokines by MDDCs exposed to vaccine formulations. Concentrations used: 5 μg/ml AER, 100 ng/ml LPS and 5 ng/ml TNFα, 1.56 μg/ml CpG and 0.625 μg/ml MPLA, 250 μg/ml PLGA, 250 μg/ml liposomes/lipids, exposure 1 hour, n = 4 (cell donors). The results represent median ± IQR.

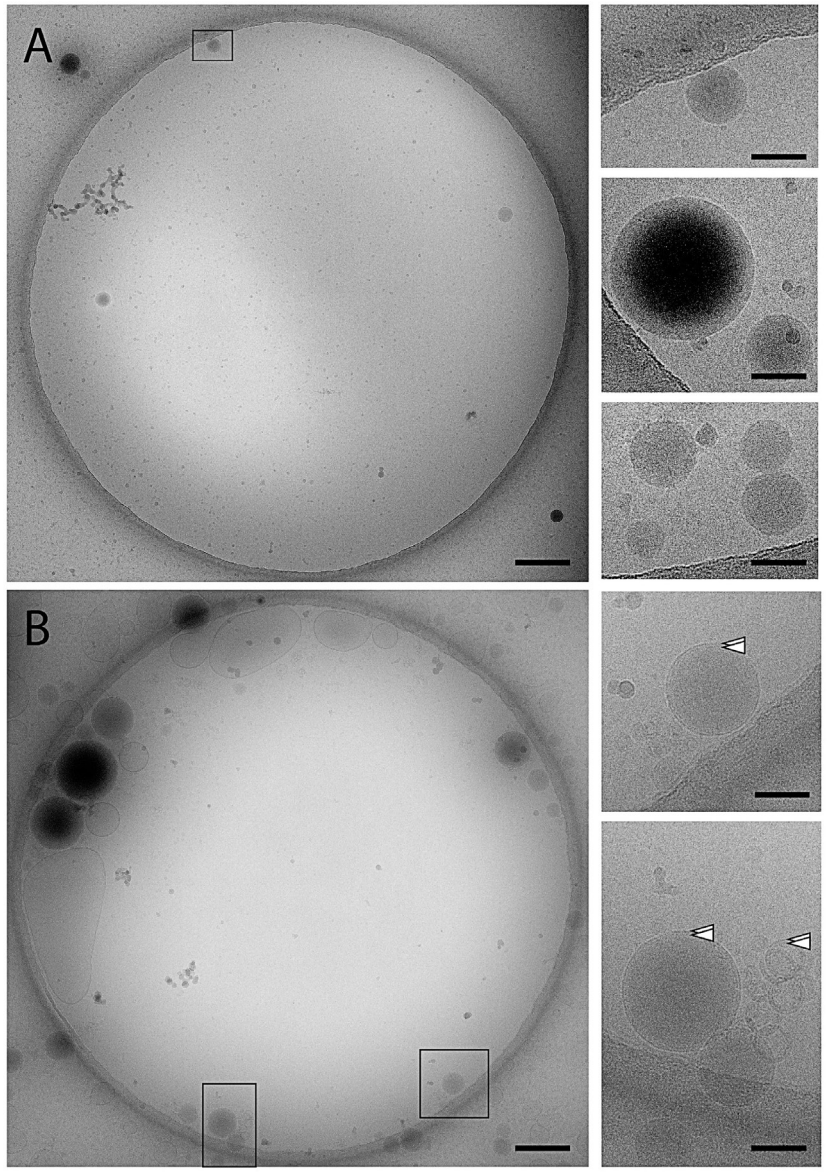

Figure S5. A) PLGA NPs (without lipids added). CryoEM overview image of a typical 2-micron diameter hole in the carbon film with three PLGA spheres. The box's area is magnified on the top right. Several other spheres from other images are shown below that image. The edges of the spheres are not sharply defined. B) Lipid-PLGA hybrid NPs. CryoEM overview of a typical 2-micron diameter hole in the carbon film showing multiple lipid-PLGA spheres. Irregularly shaped lipid vesicles were found occasionally. The boxes' areas are magnified and show PLGA spheres with clear lipid bilayer-resembling features, which can also be observed in small lipid vesicles (arrowheads). The borders of the spheres are more distinctive. In both A and B scale bars are 200 nm (overview images) and 50 nm (insets).

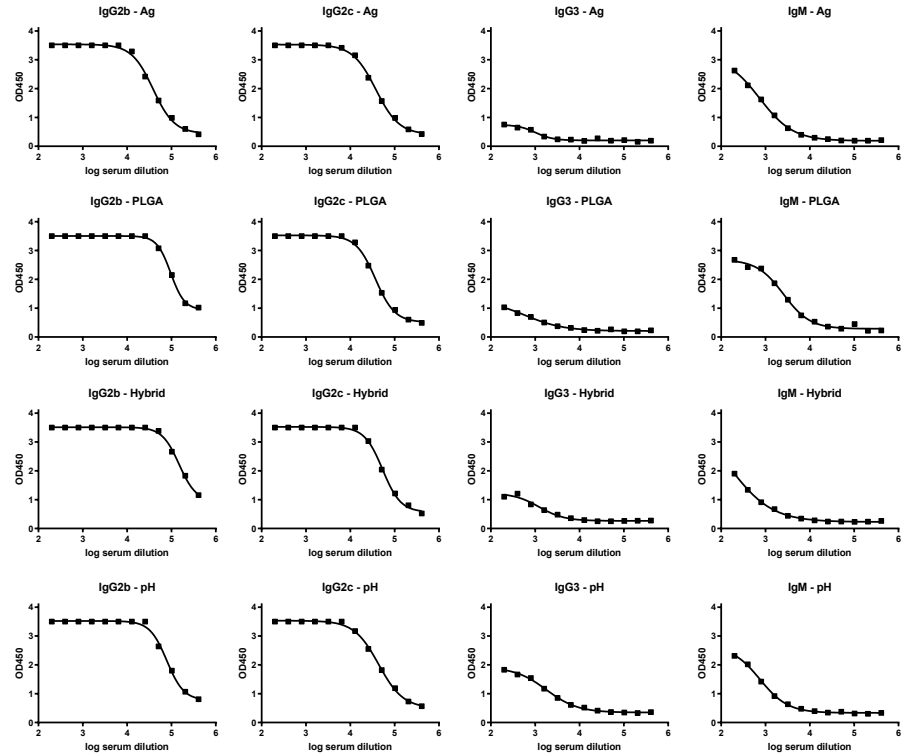

Figure S6. Quantification of AER-specific antibodies in sera. The type of antibody measured is indicated above each graph as well as the vaccination group. Values represent OD450 ELISA, and serum dilutions are shown on the x-axis. Groups are indicated in the legend. Naïve controls were not included because of the undetected (total) AER-specific antibodies (Figure 7). n = 2 (mice).

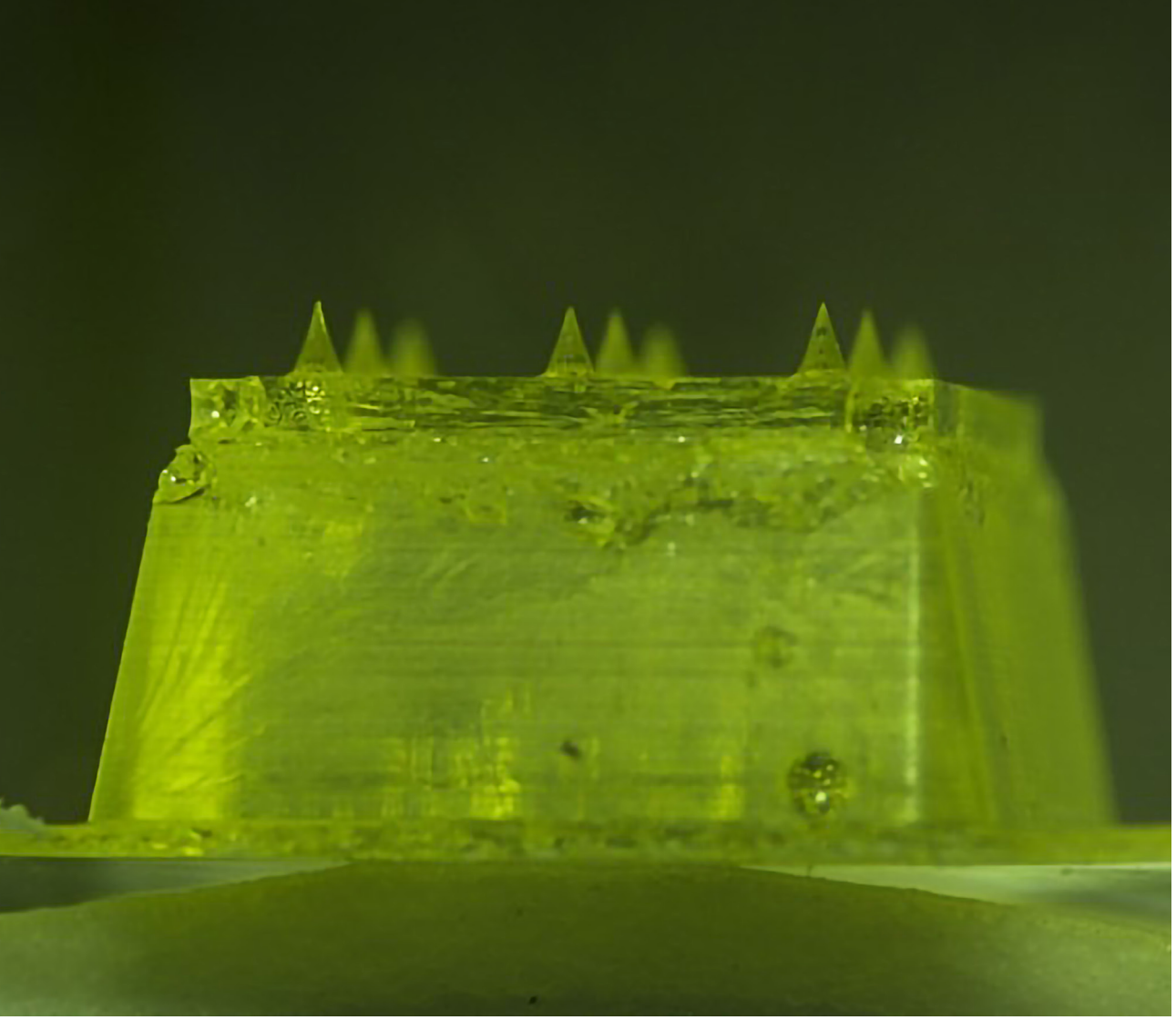

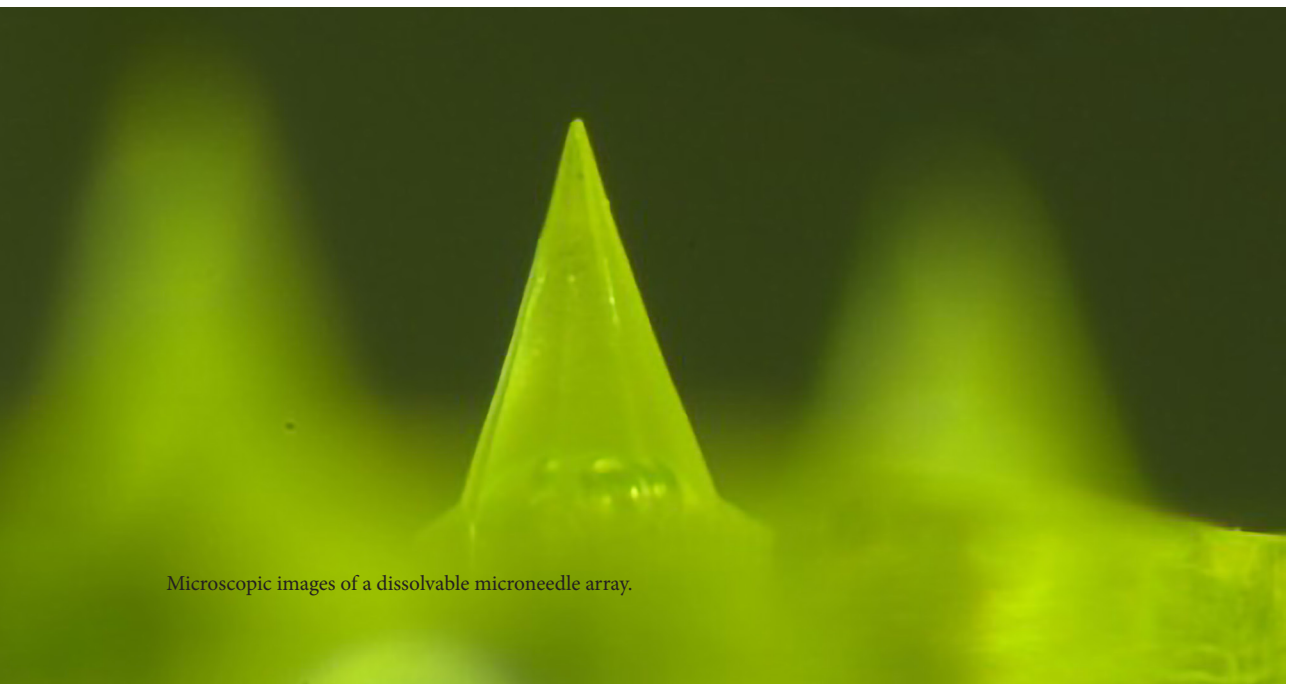

Microscopic images of a dissolvable microneedle array.

CHAPTER 5

INTRADERMAL VACCINATION WITH PLGA NANOPARTICLES VIA DISSOLVING MICRONEEDLES AND CLASSICAL INJECTION NEEDLES

Adapted from Pharm Res. 2024;41(2):305-19

M.A. Neustrup[1,2*], J. Lee[1*], B. Slütter[1], C. O'Mahony[3], J.A. Bouwstra[1], K. van der Maaden[1,4]

[*] Authors contributed equally

[1] Division of BioTherapeutics, Leiden Academic Centre for Drug Research, Leiden University, Leiden, The Netherlands
[2] Department of Infectious Diseases, Leiden University Medical Center, Leiden, The Netherlands
[3] Tyndall National Institute, Lee Maltings, Prospect Row, Cork, Ireland
[4] Tumor Immunology Group, Department of Immunology, Leiden University Medical Center, Leiden, The Netherlands

ABSTRACT

A dissolving microneedle array (dMNA) is a vaccine delivery device with several advantages over conventional needles. By incorporating particulate adjuvants in the form of poly(D,L-lactic-*co*-glycolic acid) (PLGA) nanoparticles (NPs) into the dMNA, the immune response against the antigen might be enhanced. This study aimed to prepare PLGA-NP-loaded dMNA and to compare T-cell responses induced by either intradermally injected aqueous-PLGA-NP formulation or PLGA-NP-loaded dMNA in mice. PLGA NPs were prepared with microfluidics, and their physicochemical characteristics with regard to encapsulation efficiencies of ovalbumin (OVA) and CpG oligonucleotide (CpG), zeta potentials, polydispersity indexes, and sizes were analysed. PLGA NPs incorporated dMNA was produced with three different dMNA formulations by using the centrifugation method, and the integrity of PLGA NPs in dMNAs was evaluated. The immunogenicity was evaluated in mice by comparing the T-cell responses induced by dMNA and aqueous formulations containing ovalbumin and CpG (OVA/CpG) with and without PLGA NP. Prepared PLGA NPs had a size of around 100 nm. The dMNA formulations affected the particle integrity, and the dMNA with poly(vinyl alcohol) (PVA) showed almost no aggregation of PLGA NPs. The PLGA:PVA weight ratio of 1:9 resulted in 100% of penetration efficiency and the fastest dissolution in ex-vivo human skin (< 30 min). The aqueous formulation with soluble OVA/CpG and the aqueous-PLGA-NP formulation with OVA/CpG induced the highest $CD4^+$ T-cell responses in blood and spleen cells. PLGA NPs incorporated dMNA was successfully fabricated and the aqueous formulation containing PLGA NPs induce superior $CD4^+$ and $CD8^+$ T-cell responses.

INTRODUCTION

Vaccination is one of the most successful interventions to save lives against infectious diseases. However, for intracellular pathogens (and also for cancers), vaccines often lack efficacy. Vaccines against those diseases require the induction of T cells. To boost the induction of T cells by vaccination, two efficient approaches can be applied, (i) deliver the vaccine into organs that are naturally rich in antigen-presenting cells (APCs) and (ii) increase the uptake of the vaccine by APCs using nanoparticles (NPs).

Skin is an excellent organ to deliver T-cell vaccines since it has a high population of APCs, such as dendritic cells and macrophages. Therefore, intradermal vaccine delivery can promote stronger immune responses for both T cells and B cells. However, conventional needles demand vaccines in liquid form which required a cold chain for storage. Also, they can bring sharp waste, needlestick injury, needle-phobia, and tissue damage if not used correctly [1–3]. These drawbacks show the need for novel vaccine delivery devices. Therefore, dissolving microneedle array (dMNA) has been introduced as one of the efficient approaches, which could revolutionise the way drugs are delivered. dMNAs are frequently made of biodegradable polymers or sugars, and the microneedles typically have a length below 1000 μm. Once the microneedles are inserted into the skin, they dissolve in the skin and release the loaded antigens. In spite of their limited mechanical strength and expensive production cost due to antigen waste [4], dMNA offers numerous advantages over conventional needles. One of the primary advantages is the improved safety profile [5–7]. Unlike conventional needles, dMNA does not produce sharp waste as they dissolve after insertion so that prevents contamination from reuse [8]. Besides, dMNA reduces pain sensation during administration because it barely reaches the nerves. Lastly, dMNA also has protective efficacy as they frequently brought comparable immune responses to hypodermic needle injection even with lower doses [9, 10].

To trigger an immune response against an antigen, it is often necessary to add adjuvants [11]. Not only the immune response can be enhanced by including adjuvants, but a specific immune response can also be generated [12, 13]. A particulate adjuvant, such as poly (D,L-lactic-*co*-glycolic acid) (PLGA) NPs, is a delivery system [13], provides sustained release, ensures co-delivery of antigen and molecular adjuvant, and increases uptake by dendritic cells [14–16]. PLGA is a biodegradable polymer that is approved by the Food and Drug Administration and the European Medicines Agency for different pharmaceutical applications [17], and PLGA NPs have also been used as delivery systems in subunit vaccines in mice studies [15]. The physicochemical characteristics of the particulate adjuvants, such as size, charge, and rigidity, have been shown to affect immunogenicity [12]. NPs seem to favour Th1 and $CD8^+$ T-cell-mediated immune responses, whereas microparticles seem to favour Th2 and B-cell-mediated immune responses [12]. Furthermore, dendritic cells which are key in presenting antigens to T cells, as well as activating them, favour the

uptake of particles below 200 nm [18]. While B-cell-mediated immune responses have been widely introduced for prophylactic vaccines, newer vaccines focus on Th1 and $CD8^+$ T-cell immune responses which are needed to combat multiple intracellular pathogens, such as influenza A and tuberculosis [19].

A key strategy in the formulation of new vaccines is to combine both molecular and particulate adjuvants [20, 21]. A molecular adjuvant, such as the Toll-like receptor (TLR) 9 ligand CpG oligonucleotide (CpG), is an analogue of a pathogen-associated molecular pattern which is recognised by pattern recognition receptors on APCs [22]. The combination of TLR ligands with PLGA particles has generated better immune responses compared to using only one adjuvant [23–25]. Furthermore, subunit vaccines with CpG can induce specific Th1 and $CD8^+$ T-cell responses in mice and generate long-term survivability against infectious diseases [26, 27].

Conventional methods for producing PLGA NPs, such as single or double-emulsification-based methods, often require large amounts of solvent, are labour-intensive, and are not highly reproducible [28–30]. Compared to conventional methods, microfluidics offers several advantages, including control over the production process, high efficiency, and reduced costs [29, 31]. Therefore, microfluidics is increasingly being used to produce PLGA NPs [32]. In microfluidics, solvents flow through a micro-system consisting of capillaries and chambers allowing precise manipulation of the fluids [33]. This facilitates continuous operation and the production of size-controlled NPs with a narrow size distribution [34], and the technique could therefore be used to produce PLGA NPs with a size below 200 nm, which is needed for Th1 and $CD8^+$ T-cell response.

In this study, we evaluate two approaches to improve T-cell induction via (i) PLGA NPs and (ii) dMNA. We first engineered ovalbumin and CpG (OVA/CpG) encapsulated PLGA NPs, and subsequently loaded them into dMNA. In order to ensure the stability of NPs in dMNA, we screened the most suitable polymer formulation of dMNA among three candidates (polyvinylpyrrolidone (PVP), polyvinyl alcohol (PVA), and trehalose) based on the size and polydispersity indexes (PDI) of PLGA NPs. dMNA was fabricated with the selected formulation, and skin penetration dissolution tests were executed. The loading and delivery of OVA/CpG were quantified. Finally, immune responses from OVA/CpG encapsulated NPs in dMNA and in aqueous formulation were compared.

MATERIALS AND METHODS

Materials

NE300 syringe pumps were purchased from ProSense B.V. (Oosterhout, The Netherlands). Pierce Micro bicinchoninic acid (BCA) protein assay kit, Qubit™ ssDNA Assay Kit, 500 µL Hamilton gastight, and polyether ether ketone (PEEK) capillary tubing were bought from Fisher Emergo B.V. (Landsmeer, the Netherlands). 10 mL Hamilton gastight syringes were purchased from Brunschwig Chemie B.V (Amsterdam, the Netherlands). A Teflon tube was purchased from Waters Chromatography B.V. (Etten-Leur, the Netherlands). One-piece fittings, female fitting Luer-lock adapters, two-piece adapters, interconnect tees were purchased from Mengel Engineering (Virum, Denmark). Silica capillary tubings were purchased from BGB Analytic Benelux B.V. (Harderwijk, the Netherlands). PLGA (acid terminated, lactide:glycolide 50:50, Mw 24—38 k), sodium dodecyl sulfate, sodium phosphate dibasic dihydrate, sodium phosphate monobasic dihydrate, pure sodium hydroxide pellets were purchased from Merck Chemicals B.V. (Amsterdam, the Netherlands). PVA (Mw 9k), trehalose (Mw 378), PVP (Mw 40 k), and trypan blue were purchased from Millipore Sigma (Zwijndrecht, the Netherlands). Analytical grade dimethyl sulfoxide (DMSO) and acetonitrile purchased from Biossolve B.V. (Valkenswaard, the Netherlands). EndoFit™ Ovalbumin and CpG ODN 1826 (Class B) were purchased from InvivoGen, Bio-Connect B.V. (Huissen, the Netherlands). Spectra-Por® Float-A-Lyzer® G2 1 mL (1000 kDa MWCO) purchased from VWR International B.V. (Amsterdam, the Netherlands). Millex®-VV filter units (0.1 µm) was purchased from Merck Life Science N.V. (Amsterdam, the Netherlands). Silicon microneedle arrays were provided by Tyndall National Institute (Cork, Irland). SYLGARD 184 base silicone elastomer and curing agent silicone elastomer were purchased from Dow Corning (Midland, MI, USA). Epoxy glue was purchased from by Bison International B.V. (Goes, The Netherlands).

Setup of the microfluidic system

The PLGA NPs were prepared with a three-syringe microfluidic system. The setup is depicted in Fig. 1. To assemble the microfluidic system, Luer-lock adaptors were screwed on Syringe 1, 2, and 3. Two 14-cm-long capillaries with inner diameters of 75 µm and 250 µm were attached to the Luer-lock adaptors with 360-µm fittings on Syringe 1 and Syringe 2, respectively. A 360-µm-interconnect tee with three ports in a T shape designated Port A, Port B, and Port C, where port A and C were opposite of each other and port B was positioned at an angle of 90° from Port A and B, was connected through Port A to the capillary from Syringe 1 with a 360-µm fitting. The capillary from Syringe 2 was connected to Port B with a 360-µm fitting. Port C was connected to a 14-cm-long capillary with an inner diameter of 250 µm with a 360-µm fitting. When the capillaries were attached, the capillaries were pushed to the end of the 360-µm fitting tip before insertion. A 1.6-mm-interconnect tee with three ports in a T shape designated Port 1, Port 2, and Port 3, where port 1 and 3 were opposite of each other and port 2 was positioned at an angle of 90°, was connected through Port 3 to a 7-cm-long piece of PEEK tube with a 1.6 mm fitting. A 360-µm-to-1.6-mm adapter was attached to the Luer-lock adapter on Syringe 3 and a 20-cm-long Teflon tube with an outer diameter of 1.6 mm was attached to it with a 1.6-mm fitting. The other end of the Teflon tube was attached to Port 2 with a 1.6-mm fitting. When the tubes were attached, they were first pushed fully into the 16-mm-interconnect tee before the 1.6-mm

fitting was screwed on. A 1.6-mm-to-360-µm adapter was attached to Port 1. The capillary attached to Port C was inserted through a 360-µm fitting and pushed through the 1.6-mm-interconnect tee and PEEK tube, till it reached 1 cm through the PEEK tube, after which the 360-µm fitting was screwed on the 1.6-mm-to-360-µm adapter. To complete the setup, the syringes were mounted on the syringe pumps. When the formulations were collected from the end of the PEEK tube, the tube was held perpendicular to the sample collectors, and an initial volume of approximately 150 µL was discarded before the sample was tapped.

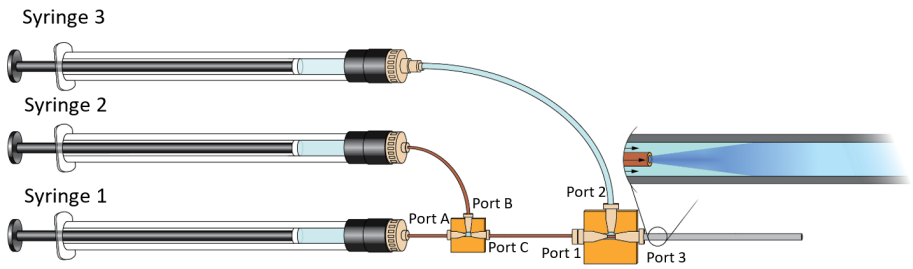

Figure 1. Schematic representation of the microfluidic-system setup. The fluid from Syringe 1 meets the fluid from Syringe 2 in a T-junction and the combined fluid meets the fluid in Syringe 3 in a co-flow where the combined fluid from Syringe 1 and 2 constitutes the inner fluid and the fluid from Syringe 3 constitutes the outer fluid.

Preparation of PLGA NPs with OVA and CpG

Two PLGA-NP formulations with OVA and CpG were prepared with a three-syringe microfluidic system: one to inject via a classical injection needle (aqueous-PLGA-NP formulation) and one used to prepare the dMNAs (dMNA-PLGA-NP formulation). For the preparation of the dMNA-PLGA-NP formulation, Syringe 1 of the microfluidic system was loaded with OVA and CpG dissolved in ultrapure water at concentrations of 4.0 mg/mL and 2.0 mg/mL, respectively. Syringes 2 and 3 were loaded with PLGA dissolved in acetonitrile at a concentration of 5.0 mg/mL and PVA (Mw of 9.5 kDa) dissolved in ultrapure water at a concentration of 14.1 mg/mL, respectively. The flow rates of the liquids dispensed from Syringes 1, 2, and 3 were set to 62.5, 625, and 2000 µL/min, respectively. After the syringe pumps were started the formulation was collected. A flow of nitrogen was used to evaporate the organic solvents from the formulation. Ultrapure water and 0.1 µm sterile filtered 100 mM phosphate buffer (75 mM Na_2HPO_4, 25 mM NaH_2PO_4) were added to achieve the final dMNA-PLGA-NP formulation, which consisted of 200 µg/mL OVA, 100 µg/mL CpG, 2.5 mg/mL PLGA, and 22.5 mg/mL PVA in 10 mM phosphate buffer (7.5 mM Na_2HPO_4, 2.5 mM NaH_2PO_4, pH 7.4).

We aimed to administer the same doses of OVA and CpG with the dMNAs and the injections with classical hypodermic needles in the immunization study. Therefore, the theoretically delivered quantities of these constituents from the dMNAs were calculated. One dose was delivered via two dMNAs, which theoretically would deliver 4.4 µg of OVA and 3.9 µg of CpG in total. To administer the same dose of OVA and CpG with the aqueous-PLGA-NP formulation (30 µL), the concentration of OVA in Syringe 1 was adjusted to 2.3 mg/mL. The remaining procedure was the same as for preparing the dMNA-PLGA-NP formulation. The final aqueous-PLGA-NP formulation consisted of 146 µg/mL OVA, 130 µg/mL CpG, 3.3 mg/mL PLGA, and 29.3 mg/mL PVA in 10 mM phosphate buffer. The soluble OVA and CpG were not removed from the dMNA-PLGA-NP formulation as dialysis would remove some of the PVA, which is a constituent needed to maintain stable dMNAs. To keep the aqueous-PLGA-NP and the dMNA-PLGA-NP formulations similar, the soluble OVA and CpG were also not removed from the aqueous-PLGA-NP formulation. The formulations were stored at 4 °C until use.

Determination of the hydrodynamic particle size and the zeta potential

The PLGA-NP formulations were analysed on a Zetasizer Nano ZS (Malvern Panalytical B.V., Almelo, the Netherlands) to determine the intensity-weighted mean hydrodynamic particle diameters (sizes) and PDIs with dynamic light scattering (detection angle of 173°), and the zeta potentials with laser Doppler electrophoresis. Before the measurements, the formulations were diluted 1:19 v/v in 10 mM phosphate buffer (n = 3).

Determination of the encapsulation efficiencies of OVA/CpG

To compare the aqueous-PLGA-NP formulation with the dMNA-PLGA-NP formulation, the encapsulation efficiencies of OVA/CpG in the PLGA NPs were determined by measuring the total concentrations of OVA/CpG before and after dialysis as dialysis removes the OVA/CpG in the continuous phase. A sample was taken before the dialysis and 1 mL of each formulation was added to Float-A-Lyzer® dialysis device. Each dialysis device was submerged in 300 mL of 10 mM phosphate buffer (PB) and the formulations were dialysed for 72 h at 4 °C.

To determine the concentrations of OVA in the samples before and after dialysis, the samples were mixed in a volume ratio of 1:1 with a mixture of 30 vol% DMSO, 0.1 M NaOH, and 10 mg/mL sodium dodecyl sulfate, to disrupt the PLGA NPs, and incubated at 37 °C for 2 h. The standard curve was prepared with OVA in 15 vol% DMSO, 0.05 M NaOH, and 5 mg/mL sodium dodecyl sulfate. Each sample was prepared in triplicates and plated on a clear flat-bottom 96-well plate. The amounts of OVA were quantified with the micro BCA assay. The absorbance was measured at 562 nm with a plate reader (Tecan Spark®, Männedorf, Switzerland).

The concentrations of CpG in the samples before and after dialysis were quantified with a Qubit™ ssDNA Assay Kit. The calibration curve was made with CpG dissolved in ultrapure water and the solutions for the calibration curve were treated the same way as the samples. Each sample was prepared in triplicate. A volume of 40 µL from each sample was added to Eppendorf tubes and dried at 37 °C overnight to remove the water. They were reconstituted

in 40 µL DMSO to disrupt the particles, and the vials were incubated at 37 °C for 2 h. The contents in the vials were spun down with a Microfuge® 18 centrifuge (1000 g, 5 min, Beckman Coulter Nederland B.V., Woerden, the Netherlands) and 30 µL of each sample was mixed with 270 µL of work reagent. After 2 min of equilibration time, 95 µL of each sample was plated on a black flat-bottom 96-well plate and 100 µL acetonitrile was added to each well. After 5 min, the fluorescence intensities (λ_{ex} 495 nm/λ_{em} 530 nm) were measured on a plate reader. The encapsulation efficiencies (EE%s) of OVA/CpG were calculated using the following equation:

$$EE\% = \frac{C(Sample\ after\ dialysis)}{C(Sample\ before\ dialysis)} \cdot 100\%$$

Preparation of PDMS mould

The silicone microneedle arrays that serves as a template consists of nine (3 × 3) microneedles [35]. Each microneedle has a height of 500 µm and a base diameter of 330 µm. Nine (3 × 3) microneedle arrays are attached to the pedestal of a polymethylmethacrylate (PDMS) grid. The combination of this grid and nine silicone microneedle arrays is the master structure. In order to create the PDMS mould, a mixture of sylgard 184 base silicone elastomer and curing agent (10:1 weight ratio) is poured into the master structure and cured overnight at 60 °C [36]. The next day, the cured PDMS mould was removed from the master structure.

Fabrication of dMNA and screening of the dMNA formulation

Securing the stability of PLGA NPs in dMNA is crucial to maintain the functionality of antigens. In order to find the most suitable polymer formulation for PLGA NPs incorporated dMNA, three different candidates of polymer formulation were used for dMNA production: 5% (w/v) PVA, 5% (w/v) PVP, and 30% (w/v) trehalose. These three different polymer formulations were screened based on the size and PDI of PLGA NPs in dMNAs.

To this end, dMNAs were fabricated with three different formulations as previously described [37]. First, empty (without OVA/CpG) PLGA NPs were added into each dMNA formulation with 1:4 of PLGA:polymer weight ratio, and the mixture was homogenised. Then, 90 µL of the mixture was loaded into the PDMS mould and centrifuged for 3 h at 25 °C with 11400 g. The centrifuged mould was dried at 37 °C overnight. The next day, silicone and epoxy glue were applied to each array to build a backplate. After another drying at 37 °C overnight, dMNAs were carefully removed from the mould. The shape and sharpness of dMNA were analysed with a brightfield microscope (Stemi 2000-C, Carl Zeiss Microscopy GmbH, Gottingen, Germany).

During the fabrication process, the size and PDI of PLGA NPs were measured three times using a Zetasizer as described in Determination of the hydrodynamic particle size and the zeta potential section (n = 3). They were measured (i) before and (ii) after adding into the polymer formulation. Subsequently, they were measured (iii) after re-suspending dMNA in 300 µL of PB (10 mM, pH 7.4). Among three candidates, the formulation that displayed the best retainment of PLGA NPs size and PDI (target size: < 200 nm, target PDI: < 0.3) was selected for further studies.

Skin penetration and dissolution tests

Penetration ability is a necessary function of dMNA in order to deliver the incorporated content into the skin. With the selected formulation from the previous section (5% (w/v) PVA with 1:4 PLGA:PVA ratio, see *Fabrication of dMNA and screening of the dMNA formulation*), PLGA NP loaded dMNA was fabricated and skin penetration test was performed [35].

Human abdominal skin was collected from a local hospital after cosmetic surgery, and stored at -80 °C after removing the fat. Before use, the skin was thawed for an hour at 37 °C and stretched on parafilm-covered styrofoam. Next, the skin was wiped with 70% (v/v) ethanol to clean. dMNA was attached to an applicator (UFAM v1.0, uPATCH B.V., Delft, The Netherlands) to pierce the skin with a reproducible velocity. The dMNA was applied onto the skin with 65 ± 1 cm/s of velocity (n = 3), and removed after one second. Then, 75 µL of 0.4% trypan blue was applied on the dMNA applied skin site for 45 min. After removal of the trypan blue solution, the stratum corneum was removed by performing tape striping until the skin appeared shiny. Next, the skin was visualised using a brightfield microscope and the penetration efficiency was calculated by dividing the number of penetrated microneedles by the number of total microneedles in one dMNA.

Fast dissolution of microneedles is important to shorten the application time and facilitate the use of dMNA for patients. For the fast delivery, we aimed for 70% (volume) dissolution within 30 min. A dMNA was applied onto the skin in the same manner as for the penetration study. However, dMNA stayed for 30 and 60 min (n = 3) in the skin instead of being removed after one second. After removal, dMNA was imaged using a brightfield microscope and the leftover microneedle volume was calculated. From the dissolution test, empty PLGA NPs loaded dMNA fabricated with the selected formulation did not show sufficient volume reduction even after 60 min. Therefore, this formulation required optimisation to ensure fast dissolution.

To this end, the total concentration of dMNA formulation was decreased from 5% (w/v) to 2.5% (w/v), and the weight ratio of PLGA:PVA was changed from 1:4 to 1:9. With this optimised formulation, PLGA NPs loaded dMNA was fabricated. Then, skin penetration and dissolution tests were repeated, whereby the dissolution time in the skin was 15 and 30 min.

Quantification of OVA in OVA encapsulated PLGA loaded dMNA

Centrifugation is an effective method to produce dMNA. However, fabrication via this method leads to drug distribution in both the microneedles and backplate. Since the drug in the backplate will not be delivered into the skin, it is important to first quantify the antigen entrapped in only the microneedles in order to deliver the target dose (4 μg) of OVA. For this, soluble OVA/CpG loaded dMNA and OVA/CpG encapsulated PLGA NPs loaded dMNA were prepared (n = 3). For control groups, empty PLGA NPs loaded dMNAs and empty PLGA NPs with soluble OVA loaded dMNAs were prepared (n = 3). To quantify the OVA in microneedles, nine microneedles were separated from the backplate (Fig. S1) and reconstituted in 170 μL of DMSO/sodium dodecyl sulfate/NaOH solvent. After homogenising overnight, a BCA assay was performed. Briefly, 150 μL of homogenised solution was loaded into a 96-well plate followed by 150 μL of working reagent. The plate was incubated for 2 h at 37 °C, and the absorbance was measured at 562 nm by using a plate reader.

Fabrication of soluble OVA loaded dMNA

In order to determine the effect of PLGA NPs on immune responses, both (i) soluble OVA/CpG loaded dMNA and (ii) OVA/CpG encapsulated PLGA NPs loaded dMNA were prepared for an immunisation study. To have the same dose of antigen in both groups, the same amount of OVA should be added to both of them during production. Therefore, the OVA amount in nine microneedles of OVA/CpG encapsulated PLGA NPs loaded dMNA was analysed in the previous section. Based on this quantification, the amount of OVA that should be added for soluble OVA/CpG loaded dMNA was determined which can have the same amount as OVA/CpG encapsulated PLGA NPs loaded dMNA.

For this, soluble OVA/CpG loaded dMNAs were fabricated with four different concentrations of OVA/CpG in 2.25% (w/v) PVA: 0.02% (w/v) OVA/0.01% (w/v) CpG, 0.1% (w/v) OVA/0.05% (w/v) CpG, 0.2% (w/v) OVA/0.1% (w/v) CpG, and 0.5% (w/v) OVA/0.25% (w/v) CpG. As described in the previous section, nine microneedles were separated from the backplate. Then, OVA loading in nine microneedles was quantified using a BCA assay. Based on the quantified OVA in microneedles of four individual arrays (Figure S3), the required OVA amount for the production of soluble OVA/CpG loaded dMNA was determined.

Quantification of CpG

Together with OVA, CpG was also encapsulated in PLGA NPs and added in dMNA in quantities of 50% w/w of the amount of OVA. To investigate the amount of CpG in microneedles, 0.05% (w/v) OVA and 0.025% (w/v) CpG were loaded in soluble CpG/OVA loaded dMNA based on the result of the studies described in the previous section. Empty PLGA NPs loaded dMNA and empty PLGA NPs with soluble OVA/CpG loaded dMNA were prepared for control groups.

Similar to OVA quantification described in *Quantification of OVA in OVA encapsulated PLGA loaded dMNAs* section, nine microneedles were separated and reconstituted in 170 μL of DMSO/sodium dodecyl sulfate/NaOH. For the quantification of CpG, a Qubit™ ssDNA assay was executed as described in *Determination of the encapsulation efficiencies of OVA/CpG* section. For the calibration curve, 0.2 mg/mL and 0.15 mg/mL of CpG in Limulus amebocyte lysate water were prepared followed by a two-fold dilution. The fluorescence intensity was measured at λ_{ex} 538 nm/λ_{em} 488 nm using a plate reader.

Animals

For the immunisation study, we used 35 female C57BL/6 mice, one OT-I mouse, which is a transgenic mouse on a C57BL/6 genetic background with T-cell receptors that pair with CD8 and recognise $OVA_{257-264}$ presented on MHC class I (haplotype H-$2K^b$) molecules, and two OT-II mice, which are transgenic mice on a C57BL/6 genetic background with T-cell receptors that pair with CD4 and recognise $OVA_{323-339}$ on MHC class II (haplotype I-A^b) molecules. They were 7–12 weeks old at the start of the experiment and were kept under standard laboratory conditions at the animal facility of Leiden Academic Centre for Drug Research, Leiden University. The animal experiment was approved by the ethical committee of Leiden University, and the animal work was performed in compliance with the Dutch government guidelines and Directive 2010/63/EU of the European Parliament.

Immunisation study

To determine if the aqueous formulations and dMNA were able to activate OVA-specific T cells, an immunisation study was performed in mice according to the schedule (Table 1).

Table 1. The schedule for the immunisation study.

Day	Action
1	Transfer OVA-specific $CD8^+$ T cells and OVA-specific $CD4^+$ T cells
2	Immunise mice
9	Harvest blood and spleens

On day 1, each of the 35 C57BL/6 mice was injected in the tail vein with 50,000 OVA-specific $CD8^+$ T cells which were isolated from a spleen collected from an OT-I mouse and 100,000 OVA-specific $CD4^+$ T cells which were isolated from two spleens collected from two OT-II mice [38] using a BD Microlance™ 3 0.3 × 13 mm needle (Becton Dickinson N.V., Vianen, Holland). On day 2, mice were weighed, marked, and allocated into seven groups of five mice, balanced with regard to weight and age. Each group was randomly assigned to seven different vaccine regimens (Table 2).

The mice group 1–3, 6, and 7 had their flanks shaved. The mice group 1–5 were anaesthetised by intraperitoneal injection with ketamine (100 mg/kg) and xylazine (10 mg/mL) for 10 min before administration of dMNAs (two dMNAs per mouse). The mice were placed on

a Heatel Teera Heatmat (Heatel B.V., Poeldijk, the Netherlands) and ophthalmic ointment was applied to their eyes. The mice group 2–5 were expected to receive 4.4–4.9 μg OVA and 3.9–4.3 μg CpG. The mice enrolled in Regimen 1 did not receive OVA/CpG. The dMNA was administrated into the skin for 30 min one at a time on either the flank or the ear. The dMNA was visualised using a bright-field microscope after being removed from the skin.

Table 2. Mice groups for the immunisation study.

Mice group	Regimens	Administration site	Target dose OVA/CpG (μg)
1	Empty dMNA (negative control)	Flank	0/0
2	Soluble OVA/CpG loaded dMNA*	Flank	4.4–4.9/ 3.9–4.3
3	OVA/CpG encapsulated PLGA NPs loaded dMNA*	Flank	4.4–4.9/ 3.9–4.3
4	Soluble OVA/CpG loaded dMNA*	Ear	4.4–4.9/ 3.9–4.3
5	OVA/CpG encapsulated PLGA NPs loaded dMNA*	Ear	4.4–4.9/ 3.9–4.3
6	OVA/CpG in PBS	Flank	4.4/3.9
7	Aqueous-PLGA-NP	Flank	4.4/3.9

*Dose in dMNAs was estimated based on dissolution.

The mice group 6 and 7 received 4.4 μg OVA and 3.9 μg CpG intradermally (flank) in a volume of 30 μL by using BD micro-fine™ + Demi U100 0,3 mL 30G insulin needles (Fisher Emergo B.V., Landsmeer, the Netherlands). Unfortunately, two mice died because of the anaesthesia (mice receiving Regimen 2 or 4), and one mouse receiving Regimen 2 was euthanised by cervical dislocation after reaching humane endpoints (limping and 17% weight reduction). On day 9, blood was collected by tail bleeding in micorvette® CB K2EDTA 300 μL tubes (Sarstedt B.V., Etten-Leur, the Netherlands). The mice were euthanised by cervical dislocation whereafter the spleens were harvested. The spleens were immersed in PBS and the blood and spleens were kept on ice till further use.

Table 3. Physicochemical characteristics of the PLGA NPs with OVA/CpG used for the aqueous-NP formulation and the dMNA. The physicochemical characteristics of the dMNA-NP formulation are measured while the formulation is liquid i.e. before they are added to the dMNA.

NP formulation	Size (nm)	PDI	ZP (mV)	EE%	
				OVA	CpG
Aqueous-PLGA-NP formulation	96.1 ± 0.4	0.090 ± 0.023	-0.85 ± 0.67	36.7	35.6
dMNA-PLGA-NP formulation	100.2 ± 1.7	0.097 ± 0.015	-1.94 ± 0.62	52.7	45.0

Average ± SD of three technical replicates. Size: intensity-weighted mean hydrodynamic particle diameters, PDI: polydispersity index, ZP: zeta potential, EE%: encapsulation efficiency.

Flow cytometric analysis of CD8⁺ and CD4⁺ T cells

To assess the OVA-specific T-cell responses in the immunised mice, the cells in the blood and spleens were stained with fluorophore-tagged antibodies. The spleens were strained to obtain single-cell suspensions and then erythrocytes were depleted from the splenocyte-containing single-cell suspensions using ammonium-chloride-kalium (ACK) lysing buffer. Hereafter, the splenocytes were resuspended in 2 mL complete Roswell Park Memorial Institute medium (cRPMI) and 100 μL of each suspension was added to a 96-well U-bottom plate. The erythrocytes in the blood were depleted in a similar way: the blood cells were suspended in 2 mL ACK lysing buffer and the lysis was stopped after 5 min by adding 5 mL cRPMI medium. The remaining blood cells were washed in 5 mL cRPMI medium and resuspended in 300 μL cRPMI medium. 100 μL of each blood-cell suspension was added to the 96-well round bottom plate. The plate with the blood and spleen cells was centrifuged (5 min, 550 g, 4 °C) and the supernatants were removed. The cells were resuspended in 100 μL surface marker staining solution (containing the fluorophore-tagged antibodies CD45.1 PE-Dazzle-594 (clone A20), Thy1.2 PE/Cyanine7 (clone 53–2.1), CD8a Brilliant Violet 510 (clone 53–6.7) (all from BioLegend Europe B.V., Amsterdam, the Netherlands), CD4 eFlour 450 (clone GK1.5), and 7-AAD Viability Staining Solution (live/dead marker) (both from eBioscience™, Fisher Emergo B.V.) in FACS buffer (1 mM EDTA, 2% fetal bovine serum, 0.1% sodium azide)), and the plate was covered with aluminium foil and incubated for 30 min at 4 °C. The plate was centrifuged (5 min, 550 g, 4 °C) and the supernatants were removed. The cells were washed two times and resuspended in 100 μL FACS buffer. Hereafter, the cells were analysed by flow cytometry (CytoFLEX S V4-B2-Y4-R3, Beckman Coulter, California, USA) with the acquisition software CytExpert (v2.3.1.22, Beckman Coulter). The sample flow rate and recorded volume were set to 60 μL/min and 80 μL, respectively. Data were analysed and manually compensated by using FlowJo software v10 (Treestar, Oregon, USA). The live CD8⁺ or CD4⁺ T cells were detected by first gating for single cells, then live (live/dead marker negative) T cells (Thy1.2 marker positive), and subsequently CD4⁺ (CD4 marker positive) or CD8⁺ (CD8a marker positive) cells. The OVA-specific cells in the live CD4⁺ or CD8⁺ T-cell populations were detected by measuring the frequency of CD45.1 (donor cells from the OT-I and OT-II mice) positive cells.

Statistical analysis

The data from the animal experiment was analysed in GraphPad Prism® version 8.0.1 (GraphPad Software, CA, USA). The statistical significance was determined with a one-way analysis of variance, followed by Bonferroni's multiple comparisons test and $P < 0.05$ was considered statistically significant (*$P < 0.05$, **$P < 0.01$, ***$P < 0.001$, ****$P < 0.0001$).

RESULTS

Characterisation of PLGA NPs and encapsulation efficiencies of OVA/CpG

The aqueous-PLGA-NP formulation and the dMNA-PLGA-NP formulation used to fabricate dMNA were prepared with the microfluidic system. When preparing the two formulations, the setup of the microfluidic system remained unchanged including concentrations of CpG, PLGA, and PVA in the syringes and the flow rates. The altered components were the OVA concentration in Syringe 1 and the final concentration of the two formulations. The OVA concentration in Syringe 1 was lower for the aqueous-PLGA-NP formulation than the dMNA-PLGA-NP formulation. The CpG:OVA:PLGA:PVA weight ratio was 1:2:25:225 for the dMNA-PLGA-NP formulation and 1:1.13:25:225 for the aqueous-PLGA-NP formulation resulting in a higher OVA concentration in the aqueous-PLGA-NP formulation than in the dNMA-PLGA-NP formulation. In the final formulations, the concentration of CpG, PLGA, and PVA was slightly higher for the aqueous-PLGA-NP formulation as it was concentrated more. The two formulations were characterised with regard to size, PDI, zeta potential, and encapsulation efficiencies of OVA/CpG (Table 3). The minor change in the method did not affect the physicochemical characteristics of the PLGA NPs massively. Both formulations were monodisperse, indicated by having PDIs below 0.1, sizes around 100 nm and slightly negative zeta potentials. OVA/CpG were effectively encapsulated into the PLGA NPs in both formulations with encapsulation efficiencies above 35%. The encapsulation efficiencies of OVA/CpG were highest in the dMNA-PLGA-NP formulation. Soluble OVA/ CpG were not removed. Therefore, OVA/ CpG are only partly encapsulated in the PLGA NPs when it is administered into the mice.

Fabrication of dMNA and screening of the dMNA formulation

dMNAs were fabricated with three different polymer formulation: 5% (w/v) PVA, 5% (w/v) PVP, and 30% (w/v) trehalose. All three formulations successfully formed nine sharp microneedle tips in each array (Fig. 2). Therefore, PLGA NPs could be incorporated in dMNAs with all three polymer formulations. The size and PDI of PLGA NPs were measured (i) before and (ii) after adding them to the formulation and also (iii) after re-suspending dMNA.

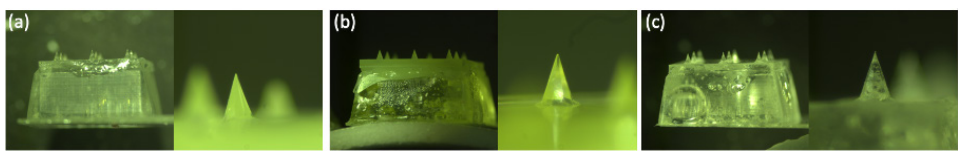

Figure 2. Fabricated dMNAs with (a) 5% (w/v) PVA, (b) 5% (w/v) PVP, and (c) 30% (w/v) trehalose.

As shown in Fig. 3a, the mean size of PLGA NPs was slightly increased after adding them to the formulations compared to before adding them. It increased 16.1% for 5% (w/v) PVA, 3.0% for 5% (w/v) PVP, and 1.5% for 30% (w/v) trehalose. These values considerably increased after re-suspending PVP dMNA (177.3%) and trehalose dMNA (396.3%). Only PVA dMNA displayed a slight increase in size (26.1%). PDI also showed similar trends. The size and PDI of PLGA NPs in only PVA dMNA were within the target range which were below 200 nm and 0.3, respectively (Fig. 3b). Therefore, 5% (w/v) PVA was selected as the dMNA formulation for further studies.

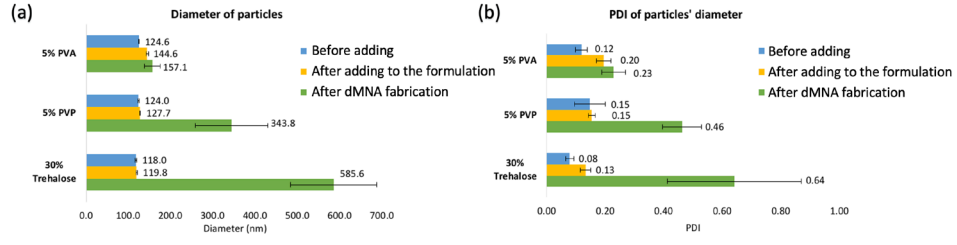

Figure 3. The (a) average size and (b) PDI of PLGA NPs in three different formulations and re-suspended dMNAs. Blue: before adding PLGA NPs to the dMNA formulation, yellow: after adding PLGA NPs to the dMNA formulation, green: after re-suspending the dMNA.

Skin penetration and dissolution of dMNA

Based on the results of PLGA NPs stability in the previous section, 5% (w/v) PVA was selected as a dMNA formulation. In order to investigate the mechanical strength and dissolution ability of dMNA, skin penetration and dissolution tests were performed. The penetration study demonstrated excellent penetration efficiency of 100% as all nine microneedles penetrated the skin (n = 3, Fig. 4a). In the dissolution test, however, only 3.6 ± 0.4% and 5.7 ± 0.4% of microneedle volume were dissolved in the skin within 30 and 60 min, respectively (Fig. 4b-c).

Hence, the dMNA formulation was further optimised by reducing the total concentration of dMNA formulation (2.5% (w/v)) and decreasing the proportion of PLGA NPs in the formulation (1:9 PLGA:PVA weight ratio). Skin penetration and dissolution tests were executed again with dMNAs produced with the optimised formulation. As a results, 2.5% (w/v) PVA dMNA (1:9 PLGA:PVA) demonstrated smilar penetration efficiency (100%) and a faster dissolution ability compared to 5% (w/v) total concentration of dMNA formulation with 1:4 PLGA:PVA weight ratio (Fig. 4d). Within 15 and 30 min, 55.8 ± 0.3% and 73.2 ± 2.8% of the microneedle volume dissolved, respectively (Fig. 4e-f). For further studies, 2.5% (w/v) total concentration of dMNA formulation with 1:9 PLGA:PVA weight ratio was used.

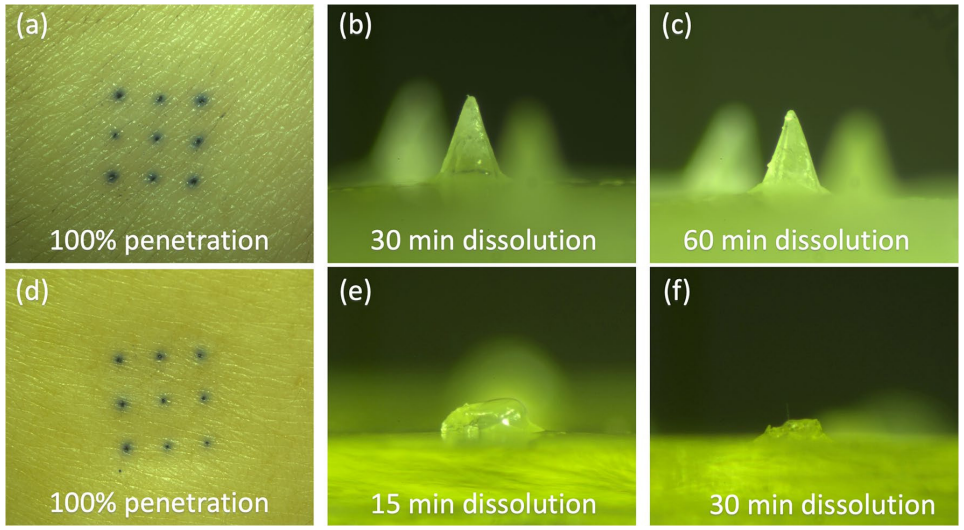

Figure 4. (a) Penetrated skin and (b) dissolved microneedle after 30 min (c) 60 min of dissolution with 5% (w/v) PVA dMNA with a 1:4 PLGA:PVA ratio. (d) Penetrated skin and (e) dissolved microneedle after 15 min (f) 30 min of dissolution with 2.5% (w/v) PVA dMNA with a 1:9 PLGA:PVA ratio.

Quantification of OVA

dMNA fabrication using a centrifugation method results in a substantial amount of antigen loading in the backplate. Therefore, quantifying OVA in only microneedles is necessary to determine the delivered dose.

Theoretically, 225 μg of PLGA NPs and 18 μg of OVA were expected to be loaded in each dMNA (including backplate) since the ratio of OVA:PLGA:PVA was 2:25:225. Based on the BCA assays, it was determined that 3.2 ± 0.4 μg of OVA was loaded in nine microneedles (17.8% of the total amount loaded in one dMNA). Based on the 70–76% dissolved volume of the microneedles (see the previous section), 2.2–2.4 μg of OVA was estimated to be delivered to the skin.

Fabrication of soluble OVA loaded dMNA

For the immunisation study, soluble OVA/CpG loaded dMNA and OVA/CpG encapsulated PLGA NPs loaded dMNA should carry an identical dose in nine microneedles which is 3.2 μg (see the previous section). Therefore, four different concentrations of OVA/CpG loaded dMNAs were prepared, and OVA in nine microneedles was quantified. As a result, 1.6 μg, 5.6 μg, 10.4 μg, and 16.1 μg of OVA were loaded in nine microneedles of 0.02% (w/v), 0.1% (w/v), 0.2% (w/v), and 0.5% (w/v) of OVA loaded dMNAs, respectively. Based on these results, a calibration curve was generated (Fig. S3) to display the OVA concentration of four different dMNAs and the corresponding OVA amount in nine microneedles. From the calibration curve, the OVA concentration for soluble OVA/CpG loaded dMNA production was determined which can carry 3.2 μg OVA in nine microneedles. Hence, 0.05% (w/v) of OVA should be loaded in soluble OVA/CpG loaded dMNA in order to carry the same OVA amount as OVA/CpG encapsulated PLGA NPs loaded dMNA.

Quantification of CpG

In PLGA NPs, CpG was also encapsulated as an adjuvant with a half weight ratio of OVA. Therefore, 0.05% (w/v) of OVA and 0.025% (w/v) of CpG were added in soluble OVA/CpG loaded dMNA based on the result of the previous section. By using the Qubit™ ssDNA assay, it was determined that 2.81 ± 0.04 μg of CpG was carried in nine microneedles. After 70—76% of dissolution, 2.0—2.1 μg of CpG is expected to be delivered to the skin.

Immunisation study

An immunisation study was performed to determine whether the presence of PLGA NPs and the administration form and location affects the T-cell responses in vivo. Transferred OVA-specific T-cell mice received seven different regimens which consisted of dMNAs or aqueous formulations with either soluble OVA/CpG or OVA/CpG partly encapsulated in PLGA NP (Table 3). The dMNAs were administered at two different locations: the flanks or the ear pinnae. Seven days after the immunisation, the T-cell responses in the blood and spleen were analysed by flow cytometry. The gating strategies are shown in Fig. S2.

The two aqueous formulations: OVA/CpG in PBS (group 6) and the aqueous PLGA NPs formulation (group 7) induced high expansion of the transferred OVA-specific $CD4^+$ T cells in the blood and spleen cells. OVA/CpG in PBS induced the highest response of OVA-specific $CD4^+$ T cells in the blood (2.5 ± 0.3% of the $CD4^+$ T-cell population) (Fig. 5a) and it was significantly higher than the response from the negative control (group 1, $P < 0.001$). The aqueous PLGA NPs formulation also induced a significantly higher OVA-specific $CD4^+$ T-cell response (1.9 ± 0.8% of the $CD4^+$ T-cell population) ($P < 0.05$) compared to the negative control. There was no significant difference between the $CD4^+$ T-cell responses induced by the two aqueous formulations. The same pattern was seen for the OVA-specific $CD4^+$ T-cell responses in the spleens (Fig. 6a); however, the responses were higher. OVA/CpG in PBS induced the highest response of OVA-specific $CD4^+$ T cells in the spleen (5.7 ± 1.4% of the $CD4^+$ T-cell population), and it was significantly higher than the negative control ($P < 0.0001$). The aqueous PLGA NPs formulation also induced a significantly higher OVA-specific $CD4^+$ T-cell response (5.4 ± 1.7% of the $CD4^+$ T-cell population) ($P < 0.0001$) compared to the negative control. Similar to the blood cells, there was no significant difference between the $CD4^+$ T-cell responses induced by the two aqueous formulations (group 6 and 7). The aqueous PLGA NPs formulation induced the highest OVA-specific $CD8^+$ T-cell response in the blood (17.0 ± 6.9% of the $CD8^+$ T-cell population) (Fig. 5b), this was statistically higher compared to the negative control ($P < 0.0001$). OVA/CpG in PBS induced an OVA-specific $CD8^+$ T-cell response of 2.7 ± 1.0%, however, this was not statistically significant compared to the negative control, though it was higher than the

0.4–0.6% baseline established by the dMNA with (group 3 and 5) and without PLGA NPs (group 2 and 4). In this case, the aqueous PLGA NPs formulation induced a significantly higher OVA-specific $CD8^+$ T-cell response ($P < 0.0001$) compared to OVA/CpG in PBS. The same pattern was seen in the spleen, however, the responses were higher. The aqueous PLGA NPs formulation induced an OVA-specific $CD8^+$ T-cell response of 29.6 ± 9.1% (of the $CD8^+$ T-cell population) (Fig. 6b), which was statistically significant compared to the negative control and the response in the spleen was again higher than the $CD8^+$ T-cell response in the blood.

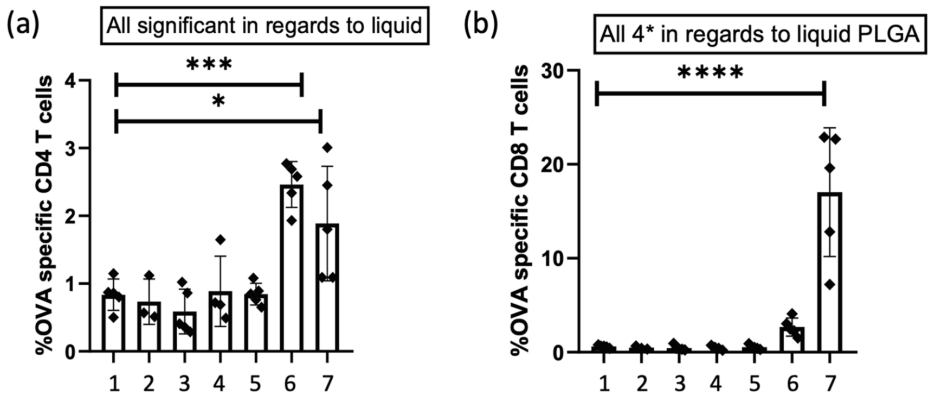

Figure 5. The percentage of OVA-specific $CD4^+$ (a) and $CD8^+$ (b) T cells of the total amount of $CD4^+$ and $CD8^+$ T cells, respectively, in the harvested blood. (mean ± SD, n = 5, except for flank MNA CpG and OVA n = 3, and ear MNA CpG and OVA n = 4). The formulations were compared with the empty dMNA, which was the negative control, for statistical significance. *P < 0.05, **P < 0.01,***P < 0.001, ***P < 0.0001.

The regimens with dMNAs (group 2–5) did not significantly change the OVA-specific $CD4^+$ T-cell responses compared to the negative control in the blood cells, and there was no significant change in the responses between the dMNAs inserted into the flank (group 2 and 3) and the ear (group 4 and 5). Neither was there a significant change in the responses between the dMNAs with (group 3 and 5) and without PLGA NPs (group 2 and 4), where all of the dMNAs induced OVA-specific $CD4^+$ T-cell responses of 0.6–0.9% in the $CD4^+$ T-cell populations. The same pattern was observed for the OVA-specific $CD4^+$ T-cell responses in the spleens, however, the T-cell responses were slightly higher for all of the regimens (Fig. 6a), where the dMNAs all induced around 1.3–1.5% of the $CD4^+$ T-cell population. The dMNA formulations (group 2–5) did not induce significant $CD8^+$ T-cell responses compared to the control in the blood and spleen either.

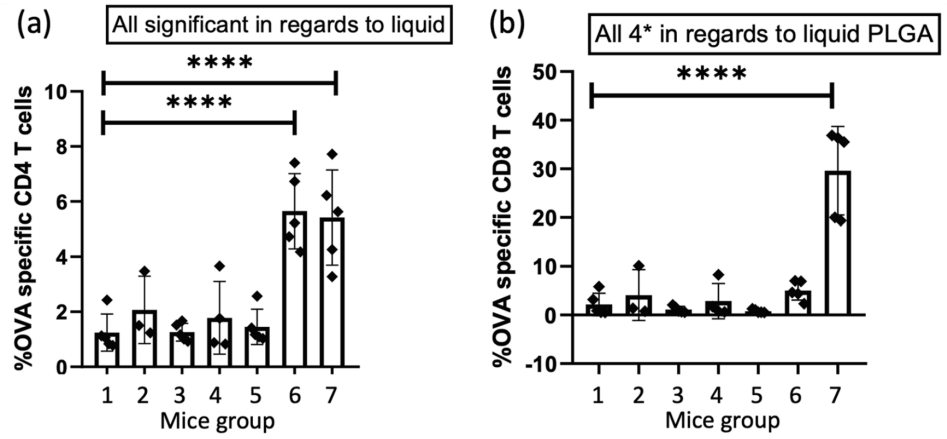

Figure 6. The percentage of OVA-specific $CD4^+$ (a) and $CD8^+$ (b) T cells of the total amount of $CD4^+$ and $CD8^+$ T cells, respectively, in the harvested spleens. (mean ± SD, n = 5, except for flank MNA CpG and OVA n = 3, and ear MNA CpG and OVA n = 4). The formulations were compared with the empty dMNA, which was the negative control, for statistical significance. *P < 0.05, **P < 0.01,***P < 0.001, ***P < 0.0001.

DISCUSSION

In this study, we developed OVA/CpG encapsulated PLGA NPs loaded dMNA. NPs work as adjuvant and enhance taking up of antigens by APCs. By delivering them to the skin which has abundant APCs, it is expected to boost the induction of T cells. For this, we chose two different approaches: (i) encapsulate antigens and adjuvant in PLGA NPs and (ii) deliver them intradermally using dMNA.

We chose to incorporate the antigen (OVA) and the molecular adjuvant (CpG) into the formulations. OVA is readily available and is often used to study antigen-specific immune responses in mice [39]. By performing an adoptive transfer of T cells from OT mice, whose T cells recognize specific OVA-derived peptide residues, the T-cell response is enlarged compared to wild-type mice, which normally require multiple vaccinations before OVA-specific immune responses can be measured. We chose CpG as adjuvant as previous studies have shown that subunit vaccines against SARS-CoV and HIV-1 containing CpG have activated dendritic cells [40] and induced specific Th1 and $CD8^+$ T-cell responses [26, 27]. We incorporated OVA/CpG into the PLGA NPs with a modular microfluidic system. The NPs sizes for the immunisation study were aimed at 100 nm as particles under 200 nm are more easily taken up by DC and supposedly give Th1 and $CD8^+$ T-cell responses [18, 41]. Furthermore, a previous study have compared PLGA NPs with OVA/CpG with sizes from 300 nm to 17 μm. The PLGA particles with 300 nm induced the highest expression of the DC activation markers CD86 and MHC class I, compared to naïve cells, soluble OVA/CpG

and PLGA microparticles with sizes of 17 μm, 7 μm, 1 μm. We succeeded at producing two formulations with monodisperse particles at around 100 nm with the microfluidic system. The sizes are normally larger with conventional methods, as double-emulsion and nanoprecipitation methods lead to PLGA NP with a minimum sizes at approximately 150 nm [42, 43]. Both of the NP formulations had zeta potentials of around -1 mV. This is a bit higher than PLGA particles prepared without PVA (-32 mV [28]). This is likely due a PVA layer on the surface of the NPs that shields the charge [44]. The soluble OVA/CpG was not removed from the PLGA-NP formulations because PVA, which is a small molecule (Mw 9 kDa), also would be removed during the dialysis. PVA is both a surfactant and the material chosen to produce the dMNA. Its concentration is crucial for dMNA production since mechanical strength of dMNA is proportional to the PVA concentration. We measured the encapsulation efficiencies of OVA/CpG. OVA had an encapsulation efficiency of 37–57%, which is higher than generally obtained with other microfluidic devices [28], but lower than via the conventional double emulsion method [42]. However, the methods are not directly comparable, as some of the small PLGA particles with a lower encapsulation efficiency probably is removed during the conventional method.

We also chose dMNA to deliver vaccines to the skin which has high population of APCs. The fabrication of PLGA NPs incorporated dMNA was successful. In terms of size and PDI, the NPs maintained stability even after being loaded into dMNA. Also, PLGA NPs loaded dMNA proved adequate mechanical strength by penetrating the skin effectively. The immunogenicity was expected to be elevated by introducing NPs in dMNA, since NPs allows targeted co-delivery of antigen and adjuvant. Unexpectedly, the immune responses from mice groups that received both soluble OVA/CpG and OVA/CpG encapsulated PLGA NPs using dMNAs (group 2–5) were significantly lower compared to those who received aqueous formulations (group 6 and 7). In recent studies, the combination of NPs and dMNAs failed to elicit immune responses. For example, OVA and poly(I:C) encapsulated PLGA NPs loaded dMNA failed to evoke $CD8^+$ T-cell responses [42].

In our study, the major reason for the poor immune responses from dMNA-received groups was poor dissolution and, as a result, insufficient dosages. Through an in-vitro skin dissolution test, it was proved that the majority of the microneedle volume was dissolved in human abdominal skin within 30 min (Fig. 4F). However, dMNA applied on in vivo mouse skin showed poor dissolution with the same application time (30 min) compared to the in vitro human skin so that the leftover volume of microneedle was larger than in vitro dissolution test (Fig. S4). This poorer dissolution in mouse skin might be resulted due to uneven surface of mouse skin compared to human skin, since the human skin was stretched on the flat and smooth Styrofoam during the in-vitro skin dissolution test.

Poor dissolution also could be caused by uneven distribution of PLGA NPs in microneedle. Centrifugal force made PLGA NPs concentrated in the tip of microneedles due to their weight, as observed by using fluorescently-labelled PLGA NPs loaded microneedles (Fig. S5). Since microneedle dissolution starts from the tip, the localisation of hydrophobic PLGA NPs in the tip disturbs rapid dissolution. Therefore, it is important to select proper production methods for the dMNA, which can distribute the drug formulation homogeneously in the microneedle. For example, filling the PDMS mould by spraying drug formulations can make homogeneously distributed microneedles [45]. Moreover, this spraying technique also can load multiple layers of drug and controlling the release by using multiple sprays. However, when a formulation is sprayed it spreads over the mould including on the surface outside of the microneedles, which leads to antigen waste. Elongating the dispensed drug formulation by placing it between two plates also contributes to the even distribution of drug formulation in the microneedle [46]. With this droplet-born air blowing technique, the length of microneedle is controllable and antigen waste can be avoided. Dispensing drug formulations is another way to reduce the localisation of NPs in the tip [35]. It can save antigen by loading the formulation only into the tips and automised system is possible by adding moving stages. However, the dispensable formulation is limited to the low viscosity.

CONCLUSION

To induce high antigen-specific T-cells responses, we chose two approaches: (i) incorporate the antigen and the molecular adjuvant into particles as they are more readily taken up by DCs which are key players in the induction of antigen-specific T-cell responses and (ii) deliver the formulations to a DC rich organ using dMNA. To achieve this, we developed OVA/CpG encapsulated PLGA NPs, and incorporated them into dMNA.

The fabrication of dMNA was successful as it displayed complete penetration efficiency with a major dissolution. Upon intradermal injection of aqueous formulation the PLGA NPs induced high $CD4^+$ T-cell and superior $CD8^+$ T-cell responses in the blood and spleen, showing the powerful approach of formulating for improved APCs uptake.

References

1. Hofmann F, Kralj N, Beie M. [Needle stick injuries in health care - frequency, causes und preventive strategies]. Gesundheitswesen [Internet]. 2002 May 1 [cited 2023 Mar 22];64(5):259–66. Available from: https://europepmc.org/article/med/12007067.
2. Prüss-Üstün A, Rapiti E, Hutin Y. Estimation of the global burden of disease attributable to contaminated sharps injuries among health-care workers. Am J Ind Med [Internet]. 2005 Dec 1 [cited 2023 Mar 22];48(6):482–90. Available from: https://onlinelibrary.wiley.com/doi/full/https://doi.org/10.1002/ajim.20230.
3. Biswas J, Dhali A, Panja S, Karpha K, Nath S, Dhali GK. Effect of hypodermic needle versus safety lancet on the fear and anxiety of needle prick among undergraduate medical students during hematology practical: a cohort study from a resource-limited setting. Cureus [Internet]. 2022 Jul 29 [cited 2023 Mar 22];14(7). Available from: /pmc/articles/PMC9420539/.
4. Ita K. Dissolving microneedles for transdermal drug delivery: Advances and challenges. Biomed Pharmacother. 2017;1(93):1116–27.
5. Liu S, Jin MN, Quan YS, Kamiyama F, Kusamori K, Katsumi H, et al. Transdermal delivery of relatively high molecular weight drugs using novel self-dissolving microneedle arrays fabricated from hyaluronic acid and their characteristics and safety after application to the skin. Eur J Pharm Biopharm. 2014;86(2):267–76.
6. Zhang L, Guo R, Wang S, Yang X, Ling G, Zhang P. Fabrication, evaluation and applications of dissolving microneedles. Int J Pharm. 2021;15(604):120749.
7. Chen S, Matsumoto H, Moro-oka Y, Tanaka M, Miyahara Y, Suganami T, et al. Microneedle-array patch fabricated with enzyme-free polymeric components capable of on-demand insulin delivery. Adv Funct Mater [Internet]. 2019 Feb 1 [cited 2023 Apr 24];29(7):1807369. Available from: https://onlinelibrary.wiley.com/doi/full/https://doi.org/10.1002/adfm.201807369.
8. Adams SB, Acvs D, Moore GE, Acvim D, Elrashidy M, Mohamed A, et al. Effect of Needle Size and Type, Reuse of Needles, Insertion Speed, and Removal of Hair on Contamination of Joints with Tissue Debris and Hair after Arthrocentesis. Veterinary Surgery [Internet]. 2010 Aug 1 [cited 2023 Apr 24];39(6):667–73. Available from: https://onlinelibrary.wiley.com/doi/full/https://doi.org/10.1111/j.1532-950X.2010.00649.x.
9. Mungmunpuntipantip R, Wiwanitkit V. Cost-utility-safety analysis of alternative intradermal versus classical intramuscular COVID-19 vaccination. Int J Physiol Pathophysiol Pharmacol [Internet]. 2022 [cited 2023 May 8];14(2):129. Available from: /pmc/articles/PMC9123469/.
10. Egunsola O, Clement F, Taplin J, Mastikhina L, Li JW, Lorenzetti DL, et al. Immunogenicity and safety of reduced-dose intradermal vs intramuscular influenza vaccines: a systematic review and meta-analysis. JAMA Netw Open [Internet]. 2021 Feb 1 [cited 2023 Feb 26];4(2):e2035693–e2035693. Available from: https://jamanetwork.com/journals/jamanetworkopen/fullarticle/2776045.
11. Di Pasquale A, Preiss S, Da Silva FT, Garçon N. Vaccine adjuvants: From 1920 to 2015 and beyond. Vaccines. 2015;3:320–43.
12. Benne N, van Duijn J, Kuiper J, Jiskoot W, Slütter B. Orchestrating immune responses: How size, shape and rigidity affect the immunogenicity of particulate vaccines. J Control Rel. 2016;234:124–34.
13. Salvador A, Igartua M, Hernández RM, Pedraz JL. An Overview on the Field of Micro- and Nanotechnologies for Synthetic Peptide-Based Vaccines. J Drug Deliv. 2011;2011:181646.
14. Vartak A, Sucheck SJ. Recent advances in subunit vaccine carriers. Vaccines. 2016;4:12.
15. Silva AL, Soema PC, Slütter B, Ossendorp F, Jiskoot W. PLGA particulate delivery systems for subunit vaccines: Linking particle properties to immunogenicity. Human Vacc Immunother. 2016;12:1056–69.
16. Makadia HK, Siegel SJ. Poly Lactic-co-Glycolic Acid (PLGA) as biodegradable controlled drug delivery carrier. Polymers (Basel). 2011;3(3):1377–97.
17. Koerner J, Horvath D, Groettrup M. Harnessing dendritic cells for poly (D, L-lactide-co-glycolide) microspheres (PLGA MS)-mediated anti-tumor therapy. Front Immunol. 2019;10:707.
18. Shima F, Uto T, Akagi T, Baba M, Akashi M. Size effect of amphiphilic poly(γ-glutamic acid) nanoparticles on cellular uptake and maturation of dendritic cells in vivo. Acta Biomater. 2013;9(11):8894–901.
19. Ottenhoff THM, Kaufmann SHE. Vaccines against tuberculosis: Where are we and where do we need to go? PLoS Pathog. 2012;8:e1002607.
20. Christensen D, Korsholm KS, Andersen P, Agger EM. Cationic liposomes as vaccine adjuvants. Expert Rev Vaccines. 2011;10:513.
21. Hafner AM, Corthésy B, Merkle HP. Particulate formulations for the delivery of poly(I: C) as vaccine adjuvant. Adv Drug Del Rev. 2013;65:1386–99.
22. Duthie MS, Windish HP, Fox CB, Reed SG. Use of defined TLR ligands as adjuvants within human vaccines. Immunol Rev. 2011;239(1):178–96.
23. Wischke C, Zimmermann J, Wessinger B, Schendler A, Borchert HH, Peters JH, et al. Poly(I:C) coated PLGA microparticles induce dendritic cell maturation. Int J Pharm. 2009;365(1–2):61–8.
24. Hamdy S, Elamanchili P, Alshamsan A, Molavi O, Satou T, Samuel J. Enhanced antigen-specific primary CD4+ and CD8+ responses by codelivery of ovalbumin and toll-like receptor ligand monophosphoryl lipid A in poly(D, L-lactic-co-glycolic acid) nanoparticles. J Biomed Mater Res A. 2007;81(3):652–62.
25. Diwan M, Tafaghodi M, Samuel J. Enhancement of immune responses by co-delivery of a CpG oligodeoxynucleotide and tetanus toxoid in biodegradable nanospheres. J Control Release. 2002;85(1–3):247–62.
26. Wille-Reece U, Wu CY, Flynn BJ, Kedl RM, Seder RA. Immunization with HIV-1 Gag protein conjugated to a TLR7/8 agonist results in the generation of HIV-1 Gag-specific Th1 and CD8+ T cell responses. J Immunol. 2005;174(12):7676–83.
27. Zhao K, Wang H, Wu C. The immune responses of HLA-A*0201 restricted SARS-CoV S peptide-specific CD8+ T cells are augmented in varying degrees by CpG ODN, PolyI: C and R848. Vaccine. 2011;29(38):6670–8.
28. Roces CB, Christensen D, Perrie Y. Translating the fabrication of protein-loaded poly(lactic-co-glycolic acid) nanoparticles from bench to scale-independent production using microfluidics. Drug Deliv Transl Res. 2020;10(3):582–93.
29. Yu B, Lee RJ, Lee LJ. Microfluidic methods for production of liposomes. Methods Enzymol. 2009;465:129–41.
30. Sah E, Sah H. Recent trends in preparation of poly(lactide-co-glycolide) nanoparticles by mixing polymeric organic solution with antisolvent. J Nanomater. 2015;2015:22.
31. Ahn J, Ko J, Lee S, Yu J, Kim YT, Jeon NL. Microfluidics in nanoparticle drug delivery; From synthesis to pre-clinical screening. Adv Drug Del Rev. 2018;128:29–53.
32. Li X, Jiang X. Microfluidics for producing poly (lactic-co-glycolic acid)-based pharmaceutical nanoparticles. Adv Drug Del Rev. 2018;128:101–14.
33. Zhao C, Ge Z, Yang C. Microfluidic techniques for analytes concentration. Micromachines (Basel). 2017;8(1):28.
34. Jahn A, Reiner JE, Vreeland WN, DeVoe DL, Locascio LE, Gaitan M. Preparation of nanoparticles by continuous-flow microfluidics. J Nanopart Res. 2008;10:925–34.
35. Lee J, van der Maaden K, Gooris G, O'Mahony C, Jiskoot W, Bouwstra J. Engineering of an automated nano-droplet dispensing system for fabrication of antigen-loaded dissolving microneedle arrays. Int J Pharm [Internet]. 2021 May 1 [cited 2021 Mar 29];600:120473. Available from: http://www.ncbi.nlm.nih.gov/pubmed/33737094.
36. Leone M, Priester MI, Romeijn S, Nejadnik MR, Mönkäre J, O'Mahony C, et al. Hyaluronan-based dissolving microneedles with high antigen content for intradermal vaccination: formulation, physicochemical characterization and immunogenicity assessment. Eur J Pharm Biopharm. 2019;134:49–59.
37. Tian Y, Lee J, van der Maaden K, Bhide Y, de Vries-Idema JJ, Akkerman R, et al. Intradermal administration of influenza vaccine with trehalose and pullulan-based dissolving microneedle arrays. J Pharm Sci [Internet]. 2022 Apr 1 [cited 2022 Mar 31];111(4):1070–80. Available from: http://www.ncbi.nlm.nih.gov/pubmed/35122832.
38. Benne N, Leboux RJT, Glandrup M, van Duijn J, Lozano Vigario F, Neustrup MA, et al. Atomic force microscopy measurements of anionic liposomes reveal the effect of liposomal rigidity on antigen-specific regulatory T cell responses. J Control Release [Internet]. 2020 Feb 1 [cited 2023 Oct 17];318:246–55. Available from: https://pubmed.ncbi.nlm.nih.gov/31812539/.
39. Immunology: Ovalbumin (OVA) Challenge [Internet]. Available from: https://www.taconic.com/find-your-model/gems/cryopreserved-models/knockout-repository/phenotypic-data-packages/comprehensive/ovalbumin-challenge.html.
40. Shi S, Zhu H, Xia X, Liang Z, Ma X, Sun B. Vaccine adjuvants: Understanding the structure and mechanism of adjuvanticity. Vaccine. 2019;37(24):3167–78.
41. Benne N, van Duijn J, Kuiper J, Jiskoot W, Slütter

B. Orchestrating immune responses: How size, shape and rigidity affect the immunogenicity of particulate vaccines. J Control Release [Internet]. 2016 Jul 28 [cited 2023 May 10];234:124–34. Available from: https://pubmed.ncbi.nlm.nih.gov/27221070/.
42. Mönkäre J, Pontier M, van Kampen EEM, Du G, Leone M, Romeijn S, et al. Development of PLGA nanoparticle loaded dissolving microneedles and comparison with hollow microneedles in intradermal vaccine delivery. Eur J Pharm Biopharm. 2018;129:111–21.
43. Hajavi J, Ebrahimian M, Sankian M, Khakzad MR, Hashemi M. Optimization of PLGA formulation containing protein or peptide-based antigen: Recent advances. J Biomed Mater Res - Part A. 2018;106:2540–51.
44. Sahoo SK, Panyam J, Prabha S, Labhasetwar V. Residual polyvinyl alcohol associated with poly (D, L-lactide-co-glycolide) nanoparticles affects their physical properties and cellular uptake. J Control Release. 2002;82(1):105–14.
45. McGrath MG, Vucen S, Vrdoljak A, Kelly A, O'Mahony C, Crean AM, et al. Production of dissolvable microneedles using an atomised spray process: Effect of microneedle composition on skin penetration. Eur J Pharm Biopharm. 2014;86(2):200–11.
46. Kim JD, Kim M, Yang H, Lee K, Jung H. Droplet-born air blowing: novel dissolving microneedle fabrication. J Control Release [Internet]. 2013 Sep 28 [cited 2022 Sep 1];170(3):430–6. Available from: http://www.ncbi.nlm.nih.gov/pubmed/23742882.

SUPPLEMENTARY MATERIAL

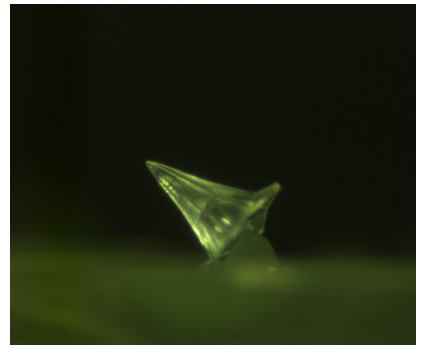

Figure S1. Separated microneedle from the array. All nine microneedle was separated from the array using blade to quantify the loading of OVA/CpG.

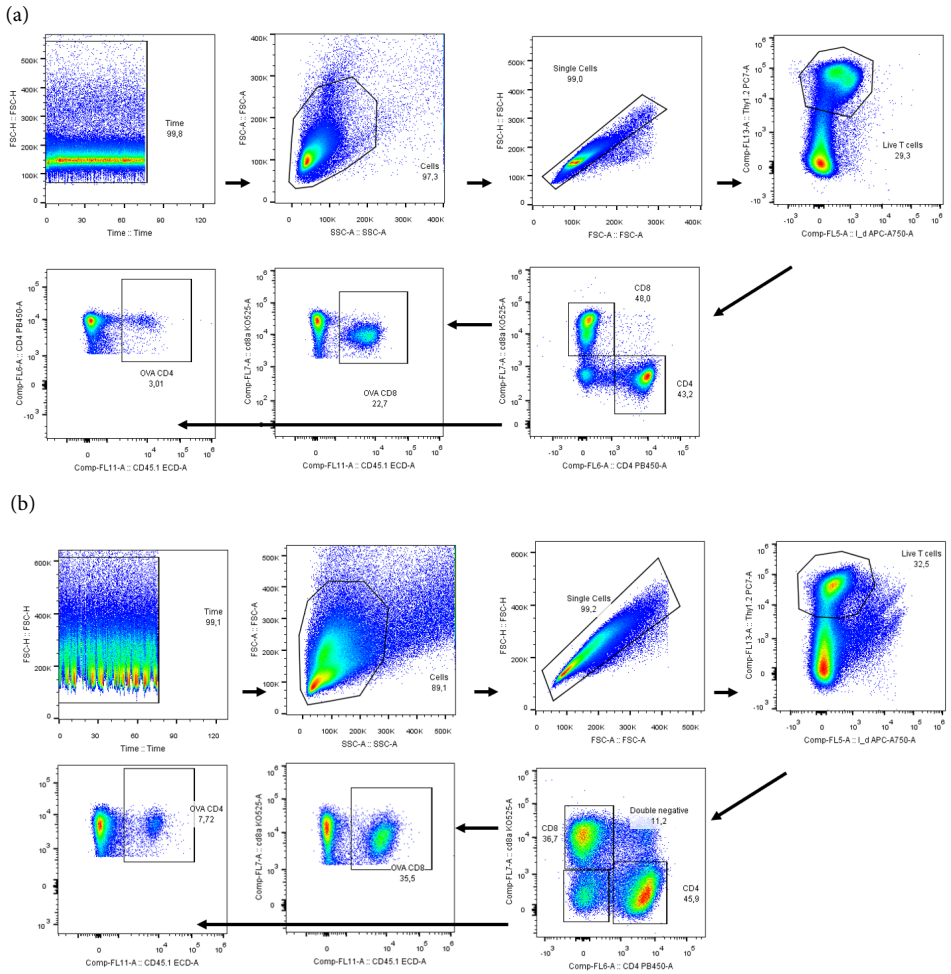

Figure S2. The gating strategy of (a) blood cells and (b) spleen cells for the OVA-specific T cell responses. First the cells were gated, then single cells, followed by live T cells, $CD4^+$ and $CD8^+$ cells, and then OVA-specific T cells.

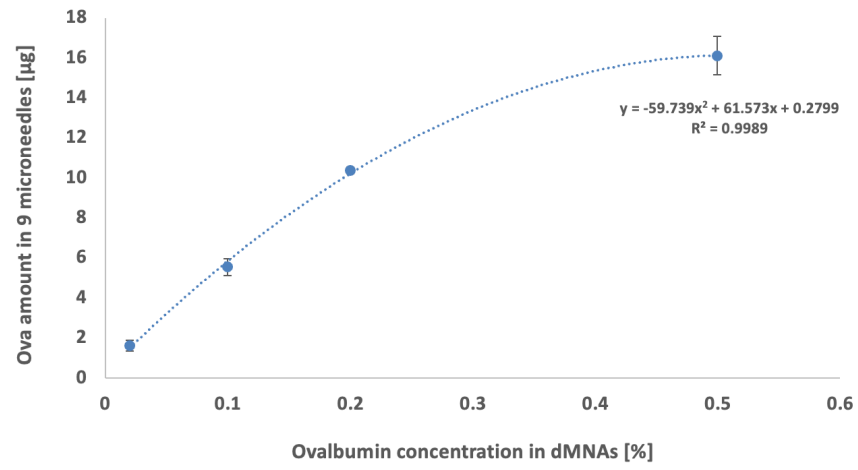

Figure S3. OVA amount in nine microneedles of 0.02%, 0.1%, 0.2%, 0.5% (w/v) OVA loaded dMNAs

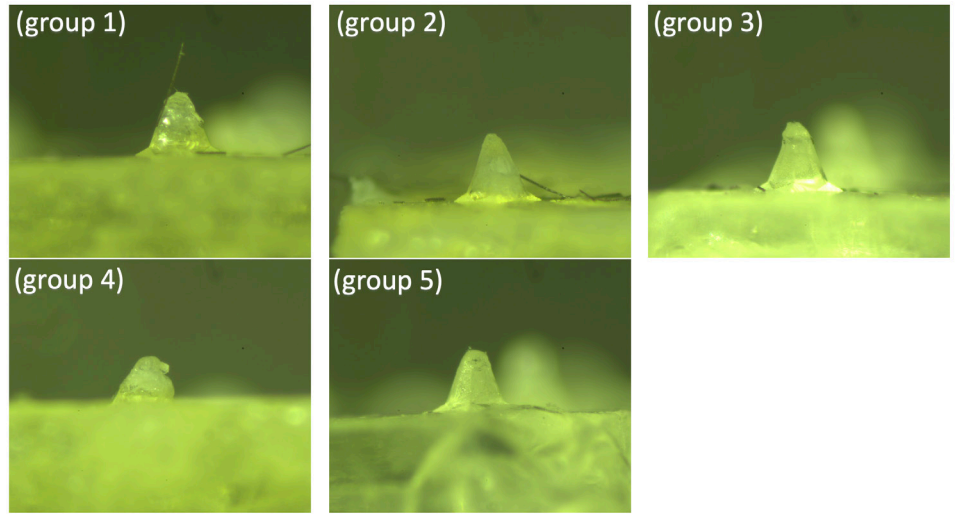

Figure S4. Leftover dMNAs and microneedles after vaccination

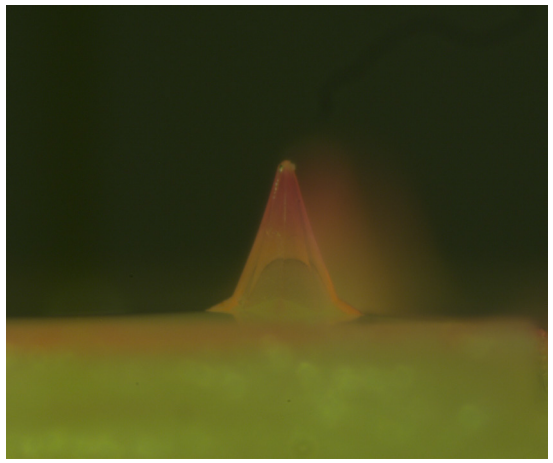

Figure S5. Rhodamine b labelled PLGA NPs loaded PVA microneedle. The weight ratio between PLGA NPs and PVA is 1:4, and centrifugal force make PLGA NPs concentrated to the tip of the microneedle.

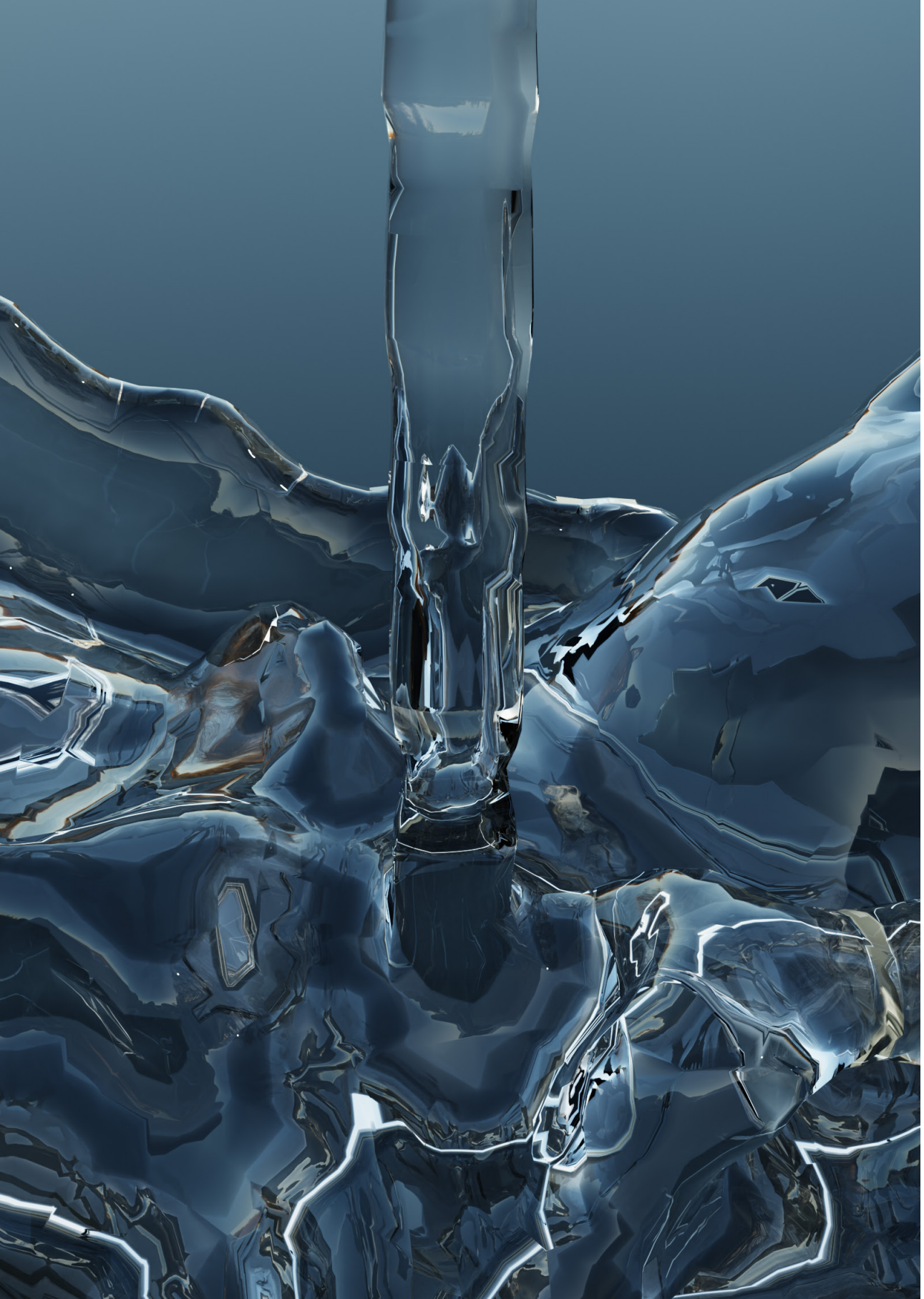

CHAPTER 6

SUMMARY OF THE DISSERTATION
GENERAL DISCUSSION
PROSPECTS
CONCLUSION

SUMMARY OF THE DISSERTATION

This dissertation focuses on nanoparticulate vaccine formulations and delivery routes to enhance antigen-specific induction of proinflammatory immune responses in the pursuit of creating new tuberculosis (TB) vaccination strategies.

To formulate a new TB vaccine, a TB antigen or antigen-encoding part is needed. The recombinant protein Ag85B-ESAT6-Rv2034 (AER), which consists of three *Mycobacterium tuberculosis* (Mtb)-expressed proteins fused together, is a promising TB antigen that provides T-cell epitopes in the human immune system [1]. However, subunit vaccines, which are vaccines based on purified antigens, such as the AER protein, are often poorly immunogenic [2–4]. Therefore, it is necessary to include molecular or particulate adjuvants in the vaccine formulation or, ideally, a combination of both, as adjuvants can help improve the potency and redirect the immune system toward an effective response [3, 4]. The emphasis in this thesis was on three particulate adjuvant types: i) cationic liposomes, ii) poly(D,L-lactic- *co*-glycolic acid) (PLGA) particles, and iii) PLGA- lipid hybrids. The research described in this dissertation focused on preparing and characterising these nanoparticles and comparing the immune responses induced by these three particulate adjuvant types.

i) Cationic liposomes are excellent subunit vaccine delivery systems that can induce cluster of differentiation (CD)4^+ (skewed towards a T helper type 1 (Th1) response) and $CD8^+$ T-cell responses [5–7]. These responses are deemed important in protection against TB [8]. A subgroup of cationic liposomes is the pH-sensitive cationic liposomes. They are stable at physiological pH; however, when they are internalised by antigen-presenting cells and exposed to the decreasing pH in the endosomes, where the liposomal bilayer becomes unstable, fuses with the endosomal membrane and the content leaks into the cytosol [9, 10]. This can promote $CD8^+$ T-cell responses [11]. The research described in this dissertation focused on optimising the lipid composition of liposomes to determine which lipid compositions could activate dendritic cells (DCs) and $CD4^+$ T cells.
ii) The second particulate adjuvant type described in this dissertation is PLGA nanoparticles. Particles made of this material have an excellent safety profile, being both biodegradable and biocompatible [12], and their properties (hydrophilicity/hydrophobicity, drug loading, drug release rate, etc.) are tuneable, which allows for the customisation of their properties to fit specific applications [13]. PLGA nanoparticles, without any added molecular adjuvants, do generally not elicit much of an immune response [5]. However, with a molecular adjuvant included, such nanoparticles can induce Th1-biased responses in mice [5].
iii) The third nanoparticle type investigated in the studies described in this dissertation is based on lipid-PLGA hybrids, which combine liposomes and PLGA nanoparticles by being nanoparticles with a PLGA core covered by lipids or vice versa [14]. Lipid-PLGA hybrids have successfully been used in drug and vaccine delivery preclinical research, where they induced equal IFNγ^+CD4^+CD44^{high}(Th1)-cell responses to liposomes with the same lipid composition in vivo [14].

While PLGA nanoparticles and lipid-PLGA hybrids are promising as drug delivery systems and nanoparticulate adjuvants, the typical bulk production methods for producing PLGA nanoparticles and lipid-PLGA hybrids are time-consuming and complex to control. It is crucial to improve and develop novel nano-preparation methods to increase their applicability, which can be done using microfluidics. Microfluidics is a technique that enables the manipulation of fluid streams through microscale fluidic channels [15]. It has emerged as a method to prepare PLGA nanoparticles with controlled diameters, which results in excellent batch-to-batch reproducibility and a narrow particle size distribution [15]. The studies described in this dissertation focus on the production of PLGA nanoparticles and PLGA hybrids using microfluidics.

Finally, a potent vaccination strategy could be to target the skin. The dermis is highly populated with different subsets of DCs, in contrast to subcutaneous and muscle tissue, which are the conventional administration routes [16]. Therefore, intradermal delivery of a TB vaccine could be of interest. Indeed, the only available TB vaccine, *Mycobacterium bovis* Bacille Calmette-Guérin (BCG), is mainly administered intradermally. Among the intradermal administration techniques, dissolvable microneedle arrays (dMNAs) are of special interest, as they: i) can secure the stability of loaded drugs by keeping them in their dry form, ii) be self-administered because of the easy application of the microneedle patch with microneedle lengths that would target the dermis, and iii) create zero needle waste as the microneedle dissolves, preventing needle-associated spread of blood-borne pathogens [17]. The research described in this dissertation investigated the first steps required for incorporating PLGA nanoparticles into dMNAs.

This dissertation delved into various aspects of developing a new TB subunit vaccine. **Chapter 1** comprehensively introduces TB immunology and the imperative for innovative vaccine solutions, culminating in this dissertation's aim and outline.

Chapter 2 describes how AER was formulated into cationic liposomal formulations with different lipid compositions and how the immune responses were assessed in vitro. The AER-containing liposomal formulations were formulated using the thin-film dehydration-rehydration method, followed by tip-sonication. The liposomes consisted of a positively charged lipid, cholesterol and a helper lipid (zwitterion) in different molar ratios. The physiochemically stable formulations were subsequently studied in a series of in vitro assays: i) a human monocyte-derived DC (MDDC) assay, where the viability and activation of DCs were assessed post-incubation with the formulations, ii) an uptake assay, whereby the uptake of liposomes was measured in MDDCs and M1 (classically activated macrophages that exhibit a proinflammatory phenotype) and M2 (alternatively activated

macrophages that exhibit an anti-inflammatory phenotype) macrophages, and iii) a T-cell assay in which the best-performing formulations were tested by incubating the activated DCs with specific $CD4^+$ T cells, to determine if the latter upregulated the activation marker CD154 and their interferon (IFN)-γ production.

The formulations containing cholesterol and the cationic lipids 1,2-dioleoyl-3-trimethylammonium-propane chloride (DOTAP), dimethyldioctadecylammonium bromide (DDA), 1,2-dioleoyl-*sn*-glycero-3-ethylphosphocholine chloride (EPC), or N^4-cholesteryl-spermine hydrochloride (GL-67) induced the highest upregulation of the MDDC-activation markers CD40, CD80, and CCR7. However, the formulation containing GL-67 induced high cell death and was therefore excluded from the T-cell assay. Among the remaining formulations, the AER/DOTAP:cholesterol:1,2-dioleoyl-*sn*-glycero-3-phosphocholine (DOPC) and AER/EPC:cholesterol:DOPC formulations significantly increased the level of IFN-γ^+CD154^+ T cells compared to their AER-empty counterparts. However, in a separate study (unpublished), the DOTAP liposomes were less immunogenic. Therefore, only the AER/EPC:cholesterol:DOPC formulation's lipid ratio was optimised further, where a molar lipid ratio of 2:1:2 was the most promising formulation, as it induced the highest level of DC activation markers and cytokine/chemokine production. In conclusion, the chapter describes a screening method for particulate vaccine formulations, where the most promising liposomal formulation in regards to inducing Th1 responses was the EPC:cholesterol:DOPC formulation.

Chapter 3 presents the set-up of a novel low-cost modular microfluidic system for producing PLGA nanoparticles and describes how the flow rates, solvents, and PLGA concentrations impact the PLGA nanoparticle formation in this system. The usability of this system for producing particles for controlled drug delivery was explored by incorporating positively and negatively charged proteins into PLGA nanoparticles. The simplest form of the modular microfluidic system involves a co-flow configuration, where an inner flow of PLGA-containing organic solvent meets an outer flow of an aqueous fluid. Mixing these two solvents triggers PLGA precipitation, leading to nanoparticle formation.

The results presented in this chapter show that the formation of nanoparticles is affected by the PLGA concentration, where an increasing PLGA concentration leads to larger particle diameters. Furthermore, it was observed that increasing the total flow rate results in the formation of smaller nanoparticles. Utilising ultrapure water as an aqueous phase resulted in negatively charged nanoparticles and uncontrolled precipitation at the outlet with high PLGA concentrations. Meanwhile, adding poly(vinyl alcohol) to the aqueous phase created neutral particles and eliminated precipitation issues. Negatively charged particles were controllably obtained utilising ethanol-water mixtures. Incorporation of the proteins ovalbumin or lysozyme (negatively and positively charged, respectively) with a three-syringe system resulted in encapsulation efficiencies above 40%. In conclusion, a cheap and easily adjustable modular microfluidic system was developed to prepare PLGA nanoparticles with precise control over the particle diameter and the possibility of including proteins, making it an excellent tool for drug and vaccine delivery applications.

In **Chapter 4**, studies on three different nanoparticulate adjuvants were reported: cationic pH-sensitive liposomes, prepared with sonication, and two modular-microfluidic-system prepared nanoparticles: PLGA nanoparticles and lipid-PLGA hybrids.

The immunogenicity of the particulate adjuvants formulated with the antigen AER with and without the molecular adjuvants monophosphoryl lipid A (MPLA) and cytosine-phosphate-guanine oligodeoxynucleotides (CpG ODNs) 1826 was assessed in vitro in MDDCs. The uptake of the particulate adjuvants in MDDCs without the molecular adjuvants was evaluated. Lipid-PLGA hybrids and pH-sensitive liposomes were taken up efficiently by MDDCs, but PLGA nanoparticles were not. MDDCs were stimulated with the particulate adjuvants, with and without the molecular adjuvants, and examined in terms of activation markers and cytokine production. Among the particulate formulations without molecular adjuvants, the cationic pH-sensitive liposomes were less efficient than the lipid-PLGA hybrids at upregulating DC surface markers and cytokine production, while PLGA nanoparticles were the least efficient. PLGA particles and pH-sensitive liposomes without molecular adjuvants hardly induced the excretion of cytokines/chemokines. The lipid-PLGA hybrids, PLGA nanoparticles, and the pH-sensitive liposomes with molecular adjuvants were all efficient at upregulating DC surface markers and cytokine production.

The protective efficacy of the liposomes, PLGA nanoparticles, and the lipid-PLGA hybrids formulated with the molecular adjuvants were tested in vivo in C57Bl/6 mice that were challenged sequentially with Mtb to determine possible efficacy as a TB vaccine. The candidate vaccines we developed were compared head-to-head with the current BCG vaccine and AER mixed with adjuvants MPLA and CpG ODN 1826. All vaccines (BCG, liposomes, PLGA nanoparticles, and the lipid-PLGA hybrids), except the AER-molecular-adjuvant mix, induced protection in Mtb-challenged C57/Bl6 mice, as indicated by a significant reduction in bacterial burden in the lungs and spleens of the animals compared to Mtb-challenged unvaccinated mice. Mice vaccinated with PLGA nanoparticles had a lower median number of Mtb bacteria in the spleens and lungs compared to BCG and the other two nanoparticle-based vaccines; however, this difference was not statistically significant between these relatively small groups. In conclusion, the nanoparticle-based formulation vaccines lowered the Mtb bacterial burden in the mice. The PLGA particles tended to have the best protective efficacy, even though the lipid-PLGA hybrids induced slightly better results in vitro.

In **Chapter 5**, studies are described in which the effect of intradermal administration of PLGA nanoparticles with CpG ODN 1826 and ovalbumin in dMNAs versus intradermal administration with hypodermic needles in vivo was determined. Intradermal injection of nanoparticles has been an effective administration route for vaccines.

In this study, we first had to design stable dMNAs with PLGA nanoparticles because the different polymers used for dMNA preparation affected the nanoparticle integrity. The dMNAs prepared with poly(vinyl alcohol) showed almost no aggregation of PLGA nanoparticles. The PLGA:poly(vinyl alcohol) weight ratio of 1:9 resulted in 100% penetration efficiency and the fastest dissolution in ex-vivo human skin (below 30 min). Subsequently, aqueous formulations and dMNAs with ovalbumin and CpG ODN 1826 with and without PLGA nanoparticles were tested in mice. The aqueous formulations with ovalbumin and CpG ODN 1826 with and without PLGA nanoparticles induced significant $CD4^+$ T-cell responses in mice compared to the other formulations. The formulation with ovalbumin and CpG ODN 1826 with PLGA nanoparticles induced significant $CD8^+$ T-cell responses compared to the other formulations. Unfortunately, the dMNAs did not dissolve entirely in the mouse skin, which could be why they did not induce $CD4^+$ and $CD8^+$ T-cell responses.

In conclusion, the aqueous formulations performed better than the dMNAs, probably due to the poor dissolution of the dMNAs in murine skin in the in vivo experiment. However, the dissolution was good in the ex-vivo human skin, demonstrating the differences between models. The dMNA formulation should, therefore, be adapted for murine testing. Even though we did not induce immune responses utilising dMNAs, dMNAs with incorporated PLGA nanoparticles were successfully prepared as the particles retained their physicochemical properties after dissolution. The aqueous formulation with PLGA nanoparticles prepared with the modular microfluidic system was especially potent at inducing $CD4^+$ and $CD8^+$ T-cell responses.

GENERAL DISCUSSION

Physicochemical properties of nanoparticles

To elicit robust $CD8^+$ T-cell responses and Th1-skewed $CD4^+$ T-cell profiles, we utilised particle diameters of approximately 150 nm for both the in vivo and in vitro experiments, as previous studies have demonstrated that particles within the size range of 10 to 200 nm tend to induce Th1-skewed $CD4^+$ and $CD8^+$ T-cell responses [18]. In contrast, larger particles (200-500 nm) often lead to Th2 responses [18]. However, the optimal size for liposomes may be different. It has been observed that small liposomes (below a size of 200 nm) generate Th2-skewed immune responses, whereas liposomes above 200 nm induce Th1-skewed responses [18]. This might be because small antigen-containing liposomes are degraded fast in the lysosomes, which could lead to ineffective antigen presentation, whereas the larger liposomes are degraded slower in the phagosomes [18]. This might explain why we see a tendency of lower protective efficacy against TB for the liposomes described in **Chapter 4** when compared with the TB vaccine based on PLGA particles and lipid-PLGA hybrids.

Particle rigidity also plays a crucial role in immune responses. Studies have shown that rigid particles are more readily taken up by macrophages, endothelial cells, and DCs than less rigid particles [18, 19]. They are also more likely to induce Th1 responses [18, 20]. When cholesterol is incorporated into the bilayer of liposomes with a liquid-disordered organisation, a liquid-ordered phase, which is more rigid, is formed [19, 21]. Our results in **Chapter 2** align with these findings, as liposomes containing cholesterol were generally more efficiently taken up by cells and could induce Th1-skewed $CD4^+$ T-cell responses (the $CD8^+$ T-cell responses were not tested). We have previously characterised the rigidity of PLGA particles, finding them significantly more rigid than liposomes (Young's modulus value of around 14.4 MPa, which is the same for cartilage [19]). In comparison, liposomes have, dependent on the lipid composition, Young's modulus values of around 500 kPa to 4 MPa [19]. The rigidity of lipid-PLGA hybrids is expected to be between these two values, as they often consist of a PLGA core surrounded by lipid layers [14]. Despite this, MDDCs took up lipid-PLGA hybrids more efficiently in our experiments. This suggests that the positive charge of the lipid-PLGA hybrids, in contrast to the negative charge of PLGA particles, mainly plays a role in cellular uptake, which also is seen for liposomes in literature, where positively charged particles are taken up more than neutral and negatively-charged liposomes [7].

Conventional methods versus microfluidics for PLGA nanoparticle production

PLGA particles prepared with conventional methods do not induce high antigen-specific $CD4^+$ and $CD8^+$ T-cell responses (the PLGA particles induced ~1% and 0.2-1% antigen-specific $CD4^+$ and $CD8^+$ T cells, respectively, out of the total $CD4^+$ or $CD8^+$ T cell population in the spleen [5]). However, the PLGA particles produced with the modular microfluidic system show high antigen-specific $CD4^+$ and $CD8^+$ T-cell responses in a similar experiment (5% and 30% antigen-specific $CD4^+$ and $CD8^+$ T cells in the spleen), as shown in **Chapter 3**. This is despite the physicochemical characteristics of the particles being more or less the same when prepared with the conventional method (average particle diameter: 157-160 nm, polydispersity index (PDI): 0.052-0.060, and zeta potential: -18 to -22 mV [5]) and the modular microfluidic system (average particle diameter: 96 nm, PDI 0.09, and zeta potential: -0.8 mV in **Chapter 3**). The differences in the responses could be due to the different ovalbumin (antigen) doses (0.31 µg and 4.4 µg for PLGA particles prepared with the conventional method and microfluidics, respectively). However, it could also be due to the particle preparation method. From personal experience, I have observed that even though PLGA particle formulations prepared with the conventional double-emulsion

method often seem acceptable when the particle diameter is measured with dynamic light scattering, the particles are usually visible to the naked eye. The PLGA particles are often spun down and washed, which removes the surfactant and lowers the zeta potential, and the steric hindrance between the particles leads to more aggregation. It is possible to avoid these aggregates in the measurement by sampling from the surface. It could also be due to differences in the surface morphology, density, or porosity, or other non-tested factors. In general, it appears that microfluidic methods are better at preparing PLGA particles with uniform particle diameters throughout the sample that can induce higher $CD4^+$ or $CD8^+$ T-cell responses than the conventional methods.

Which response is needed against tuberculosis

The immune response that correlates with protection against TB is not entirely established. It is, therefore, hard to determine if a new TB vaccine is protective in preclinical studies without performing an Mtb challenge study. Historically, it was believed that Th1 responses were essential for an effective TB vaccine, and a conventional strategy was to aim to induce Th1/Th17 responses while minimising Th2/Treg responses [22]. However, recent understanding suggests that this theory should be complemented by the interplay between Th1, Th2, and B-cell responses [22].

All the AER-containing nanoparticle vaccines in **Chapter 4** induced polyfunctional IL-2, IFN-γ, and TNF-α producing $CD4^+$ and $CD8^+$ T cells and monofunctional IFNγ-producing $CD8^+$ T cells with a central memory phenotype ($CD62L^+$). Even though the lipid-PLGA hybrids and pH-sensitive liposomes seemed to have the best cellular responses in vitro in MDDCs and in AER restimulated splenocytes from immunised non-Mtb-challenged mice, the PLGA nanoparticles with molecular adjuvants tended to have the most protective effect against TB, which demonstrates that the immune correlate is still not established.

PROSPECTS

Future directions of TB vaccine formulations

The work in this dissertation offers valuable insights into developing future TB vaccines. To translate these findings clinically, the field should focus on three significant aspects:

- Dosing and release kinetics
- Dissolvable microneedles to improve global vaccine distribution
- Production of the vaccine: assembly line with Quality Control (QC)

Dosing and release kinetics

The antigen and molecular adjuvant dose administered in the animal experiments described in this dissertation were based on previous work within the BioTherapeutics research group (dose of ovalbumin per immunisation: 5 μg [5], ovalbumin-to-CpG-ODN ratio 1:1 [23], antigen-to-liposome weight ratio 1:50 [23], dose of AER: antigen dose in antigen adjuvant mix: 25 μg) and have not been further optimised. To further improve the vaccine, the antigen dose, molecular adjuvant concentration, and antigen-to-particle weight ratio in the vaccine formulation can be further optimised. Given that the antigen dose can significantly influence both B-cell and T-cell responses [24], determining the optimal dose and antigen-to-particle weight ratio in mice and, subsequently, in humans is essential for future translation of the vaccine.

As dosing schedules have been shown to influence immune responses in both mice [25] and humans [26], the number of doses and interval between the prime and possible booster(s), as well as the release profile of the antigen, are crucial. Prolonged dosing schedules have been observed to increase neutralising antibody titres [26], suggesting several potential strategies to improve vaccination efficacy. These include exploring different intervals between prime and booster doses. This could be implemented by testing different intervals between prime and boosters or by incorporating the antigen (and molecular adjuvant) into delivery systems with diverse release profiles (e.g., mimicking the natural course of an infection). Consequently, characterising the release profiles of the different produced particles; liposomes, PLGA nanoparticles, and polymer-lipid hybrids, is of relevance. This would determine whether the vaccines release antigen in discrete bursts or continuously, and establish if a combination of these delivery systems could achieve a prolonged dosing schedule.

Dissolvable microneedles

Maintaining an expensive cold chain is often necessary to distribute liquid vaccines. This can be circumvented by incorporating vaccines into dissolvable microneedles. Furthermore, dissolvable microneedles offer additional benefits, including reduced pain compared to conventional intradermal injections and elimination of biohazardous needle waste [17].

The dissolution properties of the dissolvable microneedles with nanoparticles incorporated, described in **Chapter 5,** require improvement. While demonstrating acceptable dissolution kinetics in ex vivo human skin, the in vivo animal experiments yielded suboptimal results. Therefore, to better inform subsequent in vivo studies, initial ex vivo experiments should be conducted using mouse skin, which exhibits significant differences from human skin (e.g., reduced thickness, increased flexibility). The influence of compromised human skin (various skin conditions) on microneedle dissolution [27] could also be considered. Furthermore, for the development of a dissolvable microneedle-based vaccine, the stability of the microneedle arrays should be evaluated under a range of environmental conditions, including variations in humidity and temperature.

Several strategies can be explored to enhance the dissolution rate of the microneedles. These include:

- Evaluating alternative matrix materials: Previous investigations involving poly(vinyl alcohol), polyvinylpyrrolidone, and trehalose revealed that the latter two induced PLGA nanoparticle aggregation upon resuspension of the nanoparticles from the microneedles. Further studies should, therefore, examine a broader range of polymers, sugars, or combinations to identify formulations that minimise dissolution time while preventing aggregation of the nanoparticles.
- Investigating alternative fabrication methodologies: The centrifugation method, which was employed in **Chapter 5**, led to PLGA particle accumulation at the microneedle tips due to the higher density of the nanoparticles relative to the polymer matrix. This might be the reason for the high dissolution rate. Alternative methods that enable homogeneous particle distribution within the microneedles, such as dispensing with robotics and nanodispensing [28], or incorporating a rapidly dissolving layer just above the microneedle tip, could address this issue.
- Investigating alternative microneedle array designs, such as increasing the amount of microneedles in the array. This could lead to a reduction in the concentration of PLGA particles per microneedle while maintaining the overall dose.
- Examining alternative microneedle geometries to optimise the dissolution rate (e.g., increase the microneedle surface area).

Assembly Line

For vaccine production, the goal is to establish a continuous production assembly line with integrated QC to ensure product consistency over time. This approach aims to reduce production costs and increase speed by minimising manual labour. All processes must adhere to Good Manufacturing Practice (GMP) to ensure the vaccine is consistently produced according to quality standards and meets regulatory requirements. The modular microfluidic system is well-suited, as the vaccine formulation could be produced continuously. However, the purification method used in this dissertation (using dialysis chambers) requires improvement, as it creates batches. Alternative purification methods that are already available on the market, i.e., continuous-flow dialysis, could be explored to continuously remove organic solvents, free antigens, and non-encapsulated molecular adjuvants.

Quality Control

During the assembly line production of vaccines, the product should be analysed and assessed at critical points to ensure consistent quality. This begins with the components introduced into the microfluidic system.

There are no standardised interlaboratory methods for assessing the antigen or antigen-encoding component before its incorporation into a vaccine. In this dissertation, the antigen AER was not monomeric when dissolved (analysed with size-exclusion chromatography and asymmetric flow field-flow fractionation), and gel electrophoresis indicated inconsistent protein synthesis. This aggregation made it difficult to formulate the antigen into liposomes using the extrusion method, necessitating the sonication method instead. Even the model antigen ovalbumin, obtained from major manufacturers, was sometimes dimeric and sometimes only partially passed through a 1000 kDa dialysis membrane. Furthermore, lipophilic antigens tend to form particles that cannot penetrate a dialysis chamber, making it challenging to determine the amount of antigen incorporated into the nanoparticles.

To address these issues, thorough product analysis and interlaboratory standards for antigen characterisation, including standard characterisation methods for the nanoparticles, should be established, as they are crucial for advancing the field and improving GMP compliance.

CONCLUSION

The findings in the studies described in this dissertation highlight the interplay between nanoparticle physicochemical properties and their ability to induce robust T-cell responses. The preparation method of nanoparticles can influence their immunogenicity. Compared to conventional methods, we observed that PLGA nanoparticles produced using the modular microfluidic system induced significantly higher antigen-specific $CD4^+$ and $CD8^+$ T-cell responses. This might be attributed to the improved uniformity and reduced aggregation achieved through microfluidic fabrication. The choice of nanoparticle platform, such as liposomes, PLGA particles, or lipid-PLGA hybrids, can also impact the type of immune response elicited, as the different particle types have different physicochemical properties in regard to rigidity and charge. While each platform has its advantages and disadvantages, our results suggest that PLGA nanoparticles with incorporated antigen and molecular adjuvants produced with the modular microfluidic system may be a promising candidate for inducing robust T-cell responses with protective potential against TB.

In conclusion, the studies described in this dissertation underscore the importance of carefully considering the physicochemical properties of nanoparticles to obtain the desired immunological response. As discussed in the prospects, several other things should be considered before the research can be carried out further, such as optimising the vaccine dosage, streamlining the production method, and improving the dissolvable microneedle dissolution rate.

References

1. Commandeur S, van den Eeden SJF, Dijkman K, Clark SO, van Meijgaarden KE, Wilson L, et al. The in vivo expressed Mycobacterium tuberculosis (IVE-TB) antigen Rv2034 induces CD4+ T-cells that protect against pulmonary infection in HLA-DR transgenic mice and guinea pigs. Vaccine. 2014;32(29):3580-8. https://doi.org/10.1016/j.vaccine.2014.05.005.
2. Reyes C, Patarroyo MA. Adjuvants approved for human use: What do we know and what do we need to know for designing good adjuvants? Eur J Pharmacol. 2023;945:175632. https://doi.org/10.1016/j.ejphar.2023.175632.
3. Di Pasquale A, Preiss S, Tavares Da Silva F, Garçon N. Vaccine Adjuvants: from 1920 to 2015 and Beyond. Vaccines (Basel). 2015;3(2):320-43. https://doi.org/10.3390/vaccines3020320.
4. Johnston D, Zaidi B, Bystryn JC. TLR7 imidazoquinoline ligand 3M-019 is a potent adjuvant for pure protein prototype vaccines. Cancer Immunol Immunother. 2007;56(8):1133-41. https://doi.org/10.1007/s00262-006-0262-3.
5. Du G, Hathout RM, Nasr M, Nejadnik MR, Tu J, Koning RI, et al. Intradermal vaccination with hollow microneedles: A comparative study of various protein antigen and adjuvant encapsulated nanoparticles. J Control Release. 2017;266:109-18. https://doi.org/10.1016/j.jconrel.2017.09.021.
6. Barnier Quer C, Elsharkawy A, Romeijn S, Kros A, Jiskoot W. Cationic liposomes as adjuvants for influenza hemagglutinin: More than charge alone. Eur J Pharm Biopharm. 2012;81(2):294-302. https://doi.org/10.1016/j.ejpb.2012.03.013.
7. Nakanishi T, Kunisawa J, Hayashi A, Tsutsumi Y, Kubo K, Nakagawa S, et al. Positively charged liposome functions as an efficient immunoadjuvant in inducing cell-mediated immune response to soluble proteins. J Control Release. 1999;61(1-2):233-40. https://doi.org/10.1016/s0168-3659(99)00097-8.
8. Ottenhoff TH, Kaufmann SH. Vaccines against tuberculosis: where are we and where do we need to go? PLoS Pathog. 2012;8(5):e1002607. https://doi.org/10.1371/journal.ppat.1002607.
9. Karanth H, Murthy RS. pH-sensitive liposomes--principle and application in cancer therapy. J Pharm Pharmacol. 2007;59(4):469-83. https://doi.org/10.1211/jpp.59.4.0001.
10. Balamuralidhara V, Pramodkumar T, Srujana N, Venkatesh M, Gupta NV, Krishna K, et al. pH sensitive drug delivery systems: a review. Am J Drug Discov Dev. 2011;1(1):24-48. https://doi.org/10.3923/ajdd.2011.24.48.
11. Liu G, Zhu M, Zhao X, Nie G. Nanotechnology-empowered vaccine delivery for enhancing CD8+ T cells-mediated cellular immunity. Adv Drug Deliv Rev. 2021;176:113889. https://doi.org/10.1016/j.addr.2021.113889.
12. Anderson JM, Shive MS. Biodegradation and biocompatibility of PLA and PLGA microspheres. Adv Drug Deliv Rev. 2012;64:72-82. https://doi.org/10.1016/j.addr.2012.09.004.
13. Prabhu P, Patravale V. Potential of nanocarriers in antigen delivery: the path to successful vaccine delivery. Nanocarriers. 2014;1:10-45. https://doi.org/10.2478/nanca-2014-0001.
14. Rose F, Wern JE, Ingvarsson PT, van de Weert M, Andersen P, Follmann F, et al. Engineering of a novel adjuvant based on lipid-polymer hybrid nanoparticles: A quality-by-design approach. J Control Release. 2015;210:48-57. https://doi.org/10.1016/j.jconrel.2015.05.004.
15. Valencia PM, Farokhzad OC, Karnik R, Langer R. Microfluidic technologies for accelerating the clinical translation of nanoparticles. Nat Nanotechnol. 2012;7(10):623-9. https://doi.org/10.1038/nnano.2012.168.
16. Romani N, Flacher V, Tripp CH, Sparber F, Ebner S, Stoitzner P. Targeting skin dendritic cells to improve intradermal vaccination. Curr Top Microbiol Immunol. 2012;351:113-38. https://doi.org/10.1007/82_2010_118.
17. Kim Y-C, Park J-H, Prausnitz MR. Microneedles for drug and vaccine delivery. Adv Drug Deliv Rev. 2012;64(14):1547-68. https://doi.org/10.1016/j.addr.2012.04.005.
18. Benne N, van Duijn J, Kuiper J, Jiskoot W, Slütter B. Orchestrating immune responses: How size, shape and rigidity affect the immunogenicity of particulate vaccines. J Control Release. 2016;234:124-34. https://doi.org/10.1016/j.jconrel.2016.05.033.
19. Benne N, Leboux RJT, Glandrup M, van Duijn J, Lozano Vigario F, Neustrup MA, et al. Atomic force microscopy measurements of anionic liposomes reveal the effect of liposomal rigidity on antigen-specific regulatory T cell responses. J Control Release. 2020;318:246-55. https://doi.org/10.1016/j.jconrel.2019.12.003.
20. Baranov MV, Kumar M, Sacanna S, Thutupalli S, van den Bogaart G. Modulation of Immune Responses by Particle Size and Shape. Front Immunol. 2020;11:607945. https://doi.org/10.3389/fimmu.2020.607945.
21. Krause MR, Regen SL. The Structural Role of Cholesterol in Cell Membranes: From Condensed Bilayers to Lipid Rafts. Acc Chem Res. 2014;47(12):3512-21. https://doi.org/10.1021/ar500260t.
22. Szachniewicz MM, Neustrup MA, van den Eeden SJF, van Meijgaarden KE, Franken K, van Veen S, et al. Evaluation of PLGA, lipid-PLGA hybrid nanoparticles, and cationic pH-sensitive liposomes as tuberculosis vaccine delivery systems in a Mycobacterium tuberculosis challenge mouse model - A comparison. Int J Pharm. 2024;666:124842. https://doi.org/10.1016/j.ijpharm.2024.124842.
23. Slütter B, Bal SM, Ding Z, Jiskoot W, Bouwstra JA. Adjuvant effect of cationic liposomes and CpG depends on administration route. J Control Release. 2011;154(2):123-30. https://doi.org/10.1016/j.jconrel.2011.02.007.
24. Billeskov R, Beikzadeh B, Berzofsky JA. The effect of antigen dose on T cell-targeting vaccine outcome. Hum Vaccin Immunother. 2019;15(2):407-11. https://doi.org/10.1080/21645515.2018.1527496.
25. Schipper P, van der Maaden K, Romeijn S, Oomens C, Kersten G, Jiskoot W, et al. Repeated fractional intradermal dosing of an inactivated polio vaccine by a single hollow microneedle leads to superior immune responses. J Control Release. 2016;242:141-7. https://doi.org/10.1016/j.jconrel.2016.07.055.
26. Rodrigues CMC, Plotkin SA. The influence of interval between doses on response to vaccines. Vaccine. 2021;39(49):7123-7. https://doi.org/10.1016/j.vaccine.2021.10.050.
27. Limcharoen B, Wanichwecharungruang S, Kröger M, Sansureerungsikul T, Schleusener J, Lena Klein A, et al. Dissolvable microneedles in the skin: Determination the impact of barrier disruption and dry skin on dissolution. Eur J Pharm Biopharm. 2024;199:114303. https://doi.org/10.1016/j.ejpb.2024.114303.
28. Lee J, van der Maaden K, Gooris G, O'Mahony C, Jiskoot W, Bouwstra J. Engineering of an automated nano-droplet dispensing system for fabrication of antigen-loaded dissolving microneedle arrays. Int J Pharm. 2021;600:120473. https://doi.org/10.1016/j.ijpharm.2021.120473.

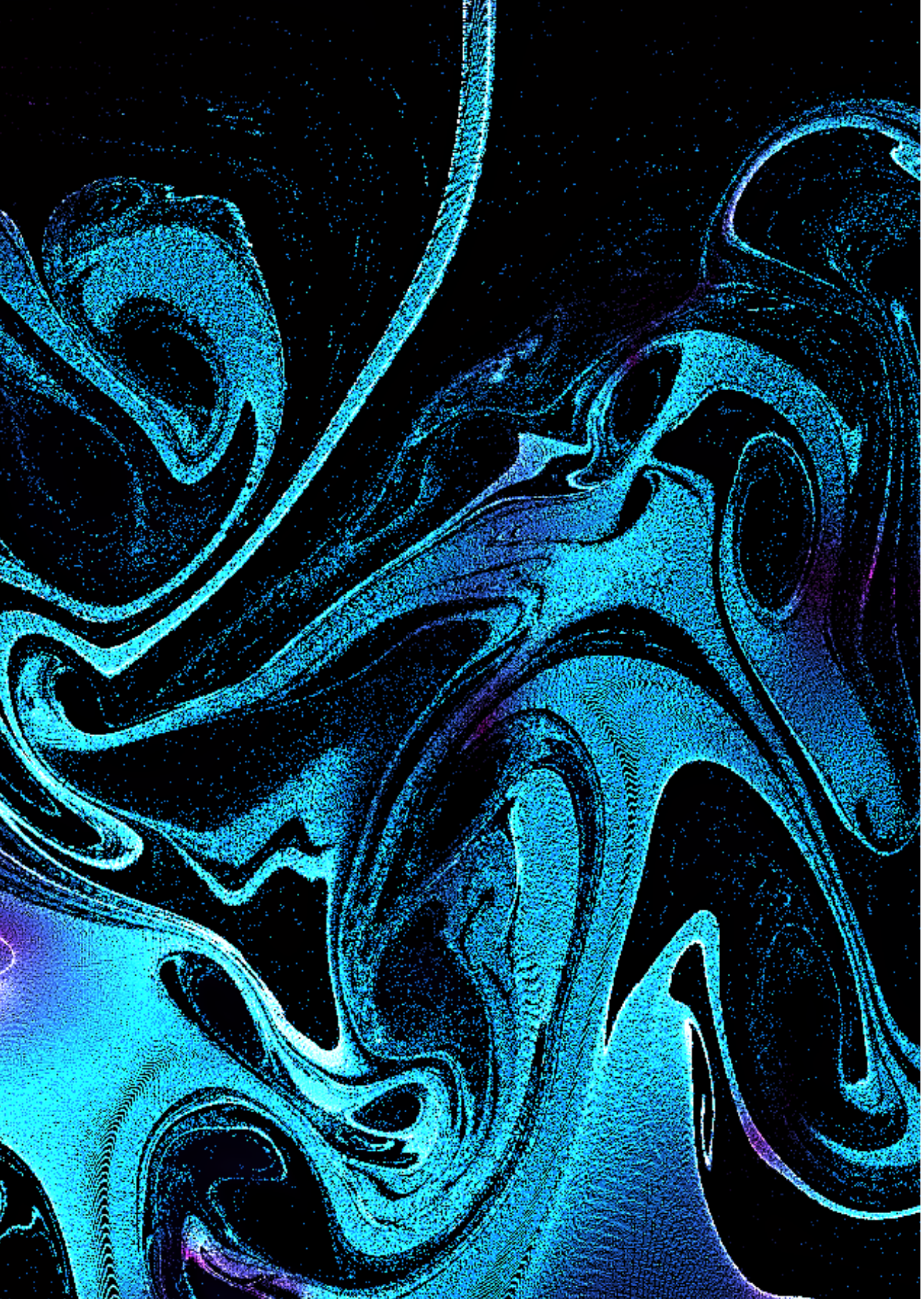

APPENDICES

SAMENVATTING VAN HET PROEFSCHRIFT
CURRICULUM VITAE
LIST OF PUBLICATIONS
ABBREVIATION LIST

SAMENVATTING VAN HET PROEFSCHRIFT

Het onderzoek beschreven in dit proefschrift richt zich op nanoparticulaire vaccinformuleringen en toedieningsroutes om de antigen-specifieke inductie van pro-inflammatoire immuunreacties te verbeteren in de zoektocht naar nieuwe vaccinatiestrategieën om tuberculose (TB) te voorkomen.

Dit proefschrift behandelt verschillende aspecten betreffende de ontwikkeling van een nieuw TB-subunitvaccin. In **Hoofdstuk 1** wordt de TB-immunologie en de noodzaak van innovatieve vaccinoplossingen geïntroduceerd. Hierna wordt het doel van het onderzoek in dit proefschrift beschreven. Tenslotte wordt de opzet van het proefschrift besproken.

In **Hoofdstuk 2** zijn studies beschreven waarin het recombinante eiwit Ag85B-ESAT6-Rv2034 (AER) verpakt werd in positief geladen liposomale formuleringen met variërende lipidensamenstellingen. Vervolgens werden de immuunreacties van de formuleringen in vitro bepaald. De AER-bevattende liposomen werden geformuleerd met behulp van de dunne-filmlaag dehydratatie-rehydratie methode, gevolgd door tip-sonicatie. De liposomen bestonden uit een positief geladen lipide, cholesterol en een helperlipide (zwitterion) in verschillende molaire verhoudingen. De fysicochemisch stabiele formuleringen werden vervolgens onderzocht met een reeks in vitro testen: i) een assay met humane monocyten-afgeleide dendritische cellen (MDDC), waarbij de levensvatbaarheid en activering van dendritische cellen (DC) werden beoordeeld na incubatie van die DCs met de formuleringen, ii) een assay waarbij de opname van liposomen werd gemeten in MDDC en M1 (klassiek geactiveerde macrofagen die een pro-ontstekings fenotype vertonen) en M2 (alternatief geactiveerde macrofagen die een anti-ontstekings fenotype vertonen) cellen, en iii) een T-cel assay waarin de best presterende formuleringen werden getest door de geactiveerde DCs te incuberen met T helpercellen, om te bepalen of bij de laatste de expressie van de activeringsmarker CD154 en hun interferon (IFN)-γ-productie verhoogd werden.

De formuleringen met cholesterol en de positief geladen lipiden 1,2-dioleoyl-3-trimethylammonium-propaanchloride (DOTAP), dimethyldioctadecylammonium-bromide (DDA), 1,2-dioleoyl-*sn*-glycero-3-ethylphosphocholine chloride (EPC) of N4-cholesteryl-spermine hydrochloride (GL-67) induceerden de hoogste upregulatie van de MDDC-activeringsmarkers CD40, CD80 en CCR7. De formulering met GL-67 induceerde echter een hoge celdood en werd daarom niet geselecteerd voor de T-celassay. Wat betreft de resterende formuleringen verhoogden de AER/DOTAP:cholesterol:1,2-dioleoyl-snglycero-3-phosphocholine (DOPC) en AER/EPC:cholesterol:DOPC formuleringen de productie van $IFN\gamma^+$ en de expressie van $CD154^+$ significant in T helpercellen vergeleken met hun AER-lege tegenhangers. Echter, in een afzonderlijke studie (ongepubliceerd) waren de DOTAP-liposomen minder in staat T celgemedieerde immuunreacties op te wekken. Daarom werd alleen de lipideverhouding van de AER/EPC:cholesterol:DOPC-formulering verder geoptimaliseerd, waarbij een molaire lipidenverhouding van 2:1:2 de meest veelbelovende formulering was, omdat deze het DC-activeringsmarkers en cytokine/chemokineproductie het sterkst verhoogde. Samengevat, dit hoofdstuk beschrijft een screeningmethode voor vaccinformuleringen, waarbij de EPC:cholesterol:DOPC-formulering het sterkste T-helper type 1 responsen induceert en dus de meest belovende formulering is voor verdere ontwikkeling als TB vaccin.

In **Hoofdstuk 3** wordt een nieuw, kosteneffectief modulair microfluïdisch systeem geïntroduceerd voor de productie van poly(D,L-lactide-*co*-glycolide) (PLGA)-nanodeeltjes. De eenvoudigste vorm van het modulaire microfluïdische systeem omvat een co-flowconfiguratie, waarbij een binnen stroom van PLGA-bevattend organisch oplosmiddel een buitenste stroom van een waterige vloeistof ontmoet. Het mengen van deze twee oplosmiddelen veroorzaakt PLGA nanoprecipitatie, wat leidt tot de vorming van nanodeeltjes. Onderzocht werd hoe de stroomsnelheid, type oplosmiddel en de PLGA concentratie de vorming van nanodeeltjes beïnvloedt. De bruikbaarheid van dit systeem voor het maken van nanodeeltjes voor gecontroleerde geneesmiddelafgifte werd onderzocht door positief en negatief geladen eiwitten (model geneesmiddelen) in PLGA-nanodeeltjes te incorporeren. Uit de experimentele resultaten bleek dat de vorming van nanodeeltjes wordt beïnvloed door de PLGA-concentratie, waarbij een toenemende PLGA-concentratie leidt tot grotere deeltjesdiameters. Verder bleek dat een verhoging van de totale stroomsnelheid resulteert in de vorming van kleinere nanodeeltjes. Het gebruik van ultrapuur water in de waterfase resulteerde in negatief geladen nanodeeltjes en ongecontroleerde precipitatie in het systeem bij hoge PLGA-concentraties. Ondertussen creëerde het toevoegen van poly(vinylalcohol) aan de waterfase neutrale deeltjes en elimineerde deze toevoeging de precipitatieproblemen. Negatief geladen deeltjes werden reproduceerbaar verkregen door gebruik te maken van ethanol-watermengsels. Incorporatie van de eiwitten ovalbumine of lysozyme (respectievelijk negatief en positief geladen) met een drievloeistofkanalensysteem resulteerde in encapsulatieefficiënties van boven de 40%. Hieruit kan geconcludeerd worden dat in dit onderzoek een goedkoop en gemakkelijk aanpasbaar modulair microfluïdisch systeem werd ontwikkeld om PLGA-nanodeeltjes te bereiden met een controleerbare deeltjesdiameter. Ook maakt dit systeem het mogelijkheid om eiwitten in te bouwen, waardoor dit systeem veelbelovend is voor het maken van nanodeeltjes-gebaseerde geneesmiddel- en vaccintoepassingen.

In **Hoofdstuk 4** worden studies beschreven waarin drie verschillende nanodeeltjes worden vergeleken: kationische pH-gevoelige liposomen, bereid door middel van sonicatie, en twee nanodeeltjes bereid met het modulair-microfluïdisch-systeem, namelijk PLGA-nanodeeltjes en PLGA-nanodeeltjes met aan de buitenkant een lipidenlaag (lipide-PLGA-hybriden).

De immunogeniciteit van de nanodeeltjes met het antigeen AER met en zonder de adjuvanten (een molecuul dat de immuunreactie kan verhogen of veranderen) monophosphoryl lipide A (MPLA) en cytosine-fosfaat-guanine-motieven oligodeoxynucleotiden (CpG ODN) 1826 werd in vitro in MDDCs (zoals beschreven in hoofdstuk 2) beoordeeld. Eerst werd de opname van de nanodeeltjes in MDDCs zonder de adjuvanten geëvalueerd. Lipide-PLGA-hybriden en pH-gevoelige liposomen werden efficiënt opgenomen door MDDCs, maar PLGA-nanodeeltjes niet. Daarna werden MDDCs gestimuleerd met de nanodeeltjes met en zonder de adjuvanten. De MDDCs werden onderzocht op activeringsmarkers en cytokineproductie. Bij de nanodeeltjes formuleringen zonder adjuvanten waren de kationische pH-gevoelige liposomen minder efficiënt dan de lipide-PLGA-hybriden in het upreguleren van dendritische cel-activeringsmarkers en cytokineproductie, terwijl PLGA-nanodeeltjes het minst efficiënt waren. PLGA-deeltjes en kationische pH-gevoelige liposomen zonder adjuvanten induceerden nauwelijks de secretie van cytokines/chemokines. De lipide-PLGA-hybriden, PLGA-nanodeeltjes en de pH-gevoelige liposomen met adjuvanten waren allemaal efficiënt in het up-reguleren van dendritische cel-oppervlaktemarkers en cytokineproductie.

De beschermende werkzaamheid van de liposomen, PLGA-nanodeeltjes en de lipide-PLGA-hybriden geformuleerd met de moleculaire adjuvanten werd in vivo getest in C57Bl/6-muizen die besmet werden met *Mycobacterium tuberculosis* (Mtb) om de mogelijke bescherming van het TB-vaccin te onderzoeken. De kandidaatvaccins die we ontwikkelden werden vergeleken met het huidige *Mycobacterium bovis* Bacille Calmette-Guérin (BCG)-vaccin en AER gemengd met de twee adjuvanten MPLA en CpG ODN 1826. Alle vaccins (BCG, liposomen, PLGA-nanodeeltjes en de lipide-PLGA-hybriden), behalve het AER- adjuvant mengsel induceerden bescherming tegen TB in C57BL/6 muizen. Dit bleek uit een significante vermindering van de bacteriële lading TB in de longen en milt van de dieren in vergelijking met de bacteriële lading niet-gevaccineerde muizen. Muizen gevaccineerd met PLGA-nanodeeltjes hadden een lager aantal Mtb-bacteriën in de milt en longen vergeleken met het BCG-vaccin en de twee vaccins gebaseerd op nanodeeltjes; het verschil was echter niet statistisch significant, omdat de groepen uit een klein aantal muizen bestonden. Samengevat, uit deze studies kan geconcludeerd worden dat nanodeeltjes-gebaseerde formuleringen de Mtb-bacteriële lading bij de muizen verlaagde. De PLGA-nanodeeltjes leidde tot de beste bescherming, hoewel de lipide-PLGA-hybriden iets betere resultaten in vitro lieten zien.

In **Hoofdstuk 5** worden studies beschreven waarin het effect van intradermale toediening van PLGA-nanodeeltjes met CpG ODN 1826 en ovalbumine in oplosbare micronaaldarrays (dMNAs) vergeleken werd met intradermale toediening met hypodermische (klassieke injectie) naalden in vivo. Intradermale injectie van nanodeeltjes is een effectieve toedieningsroute voor vaccins, zoals beschreven in **Hoofdstuk 4**.

In deze studie moesten we eerst stabiele dMNAs met daarin PLGA-nanodeeltjes ontwikkelen. Dit was belangrijk omdat de verschillende polymeren die werden gebruikt voor de bereiding van dMNAs de integriteit – en daarmee de functionaliteit – van de nanodeeltjes kan beïnvloeden. De dMNAs bereid met poly(vinylalcohol) vertoonden bijna geen aggregatie van PLGA-nanodeeltjes in de oplosbasbare dMNAs. De PLGA:poly(vinylalcohol)-gewichtsverhouding van 1:9 resulteerde in 100% huid-penetratie efficientie en de snelste oplosbaarheid in ex-vivo humane huid (de dMNAs losten op binnen 30 minuten). Vervolgens werden injecteerbare formuleringen en dMNAs beiden met ovalbumine en CpG ODN 1826 met en zonder PLGA-nanodeeltjes getest in muizen. De injecteerbare formuleringen met ovalbumine en CpG ODN 1826 met en zonder PLGA-nanodeeltjes induceerden significante T helpercelresponsen in muizen vergeleken met de andere formuleringen. De formulering met ovalbumine en CpG ODN 1826 met PLGA-nanodeeltjes induceerde significante cytotoxische T-celresponsen vergeleken met de andere formuleringen. Helaas losten de dMNAs niet volledig op in de muizenhuid, wat mogelijk de reden is waarom de toediening via dMNAs geen helper en cytotoxische T-cel responsen induceerden.

Hieruit kan geconcludeerd worden dat de injecteerbare formuleringen beter presteerden dan de dMNAs, waarschijnlijk vanwege de slechte oplosbaarheid van de dMNAs in muizenhuid in het in vivo experiment. De oplosbaarheid was echter goed in de ex-vivo humane huid, wat de verschillen tussen de modellen bloot legt. De dMNA-formulering moet in de toekomst daarom worden aangepast voor studies met muizen. Hoewel we geen immuun responsen induceerden met behulp van dMNAs, konden dMNAs met PLGA-nanodeeltjes met succes worden bereid, aangezien de deeltjes hun fysisch-chemische eigenschappen behielden na oplossen. De injecteerbare formulering met PLGA-nanodeeltjes bereid door middel van het modulaire microfluïdische systeem was bijzonder krachtig in het induceren van helper en cytotoxische T-celresponsen.

CURRICULUM VITAE

Born in Copenhagen, Denmark, in 1990, Malene Aaby Neustrup pursued her undergraduate and graduate studies in Pharmacy at the School of Pharmaceutical Sciences, University of Copenhagen, Denmark, from 2011 to 2017. During her academic journey, she gained practical experience as a student assistant in the product quality department at the company Haldor Topsøe.

Her master's thesis research, conducted at the Danish State Serum Institute and the Department of Pharmacy, University of Copenhagen, was supervised by dr. Signe Tandrup Schmidt, prof.dr. Camilla Foged, and dr. Dennis Christensen, and resulted in her thesis titled: "Formulation and Characterisation of Nanoemulsion-Based Adjuvants Mediating Vaccine-Induced $CD8^+$ T-Cell Responses".

In September 2017, Malene Aaby Neustrup commenced her PhD studies at the Leiden Academic Centre for Drug Research, Leiden University, and Leiden University Medical Centre under the guidance of prof.dr. Joke A. Bouwstra, prof.dr. Tom H.M. Ottenhoff, and dr. Koen van der Maaden. Her doctoral research focused on developing a tuberculosis vaccine utilizing nanoparticle formulations and dissolvable microneedle technology. Teaching and mentorship were central components of Malene's studies, demonstrated by her supervision of laboratory courses, guidance of bachelor's students, and mentorship of master's students. In addition, she presented her research at several Dutch conferences.

LIST OF PUBLICATIONS

Systematic investigation of the role of surfactant composition and choice of oil: Design of a nanoemulsion-based adjuvant inducing concomitant humoral and $CD4^+$ T-cell responses
S. T. Schmidt, **M. A. Neustrup**, S. Harloff-Helleberg, K. S. Korsholm, T. Rades, P. Andersen, D. Christensen, and C. Foged. Pharm Res. 2017;34(8):1716-27.
https://doi.org/10.1007/s11095-017-2180-9

Induction of cytotoxic T-lymphocyte responses upon subcutaneous administration of a subunit vaccine adjuvanted with an emulsion containing the Toll-like receptor 3 ligand poly(I:C)
S. T. Schmidt, G. K. Pedersen, **M. A. Neustrup**, K. S. Korsholm, T. Rades, P. Andersen, D. Christensen, and C. Foged. Front Immunol. 2018;9:898.
https://doi.org/10.3389/fimmu.2018.00898

Atomic force microscopy measurements of anionic liposomes reveal the effect of liposomal rigidity on antigen-specific regulatory T-cell responses
N. Benne, R. J. T. Leboux, M. Glandrup, J. van Duijn, F. Lozano Vigario, **M. A. Neustrup**, S. Romeijn, F. Galli, J. Kuiper, W. Jiskoot, and B. Slütter. J Control Release. 2020;318:246-55.
https://doi.org/10.1016/j.jconrel.2019.12.003

Stabilin-1 is required for the endothelial clearance of small anionic nanoparticles
G. Arias-Alpizar, B. Koch, N. M. Hamelmann, **M. A. Neustrup**, J. M. J. Paulusse, W. Jiskoot, A. Kros, and J. Bussmann. Nanomedicine. 2021;34:102395.
https://doi.org/10.1016/j.nano.2021.102395

Understanding opalescence measurements of biologics - A comparison study of methods, standards, and molecules
P. Kunz, E. Stuckenberger, K. Hausmann, L. Gentiluomo, **M. A. Neustrup**, S. Michalakis, R. Rieser, S. Romeijn, C. Wichmann, R. Windisch, A. Hawe, W. Jiskoot, and T. Menzen. Int J Pharm. 2022;628:122321.
https://doi.org/10.1016/j.ijpharm.2022.122321

Intrinsic immunogenicity of liposomes for tuberculosis vaccines: Effect of cationic lipid and cholesterol
M. A. Neustrup*, M. M. Szachniewicz*, K. E. van Meijgaarden, W. Jiskoot, J. A. Bouwstra, M. C. Haks, A. Geluk, and T. H. M. Ottenhoff. Eur J Pharm Sci. 2024;195:106730.
https://doi.org/10.1016/j.ejps.2024.106730.

Intradermal vaccination with PLGA nanoparticles via dissolving microneedles and classical injection needles
M. A. Neustrup*, J. Lee*, B. Slütter, C. O'Mahony, J. A. Bouwstra, and K. van der Maaden. Pharm Res. 2024;41(2):305-19.
https://doi.org/10.1007/s11095-024-03665-7

Evaluation of PLGA, lipid-PLGA hybrid nanoparticles, and cationic pH-sensitive liposomes as tuberculosis vaccine delivery systems in a Mycobacterium tuberculosis challenge mouse model - A comparison
M. M. Szachniewicz, **M. A. Neustrup**, S. J. F. van den Eeden, K. E. van Meijgaarden, K. Franken, S. van Veen, R. I. Koning, R. W. A. L. Limpens, A. Geluk, J. A. Bouwstra, and T. H. M. Ottenhoff. Int J Pharm. 2024;666:124842.
https://doi.org/10.1016/j.ijpharm.2024.124842

A versatile, low-cost modular microfluidic system to prepare poly(lactic-*co*-glycolic acid) nanoparticles with encapsulated protein
M. A. Neustrup, T. H. M. Ottenhoff, W. Jiskoot, J. A. Bouwstra, and K. van der Maaden. Pharm Res. 2024;41(12):2347-61.
https://doi.org/10.1007/s11095-024-03792-1

*Authors contributed equally

ABBREVIATION LIST

Abbreviation	Meaning
ACK	ammonium-chloride-kalium
AER	Ag85B-ESAT6-Rv2034
Ag	antigen
Ag85B	antigen 85B
APC	antigen-presenting cell
BCA	bicinchoninic acid
BCG	*Mycobacterium bovis* Bacille Calmette-Guérin
BSA	bovine serum albumin
CCD	the Netherlands's Central Authority for Scientific Procedures on Animals
CCL	chemokine (C-C motif) ligand
CCR	C-C chemokine receptor type
CD	cluster of differentiation
CFU	colony forming unit
CpG ODN	cytosine-phosphate-guanine oligodeoxynucleotide
CXCL	chemokine (C-X-C motif) ligand
CXCR	C-X-C motif chemokine receptor
DC	dendritic cell
DC-cholesterol	3ß-[N- (N',N'-dimethylaminoethane)-carbamoyl]cholesterol hydrochloride
DDA	dimethyldioctadecylammonium bromide, bromide salt
DLS	dynamic light scattering
dMNA	dissolvable microneedle array
DMSO	dimethyl sulfoxide
DOBAQ	N-(4-carboxybenzyl)-N,N-dimethyl-2,3-bis(oleoyloxy)propan-1-aminium
DODMA	1,2-dioleyloxy-3-dimethylaminopropane
DOPC	1,2-dioleoyl-*sn*-glycero-3-phosphocholine
DOPE	1,2-dioleoyl-*sn*-glycero-3-phosphoethanolamine
DOTAP	1,2-dioleoyl-3-trimethylammonium-propane, chloride salt
DSPC	1,2-distearoyl-sn-glycero-3-phosphocholine
EE%	encapsulation efficiency
ELISA	enzyme-linked immunosorbent assay

Abbreviation	Meaning
EPC	1,2-dioleoyl-*sn*-glycero-3-ethylphosphocholine, chloride salt
ESAT-6	the 6 kDa early secretory antigenic target
EU	endotoxin unit
FBS	fetal bovine serum
FDR	false discovery rate
FRR	flow rate ratio
GL-67	N^4-cholesteryl-spermine hydrochloride
GM-CSF	granulocyte-macrophage colony-stimulating factor
GMP	Good Manufacturing Practice
His	N-terminal hexahistidine
HLA	human leukocyte antigen
HRP	horse radish peroxide
i.n.	intranasal
ID	inner diameter
IFN	interferon
Ig	immunoglobulin
IL	interleukin
IMDM	Iscove's Modified Dulbecco's Medium
IQR	interquartile range
KLRG1	killer cell lectin-like receptor subfamily G member 1
LAL	limulus amebocyte lysate
LN	lymph node
MACS	magnetic cell isolation
M-CSF	macrophage colony-stimulating factor
MDDC	monocyte-derived dendritic cell
MDMF	monocyte-derived macrophages
MDR-TB	multidrug-resistant tuberculosis
MHC	major histocompatibility complex
MPLA	monophosphoryl lipid A
Mtb	*Mycobacterium tuberculosis*
MVL5	N1-[2-((1S)-1-[(3-aminopropyl)amino]-4-[di(3-amino-propyl) amino]butylcarboxamido)ethyl]-3,4-di[oleyloxy]-benzamide
NP	nanoparticle

Abbreviation	Meaning
OD	outer diameter
OVA	ovalbumin
PAMP	pathogen-associated molecular pattern
PB	phosphate buffer
PBMC	peripheral blood mononuclear cell
PBS	phosphate-buffered saline
PCR	polymerase chain reaction
PD-1	programmed cell death protein 1
PDI	polydispersity index
PDMS	polymethylmethacrylate
PE	phosphatidylethanolamine
PEEK	polyether ether ketone
PLGA	poly(D,L-lactic-*co*-glycolic acid)
PPD	purified protein derivative
PRR	pattern-recognition receptor
PTFE	polytetrafluoroethylene
PVA	poly(vinyl alcohol)
PVP	polyvinylpyrrolidone
QC	Quality Control
rpm	rounds per minute
RPMI	Roswell Park Memorial Institute
s.c.	subcutaneous
SA	stearylamine
SDGs	Sustainable Development Goals
SOI	site of injection
TB	tuberculosis
TCR	α:β T-cell receptor
T_{FH} cell	T follicular helper cell
TFR	total flow rate
Th	T helper
Th1	T helper type 1
Th1/Th2/Th17	T-helper type 1/2/17 cell
TLR	Toll-like receptor
TMB	tetramethylbenzidine

Abbreviation	Meaning
TNF	tumor necrosis factor
T_{reg} cell	regulatory T cell
Ultrapure water	Spectra-Por® Milli-Q® water
UMAP	uniform manifold approximation and projection
WHO	World Health Organization